ISSN 1341-562X

JOURNAL OF FOREST PLANNING

Vol. 13 Special Issue "Silvilaser"

Japan Society of Forest Planning

February, 2008

JOURNAL OF FOREST PLANNING

Submission of Manuscripts

Manuscripts should be submitted to following Editorial Office.

Dr. Seiji ISHIBASHI
JOURNAL OF FOREST PLANNING
University Forest in Chichibu,
Graduate School of Agricultural and Life Sciences,
The University of Tokyo
1-1-49 Hinoda-cho, Chichibu, Saitama 368-0034, Japan
Phone: +81-494-22-0272, Fax: +81-494-23-9620
E-mail:bashi@uf.a.u-tokyo.ac.jp

Subscription Information

JOURNAL OF FOREST PLANNING is pubished halfyearly. The subscription for 2003 is 5,000 yen and the single issue price is 2,500 yen. Subscription orders can be sent to following office.

Toho Shoten
343 Yamabuki-cho
Shinjuku-ku, Tokyo 162-0801, Japan
Phone: +81-3-3269-2131, Fax: +81-3-3269-8655
http://www.toho-shoten.co.jp

JOURNAL OF FOREST PLANNING is published by
Japan Society of Forest Planning
Iwate University, 3-18-8 Ueda, Morioka, Iwate 020-8550, Japan

JOURNAL OF

FOREST PLANNING

Vol.13, Special Issue "Silvilaser" February, 2008

Japan Society of Forest Planning

CONTENTS

Foreword

Special Issue - Silvilaser 2006 LiDAR Applications in Forest Inventory and Assessment
Yasumasa Hirata 139

Articles

Estimation of Stand Density of Young Plantations using Digitized Aerial Photographs in Ehime Prefecture, Japan
Rikiya Kaneko, Yasushi Suzuki, Jun'ichi Gotou, Chitosi Eino, Kosuke Makino, Hayato Tsuzuki and Tatsuo Sweda 141

Development of the Forest Road Design Technique using LiDAR Data of the Funyu Experimental Forest
Masashi Saito, Kazuhiro Aruga, Keigo Matsue and Toshiaki Tasaka 147

Estimation of Tree Height and Forest Biomass from GLAS Data
G. Sun, K.J. Ranson, J. Masek, Z. Guo, Y. Pang, A. Fu and D. Wang 157

The Estimation of Wind Risk in Forests Stands using Airborne Laser Scanning (ALS)
Juan Suárez, Rafael Garcia, Barry Gardiner and Genevieve Patenaude 165

Estimation of Biophysical Parameters of Individual Tree Stands derived from LiDAR and Digital Matrix Camera Image
Takahiro Endo, Tatsuya Nawamura, Hitoshi Taguchi, Pranab Jyoti Baruah, Masahiro Setojima, Toru Katsura and Yoshifumi Yasuoka 187

Quantifying Variances of Line-Intercept-Sampling Estimators of Percentage Cover
Kaiguang Zhao, Sorin Popescu and Ross Nelson 195

Stemwood Volume Estimates for a Mixed Temperate Forest using Satellite LiDAR
Jacqueline Rosette, Peter North and Juan Suárez 205

Forest Habitability for Wildlife as Evaluated by Airborne Laser Profiling
Sayoko Ueda, Hayato Tsuzuki and Tatsuo Sweda 215

Analysis of Canopy Structure in Beech (*Fagus crenata*) Secondary Forests using an Airborne Laser Scanner
Ai Nishikami, Yukihiro Chiba, Yoshio Awaya and Yoshitaka Kakubari 225

Estimation of Stand Structure in the Deciduous Broad-leaved Forest using Multi-temporal LiDAR Data
Yasuteru Imai, Masahiro Setojima, Manabu Funahashi,
Toshio Katsuki and Masahiro Amano 233

Estimating Mean Height and Stand Volume in Broad Leaved Forest Stands using LiDAR
Eiji Kodani and Yoshio Awaya 239

Land-cover Classification of Ehime Prefecture, Japan using Airborne Laser Altimetry
Yoshiko Maeda, Hayato Tsuzuki, Ross Nelson and Tatsuo Sweda 245

Comparison of Different Sampling Density Data for Detecting and Measuring Individual-trees in a Mountainous Coniferous Forest using Small-footprint Airborne LiDAR
Tomoaki Takahashi, Kazukiyo Yamamoto and Yoshimichi Senda 249

Estimating Timber Stock of Ehime Prefecture, Japan using Airborne Laser Profiling
Hayato Tsuzuki, Ross Nelson and Tatsuo Sweda 259

Measurement of Snow Depth Distribution in a Mountainous Watershed using an Airborne Laser Scanner
Yoshio Tsuboyama, Akira Shimizu, Tayoko Kubota,
Toshio Abe, Naoki Kabeya and Tatsuhiko Nobuhiro 267

Expectation of LiDAR on Forest Measurement in Kyoto Protocol
Masahiro Amano 275

Stability of Surface LiDAR Height Estimates on a Point and Polygon Basis
Michael A. Wulder, Steen Magnussen, David Harding, Nicholas C. Coops,
Paul Boudewyn and David Seemann 279

Regional Forest Inventory using an Airborne Profiling LiDAR
Ross Nelson, Eæsset, Terje Gobakken, Göran Ståhl and Timothy G. Gregoire 287

Conifer Plantation Volume Estimation by Remote Sensing without Parameter Fittings
Gen Takao, Satoshi Ishibashi, Masayoshi Takahashi,
Tatsuo Sweda, Hayato Tsuzuki and Tomoko Kusakabe 295

Estimation of Stand Attributes in *Cryptomeria japonica* and *Chamaecyparis obtusa* Stands from Single Tree Detection using Small-Footprint Airborne LiDAR Data
Yasumasa Hirata, Naoyuki Furuya, Makoto Suzuki and Hirokazu Yamamoto 303

Guide for Contributors 311

Foreword:

Special Issue – Silvilaser 2006
LiDAR Applications in Forest Inventory and Assessment

Yasumasa Hirata*

Applications of LiDAR/laser scanning systems to characterize forested areas have expanded rapidly over the last several years, particularly in the domain of forest inventory. The application of LiDAR data is expanding over an ever increasing range of interest areas. Previous conferences relating to LiDAR application in forestry were held in Victoria, British Columbia, Canada, March 14-15, 2002; Brisbane, Queensland, Australia, April 18-19, 2002; Umeå, Sweden, September 2-4, 2003; Freiburg, Germany, October 3-6, 2004 and Blacksburg, Virginia, USA, September 29-October 1, 2005. Japan Society of Forest Planning, Forestry and Forest Products Research Institute and Ehime University organized an conference, Silvilaser 2006, which was the sixth in this international series, in Matsuyama, Ehime, Japan, November, 7-10, 2006. In the 21st century, LiDAR systems are used worldwide for natural resource assessment, and this conference generated interest in Asia as well as the rest of world.

The intention of Silvilaser 2006 was to provide a platform for information sharing and to enable the communication of experiences users have had in using LiDAR data to meet a range of information needs. Developing the linkage between LiDAR practitioners across a range of applications domains was also a conference goal. The aim of the conference was to present and exchange state-of-the-art scientific as well as practical results and techniques resulting from airborne and terrestrial LiDAR application in many domains of forestry. The conference contributed to explore links between researchers, producers, and end-users of LiDAR products. The conference was made up of 6 sessions; (1) techniques for extraction of tree information, (2) mapping and classification, (3) measurement for forest condition, (4) biomass and LAI estimation, (5) large scale forest inventory, and (6) integration of LiDAR and optical sensor data.

This special issue is a compilation of contributed papers from the Silvilaser 2006 conference. These papers represent a significant benchmark of LiDAR application in forest inventory and assessment. I believe that these studies will provide readers of the Journal of Forest Planning with useful information and clues to apply LiDAR in wider domains of forestry.

* Shikoku Research Center, Forestry and Forest Products Research Institute

Article

Estimation of Stand Density of Young Plantations using Digitized Aerial Photographs in Ehime Prefecture, Japan

Rikiya Kaneko[*1], Yasushi Suzuki[*2], Jun'ichi Gotou[*2], Chitosi Eino[*3], Kosuke Makino[*3], Hayato Tsuzuki[*4] and Tatsuo Sweda[*4]

ABSTRACT

Most of Japanese young plantation forests have reached an age when thinning is needed, but they have not yet been cut, and stand density is often too high. An economical method is needed for selecting stands that should be cut. We are developing a method of stand density estimation using aerial photography. In previous work, we devised a method for high resolution color aerial-photographs. It divides images into a series of color bands, and estimates stand densities by the brightness in a combination of different band images. Ground truthing is needed to improve precision. In our earlier work, we used a set of 22 plots for ground truthing. Here, we present ground truthing of mono-color aerial photographs obtained for a growing stock investigation project in Ehime prefecture, Japan. The project is to estimate the CO_2 sink potential for all forests in the prefecture. Vegetation profiles are measured by airborne laser altimetry assisted by a consecutive series of ground truth surveys. Performance of mono-color aerial photography method was rather poor, indicating that manual contrast adjustment should be improved.

Keywords: aerial photography, airborne laser altimetry, ground truth survey, plantation forests, stand density

INTRODUCTION

The majority of young Japanese plantation forests were planted 40-50 years ago and are reaching an age when thinning is required. Much of these forests have not yet been thinned and stand densities are too high. For the forestry industry, it would be highly advantageous to have an economical method for locating within the vast plantation tracts those dense stands that need immediate thinning. Earlier, we (Gotou *et al.*, 2006) developed a technique using high resolution color aerial photography to estimate stand density in young plantation forests. The method divides images into a series of color channels, and estimates stand densities from a combination of modified color channel images. In the development stage, ground truthing within the tree stands is required to improve precision. The present paper describes the method and results of our previous work (Gotou *et al.*, 2006). We also tested the methodology using mono-color aerial photographs of normal resolution, which are less expensive, but contain less information than color and high-resolution photographs. The ground truth data we used were obtained from an investigation for a growing stock investigation to assess the CO_2 sink potential of all forests in Ehime Prefecture, Japan. The project produces forest vegetation profiles measured by airborne laser altimetry augmented with a consecutive series of ground truth surveys (Tsuzuki *et al.*, 2006b) to derive forest leaf area indices and ground stocks (Kusakabe *et al.*, 2000 ; 2006; Tsuzuki *et al.*, 2006a). Airborne laser altimetry data is used in attempts to estimate precise stand information such as height and density of trees (e.g. Hirata, 2005a and 2005b), often for limited forest areas. Stand density estimation by aerial photography is less precise than that with airborne laser altimetry, but is less expensive and applicable to larger areas. Here, we explore the possibility of applying a less expensive method to estimate stand density in larger areas by using aerial photography. We also report on data obtained from airborne laser altimetry.

Corresponding author: Yasushi Suzuki
[*1] Graduate school of Agriculture, Kochi University, B200 Monobe, Nankoku 783-8502, Japan
[*2] Faculty of Agriculture, Kochi University, B200 Monobe, Nankoku 783-8502, Japan
[*3] FRESCO Inc., 337-1 Kume-Kubota cho, Matsuyama, 791-1101, Japan
[*4] Faculty of Agriculture, Ehime University, 3-5-7 Tarumi, Matsuyama, 790-8566, Japan

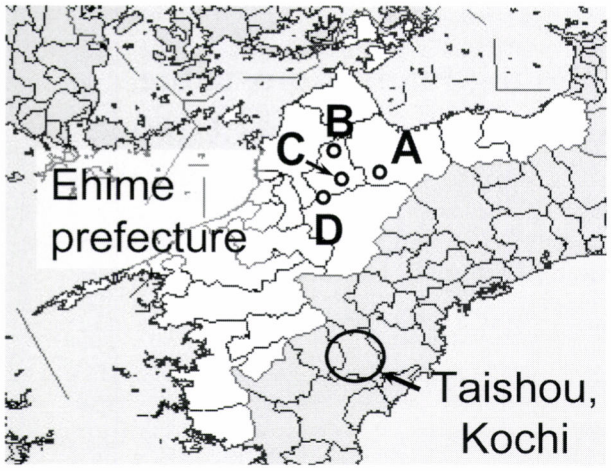

Fig. 1 Locations of aerial photography. "A", "B", "C", and "D" are labels in Table 2
Map image is from Wikipedia (http://ja.wikipedia.org/)

MATERIALS AND METHODS

Stand Density Estimation by Color-aerial Photography (methodology developed in our previous study)

Target Stands

The target stands for our earlier work (GOTOU *et al.*, 2006) were selected from a series of municipal forests in the vicinity of Taishou (a town recently subsumed into the municipality of Shimanto), located in the mid-western portion of Shikoku Island, which is in the western part of Kochi Prefecture, Japan (Fig. 1). All of the selected stands are plantations of Japanese cedar (*Cryptomeria japonica*) or Japanese cypress (*Chamaecyparis obtusa*). The color aerial photographs covering the stands were obtained from the municipal office. The images were taken in 2000 at an altitude 2,500m to investigate land use within Taishou. The altitude was lower than usual, so that image resolution was excellent.

Modification of Digitized Images

The color photographs of the target stands were scanned at 720dpi. The digital files were resolved into eight channels of color-separated images using Adbe Photoshop™. There are three color separation systems: CMYK, RGB, and Lab. CMYK consists of four color-channel images: cyan, magenta, yellow, and black. There are three color-channel images in the RGB system, viz. red, green, and blue. The Lab system also has three color-channel images, viz. brightness (L), magenta from green (a), and yellow from blue (b). Our methodology uses only the brightness channel image from the Lab system. In summary, eight channels of images are generated from single digitized aerial photographs; CMYK-cyan, CMYK-magenta, CMYK-yellow, CMYK-black, RGB-red, RGB-green, RGB-blue, and Lab-brightness.

In some images, sections were completely bleached out by sunlight. Contrast adjustment in Photoshop was used to deal with over-exposed sections of each color-channel image. Concurrently, we applied Photoshop's edge effect procedure for each image. These image enhancement methods allow for more accurate estimates of tree stand density.

Each tree crown has sunlit and shaded sides. On brightly illuminated mountain slopes, the distinction between sunlit and shaded portions of tree crowns is clear in the images, but this is not the case on shaded terrain. A variety of image enhancement methodologies has been proposed to deal with this difficulty on shaded slopes. For example, AWAYA and NISHIZONO (2005) proposed a pattern decomposition approach and applied it to Landsat TM data. We attempted to alleviate the shade effect by adjusting image contrast so that shaded sides of tree crowns were clearly distinguished from sunlit sides. The edge enhancement procedure was applied so that shaded and sunlit portions of canopy could be readily assigned to individual tree crowns.

After these enhancements, the color-channel images were converted to ortho-photographs with a ground resolution of 50cm. The conversion process used digital topographic maps overlain with 50m grids through application of a geographical correction procedure. In the final process of image conversion, the brightness of the each contrast-adjusted, edge-effect applied ortho-photograph image was measured on a digital scale of 0 to 255 in proportion to the brightness of image pixels. The digital scale of pixel brightness was used to estimate tree stand density. The brightness scale was summarized for each 10m × 10m grid unit using IrfanView™ free software, version 3.97. That is, the original 0.5m pixels were averaged into 10m pixel.

Ground Truth Data

Plots (20m × 20m) for ground truthing were set out in the forests of Taishou. There were 16 plots in total, half of Japanese cedar and half of Japanese cypress. In each plot, the number of the trees was counted. Precise positions of plots were obtained by GPS.

An additional 6 plots were selected from aerial images in which the outlines of individual tree crowns were readily identified. In this process, images were modified to make counting of individual trees easier. Three of these additional plots contained Japanese cedar and three contained Japanese cypress. Tree densities ranged from 350 to 2,600ha^{-1} and from 400 to 1,700ha^{-1} in stands of Japanese cedar and Japanese cypress, respectively.

Estimation of Stand Density with Modified Aerial Images

The brightness of each modified image was measured for every 10m × 10m grid. The ground truth plots measured 20m × 20m. Therefore, the brightness values of 10m × 10m grids were averaged over the larger corresponding ground truth plots. The number of averaged 10m × 10m grids for a plot was more than four because the edge lines of the ground truth plots were not parallel to these 10m × 10m grids. For a single ground truth plot, eight averaged brightness values were obtained from the eight channels of modified aerial images. These averaged brightness values were used as independent variables to estimate stand density as a dependent variable.

Simple linear regression analysis was carried out separately for Japanese cedar and Japanese cypress plots (n = 11 for each group). We assumed that the relation between stand density and brightness values fit an exponential function:

$$N = b\, e^{a x} \quad (1)$$

where N represents the estimated stand density (trees/ha), x denotes one of the brightness values, a and b are constants. Table 1 lists the coefficients of determination for the analysis. The coefficients for the RGB-green and CMYK-cyan channels for Japanese cedar plots were higher than those of other color channels; those of the RGB-green and the RGB-blue channels were the highest for Japanese cypress plots.

For more efficient estimation, multiple regression analysis was carried out with a combination of brightness variables from two color channels. Prior to the multiple regression analysis, we examined internal correlation between the brightness values of eight color channels. For the Japanese cedar plots, there were two combinations of color channels for which there was no significant correlation ($p > 0.01$): a) the combination of CMYK-yellow and Lab-brightness ($R = 0.504$), and b) the combination of CMYK-yellow and RGB-red ($R = 0.600$). For the Japanese cypress plots, two combinations had low internal correlation: a) the combination of CMYK-yellow and CMYK-cyan ($R = 0.569$), and b) CMYK-yellow and CMYK-magenta ($R = 0.596$). In summary, only CMYK-yellow had no significant ($p > 0.05$) internal correlation with the other seven color channels for both Japanese cedar and Japanese cypress plots.

Multiple regression analysis was carried out to examine the relationship between CMYK-yellow and the other seven color channels. For the Japanese cedar plots, the coefficient of determination (R^2) for the multiple regression using an independent variable combination of CMYK-yellow (Y) and Lab-brightness (Lab) was higher than all R^2 values for single regressions. However, the coefficients of determination for multiple regressions including other independent variable combinations were lower than those of single regressions. For the Japanese cypress plots, there was no combination of color channels that had higher coefficients of determination than single regressions. Thus, a single regression with color channel RGB-blue (B) was the most efficient for estimation of stand density in Japanese cypress plots.

The following formulae were the most efficient for stand density estimation using the modified color channel images.

Japanese cedar $N = 52.61\, e^{0.013\,Y + 0.011\,Lab}$ (2)

Japanese cypress $N = 116.81\, e^{0.0159\,B}$ (3)

where Y, Lab, and B denote the brightness values (0 - 255) of CMYK-yellow, Lab-brightness, and RGB-blue, respectively. Adjusted-R^2 values (adjusted coefficient of determination; ZAR, 1999) are 0.888 (n = 11) and 0.830 (n = 11) for formulae (2) and (3), respectively.

Applying the Stand Density Estimation Method to a Set of Data with Mono-color Images

Target Stands and Field Investigation

We applied the stand density estimation methodology and the estimation formulae to a set of ground truth data for a growing forest stock investigation project. Airborne laser altimetry was carried out in the fall of 2005. A series of ground truth investigations is now underway, and will be applied to 200 plots spread across the prefecture. We selected 25 plots from part of the completed data set. All plots are plantation forest; 15 and 10 plots contain Japanese cedar and Japanese cypress, respectively. These plots were located precisely beneath a corresponding measurement line for laser surveying.

In the field investigation, the size of the plots was variable. Each plot was square with a side length set to approximate average tree height. The average area of the selected plots was 0.0481 ha (range: 0.0152-0.0764 ha; SD = 0.0122 ha; n = 25) and the average stand density was 1,523 trees/ha (range: 521-2,473 trees/ha; SD = 494 trees/ha; n = 25). Table 2 lists the corresponding mono-color aerial images prepared for the following analysis, and Fig. 1 shows the locations of the sites. The images were taken at the usual altitude of 4,600 - 4,700m, giving lower resolution than those taken at lower altitude for the previous study.

Table 1 Coefficients of determination (R^2) for each color channel

	CMYK-cyan	CMYK-magenta	CMYK-yellow	CMYK-black	RGB-red	RGB-green	RGB-blue	Lab-brightness
Japanese cedar	0.8335	0.8160	0.6173	0.7933	0.8161	0.8452	0.8111	0.7458
Japanese cypress	0.6132	0.5733	0.5904	0.7593	0.7762	0.8320	0.8466	0.7075

Table 2 Details of sites for aerial photography

Image title	Ishizuchi 2-5	Ishizuchi 2-6	Matsuyama 6-8	Matsuyama 8-11	Matsuyama 9-9
Altitude (m)	4,700	4,700	4,600	4,600	4,600
Year	2003	2003	2002	2002	2002
Photography by	Forestry Agency	Forestry Agency	Geographical Survey Institute	Geographical Survey Institute	Geographical Survey Institute
Site label in Fig. 1	A	A	B	C	D

Conversion of Images

The images were digitized and modified as in the previous analysis, except for color channels resolution, viz. scanned at 720dpi (Fig. 2(1)), processed with the Photoshop™ edge effect detection (Fig. 2(2)), and converted to ortho-images (Fig. 2(3)). Appropriate parts of the modified images were then extracted for measurement of brightness values (Fig. 2(4)). We used gray scale photographs. Therefore only the brightness value was used for the analysis. Binary scales of pixels with a range of 0 to 255 were summarized for every 10m $\times$10m grid using IrfanView™. Summarized values were averaged for corresponding plot areas. The averaged brightness values were used as the brightness values of the plots.

The relationships between stand density ground truth data and the brightness values of the modified images were examined by regression. Following the previous study, single regression formula with an exponential fit was applied (there was only one independent variable, the brightness value (B)). Hence, the formula was of the form in equation (1), replacing x with B. The regression used is equation (3), applied to Japanese cypress data in the previous study.

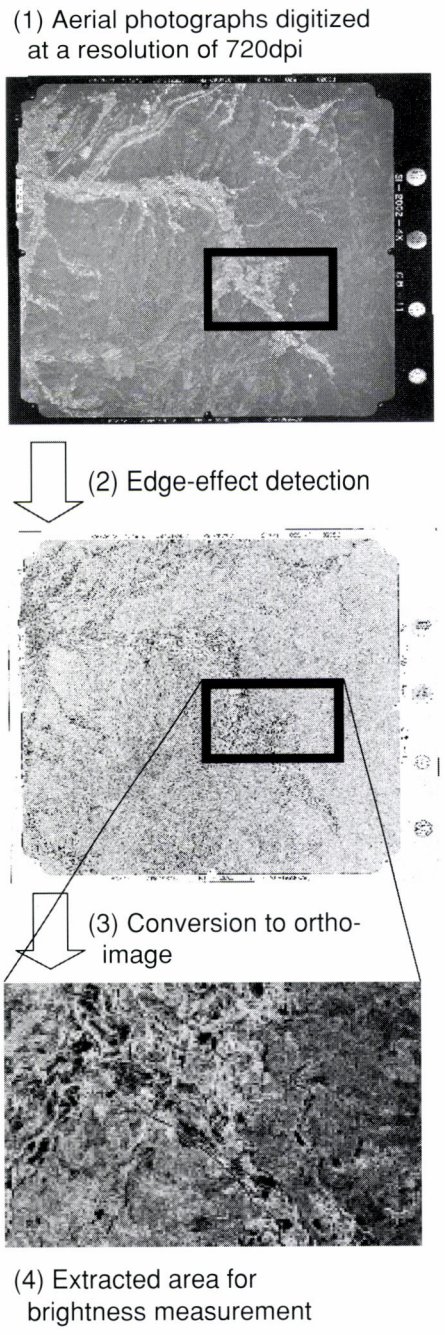

Fig. 2 Procedure for modification of aerial photographic images

RESULTS AND DISCUSSION

Fig. 3 illustrates the results for Japanese cedar and Japanese cypress. When regression equation (1) was first applied separately for Japanese cedar (n = 15) and Japanese cypress (n = 10), the results were as follows: for Japanese cedar, a = 580.02, b = 0.0064, adjusted-R^2 = 0.392, and p = 0.007; for Japanese cypress, a = 665.94, b = 0.0059, adjusted-R^2 = 0.271, and p = 0.071. There was no significant difference between constants a and b for the two tree species (p = 0.889 for a, and p = 0.574 for b). Therefore the following formula was derived for the combined data (n = 25, adjusted-R^2 = 0.413, p < 0.001):

$$N = 590.95\, e^{0.0064\,B} \qquad (4)$$

The solid curve in Fig. 3 is fitted to this formula. While there are some outliers (2 - 3 for Japanese cedar and 4 - 5 for Japanese cypress) the regression curve summarizes well the relationship between stand density and brightness value. The dashed curve in Fig. 3 is fitted to regression formula (3) obtained with data from the previous study for Japanese cypress in Taishou. The fitted line for formula (3) is quite separate from that fitted to formula (4).

Because the photographs used in the present study were taken at high altitude, parts of some were so dark that we could not identify individual tree crowns, even after application of the contrast adjustment process. The three observations marked with small letters "a", "b", and "c" in Fig. 3 represent these low quality images. The trend of the relationship between stand density and brightness value would become more similar to the fit of formula (3) were these three observations to be excluded. This suggests that a form of regression formula (3) would express the general trend between stand density and brightness value and that there would be common constant terms for the formula should more data become available. Gotou (2007) found that the CMYK-cyan channel is most effective to identify bamboo forests using color aerial photographs. The reason why particular color channels have better performance to identify tree density or to classify forest types may be related to a reflection property of leaves. Further investigation is necessary to explain the reason.

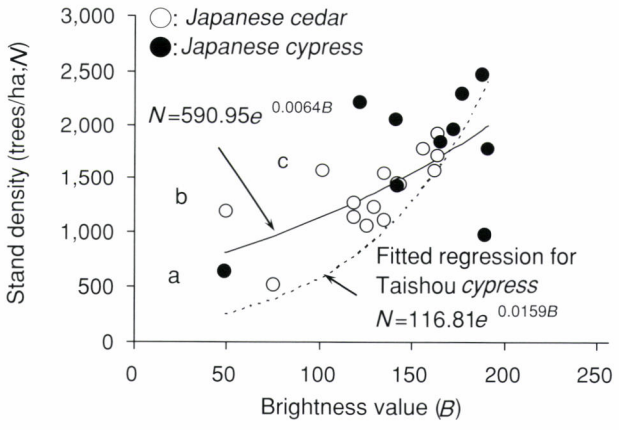

Fig. 3 Relationship between stand density and brightness value
Symbols marked "a", "b", and "c" are for plots with poor performance of contrast adjustment.

There is a problem in the contrast adjustment process. Most of the processes we used for image enhancement can be performed objectively. All operators of Photoshop™ would obtain the same result from the same data, but this is not so for the contrast adjustment process. Image contrasts are adjusted such that black and white parts are balanced. In our previous study, we adjusted the contrast so that median values of the contrast histogram in Photoshop™ would be 125. However, in the present study, the median values were set to 100 in order to make dark parts of images as clear as possible. A more objective criterion should be determined for the contrast adjustment process.

CONCLUSIONS

We applied the stand density estimation method developed for color and high resolution aerial photography to a set of gray scale, low resolution images obtained by an airborne laser altimetry project. The fitted regression formula was statistically significant, but precision was lower than in the earlier study. An improvement of contrast adjustment process is essential for the development of the method. The stand density estimation method was developed with rather small number of data in a limited area. Further verification is necessary using a sufficiently large number of testing data.

In the airborne laser altimetry project, a series of vegetation profiles was produced, with corresponding ground truth data. The line type laser can be used to estimate stand density along the flight paths. Peaks in a vegetation profile should correspond to individual trees. However, the density estimate is defined as line density, that is, trees per line, not trees per unit area. In the present study, stand density per unit area was analyzed with modified aerial images coupled with ground truthing. We are planning to investigate the possibility of estimating area density from vegetation profiles.

LITERATURE CITED

Awaya, Y. and Nishizono, T., (2005): Mapping of mixing ratio of deciduous broadleaves in Sugi cedar plantations in a heavy snow area: An analysis using Landsat TM data and forest management information. J. Jpn. For. Soc. **87**: 490-496 (in Japanese with English summary)

Gotou, J., (2007): Establishment of unutilized forest-originated biomass as practical resource by indexing the amount and development of appropriate harvesting methods. Report of Grant-

in-Aid for Scientific Research (C), No. 16580123, 76pp

GOTOU, J., KANEKO, R. and SUZUKI, Y., (2006): Image analysis of aerial photograph to estimate the unused forest resources. Proc. J. For. Soc. Congress **117**: 245 (in Japanese)

HIRATA, Y., (2005a): Influence of transmittance and sampling density of laser beams in forest measurement of a *Cryptomeria japonica* stand with an airborne laser scanner. Jpn. J. For. Plann. **39**: 81-95 (in Japanese with English summary)

HIRATA, Y., (2005b): Relationship between tree height and topography in a *Chamaecyparis obtusa* stand derived from airborne laser scanner data. J. Jpn. For. Soc. **87**: 497-503 (in Japanese with English summary)

KUSAKABE, T., TSUZUKI, H., HUGHES, G. and SWEDA, T., (2000): Extensive forest leaf area survey aiming at detection of vegetation change in subarctic-boreal zone. Polar Biosci. **13**: 133-146

KUSAKABE, T., TSUZUKI, H. and SWEDA, T., (2006): Long-range estimation of leaf area index using airborne laser altimetry in Siberian boreal forest. J. Jpn. For. Soc. **88**: 21-29 (in Japanese with English summary)

TSUZUKI, H., KUSAKABE, T. and SWEDA, T., (2006a): Long-range estimation of standing timber stock in western boreal forest of Canada using airborne laser altimetry. J. Jpn. For. Soc. **88**: 103-113 (in Japanese with English summary)

TSUZUKI, H., NELSON, R. and SWEDA, T., (2006b): Timber stock estimate by airborne laser profiling for entire Ehime prefecture, Japan. In: Y. HIRATA, Y. AWAYA, T. TAKAHASHI, T. SWEDA and H. TSUZUKI (Eds.), Proc. Int. Conference, Silvilaser 2006, November 7-10, 2006, Matuyama, Japan: 82-87

ZAR, J.H., (1999): Biostatistical analysis, 4th ed. Prentice-Hall Inc., Upper Saddle River, NJ, 663pp

(Received 25 December 2006)
(Accepted 28 August 2007)

Article

Development of the Forest Road Design Technique using LiDAR Data of the Funyu Experimental Forest

Masashi Saito[*1], Kazuhiro Aruga[*1], Keigo Matsue[*1] and Toshiaki Tasaka[*1]

ABSTRACT

The forest road design process includes extensive field investigations and dynamic real-time decision-making processes to create the best forest road design. These processes do require significant effort, and require the most experienced personnel to affect the best outcome. However, such "front end efforts" pay huge dividends in estimating construction costs, as well as benefits of the improved design in the out years in both utility of use and maintenance of the constructed road. One of the major faults of past techniques was the low reproducibility of geographical features, and the resultant impacts that subsequently were encountered during the design and construction phases of the road projects. In this research, in order to improve the above-mentioned facts, the forest road design technique was developed using the LiDAR (Light Detection and Ranging) data that presented more accurate geographical features. The forest roads constructed before and after the LiDAR measurement were surveyed. Elevations on the cross-sections of the forest road constructed before LiDAR measurement were compared with those from 1m grid DEM made from LiDAR data and 10m grid DEM made from 1/5,000 topographic map. The mean square error between actual measurements and 1m grid DEM was 1.12m. On the other hand, the mean square error between actual measurements and 10m grid DEM was 6.02m. Earthwork-volumes estimated using the actual measurement of the forest road constructed after LiDAR measurement and by the program using 1m grid DEM were 3,596.48m^3 and 3,641.51m^3 respectively, while the earthwork volume using 10m grid DEM was 10,637.6m^3. Ground surfaces produced by LiDAR data represented actual ground surfaces accurately and the results of the forest road design using LiDAR data were similar to the actual forest road. The goal of the efforts demonstrated that using LiDAR enhanced the opportunities for planners to examine alternative designs to improve ease of design, cost of construction, and maintainability.

Keywords: LiDAR data, forest road design, earthwork-volume, Funyu experimental forest, cost comparison.

INTRODUCTION

The forest road design process includes extensive field investigations and dynamic decision-making processes to create the best forest road design. While those processes are labor intensive and require the most experienced engineering and surveying staff, they also represent the key efforts that must be implemented in order to have a successful, cost-effective project. A variety of forest road design supporting techniques to reduce the workload of the forest road design have been developed using DEM (Digital Elevation Model), GPS (Global Positioning System), and similar techniques (KOBAYASHI, 1984). These techniques have, however, demonstrated lack of accuracy because of the low reproducibility of geographical features. In order to improve the above-mentioned facts, ARUGA *et al.* (2006) developed the forest road design technique using the LiDAR (Light Detection And Ranging) data that demonstrated a significant improvement in representing relatively accurate geographical features (KATO, 2004). However, the comparison with the field investigation has not been done. In this research, the 1m grid DEM generated from the LiDAR data was applied to the program and the results by the program were compared with the field

Corresponding author: Masashi Saito
[*1] Address: Utsunomiya University, 350 Mine, Utsunomiya 321-8505, Japan
+81-28-649-5544 Fax: +81-28-649-5545
zn9m-situ@asahi-net.or.jp,
aruga@cc.utsunomiya-u.ac.jp,
matsue@cc.utsunomiya-u.ac.jp,
tasaka@cc.utsunomiya-u.ac.jp

investigation measurements.

THE ACCURACY VERIFICATION OF THE LIDAR DATA

Materials and Method

The study site (Fig. 1) is the Funyu experimental forest at latitude 36 degrees 46 minutes north, longitude 139 degrees 49 minutes east and elevations between 300m and 550m. The average slope of the study site is about 28 degrees. The forest road is along the ridge and the vegetation around it is a mixed forest composed of pine, oak, azalea and so on. The length of the forest road is about 1,300m. The LiDAR measurement was conducted by a helicopter on October 21, 2003 (Table 1). The field investigation was done in November 2005.

To verify the accuracy of the LiDAR data, the forest road constructed before and after the LiDAR measurement was surveyed. First, the traverse survey of the route was conducted on the forest road from GPS control points and its closing error was 1/3,015. Then, the cross-sections were surveyed from the traverse survey points at intervals of 10m. Nine cross-sections were surveyed on the forest road constructed before the LiDAR measurement and twenty cross-sections were surveyed on the forest road constructed after the LiDAR measurement. The elevation corresponding to each survey point was determined with the 1m grid DEM generated from the LiDAR data using the bilinear interpolation. Then, those elevations were compared with the elevations obtained from the cross-section survey. In addition, elevations were determined with the 10m grid DEM generated from the 1/5,000 topographic map as one of conventional DEMs.

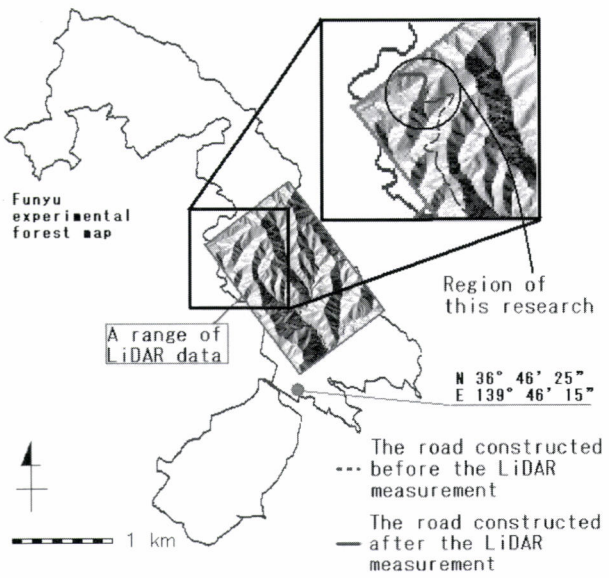

Fig. 1 A range of LiDAR data and region of this research

Table 1 Specification of the LiDAR measurement

Item	Specification
Target flight hight above ground	500m
Target flight hight speed	25m/s
Measurement density	8.82 points/m²
System	ALTM1225
Laser wave length	1.064μm
Laser pulse frequency	25,000Hz
Scan frequency	27Hz
Scan angle	24°
Return mode	First and Last
Laser beam divergence	0.2, 1.0 mrad

Result

The comparison of elevations between survey results and DEMs was conducted with all of the 90 points on the forest road constructed before LiDAR measurement and 127 points of the ground surface on the forest road constructed after LiDAR measurement. Fig. 2 is an example of the cross-section on the forest road constructed before LiDAR measurement. The natural ground surfaces before the forest road construction can be shown with LiDAR data in Fig. 3. The points of the road surface and the cut slope on the forest road constructed after LiDAR measurement were excluded from the comparison of elevations because elevations of those points were changed after LiDAR measurement (Fig. 3).

Fig. 4 shows the frequency distribution of the differences between elevations from survey results and DEMs. The root mean square error of elevations at the total 217 points between survey results and 1m grid DEM was 1.12m while the root mean square error of the 90 points on the forest road constructed before LiDAR measurement was 1.04m and that of 127 points of the ground surface on the forest road constructed after LiDAR measurement was 1.35m. On the other hand, the root mean square error of elevations between survey results and 10m grid DEM was 6.02m.

Fig. 5 shows the comparison of forest road profiles. The forest road profile from 1m grid DEM represents the actual profile of the forest road constructed before the LiDAR measurement and keeps almost constant differences from the actual profile of the forest road constructed after the LiDAR measurement. On the other hand, Fig. 5 shows the big difference between the actual profile and that from 10m grid DEM. It was clarified that the error was greatly reduced using 1m grid DEM generated from the LiDAR data compared with using 10m grid DEM.

However, the greatest difference between open air points and points in the forest occurred even though 1m grid DEM

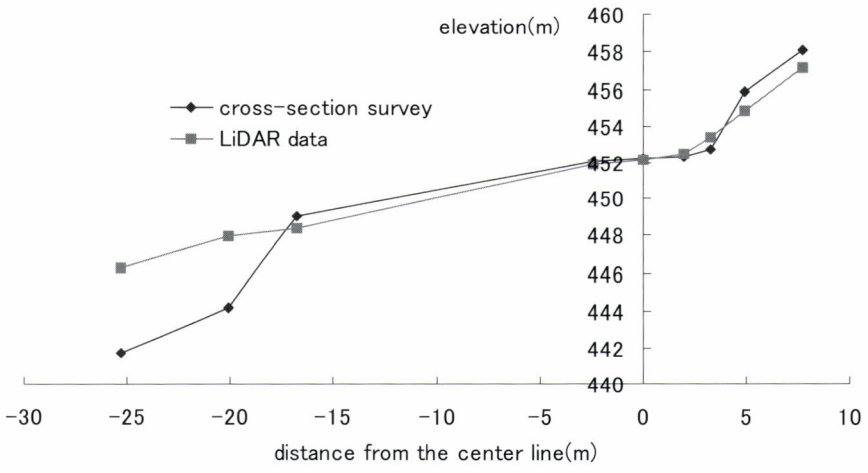

Fig. 2 Example of the cross-section on the forest road constructed before LiDAR measurement

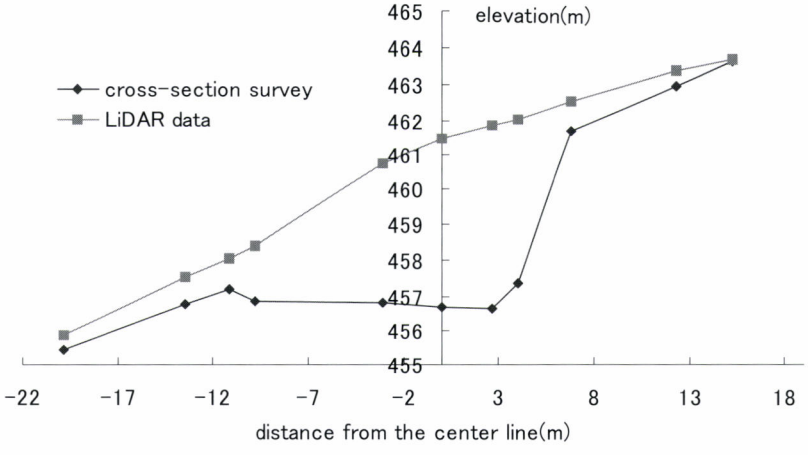

Fig. 3 Example of the cross-section on the forest road constructed after LiDAR measurement

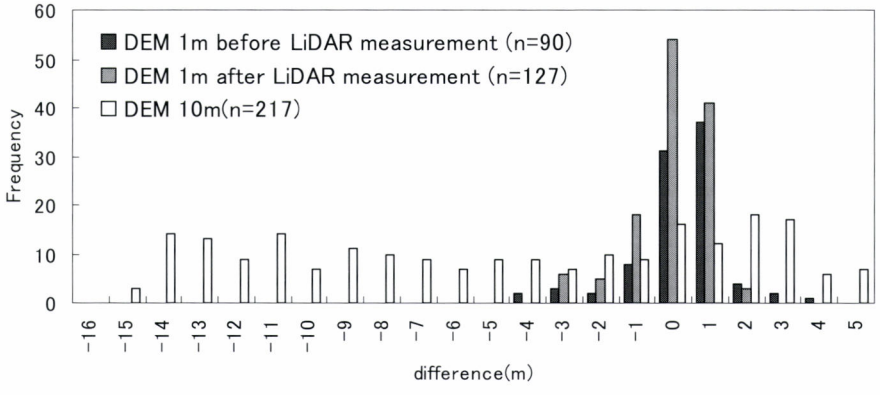

Fig. 4 Frequency distributions of differences between elevations from cross-section survey and DEMs

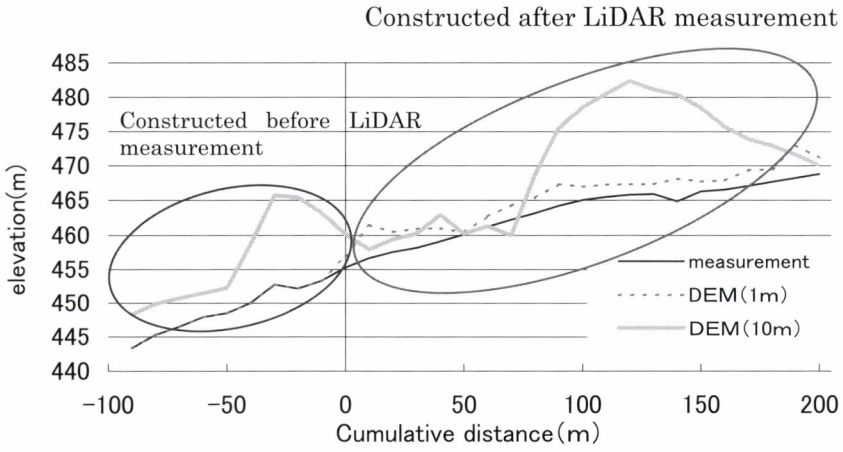

Fig. 5 The comparison of forest road profiles

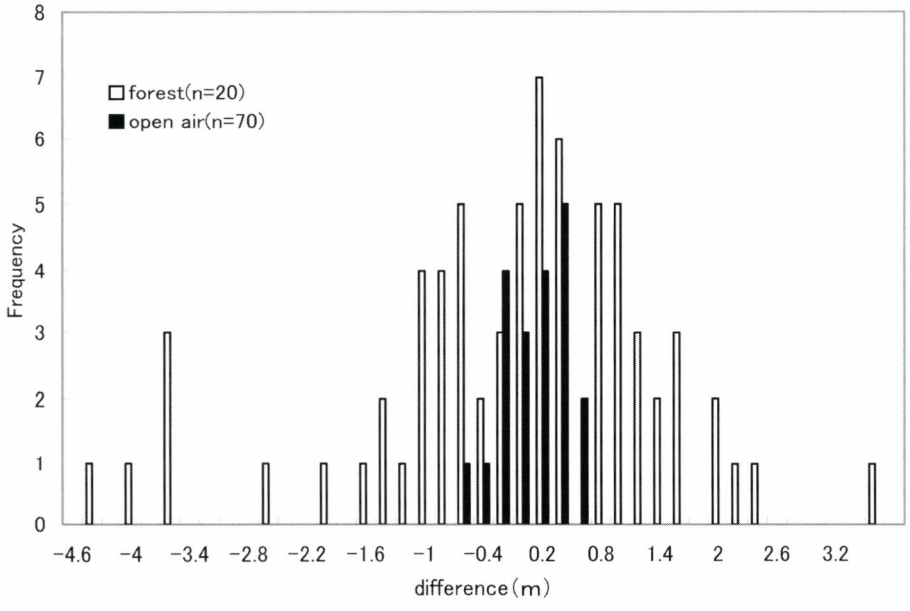

Fig. 6 Comparisons between open air points and points in the forest

was used (Fig. 6). The root mean square error of 20 open air points on the forest road constructed before LiDAR measurement was 0.33m. On the other hand, the root mean square error of 70 points in the forest along the forest road constructed before LiDAR measurement was 1.50m.

VERIFICATION OF THE FOREST ROAD DESIGN TECHNIQUE USING THE LIDAR DATA

Forest Road Design Method

The coordinate and the road height of each survey point on the forest road at intervals of 10m were provided to the program, which connected each point by cubic spline function as the forest road route (TASAKA *et al.* 1996). The cubic spline function is the following equation.

$$P(t) = A + Bt + Ct^2 + Dt^3 \quad (1)$$

$P(t)$ is a plane vector in which $x(t)$ and $y(t)$ are elements. The range of the parameter t is within the distance between the cross-sections. Coefficients A, B, C, and D of the spline curve are determined by giving positional vectors P_k, P_{k+1} and tangent vectors P'_k, and P'_{k+1} at both ends of each segment.

$$A = P_k \quad (2)$$

$$B = P'_k \tag{3}$$

$$C = \frac{3(P_{k+1} - P_k)}{t_{k+1}^2} - \frac{2P'_k}{t_{k+1}} - \frac{P'_{k+1}}{t_{k+1}} \tag{4}$$

$$D = \frac{2(P_k - P_{k+1})}{t_{k+1}^3} + \frac{P'_k}{t_{k+1}^2} + \frac{P'_{k+1}}{t_{k+1}^2} \tag{5}$$

When positional vectors, the first derivatives, and the second derivatives are continuous at the connected points, the cubic spline function curvatures are approximately continuous. The condition that the second derivative is continuous is expressed by the following equation.

$$t_{k+2}P'_k + 2(t_{k+1} + t_{k+2})P'_{k+1} + t_{k+1}P'_{k+2} = \frac{3}{t_{k+1} + t_{k+2}}\{t_{k+1}^2(P_{k+2} - P_{k+1}) + t_{k+2}^2(P_{k+1} - P_k)\} \tag{6}$$

Not only positional vector P_k but also tangent vectors P'_1 and P'_n at both ends of the cubic spline curve are required to calculate unknown tangent vectors P'_k,. The spline function is assumed to be under the free end condition because the curvature of the forest road path at the beginning and end points are 0. This condition is expressed by the following equation.

$$P'_1 = \frac{P'_2}{2} = \frac{3(P_2 - P_1)}{2t_2} \tag{7}$$

$$P'_{n-1} + 2P'_n = \frac{3(P_n - P_{n-1})}{t_n} \tag{8}$$

Coefficients *A, B, C,* and *D* of the cubic spline function are calculated and the spline function is determined from these conditions 6, 7, and 8 (Fig. 7).

In order to estimate the earthwork-volumes of the forest road designed by the program accurately, each segment between each survey point was interpolated at an interval of 1m. $hx(t)$ and $hy(t)$ which are elements of an unit vector $H(t)$ normal to an cubic spline function at an interpolated point are determined with $x'(t)$ and $y'(t)$ which are elements of an tangent vector $P'(t)$ (Fig. 8).

$$hx(t) = \cos\left(\arctan\left(-\frac{x'(t)}{y'(t)}\right)\right) \tag{9}$$

$$hy(t) = \sin\left(\arctan\left(-\frac{x'(t)}{y'(t)}\right)\right) \tag{10}$$

Each coordinate on the normal line to the cubic spline curve was determined within 15m of both sides of the cubic spline curve at an interval of 1 m based on the equations 9 and 10. Then, an elevation of each coordinate was calculated from the DEMs using the bilinear interpolation as the cross-section of the ground profiles (Fig. 9).

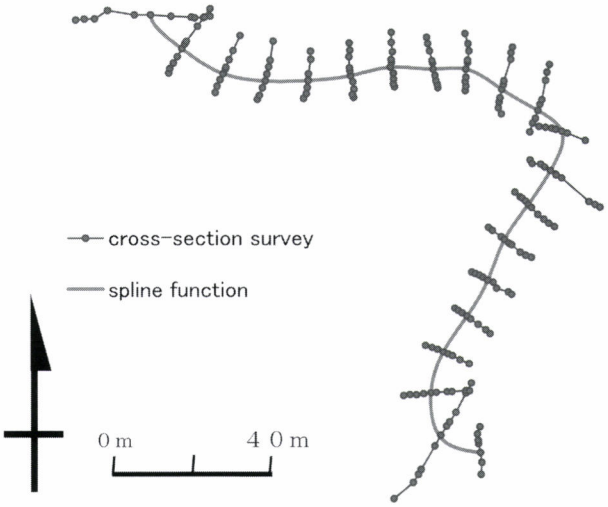

Fig. 7 Route figure obtained with spline function

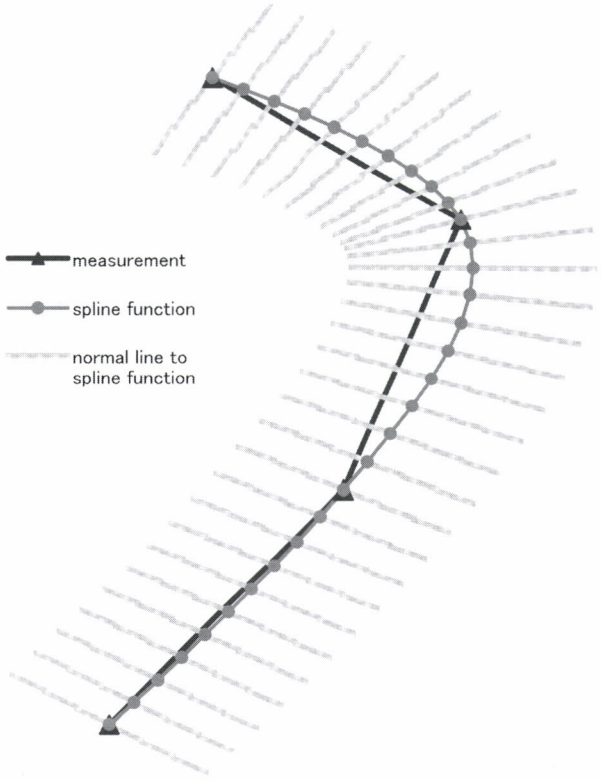

Fig. 8 A normal line to spline function

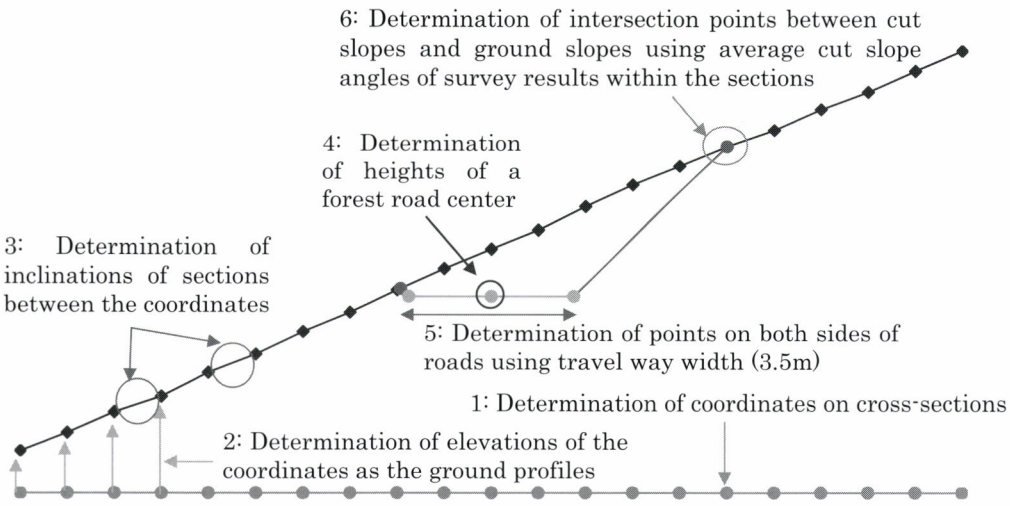

Fig. 9 The forest road design procedure

Calculation Method of Earthwork Volumes

The earthwork volumes of forest roads designed by the program were compared with those of the actual forest road constructed after the LiDAR measurement. First, in order to calculate the earthwork volumes of the actual forest road, the cut and fill areas of the cross-sections were calculated using original ground slopes and forest road templates. In this study, the LiDAR data was assumed to be original ground slopes and survey data was assumed to be forest road templates. Then, earthwork-volumes V (m^3) were calculated by the average end-area method. The average end-area method is expressed by the following equation.

$$V = \frac{d}{2}(A_i + A_{i+1}) \quad (11)$$

A_i and A_{i+1} are cross-sectional areas and d is the distance between the cross-sections.

The earthwork volumes of the forest road designed by the program were calculated using the following procedures (Fig. 9).

1: Determination of coordinates on cross-sections.
2: Determination of elevations of the coordinates as the ground profiles.
3: Determination of inclinations of sections between the coordinates.
4: Determination of heights of a forest road center line.
5: Determination of points on both sides of roads using travel way width (3.5m).
6: Determination of intersection points between cut slopes and ground slopes, using average cut slope angles of survey results within the sections.
7: Calculation of areas enclosed between ground profiles and road templates as cross-sectional areas.
8: Calculation of earthwork-volumes from the cross-sectional areas using the average end-area method (the equation 11).

Calculation Method of Construction Costs

To compare the construction cost from the amount of the calculated earthwork volume, an assumed man hours/volume handled was used. It was assumed that a bucket excavator was used for cutting, a bulldozer was used for filling and a dump truck was used for transportation. Each work efficiency was determined as follows (ANON. 2002):

1) Workload for cutting by a bucket excavator an hour Q (m^3/h) is calculated by the following equation.

$$Q = \frac{60 q_0 kfE}{C_m} \quad (12)$$

Here, q_0: capacity of a bucket (0.6m^3), k: coefficient of a bucket (0.8), f: bucket conversion coefficient (normal soil : 1/1.45), E: working efficiency (0.8), C_m: cycle time (normal soil : 32 seconds). From the equation 12, the amount of workload an hour was 29.73m^3/h.

2) Workload for smoothing by a bulldozer (11 t) an hour Q (m^3/h) is calculated by the following equation:

$$Q = 10E(11D + 8) \quad (13)$$

Here, E: working efficiency (0.6), D: depth of finishing (0.3m). From the equation 13, the amount of workload an hour was 67.8m^3/h. Moreover, workload for compacting by a bulldozer (11t) an hour Q (m^3/h) is calculated by the following equation.

$$Q = \frac{VWDE}{N} \quad (14)$$

Here, V: compacting speed (3,500m/h), W: effective width of compacting a time (0.7m), N: the number of compacting (5 times). From the equation 14, the amount of workload an hour was 88.2m³/h.

3) Earthwork volume of transportation by a dump truck an hour V_t (m³/h) is calculated by the following equation.

$$V_t = \frac{60}{C_m} qE \tag{15}$$

$$q = \frac{W}{w} \tag{16}$$

$$C_m = \beta L + \alpha \tag{17}$$

Here, q: payload a truck (m³), C_m: cycle time, E: working efficiency (0.9), W; maximum capacity (4t), w; unit weight of ground (sandy soil: 1.8t/m³), β; coefficient by transportation situation (4.8), L; one way transportation distance (2km), α; loading and other working time (11 minutes for a 0.6-m³ bucket excavator). Earthwork volume of transportation an hour was 5.7m³/h.

Each working time was calculated using the calculated earthwork-volume and each working efficiency mentioned above. Then, each working cost is calculated using each working time and unit cost for each machine (Table 2-4).

Results

The earthwork volume of the survey result was 3,596.48m³ while the earthwork volume of the forest road designed by the program was 3,641.51m³. Fig. 10 shows cumulative earthwork volumes. The error of earthwork volumes with 1m grid DEM was 2.67% compared with those of actual forest road. On the other hand, the error with 10m grid DEM was 199% (Fig. 10). Because the mesh size of 10m gird DEM is much larger than that of 1m grid DEM, the root mean square error of elevations between survey results and 10m grid DEM was much worse than that between survey results and 1m grid DEM. Subsequently, the error of earthwork volumes with 10m grid DEM was much worse than that with 1m grid DEM.

Table 2 Driving Unit Price of a Bucket Excavator (vehicle exhaust emission measures type)

Item	Unit	Unit Cost (yen)	Total Cost (yen)
Driver	0.18 person	17300	3114
Diesel Oil	18L	72	1296
Machine Depreciation	1h	4300	4300
Total	1h		8710

Table 3 Driving Unit Price of a Bulldozer (Vehicle exhaust emission measures type).

Item	Unit	Unit Cost (yen)	Total Cost (yen)
Driver	0.19 person	17300	3287
Diesel Oil	14L	72	1008
Machine Depreciation	1h	5230	5230
Total	1h		9525

Table 4 Driving Unit Price of a Dump Truck

Item	Unit	Unit Cost (yen)	Total Cost (yen)
Driver	0.16person	14500	2320
Diesel Oil	6.8L	72	490
Machine Depreciation	1h	4300	4300
Tire Tread wear Cost	1h	196	196
Total	1h		7306

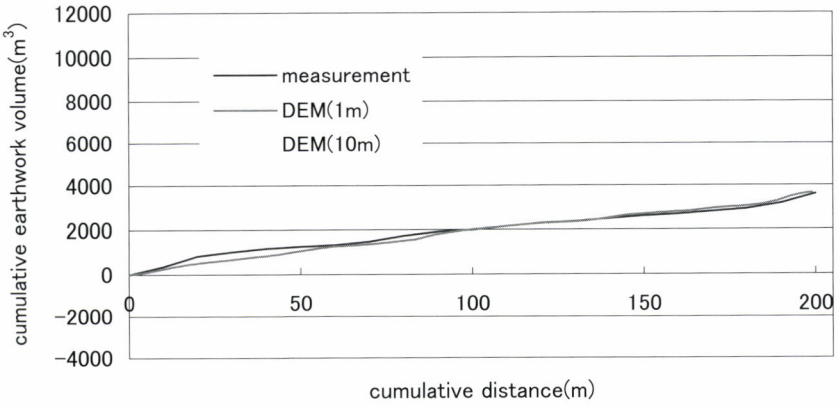

Fig. 10 Cumulative earthwork volumes

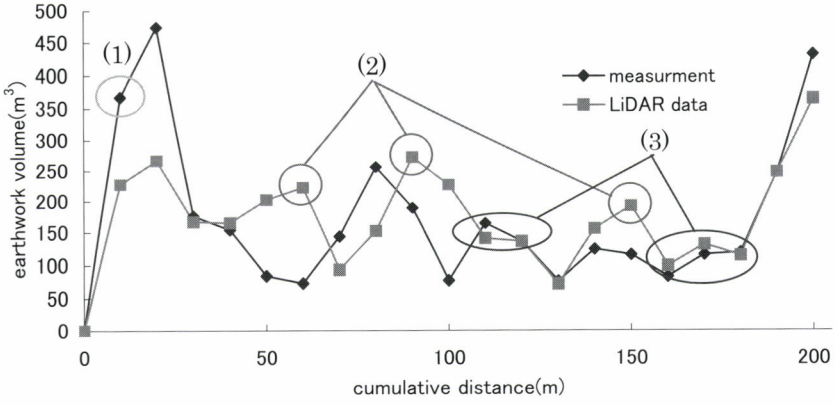

Fig. 11 Comparison of earthwork volumes

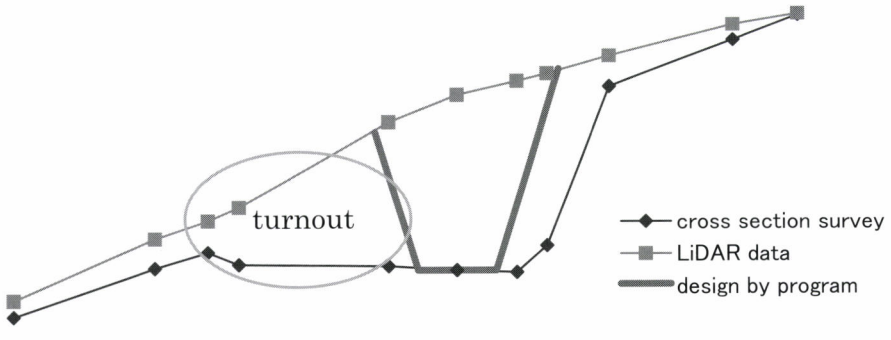

Fig. 12 Example of a turnout at the part (1) in Fig. 11

Fig. 11 shows the comparison result of the earthwork volumes every 10m by each method. The error occurred according to the sections such as (1) a turnout and (2) curve parts. The turnout is not assumed to be constructed in the program while the turnout is located at part (1) in Fig. 11 on the actual forest road (Fig. 12). Therefore, a big gap of the earthwork volumes occurred in this section. This will be improved in the future study.

Another big gap occurred at the top of the curves, the part (2) in Fig. 11 because each section was surveyed as a straight line while the program interpolated each section using a cubic spline function (Fig. 8). Moreover, the average end-area method was commonly used for straight roadways, not

curved roadways. As the program interpolated each section at an interval of 1m (a very short interval), it calculated earthwork volumes relatively accurately even using the average end-area method (ARUGA *et al.* 2005), On the other hand, earthwork volumes from survey data was not calculated accurately due to their intervals of 10m.

As for part (3) in Fig. 11, because the cross-section designed by the program was also corresponding to the survey results well at the straight-line part, the differences of the earthwork volumes were small.

DISCUSSIONS

Since this research site was relatively steep, the forest road was constructed with full bench (Fig. 3 or 12). However, earthwork volumes and costs could be reduced by constructing forest roads while balancing cut and fill volumes on the each cross-sections (zero-line method). In this section, working times and costs between the full-benched forest road and the forest road designed by the zero-line method were examined. As a result of the forest road designed by the zero-line method, the cut volume was +662.35m³, the fill volume was -994.38m³, and the cumulative earthwork volume was -282.03m³ (Fig. 13). The zero-line method significantly reduced required earthwork volumes.

Table 5 shows the working times estimated from the earthwork volumes. The working time for constructing the forest road designed by the zero-line method was also decreased greatly compared with that of the full-benched forest road because the earthwork-volumes became smaller. Table 6 displays the construction costs estimated from the calculated working times. From Table 6, it was clear that the zero-line method significantly decreased construction costs.

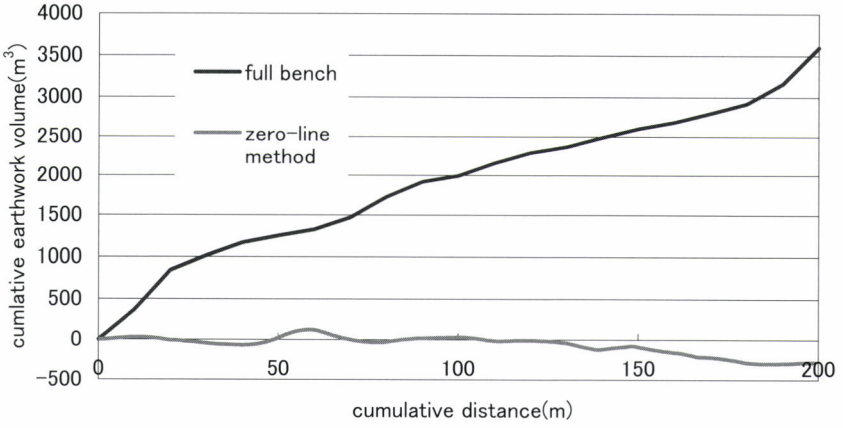

Fig. 13 Comparison of cumulative earthwork volumes

Table 5 Working times estimated from the earthwork-volumes

	Volume (m³)		Working time (hour)			
	Cut	Fill	Cut	Fill	Transport	Total
Full Bench	3596.48	0	120.72	0	630.48	751.19
Zero-Line Method	662.35	944.38	22.23	24.64	49.07	95.94

Table 6 Comparison of construction costs

		Full Bench (yen)	Zero-Line Method (yen)
Cut		1,051,429	193,640
Fill		0	234,661
Transport		2,550,920	198,525
Total		3,602,349	626,826
Cost per Meter		18,012	3,134

CONCLUSIONS

Ground surfaces produced by LiDAR data represented actual ground surfaces accurately and the results of the forest road design using LiDAR data were similar to the actual forest road as-builts. With the high reliability of the LiDAR data, various alternative proposals could be examined efficiently because of reduced workload requirements of each alternative proposal examination.

Various organizations have been measuring the LiDAR on the forested areas, and 5m grid DEM made by the LiDAR measurement begins to be offered in the urban region. The forest road design program developed and verified in this study could be more useful tool as the LiDAR measurement is more commonly used in the future.

However, LiDAR is not infallible. An error was discovered in the LiDAR data sets. The root mean square error in open sky was 0.33m and the root mean square error was 1.50m in the forest. Tree canopies and floor vegetations might interrupt the laser. Future study will develop the technique to correct and compensate for this phenomenon to create more accurate ground surface from the raw LiDAR data.

LITERATURE CITED

ANON., (2002): Rindo Hikkei Gijyutsuhen. Nihon Rindo Kyokai, Tokyo, 279pp (in Japanese)

ARUGA, K., SESSIONS, J. and AKAY, A.E., (2005): Application of an Airborne Laser Scanner to Forest Road Design with Accurate Earthwork Volumes. J. For. Res. **10**(2): 113-123

ARUGA, K., TASAKA, T., SESSIONS, J. and MIYATA, E.S., (2006): Tabu Search Optimization of Forest Road Alignments Combined with Shortest Paths and Cubic Splines. Cro. J. of For. Eng. **27**(1): 37-47

KATO, M., (2004): Sinrin Remote Sensing. Nihon Ringyo Tyosakai, Tokyo, 273pp (in Japanese)

KOBAYASHI, H., (1984): Planning System for Road-Route Locations in Mountainous Forests. J. Jap. For. Soc. **66**(8): 313-319

TASAKA, T., OCHI, S. and MATSUO, T., (1996): Planning Method of Terrain Acceptable Forest Roads Applying with Spline Function. Bulletin of the Utsunomiya University Forests **32**: 17-26

(Received 25 December 2006)
(Accepted 4 December 2007)

Article

Estimation of Tree Height and Forest Biomass from GLAS Data

G. Sun[*1,2], K.J. Ranson[*3], J. Masek[*3], Z. Guo[*2], Y. Pang[*4], A. Fu[*2] and D. Wang[*2]

ABSTRACT

The Geoscience Laser Altimeter System (GLAS) on the Ice, Cloud and land Elevation Satellite (ICESat) is the first spaceborne lidar instrument for routine global observation of the Earth. GLAS records a vertical profile of the returned laser energy from a footprint of approximate 70m diameter. The GLAS waveform data (GLA01) and the Land/Canopy Elevation product (GLA14) provide information on vegetation spatial structure. In this study the use of the GLAS data for forest structural parameters retrieval was evaluated using airborne LVIS (NASA's Laser Vegetation Imaging Sensor) data and field measurements. The tree height indices from airborne large-footprint lidars such as LVIS have been successfully used for estimation of forest structural parameters in many studies. The tree height indices, based on lidar return energy quartiles from GLAS data were compared to similar tree height indices derived from LVIS data within the GLAS footprints. The results show that the tree height indices derived from the GLAS and LVIS waveforms were highly correlated. Our analysis showed that tree height and biomass obtained from field measurements can be predicted from GLAS data. Comparisons of the near-repeat-pass GLAS data acquired in Fall of 2003 (L2A), Fall of 2004 (L3A), and early Summer of 2005 (L3C) and 2006 (L3F) show that the surface elevations from GLAS were consistent. When the mean distance between corresponding points from two 4.5km orbits (260 GLAS shots from L2A and L3F) was 82.6m, the R^2 of the elevations from these two orbits was 0.997, with a RMSE of 4.1m. The top tree heights from the near-repeat-pass GLAS orbits show significant differences, probably due to the heterogeneity of the forests.

Keywords: LiDAR, forests, tree height, biomass, GLAS

INTRODUCTION

Vegetation spatial structure must be known to adequately monitor and model the carbon cycle and forest ecosystem dynamics. Most remote sensing systems, although providing images of the horizontal distribution of canopies (e.g., Landsat, MODIS), do not provide direct information on the vertical distribution of canopy elements. The lidar waveform signature from a large-footprint airborne lidar instrument, such as the Scanning Lidar Imager of Canopies by Echo Recovery (SLICER) (HARDING *et al.*, 2001) and the Laser Vegetation Imaging Sensor (LVIS) (BLAIR *et al.*, 1999) have been successfully used to estimate tree heights and above-ground forest biomass (LEFSKY *et al.*, 1999; DUBAYAH and DRAKE, 2000; WEISHAMPEL *et al.*, 2000; DRAKE *et al.*, 2002). Using LVIS data, DRAKE *et al.* (2003) found that lidar metrics, especially the height of median energy (HOME), were strongly correlated with mean stem diameter, basal area and above ground biomass (AGBM). Their studies found that these relationships differed between regions and that environmental factors have an important influence on these relationships. HYDE *et al.* (2005) found good agreement between field and lidar measurements of height, tree cover, and biomass at the footprint level, and canopy height and biomass at the stand level. Differences between field and lidar measurements are mainly attributable to the spatial configuration of canopy elements. The studies using SLICER data by LEFSKY *et al.* (2005a), however, found that the relationships between many

Corresponding author: Guoqing Sun
[*1] Department of Geography University of Maryland, College Park, MD 20742 USA, e-mail: Guoqing.sun@gmail.com
[*2] State Key Laboratory of Remote Sensing, Institute of Remote Sensing Applications, Chinese Academy of Sciences, P. O. Box 9718, Beijing, 100101, China
[*3] NASA's Goddard Space Flight Center, Greenbelt, MD, 20771 USA
[*4] Institute of Forest Resources Information Technology, Chinese Academy of Forestry, Beijing, 100091, China

stand structure indices and lidar measured canopy structure have generality at the regional scale. LEFSKY *et al.* (2002) studied three biomes and found that a single equation explains major variance in above-ground biomass and shows no statistically significant bias in its predictions for any individual site. The differences noted in these studies may be the result of different data characteristics.

The Geoscience Laser Altimeter System (GLAS) instrument aboard the Ice, Cloud, and land Elevation (ICESat) satellite, launched on 12 January 2003. GLAS is the first lidar instrument designed for continuous global observation of the Earth (ZWALLY *et al.*, 2002). Researchers have started using GLAS data for forest studies (RANSON *et al.*, 2004a, b; CARABAJAL and HARDING, 2005; LEFSKY *et al.*, 2005b). Measurements derived from lidar waveforms were used to characterize the canopy vertical structure. These measurements include the lowest and highest detectable returns (above a threshold noise level), and the heights within the canopy where 25, 50, 75 and 100% waveform energy were received (BLAIR *et al.*, 1999). The vertical distribution of plant materials, along with the gap distribution, determines the proportion of energy scattered at a given height. The use of GLAS data for deriving accurate forest parameters for regional studies requires full understanding of their characteristics. The canopy height metrics derived from GLAS data were compared with those derived from LVIS waveforms within the GLAS footprint. The tree height and biomass within GLAS footprints measured in the field were used to test the prediction capability of the GLAS data. The results show some of the potentials and problems of the GLAS data for vegetation structure studies.

STUDY SITE AND DATA

Study Site

The study sites include a forested area within the US Department of Agriculture's Beltsville Agricultural Research Center (BARC), north of the NASA's Goddard Space Flight Center (GSFC) in Maryland, USA (39°N, 76°50'W), and forests around Tahe (52.5° N, 125° E) and Changbai Mountain (42.5° N, 128° E) areas in Northern China. LVIS data over BARC were used to compare with the GLAS data.

More than 80 GLAS footprints were measured in Northern China. After the center of GLAS footprint was located using GPS, four sampling plots with a radius of 7.5 meters (center, 22.5m to north, south-east, and south-west from center) were located within the footprint. Diameter at breast height (DBH) and tree height of all trees with DBH > 5cm were measured. Dominant trees within a ~100m circle but not inside these sampling plots were also measured. These measurements were later used to estimate the height of dominant trees and above-ground biomass in the GLAS footprints.

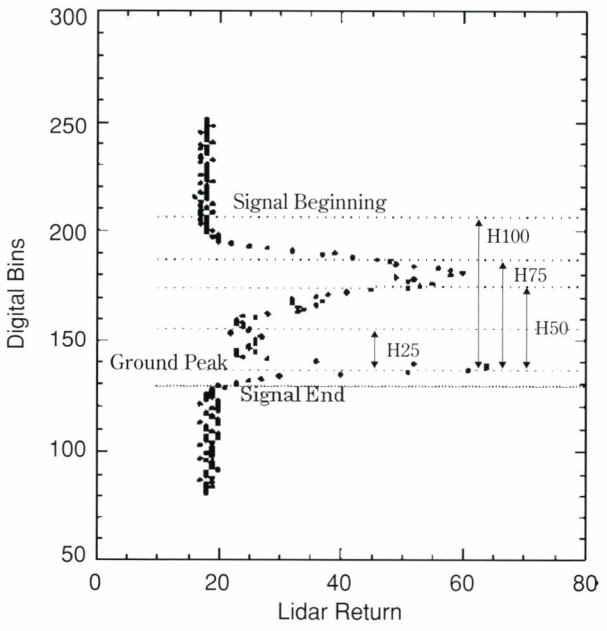

Fig. 1 A typical LVIS waveform attributes and locations of energy quartiles labeled

LVIS Data

NASA's Laser Vegetation Imaging Sensor (LVIS) is an airborne laser altimeter system designed, developed and operated by the Laser Remote Sensing Laboratory at Goddard Space Flight Center. In August 14, 2003, LVIS obtained sub-canopy and canopy-top topography data as well as canopy vertical structure information for several forested sites in the US using a footprint size of 10m (BLAIR *et al.*, 2004). Fig. 1. shows a typical LVIS waveform and provides the definitions of energy height indices. H25 is the 25% quartile height and is calculated by subtracting the ground elevation from the elevation where 25% of the returned energy occurs. H100 is the canopy top height. These quartile heights are a relatively direct measure of the vertical profile of canopy components. In addition, waveform measures are a function of the complex and variable 3-D structure of canopy components and their spectral properties including the spectral properties of the ground/litter. The gap distribution within the canopy largely determines the amount of scattered energy at a given height that returns to the sensor.

GLAS Data

GLAS carries three lasers. Laser 1 started firing on February 20, 2003 and failed only 37 days later. Anomaly studies revealed systematic problems that reduced the lifetime of the laser system. Consequently, the GLAS mission started to operate with a 91-day repeat orbit (with a 33 day sub-cycle) over selected times of the year to maximize coverage of ice-

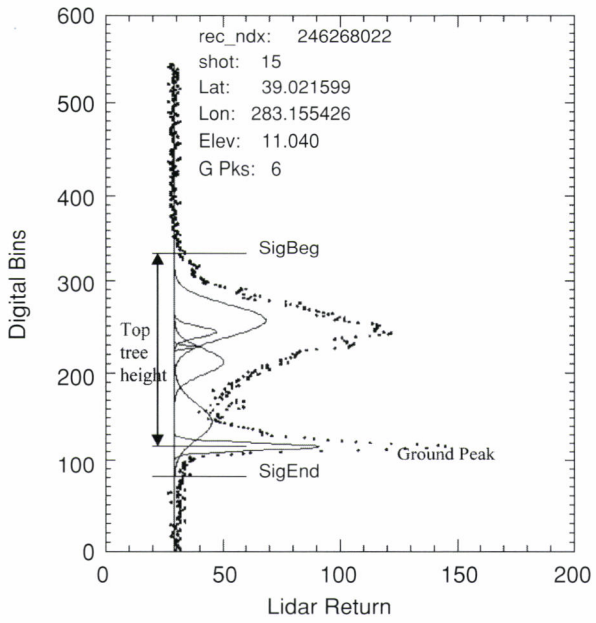

Fig. 2 A GLAS waveform from the study area: Dots-GLAS waveform data from GLA01, solid curves-Gaussian peaks used to fit the waveform from GLA14
Top tree height is the distance from signal beginning to the first Gaussian peak, i.e. the ground peak.

covered areas. From early October to November 19, 2003, GLAS completed the first 33-day sub-cycle using laser 2 (L2A). Since then, more 33-day sub-cycle data sets have been acquired in Feb-March, May-June and October-November periods each year. The use of laser 3 was initiated in October, 2004 (L3A), and continued in February-March (L3B), May-June (L3C), October-November (L3D) in 2005, and Feb-March (L3E), May-June (L3F) in 2006. These 33-day sub-cycles are nearly repeat-passes of the October-November 2003 data (L2A), providing a capability for seasonal and inter-annual change monitoring. GLAS data from L2A, L3A, L3C, L3D and L3F were used in this study.

GLAS uses 1064-nm laser pulses and records the returned laser energy from an ellipsoidal footprint. The footprint diameter is about 65m, but its size and ellipticity have varied through the course of the mission (SCHUTZ *et al.*, 2005; ABSHIRE *et al.*, 2005). GLA01 products provide the waveforms for each laser shot, but only an estimated geolocation for all 40 shots acquired within 1 second. For the land surfaces, the waveform has 544 bins with a bin size of 1-nsec or 15cm. The bin size from bin 1 to 151 has been changed to 60cm starting from acquisition L3A, so the total waveform length increased from 81.6m to about 150m. The product GLA14 (Land/Canopy Elevation) doesn't contain the waveform, but various parameters derived from the waveform. The GLAS waveforms were smoothed using filters, and the signal beginning and end were identified by a noise threshold. The smoothed waveform was initially fitted using many Gaussian peaks at different heights, and then the peaks were reduced to six by an iterative process (ZWALLY *et al.*, 2002; HARDING and CARABAJAL. 2005). GLAS14 data provides the surface elevation and the laser range offsets for the signal beginning and end, the location, amplitude, and width of the six Gaussian peaks. Fig. 2 shows a GLAS waveform from our study area with the Gaussian peaks (HOFTON *et al.*, 2000) and other parameters extracted from GLA14 data products. Assuming that the last peak near the ground is from surface reflection, the distance from the signal beginning and this ground peak is the top canopy height (referred to as H14). This works only for flat area, and requires significant energy return from ground surface. For cases with dense canopies, rough surfaces with slopes, the elevation of the ground peak becomes questionable.

The GLAS L2A data had a range precision of <2.5cm and a pointing determination accuracy better than 2 arcsec, corresponding to a horizontal geolocation error of 5.8m (ABSHIRE *et al.*, 2005). According to CARABAJAL and HARDING (2005), the horizontal geolocation error for L3A, Release 22 was 2.4m (mean) and 7.3m (standard deviation). For this study, GLAS waveforms were extracted and processed to estimate the energy quartile heights similar to those from LVIS data products.

DATA PROCESSING METHOD

GLAS Data Processing

The GLA14 data were first retrieved along with the record index, the serial number of the shot within the index (from 1 to 40), acquisition time, latitude, longitude, elevation, range offsets of signal beginning, signal ending, waveform centroid, and fitted Gaussian peaks. In the GLA01 data file, the 40 shots received in one-second are assigned only one estimated latitude and longitude. Using the record index and shot number found in GLA14 data, the individual waveform was extracted from GLA01 data along with other parameters such as estimated noise level, noise standard deviation, and transmitted pulse waveform, which were used later in waveform processing.

A method for calculating the heights of quartile waveform energy from GLAS waveform was implemented. The waveform was first filtered by a Gaussian filter with a width similar to the transmitted laser pulse. The real width was estimated from the waveform of transmitted pulse. It was about 12 ns, equivalent to a vertical distance of 1.8m. The GLA01 product gives the estimated noise level, i.e. the mean and standard deviation of background noise values in the waveform. For many cases, the noise level before the signal beginning was lower than the noise after the signal ending. Consequently, we estimated the noise levels before the signal beginning and after the signal ending from the original waveform separately using a method based on the histogram. Using three standard deviations as a

threshold above the noise level, the signal beginning and ending were located. The total waveform energy was calculated by summing all the return energy from signal beginning to ending. Starting from the signal ending, the position of the 25%, 50%, and 75% of energy were located by comparing the accumulated energy with total energy. Since the heights of these quartiles refer to the ground surface, not the signal ending, the ground peak in the waveform needs to be located. Searching backward from the signal ending, the peaks can be found by comparing a bin's value with those of the two neighboring bins. If the first peak is too close to the signal ending, i.e. the distance from signal ending to the peak is less than the half width of the transmitted laser pulse, this peak was discarded. The first significant peak found is the ground peak. As terrain slope and surface roughness increase, the ground peak of the waveform becomes wider and the signal beginning moves upwards in a proportional manner. The distance between the signal ending and the assumed signal ending was used as an adjustment to the signal beginning.

Extracting LVIS Data

The LVIS shots were dense enough to provide maps of the canopy vertical structure. All LVIS shots, the centers of which were within a circle of 60m diameters centered at each GLAS footprint, were extracted from the LVIS ground elevation (LGE) data, and the statistics of the quartile heights (H25, H50, H75, and H100) were calculated. The height indices derived from GLAS waveform and LVIS data were compared. The linear correlation of two vectors was used to evaluate their relationship.

Seasonal Effect on GLAS Data

The GLAS data from nearly repeat passes were compared. The distances between corresponding footprints ranged from a few tens of meters to a few hundreds of meters. The tree height indices from GLAS data were compared to assess any temporal differences between these GLAS overpasses.

RESULTS AND DISCUSSION

Comparisons of GLAS Height Indices with Averaged LVIS Height Indices

The correlations between tree height indices derived from LVIS and GLAS are shown in Table 1 for the GLAS data of L2A (Oct 11, 2003) and L3C (June 9, 2005). It can be seen that the linear correlation coefficient (R^2) between the averaged LVIS indices and indices derived from the GLAS waveforms is significant for most cases. For both dates, the correlations between averaged LVIS quartile heights and GLAS quartile heights are high. For the GLAS data acquired on Oct 11, 2003, the GLAS H75 has the highest correlations with the average quartile heights H50 (R^2=0.83) and H75 (R^2=0.82) from LVIS data.

Table 1 Correlations (R^2) between the tree height indices derived from GLAS waveforms and averaged LVIS data within the GLAS footprint

L2A	Height Indices From GLAS					
LVIS	wflen	H14	H25	H50	H75	H100
Mean H25	0.58	0.42	**0.54**	0.77	0.82	0.62
Mean H50	0.61	0.45	0.52	**0.77**	0.83	0.65
Mean H75	0.63	0.48	0.48	0.73	**0.82**	0.66
Mean H100	0.64	0.49	0.69	0.48	0.79	**0.66**
L3C	wflen	H14	H25	H50	H75	H100
Mean H25	0.55	0.32	**0.60**	0.66	0.63	0.54
Mean H50	0.59	0.35	0.59	**0.66**	0.65	0.58
Mean H75	0.61	0.38	0.56	0.65	**0.65**	0.60
Mean H100	0.64	0.40	0.54	0.64	0.64	**0.62**

*Bolded numbers are correlations between the same quartile energy heights from LVIS and GLAS.

In order to investigate the differences between the L2A and L3C data in this site, the differences of the regression equations: $H_{xx}^{GLAS}=A_0+A_1H_{xx}^{LVIS}$, where xx = 50, 75 and 100 between L2A and L3C were tested. *T*-tests were used to test the difference in regression slopes, and F-tests were used to test the difference in regression equations. The results show that the only significant difference is between two regression equations for H100, and all others have no significant differences at 95% confidence level. Because on both dates of Oct 11, 2003 and June 9, 2005, the canopy was fully leaved, the GLAS data were consistent compared with the LVIS data.

Tree Height from GLAS and Field Measurement

Fig. 3 shows a comparison of maximum tree height measured in the field and the estimation from GLA14 data using all 84 sampling points. The line in the figure is the 1:1 line. The correlation (r^2) between the measured and GLAS-estimated tree heights was 0.57, and residual standard error is 4.46m. Figures 4-6 are the comparisons of GLAS estimated biomass with the field measurements. Fig. 4 used all 84 GLAS footprint data in Tahe (64) and Changbai area (20). The forests in Changbai Mountain area are mainly evergreen conifer trees, while most trees in Tahe are deciduous trees (larch and birch). Fig. 5 shows the results using data from Changbai (20) and the GLAS data at Tahe acquired in late Fall (24). Fig. 6 shows the results using GLAS data (40) in Tahe acquired in June. The solid lines in these figures are 1:1 lines. The R^2 and Residual Standard Error are 0.68, 29.35 Mt/ha, 0.78, 30.58 Mt/ha, and 0.59, 24.56 Mt/ha for Fig. 4-6, respectively.

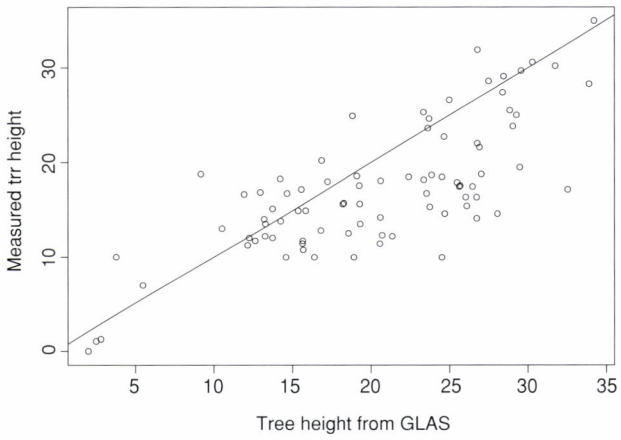

Fig. 3 Top tree heights from field measurements and GLAS estimation in Northern China

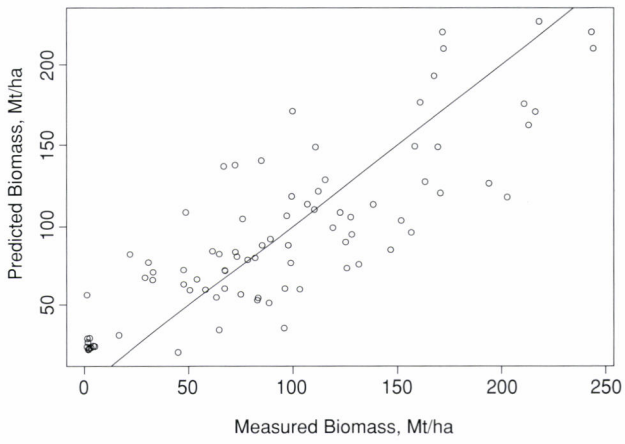

Fig. 4 Comparisons of field biomass with the prediction from GLAS indices using all GLAS footprint data in Changbai preserve forests and Tahe site

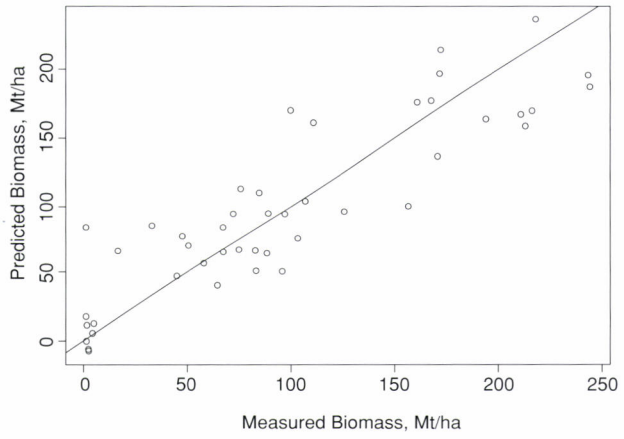

Fig. 5 Comparisons of field biomass with the prediction from GLAS indices using GLAS data in Changbai and the GLAS data acquired in late Fall in Tahe area

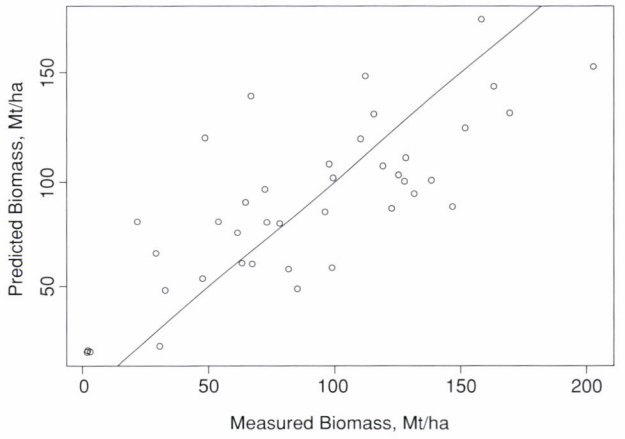

Fig. 6 Comparisons of field biomass with the prediction from GLAS indices using GLAS data acquired in early summer in Tahe area

Seasonal Changes and Forest Heterogeneity

Fig. 7 shows that the surface elevation measured by GLAS on nearly repeated passes are highly consistent. These data used were subsets of the L2A and L3F orbits, each with 260 GLAS footprints (about 4.5km long). The distances of corresponding points range from 75.4m to 89.8 m with a mean of 82.6m. The correlation between the surface elevation from these two orbits was R^2=0.997, with a RMSE of 4.1m. For the top tree height H14, R^2=0.51 and RMSE-4.62m. Figs. 8 and 9 show the comparisons of the top tree height measured by GLAS on different dates. The mean distance between the two orbits shown in Fig. 8 is 170.8m, the correlation between the top tree height from these two orbits is R^2=0.31, and RMSE=6.06m. In this case, the correlation of elevation is R^2=0.81, and RMSE=30.29. The mean distance of the two orbits shown in Fig. 9 is 58.8m, the correlation between the top tree height from these two orbits is R^2=0.46, and RMSE=4.87m. The correlation of elevation is R^2=0.995, and RMSE=5.68m. These results show that the ground surface elevation from the repeat-pass GLAS data sets was consistent, i.e. the correlations of elevation from two orbits were high. The correlations of top tree heights were much lower, and RMSEs were high. The de-correlation was determined by the distances between the two orbits, which indicates that the difference of top tree heights from two repeat-pass orbits is mainly caused by the horizontal heterogeneity of the forest canopies. The different foliage density in different seasons may be the other factor for the height differences from near-repeat pass GLAS data, but seems not significant. Further detailed studies are needed to identify the major factors.

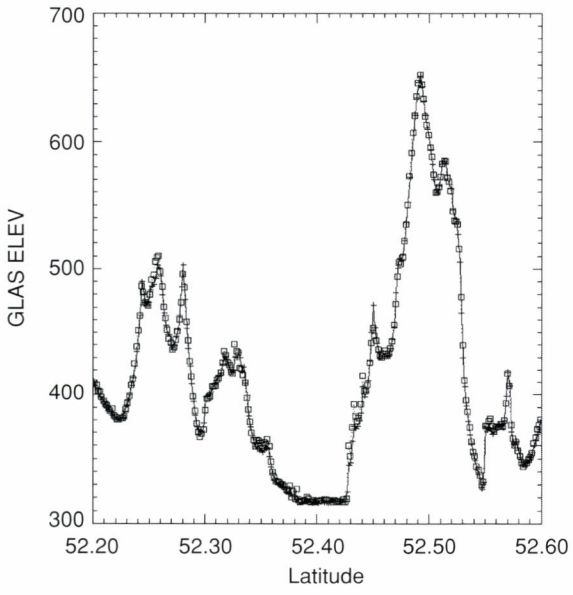

Fig. 7 Surface elevation from two GLAS orbits: data acquired by L3F on May 28, 2006 (square symbol) and by L2A on Oct 21, 2004 (plus sign)

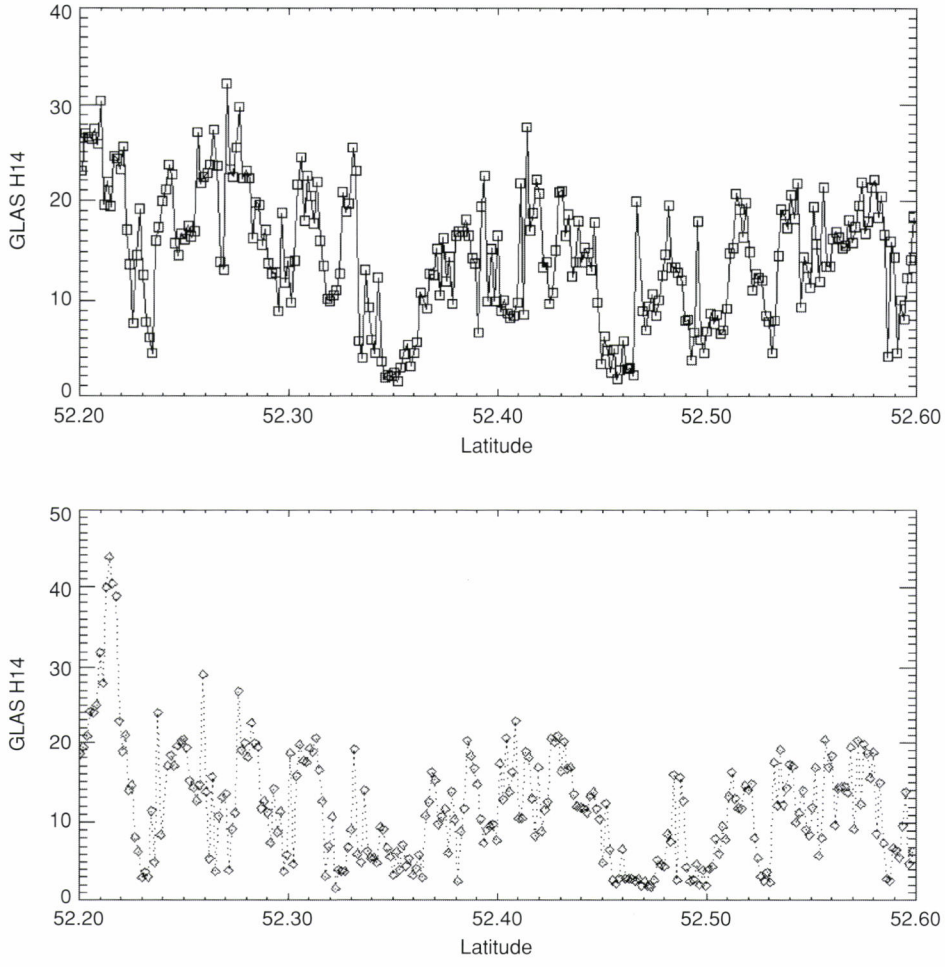

Fig. 8 Comparisons of tree heights from GLAS data acquired by L3C on May 28, 2005 (top) and by L3A on Oct 11, 2004 (bottom)
The distance between these two GLAS orbits is about 170m. Mean tree height is 14.48m and 11.90m for May 28, 2005 and Oct 11, 2004 data, respectively.

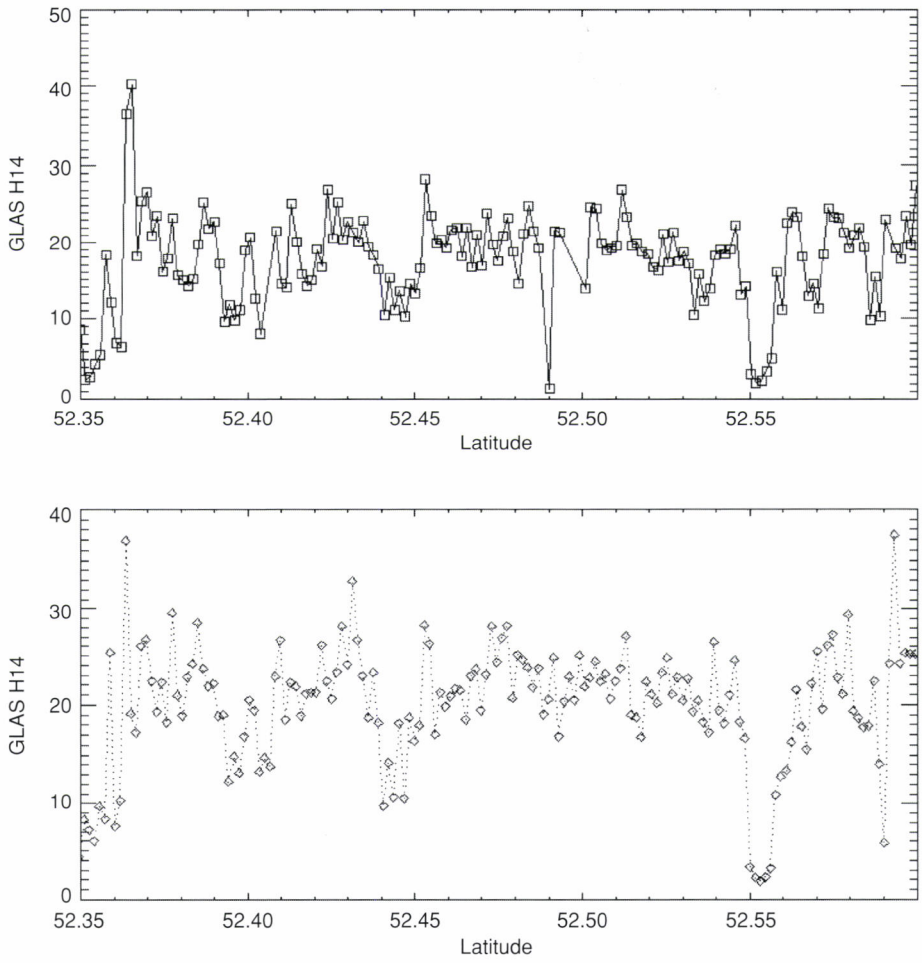

Fig. 9 Comparisons of tree heights from GLAS data acquired by L3C on June 19, 2005 (top) and by L3F on June 24, 2006 (bottom)
The distance between these two GLAS orbits is about 60m. Mean tree height is 17.75m and 18.22m for June 19, 2005 and June 24, 2006 data, respectively.

CONCLUSIONS

The Geoscience Laser Altimeter System (GLAS) is the first lidar instrument for continuous global observation of the Earth. It samples the earth surface every 175m along track with an ellipsoid footprint of about 120m by 50m for laser 2, and a circular footprint of about 65m for laser 3. In this study, the airborne Laser Vegetation Imaging Sensor (LVIS) data was used to as an independent check of the GLAS data.

Correlations between tree height indices derived from LVIS and GLAS were relatively high (e.g., R^2= 0.82 for LVIS H75 and GLAS H75; and R^2=0.83 for LVIS H50 and GLAS H75). The results indicate that the vertical information in GLAS and LVIS waveforms were similar on the scale of GLAS footprint size. The quartile waveform energy heights H50 and H75 derived from GLAS and LVIS data showed higher correlations than H100. Because of these high correlations and the fact that these height indices from airborne lidar data has been used for forest biomass estimations, we believe that the GLAS data will be useful for biomass sampling in regional to global scales, given the limitations of geographical coverage and the large footprint diameter.

The field measurements and data analysis showed that GLAS data predicted the top tree height and stand biomass well for the cases studied here. However, caution and further study should be taken in terms of the effects of seasons of data acquisition, the scale of the sample as well as terrain slope and forest types on the derived forest structure measures.

ACKNOWLEDGEMENT

This study and field work was funded by National Science Foundation of China (40571112), the 863 program (2006AA12Z114)

of China, and NASA's Science Mission Directorate. The LVIS data sets were provided by the Laser Vegetation Imaging Sensor (LVIS) team in the Laser Remote Sensing Branch at NASA Goddard Space Flight Center with support from the University of Maryland, College Park. Funding for the collection and processing of the northeastern USA data was provided by NASA's Terrestrial Ecology Program (NASA Grant number NAG512112).

LITERATURE CITED

ABSHIRE, J. B., SUN, X., RIRIS, H., SIROTA, J. M., MCGARRY, J. F., PALM, S., YI, D. and LIIVA, P., (2005): Geoscience Laser Altimeter System (GLAS) on the ICESat Mission: On-orbit measurement performance. Geophysical Research Letters **32** (22)

BLAIR, J. B., HOFTON M. A. and RABINE D. L., (2004): Processing of NASA LVIS elevation and canopy (LGE, LCE and LGW) data products, version 1.0. https://lvis.gsfc.nasa.gov, 2004

BLAIR, J. B., RABINE D. L. and HOFTON M. A., (1999): The laser vegetation imaging sensor (LVIS): a medium-altitude, digitation-only, airborne laser altimeter for mapping vegetation and topography. ISPRS Journal of Photogrammetry and Remote Sensing **54**: 115-122

CARABAJAL, C. C. and HARDING, D. J., (2005): ICESat Validation of SRTM C-Band Digital Elevation Models. Geophys. Res. Lett. **33**: L22S01

DRAKE, J. B., DUBAYAH, R. O., CLARK, D. B., KNOX, R. G., BLAIR, J. B., HOFTON, M. A., CHAZDON, R. L., WEISHAMPEL, J. F. and PRINCE, S. D., (2002): Estimation of tropical forest structural characteristics using large-footprint lidar. Remote Sensing of Environment **79**: 305-319

DRAKE, J. B., KNOX, R. G., DUBAYAH, R. O., CLARK, D. B., CONDIT, R., BLAIR, J. B. and HOFTON, M., (2003): Above-ground biomass estimation in closed canopy Neotropical forests using lidar remote sensing: factors affecting the generality of relationships. Global Ecology And Biogeography **12** (2): 147-159

DUBAYAH, R. O. and DRAKE, J. B., (2000): Lidar remote sensing for forestry. Journal of Forestry **98** (6): 44-46

HARDING, D. J. and CARABAJAL, C. C., (2005): ICESat waveform measurements of within-footprint topographic relief and vegetation vertical structure. Geophysical Research Letters **32**: L21S10, doi:10.1029/2005GL023471

HARDING, D. J., LEFSKY, M. A., PARKER, G. G. and BLAIR, J. B., (2001): Laser altimeter canopy height profiles - Methods and validation for closed-canopy, broadleaf forests. Remote Sensing Of Environment **76** (3): 283-297

HOFTON, M. A., MINSTER, J. B. and BLAIR, J. B., (2000): Decomposition of laser altimeter waveforms. Ieee Transactions On Geoscience And Remote Sensing **38** (4): 1989-1996, Part 2

HYDE, P., DUBAYAH, R., PETERSON, B., BLAIR, J. B., HOFTON, M., HUNSAKER, C., KNOX, R. and WALKER, W., (2005): Mapping forest structure for wildlife habitat analysis using waveform lidar: Validation of montane ecosystems. Remote Sensing Of Environment **96** (3-4): 427-437

LEFSKY, M. A., COHEN, W. B., ACKER, S. A., PARKER, G. G., SPIES, T. A. and HARDING, D., (1999): Lidar remote sensing of the canopy structure and biophysical properties of Douglas-fir western hemlock forests. Remote Sensing Of Environment **70** (3): 339-361

LEFSKY, M. A., COHEN, W. B., HARDING, D. J., PARKER, G. G., ACKER, S. A. and GOWER, S. T., (2002): Lidar remote sensing of above-ground biomass in three biomes. Global Ecology And Biogeography **11** (5): 393-399

LEFSKY, M. A., HARDING, D. J., KELLER, M., COHEN, W. B., CARABAJAL, C. C., ESPIRITO-SANTO, F., HUNTER, M. O. and OLIVEIRA Jr., R., (2005b): Estimates of forest canopy height and aboveground biomass using ICESat. Geophysical Research Letters **32**: L22S02, doi:10.1029/2005GL023971, 2005

LEFSKY, M. A., HUDAK, A. T., COHEN, W. B. and ACKER, S. A., (2005a): Geographic variability in lidar predictions of forest stand structure in the Pacific Northwest. Remote Sensing Of Environment **95** (4): 532-548

RANSON, K. J., SUN, G., KOVACS, K. and KHARUK, V. I., (2004a): Landcover attributes from ICESat GLAs data in central Siberia. IGARSS 2004 Proceedings, 20-24 September 2004, Anchorage, Alaska, USA

RANSON, K. J., SUN, G., KOVACS, K. and KHARUK, V. I., (2004b): Use of ICESat GLAS data for forest disturbance studies in central Siberia. IGARSS 2004 Proceedings, 20-24 September 2004, Anchorage, Alaska, USA

SCHUTZ, B. E., ZWALLY, H. J., SHUMAN, C. A., HANCOCK, D. and DIMARZIO, J. P., (2005): Overview of the ICESat Mission. Geophysical Research Letters **32** (22)

WEISHAMPEL, J. F., BLAIR, J. B., KNOX, R. G., DUBAYAH, R. and CLARK, D. B., (2000): Volumetric lidar return patterns from an old-growth tropical rainforest canopy. International Journal Of Remote Sensing **21** (2): 409-415

ZWALLY, H. J., SCHUTZ, B., ABDALATI, W., ABSHIRE, J., BENTLEY, C., BRENNER, A., BUFTON, J., DEZIO, J., HANCOCK, D., HARDING, D., HERRING, T., MINSTER, B., QUINN, K., PALM, S., SPINHIRNE, J. and THOMAS, R., (2002): ICESat's laser measurements of polar ice, atmosphere, ocean, and land. Journal of Geodynamics **34** (3-4): 405-445

(Received 12 January 2007)
(Accepted 8 May 2007)

Article

The Estimation of Wind Risk in Forests Stands using Airborne Laser Scanning (ALS)

Juan Suárez[*1], Rafael Garcia[*2], Barry Gardiner[*1] and Genevieve Patenaude[*2]

ABSTRACT

Wind is the most important abiotic hazard for forestry in Britain. Most forests have been established in upland areas in locations that are commonly affected by high winds and poor soil conditions. Strong winds cause significant loss of timber every year in Great Britain and have profound effects in wood quality though increases in the proportion of compressed wood, poor stem straightness, repeated loss of leaders and important alterations in the relationship between height and diameter. ForestGALES (Geographical Analysis of the Losses and Effects of Storms in Forestry) is a process-based model that provides a better understanding of the variability in the wind forest climatology, an estimation of the critical wind speed to cause wind damage and the return period for that damage to occur. At present, ForestGALES is currently being linked to ArcGIS and LiDAR data has been evaluated to estimate the effects of stand structure in the probability of wind damage. To do so, the model has been adapted to operate with tree lists generated by LiDAR. In this context, three canopy delineation algorithms have been tested in connection to existing allometric relationships.TreeVAW (POPESCU, 2006), TreesVIS (WEINACKER *et al.*, 2004) and ITC (GOUGEON, 2005). The results provided a valid method for evaluating the effects of stand variability on wind damage and the effectiveness of Airborne Laser Scanning for monitoring forest structure and its effects on wind stability.

Keywords: LiDAR, forestry, windthrow, tree canopy segmentation and tree dimensions.

INTRODUCTION

Wind is the most important abiotic hazard for forestry in Britain. Most forests have been established in upland areas in locations that are commonly affected by high winds and poor soil conditions. Strong winds cause significant losses of trees every year in Great Britain. In addition, the quality of the timber is also affected by an increase in the proportion of compressed wood, poor stem straightness, repeated loss of leaders and important alterations in the relationship between height and diameter.

ForestGALES (Geographical Analysis of the Losses and Effects of Storms in Forestry) is a process-based model that provides a better understanding of the wind forest climatology, an estimation of the critical wind speed at which wind damage is caused and the return period for that damage to occur. The use of a mechanistic model creates more flexibility for testing different forest management scenarios such as the choice of cultivation, thinning options, drainage improvements, the impact of clearfellings and the creation of long term retentions (GARDINER *et al.*, 2004). At present, ForestGALES is being integrated into the British Forest Enterprise corporate GIS system.

Initial validation of the model, with data from wind tunnels and field experiments (GARDINER *et al.*, 2000), has shown its sensitivity to silvicultural practices which alter the height-spacing ratios, drainage maintenance, stem taper and distance to new edges. These changes of stand conditions are attributed to forest management (or the lack of it).

During field validation, a group of 177 plots 10x10m in size and distributed across 6 monitoring areas in the UK, were surveyed to collect the necessary parameters for running the

Corresponding author: Juan Suárez
[*1] Forest Research, Northern Research Station, Roslyn, EH25 9SY, UK
juan.suarez@forestry.gsi.gov.uk, Barry.Gardiner@forestry.gsi.gov.uk
[*2] Department of Geography, University of Edinburgh, Edinburgh, EH6 9XP, UK
R.Garcia-Gonzalez@sms.ed.ac.uk, Gpatenau@staffmail.ac.ed.uk

model (tree height, diameters and spacing) and observed wind damage. The results showed an overall performance around 48% in accuracy with a considerable amount of over predictions (Table 1).

These results contrasted sharply with the better results obtained in wind tunnel experiments. Part of the reason was the excessive simplification of the input parameters that only accepted mean stand conditions. A second validation of the model used Montecarlo simulations to recreate normal stand variability using the same datasets. This time the results showed an increase in the performance of the model up to 70% (SUÁREZ *et al.*, 2001). The better results were attributed to more realistic stand characteristics that allowed variable distributions of tree heights and diameters for each plot.

Following this principle, the model has been recently adapted to operate with tree lists in order to map the effect of variable stand conditions and to have an insight into the effect of stand structure and, in particular, the spatial distribution of different types of trees on the probability of wind damage. As this information is difficult to measure in the field, airborne laser scanning (ALS) data have been tested as a cost-effective alternative to field data collection. However, the main problem when working with ALS is how to convert point clouds of data into something meaningful, where information about individual trees can be extracted.

Therefore, three canopy delineation algorithms have been tried in connection to existing allometric relationships in order to extract the dimensional parameters to operate the model at tree level: TreeVAW (POPESCU, 2006), TreesVIS (WEINACKER *et al.*, 2004) and ITC (GOUGEON, 2005). This paper will explain in detail the comparative results of each algorithm.

Table 1 Metrics of performance of ForestGALES in the wind monitoring areas.

%Damage (Sensitivity)	%NO-Damage (Specificity)	Total (Truth)	Underpred. (False -ve)	Overpred. (False +ve)
0.88	0.32	0.48	0.12	0.68

To summarise, the aims of this study are:

1. to carry out a comparative evaluation of 3 bespoke algorithms for individual tree crown delineations ITC, TreesVIS and TreeVAW;
2. to evaluate the most sensitive parameters for running ForestGALES at tree level such as tree height and diameter at breast height (DBH) using ALS;
3. to evaluate use of tree lists as an input dataset for ForestGALES in order to make more accurate predictions of wind damage than the ones generated with stand information gathered in the field;
4. to determine the spatial location of the most vulnerable trees in the forest in order to understand the effect of stand structure on the likelihood of wind damage and as an aid to future management plans.

FIELD METHODS

A study area was located around the Aberfoyle village (56° 10' North, 4° 22' West) inside the Trossachs-Ben Lomond National Park in the west coast of Scotland (Fig. 1).

ALS data were acquired in September 2002. The total area surveyed was 17.5km² at a cost of roughly £5 per ha. The characteristics of this dataset are displayed in Table 2.

Field data were also collected in order to test the accuracy of the canopy segmentation models and the predictions of wind damage. The collection of data in the field consisted on 9 square plots each a quarter of a hectare in size covering a selection of forest stands planted with Sitka spruce (*Picea*

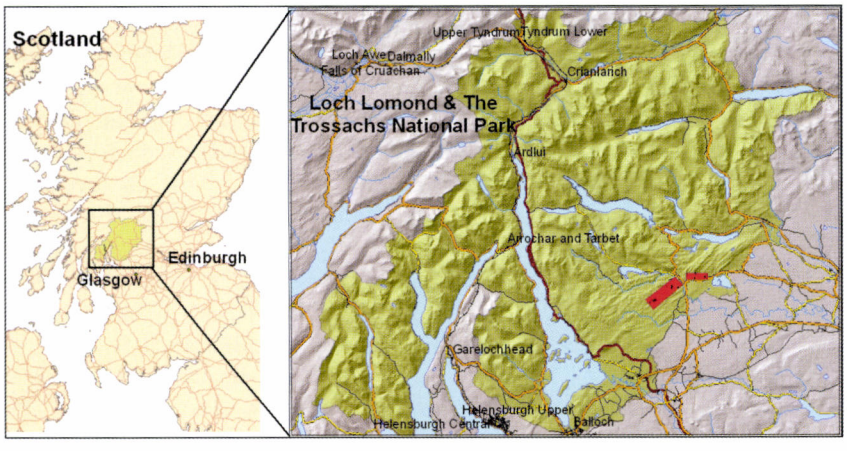

Fig. 1 Fig. 1. The study area is within the Trossachs-Ben Lomond National Park (highlighted in green). Red rectangles show the area covered by airborne LiDAR.

Table 2 Laser data characteristics of ALS survey in 2002.

Parameter	*Performance*
Sensor	Optech ALTM2033
Laser pulse frequency	33,000Hz
Flying altitude	1000m
Beam divergence	10cm
Scanning angle	20 degrees
Sampling intensity	3-4 returns per m^2
Position accuracy	X, Y < 40cm
Elevation accuracy	Z < 9- 15cm

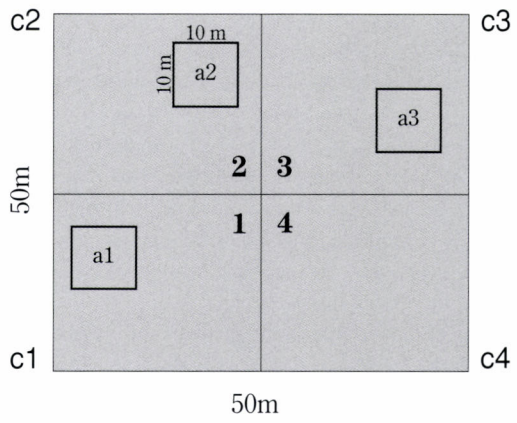

Fig. 2 Fig. 2. Configuration of the sample plot in field. Within each 50×50m plot the DBH, dominance and position for every tree were measured. Within small 10×10m plots tree height, height to first live whorl and crown diameter were also measured.

Table 3 Surveyed plots in the study area.

Plot	*Age*	*Yield Class*	*Density (stem/ha)*	*Avg DBH (cm)*	*SD DBH (cm)*	*Avg Height (m)*	*SD Height (m)*	*Top Height (m)*	*Avg Crown (m)*	*SD Crown (m)*	*Basal Area (m^2/ha)*	*Vol (m^3/ha)*
1	33	20	580	31.02	10.39	26.01	2.65	27.18	5.53	1.67	48.7	573.50
2	31	16	344	29.80	10.98	22.35	2.11	22.60	6.55	0.82	27.2	264.72
4	33	24	440	32.73	7.55	24.87	2.75	25.64	5.77	1.45	39.0	431.35
6	33	16	504	28.02	7.23	21.27	2.17	21.96	5.86	0.99	33.1	313.65
7	31	20	380	33.92	6.68	25.23	1.50	25.52	5.68	0.87	35.6	393.18
8	32	24	412	36.38	8.36	27.99	1.89	28.46	5.94	1.12	45.1	557.12
9	31	22	520	28.94	7.49	24.49	2.81	26.06	5.02	1.04	36.5	410.28
10	32	24	548	29.62	5.92	23.84	1.70	24.64	4.80	0.93	39.3	417.72
12	33	20	520	27.08	7.08	21.87	4.75	21.65	5.14	0.67	32.0	297.97

sitchensis) aged 31-33 years old (see Table 3). The plots were located on terrain, with slopes varying between 5 to 25%, except plots 2 and 4, which were located on flat terrain. Altitude varied from 25 to 170m above sea level.

Within each 50×50m plots, the diameter and position of each tree (located with a Total Station and DGPS), and its dominance were measured. Additionally, three 10×10m square plots were randomly located inside each 50×50m plot as shown in Fig. 2. Within each small plot, tree heights, crown dimensions in N-S and E-W axis and the height to the first live whorl for all trees were also measured.

METHODOLOGY

The Construction of a Digital Canopy Model

The delineation algorithms were performed on gridded data representing the height of the canopy in every pixel. The grid dimension was 0.5×0.5m, interpolated by Kriging without anisotropy. Previously, a Normalised Digital Canopy Model (NDCM) had been calculated by subtracting the difference between the cloud points in the first ALS returns and an estimation of the digital terrain model (DTM) derived after filtering out those hits being intercepted by the forest canopy and, therefore, not reaching the underlying terrain. The method involved an iterative process of selection of points within kernels of variable size according to the local minima (SUÁREZ *et al.*, 2005).

Delineation Process

The algorithm by POPESCU *et al.* (2003): TreeVAW

This algorithm estimates the location of the trees tops and the crown diameter in the NDCM. In order to find the tree

tops, the local maxima technique finds the pixel that has a higher value than the surrounding pixels in all directions within a search window. This algorithm uses two different search windows, an $n \times n$ squared window and a circular area (POPESCU *et al.*, 2003). In order to define an appropriate search window size, the technique assumes that there exists a relationship between crown size and tree height. The method requires (*a*) maximum and minimum crown diameters as initial parameters and (*b*) an empirical relationship between tree height and crown diameter.

This relationship was derived from the Forest Research Environmental Database (FRED), a field inventory dataset extracted from permanent sample plots across the country. In the construction of the relationship, all Sitka spruce in Scotland for which tree crown and height were measured were selected. The relationship between crown diameter and height was improved by fitting them to yield class, as defined by EDWARDS and CHRISTIE (1981): annual incremental growth in m^3, per hectare, per year. One equation was adjusted to lower potential productivity (yield class 16). A second equation was fitted to higher potential productivity (yield class 20, 22 and 24 combined). The initial parameters derived from data with yield class 16 were applied to plot 2 and 6. The parameters derived from yield class 20, 22 and 24 were applied to the rest of plots. Initial parameters are shown in Table 4.

Once the location of the trees is set, the NDCM is sampled at the positions of the treetop to calculate the height of each tree. Thereafter, the algorithm calculates crown diameter for each tree.

Firstly a 3×3 pixels median filter is applied over the NDCM in order to avoid noise at the top of the canopy. In order to calculate crown diameter, two perpendicular profiles are extracted from the NDCM and then, a fourth-degree polynomial equation is fitted to each profile. The algorithm finds the local minimum of the fitted functions. The edges of the crown profiles are local minimums, where the first derivative equals zero and the second derivative is positive. The crown diameter is calculated as the distance between the two edges of the crown profile. The final crown diameter is calculated as the average of the crown diameters of the two perpendicular profiles (POPESCU *et al.*, 2003). See Fig. 3.

The algorithm by WEINACKER *et al.* (2004): TreesVIS

The algorithm starts by finding treetops using a local maximum filter in the NDCM. This filter finds the local maxima as the pixel with highest value compared to its surrounding pixels (WEINACKER *et al.*, 2004).

Once the tree tops are located, a pouring algorithm, starting from the tree top, aims at the detection of the tree borders. This algorithm works similarly to the inverted watershed algorithm (SOILLE, 1999). After the application of this algorithm, some segments have sizes or shapes that are improbable to represent a tree. In order to merge this improbable tree segment with other segments, rules on defining the area and the shape of the segmented crown and the proximity with the nearest tree top are applied. A complete description of the algorithm can be found in WEINACKER *et al.* (2004). See Fig. 3.

The algorithm by GOUGEON (1995)

This algorithm was initially developed for high spatial resolution optical images, but it has recently been used with LiDAR data to delineate individual tree crowns (LECKIE *et al.*, 2003).

The algorithm is divided in two parts: firstly, the following-valley approach starts by finding the local minima in the NDCM. A pixel is considered as local minima if all its surrounding pixels have higher values. By starting at the local minima, the algorithm follows the "valley pixels", which are found between pixels with higher values. The algorithm continues to find valley pixels until a crown is delimited. Secondly, a complete delineation is done with the application of the second-rule approach that, in this case, eliminated canopies smaller than $4m^2$. This threshold was selected after the analysis of the field data stored in FRED. A complete description of the algorithm can be found in GOUGEON (1995). See Fig. 3.

Linking Process

The methodology applied in the linking process was applied in previous works by PERSSON *et al.* (2003). In order to evaluate the results, each detected tree was automatically linked to the corresponding field tree. The position for a delineated tree was assumed as the position of the tree top.

For each delineated crown tree different situations can occur: (1) within each delineated tree crown, there is only one field tree, (2) within each delineated tree crown, there are more than one field tree and (3), within each delineated tree crown there are no field trees. For (1), the delineated tree was linked directly to the field tree, for (2), the delineated tree was linked to the closest field tree within the delineated tree crown projection, and for (3), the segmented tree is a segment that

Table 4 Initial parameters used in the method described by Popescu.

Yield Class (m^3/ha-yr)	Crown diameter-height relationship	R^2	Regression significance	Max Crown Diameter (m)	Min Crown Diameter (m)	Min Height (m)
16	CWD=0.0002 h^3-0.0061 h^2+0.1958 h+0.4218	0.81	P<<0.001	8.60	1.10	7.70
20,22,24	CWD=0.0006 h^3-0.0252 h^2+0.4627 h-0.1779	0.76	P<<0.001	10.90	2.20	7.10

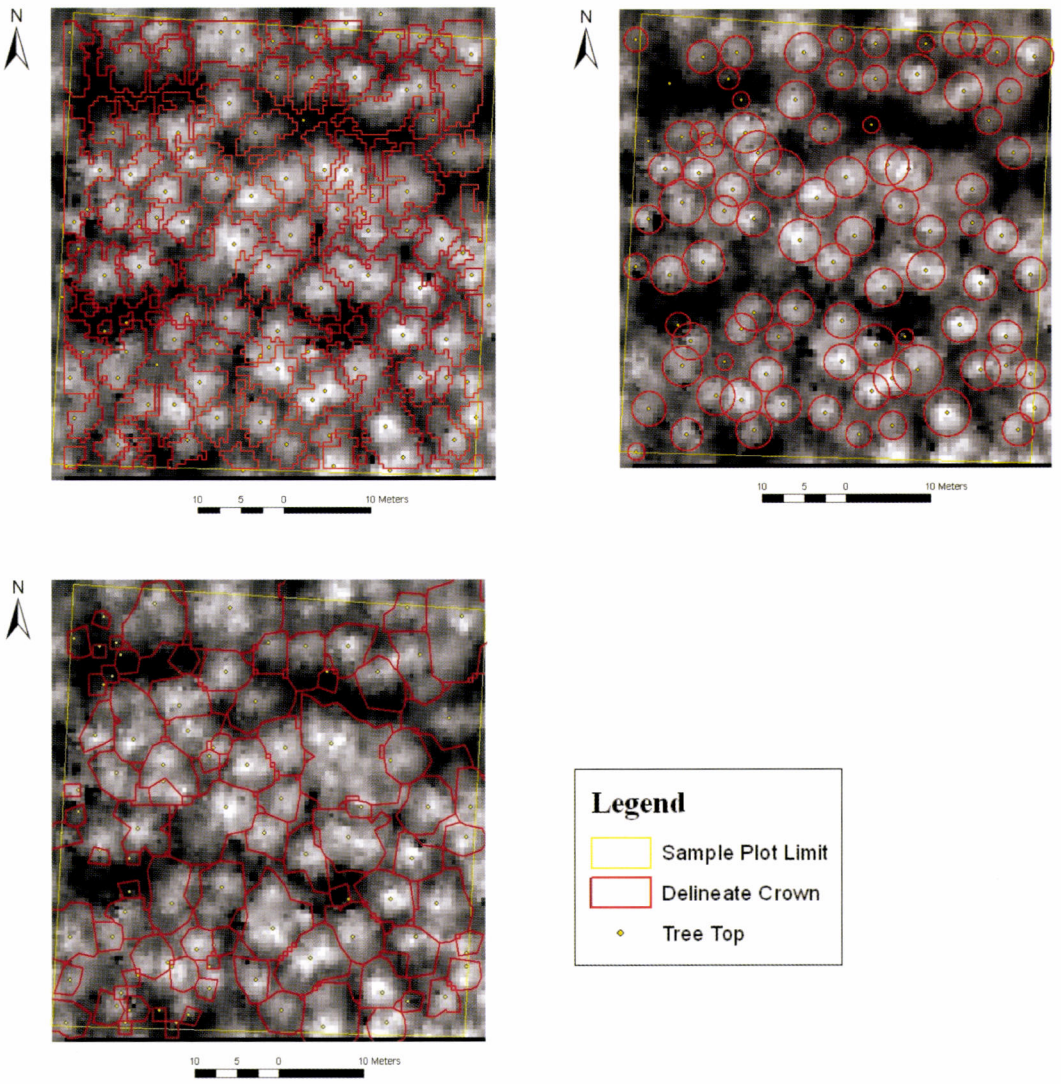

Fig. 3 Example of tree crown delineation in sample plot 8. The left, middle and right images show tree crown delineation with TreeVAW, TreesVIS and Gougeon algorithms respectively.

has no field tree. For each unlinked field tree, a search was conducted at a maximum distance of two pixels in all directions, each pixel measuring 0.5 × 0.5m. If a field detected tree was found within this buffer distance, then the segmented crown was assigned to it.

One of the most common problems was the segmentation of crowns belonging to small trees that were close to larger ones. Usually, the small undetected trees ended up with their canopies linked to the taller ones and then becoming invisible.

Tree Attributes Estimation

Individual tree parameters considered were tree height (H), crown diameter (L) and stem diameter at breast height (DBH). In order to calculate the error in the estimation of individual tree parameters, the values from each segmented tree were compared with the field measured trees after the linking process.

LiDAR tree height (H) was calculated by all the algorithms as the local maxima derived from the different canopy delineations. Crown diameter in TreeVAW was provided directly applying the algorithm by Popescu. The delineated crowns for the other algorithms were derived from the area of each crown (A). The crown diameter (L) was calculated assuming a circular shape:

$$L=\sqrt{\frac{4\cdot A}{\pi}} \tag{1}$$

In coniferous species such as Sitka spruce there is a strong relationship between DBH with crown diameter and

Table 5 Coefficients for the relationship between DBH and crown diameter and tree height.

Equation	Adjusted R^2	Standard error (cm)	Regression significance	Regresion coeficientes		
				a_1	a_2	a_3
DBH (cm)=a_1L(m)+a_2H(m)+a_3	0.89	2.99	p<<0.001	3.3236	0.8521	-3.8540

Aberfoyle_all_plots.txt - Notepad

File Edit Format View Help

Aberfoyle plot_ID	Age	Gougeon Species	stand Soil	Culti	Draina	SH(m)	SDBH(cm)	Indv(H)	Indv(DBH)	Spac	GAP	Weibull_A	Weibull_k
1003	33	10	1	7	1	27.18	31.02	26.55	39.48	4.47	0	3.6	1.85
1007	33	10	1	7	1	27.18	31.02	23.50	27.73	4.47	0	3.6	1.85
1014	33	10	1	7	1	27.18	31.02	21.40	26.39	4.47	0	3.6	1.85
1018	33	10	1	7	1	27.18	31.02	27.00	35.72	4.47	0	3.6	1.85
1019	33	10	1	7	1	27.18	31.02	19.40	24.68	4.47	0	3.6	1.85
1022	33	10	1	7	1	27.18	31.02	23.61	25.45	4.47	0	3.6	1.85
1027	33	10	1	7	1	27.18	31.02	20.16	20.09	4.47	0	3.6	1.85
1030	33	10	1	7	1	27.18	31.02	19.91	18.42	4.47	0	3.6	1.85
1031	33	10	1	7	1	27.18	31.02	23.85	27.72	4.47	0	3.6	1.85
1036	33	10	1	7	1	27.18	31.02	26.09	34.29	4.47	0	3.6	1.85
1037	33	10	1	7	1	27.18	31.02	23.23	27.19	4.47	0	3.6	1.85
1038	33	10	1	7	1	27.18	31.02	24.85	34.20	4.47	0	3.6	1.85
1040	33	10	1	7	1	27.18	31.02	23.65	25.86	4.47	0	3.6	1.85
1047	33	10	1	7	1	27.18	31.02	25.25	31.31	4.47	0	3.6	1.85
1050	33	10	1	7	1	27.18	31.02	25.05	40.99	4.47	0	3.6	1.85
1052	33	10	1	7	1	27.18	31.02	26.67	35.64	4.47	0	3.6	1.85
1056	33	10	1	7	1	27.18	31.02	25.04	31.76	4.47	0	3.6	1.85
1077	33	10	1	7	1	27.18	31.02	26.99	33.91	4.47	0	3.6	1.85
1094	33	10	1	7	1	27.18	31.02	23.69	24.29	4.47	0	3.6	1.85
1098	33	10	1	7	1	27.18	31.02	21.06	32.08	4.47	0	3.6	1.85
1106	33	10	1	7	1	27.18	31.02	27.12	33.41	4.47	0	3.6	1.85
1112	33	10	1	7	1	27.18	31.02	23.50	28.03	4.47	0	3.6	1.85
1122	33	10	1	7	1	27.18	31.02	24.02	38.32	4.47	0	3.6	1.85
1127	33	10	1	7	1	27.18	31.02	23.20	30.44	4.47	0	3.6	1.85

Fig. 4 Example of a tree list derived from ALS used for running the model.

tree height. For this reason, DBH has been estimated with L and H using the following regression formula:

$$DBH = a_1L + a_2H + a_3 \quad (2)$$

The a_1, a_2 and a_3 coefficients were calibrated using field observations from FRED. See Table 5.

Running ForestGALES with Tree Lists

Tree lists were generated with information derived from ALS (Fig. 4). In this case, only linked trees within the small 10x10m plots in each forest stand were considered for this analysis because tree height was only measured for those trees. Data derived from ALS (individual tree height and DBH) were combined with stand measurements (age, species code, soil type, cultivation, drainage, mean height, mean diameter, spacing and size of upwind gap) and wind climate conditions for each area (Weibull A and k values representing wind speed in ms^{-1}).

The model requires stand information such as mean height (m), mean diameter (cm) and spacing (m) in order to calculate a logarithmic wind profile above the canopy and an exponential profile within the canopy, together with the aerodynamic roughness (z_0) and the zero plane displacement (d). So, those parameters were extracted directly from the Forest Enterprise Sub-Compartment Database.

The wind loading on individual trees within the stand is then calculated as a function of the wind speed at 10 m above each canopy using the information about the drag on the canopy contained in z_0 and d (see GARDINER *et al.*, 2000 for full details). The total turning moment at the base of a tree is then calculated accounting for the bending of the stem and the overhanging mass of the canopy. Those values are derived from individual tree height and DBH values estimated by each tree canopy segmentation algorithm. Finally, adjustment is made for wind gusting, location relative to the forest edge and the width of any upwind gap using empirical correction factors derived from wind tunnel and field experiments (STACEY *et al.*, 1994; GARDINER *et al.*, 2000). Upwind gaps were set to zero as the plots are all located in the middle of the stand.

The resistance to breakage is based on the assumption that the wind stress remains constant between the base of the canopy and the stem base. This allows the calculation of the stress at breast height only, which is compared to the Modulus of Rupture, corrected by the proportion of knots in the timber. The critical wind speeds for overturning and breakage are calculated as the wind speeds required to produce bending moments in excess of the resistive factors at the base of the stem for overturning and 1.3 metres for breakage (GARDINER *et al.*, 2000). Results are produced in ms^{-1} for each individual tree.

The wind climate model used in the program is obtained from the DAMS scoring system, which is a function of elevation, topographic exposure, aspect, funnelling effects and wind zone of the country (BELL *et al.*, 1995). The actual scoring system is transformed into a Weibull distribution, where the scale parameter A represents the modal wind speed [ms^{-1}], and the k-parameter [ms^{-1}] represents the spread of the

values. In this application, a constant value of 1.85 has been assigned for all the simulations, whereas Weibull-A is estimated from the DAMS scores at each tree location. DAMS values are converted to Weibull-A using the following relationship:

$$\text{Weibull-A} = -0.9626 + 0.4279\ \text{DAMS\_Value}; \quad (3)$$

The probability of annual exceedance of the damaging winds is calculated from the probability density function represented by the Weibull distribution. These final probabilities are transformed into return periods for both overturning and breakage. The return periods are the inverse of the probabilities and they are expressed in number of years to damage.

RESULTS

Crown Delineations

TreeVAW seemed to have the highest level of crown detections around 90% in the larger plots (50×50m). TreesVIS seemed to over predict the number of crown segments due to the partition of large crowns into multiple canopies. On the contrary, the method developed by Gougeon had the opposite effect as many individual canopies were aggregated into larger ones (Table 6).

These results, although initially favourable to TreeVAW, had a limited correspondence to the reality of stand structure. Fig. 5 depicts the distribution of stem diameters in two plots

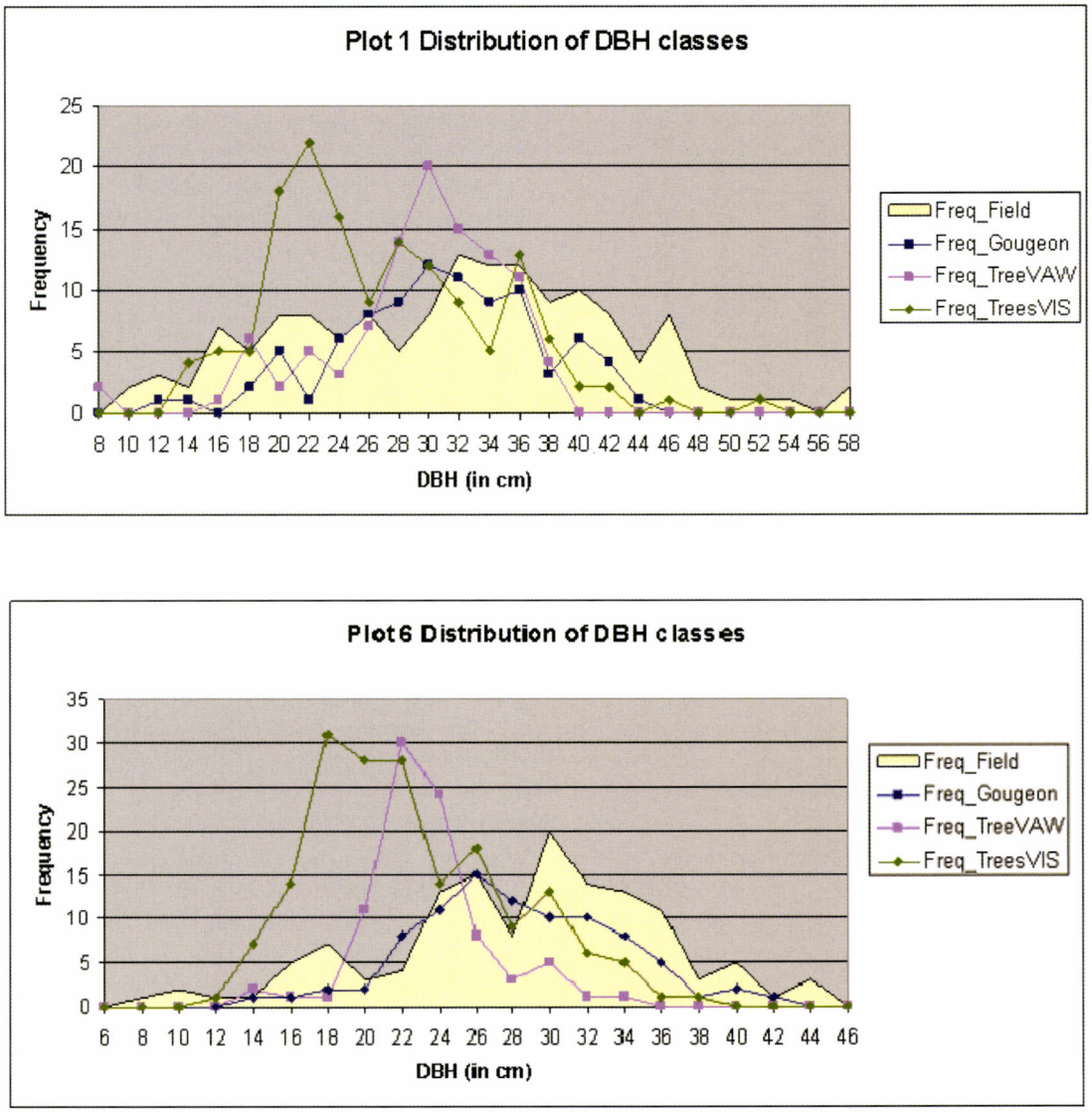

Fig. 5 Predictions of stand structure using stem diameter classes obtained with each method compared to field observations in Plots 1 and 6.

Table 6 Crown delineation with each algorithm.

		TreeVAW		TreesVIS		Gougeon	
Plot	**Field Trees**	**Delineated Trees**	%	**Delineated Trees**	%	**Delineated Trees**	%
1	145	103	71.0%	144	99.3%	89	61.4%
2	86	93	108.1%	141	164.0%	55	64.0%
4	110	100	90.9%	164	149.1%	99	90.0%
6	126	103	81.7%	176	139.7%	89	70.6%
7	95	98	103.2%	153	161.1%	82	86.3%
8	103	87	84.5%	88	85.4%	90	87.4%
9	130	105	80.8%	167	128.5%	103	79.2%
10	137	132	96.4%	168	122.6%	111	81.0%
12	130	127	97.7%	167	128.5%	109	83.8%
Total	**936**	**845**	**90.27%**	**1192**	**127.35%**	**738**	**78.84%**

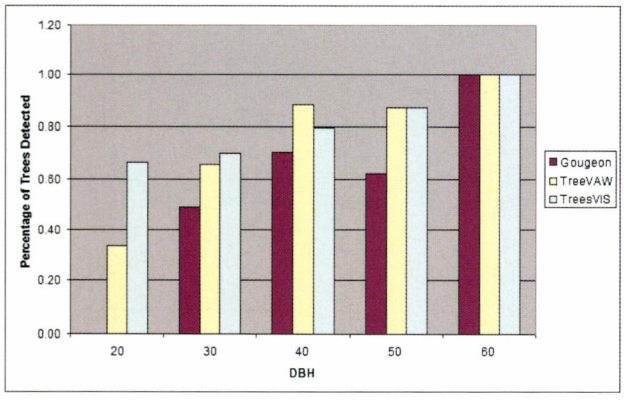

Fig. 6 Individual tree crown delineation with each method in all plots distributed by diameter classes.

estimated by each algorithm compared to field observations (area in colour). Accordingly, TreesVIS seem to over predict the number of trees with small diameters with the partition of larger crowns into a lot of spurious trees. TreeVAW also seem to concentrate predictions on low diameter classes while under predicting larger diameters ostensibly. Gougeon's method, on the contrary, seems to approximate better stand structure despite the number of predicted trees is much lower than the other two methods.

The number of trees detected by each method inside the 10×10m plots was 58% with Gougeon, 75% with TreesVIS and 76% with TreeVAW. The performance of the models by diameter classes showed a general decrease with the smallest trees. Trees with diameter classes above 40cm were accurately detected more than 80% of the time with TreeVAW and TreesVIS. On the contrary, the general performance of the Gougeon method barely reached 60% in the best case. The three models detected all trees in the 60cm DBH class (Fig. 6).

The Estimation of Individual Tree Height and DBH

The estimations of height and stem diameter at individual tree level with each algorithm were compared to field observations for all detected trees in the 10×10m plots.

Individual tree height was estimated with a RMSE (%) of 1.93m (8.12%), 2.40m (10.05%) and 2.29m (9.46%) using TreeVAW, TreesVIS and Gougeon respectively with $P << 0.001$ (See Table 7). Overall, there were no substantial differences between the three algorithms. All the models showed similar bias, underestimating tree heights between a 1.18m and 1.59m. There were no important differences between dominance status, diameter classes or observed height in the field in the distribution of the residuals. However, differences between the trends, depicted by each linear model, and the one-to-one relationship suggest that underestimations seem to increase towards the tallest trees.

TreeVAW showed a slightly better performance in all plots except plot 1, which presented the highest tree density and where the algorithm by Gougeon worked better. The discrepancies between observed and predicted values (R^2) seemed to be higher in TreesVIS (see Fig. 7 to 9).

The algorithm by Gougeon was found to be the most effective for estimating DBH with a RMSE of 6.15cm (18.798%) followed by TreeVAW with a RMSE of 7.28cm (22.82%) and TreesVIS with a RMSE of 7.67m (24.19%), all with $P << 0.001$ (See Table 8). All the algorithms generally underestimated DBH in all classes, especially in the largest diameter classes, where the negative trend seem to increase compared to the one-to-one relationship (see Fig. 7 to 9). The distribution of residuals did not infer any error pattern related to dominance status or diameter classes.

Table 7 Individual Tree Height estimation with each method.

	Observations	Average Height (m)	RMSE (m)	RMSE (%)	Mean difference (BIAS) (m)
TreeVAW	79	23.82	1.93	8.12%	−1.18
TreesVIS	80	23.91	2.40	10.05%	−1.45
Gougeon	61	24.19	2.29	9.46%	−1.59

Table 8 Individual DBH estimation with each method.

	Observations	Average DBH (m)	RMSE (m)	RMSE (%)	Mean differences (BIAS) (m)
TreeVAW	79	26.97	7.28	22.82%	−4.95
TreesVIS	80	26.84	7.67	24.19%	−4.86
Gougeon	61	29.43	6.15	18.79%	−3.31

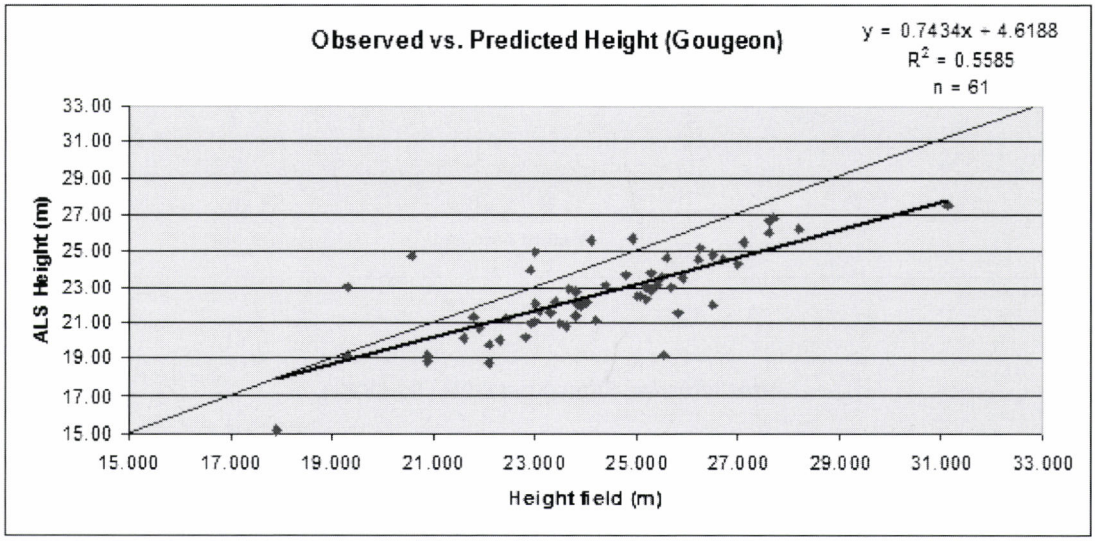

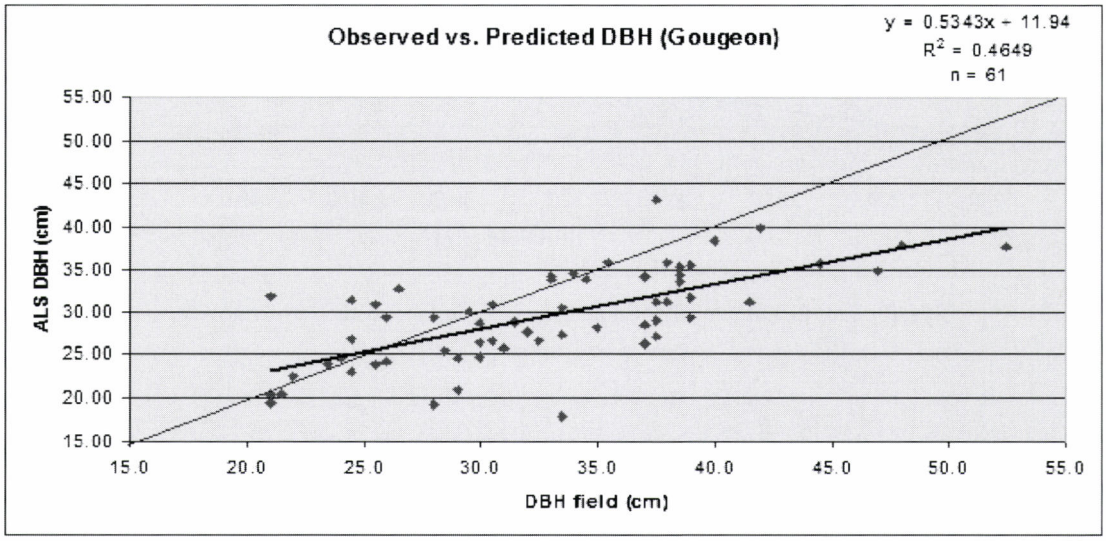

Fig. 7 Tree height and DBH estimations following the method by Gougeon.

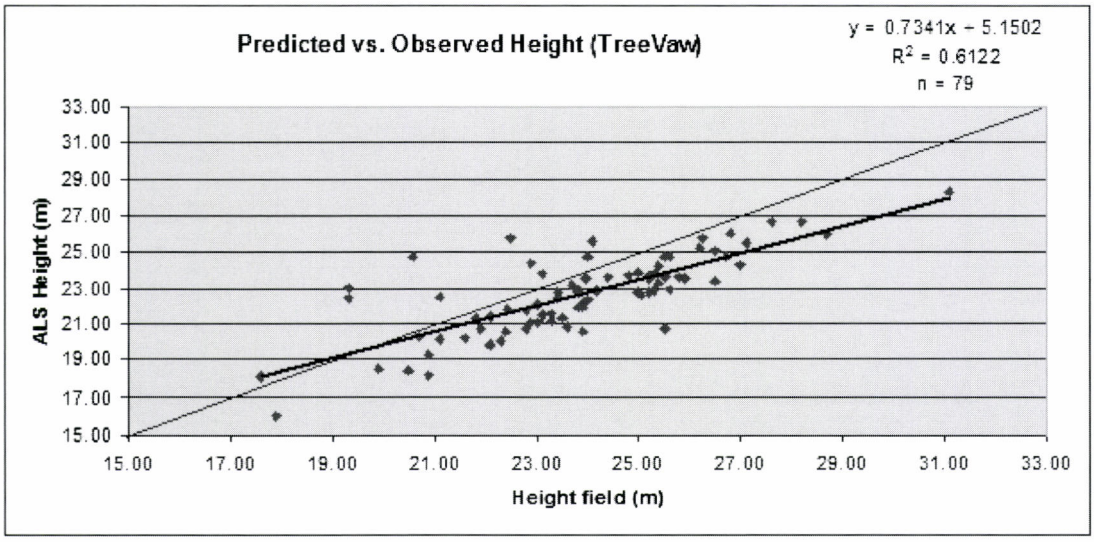

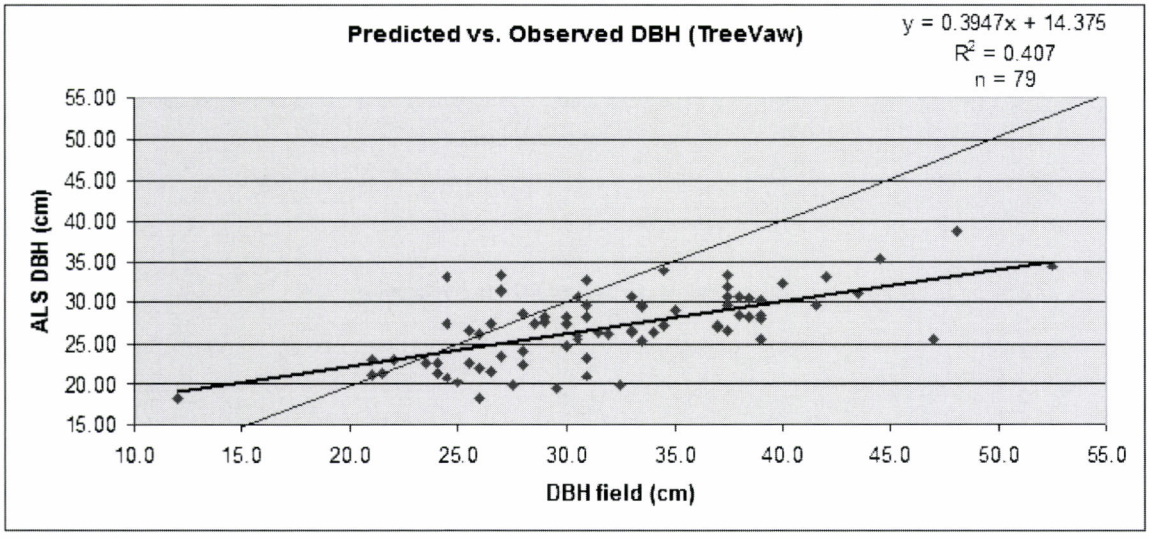

Fig. 8 Tree height and DBH estimations following the method by TreeVAW.

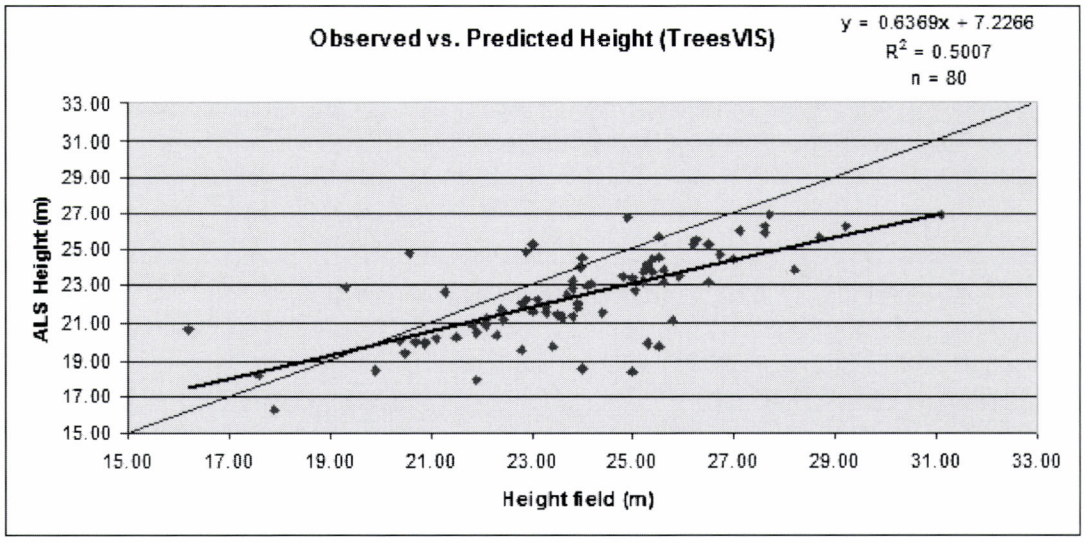

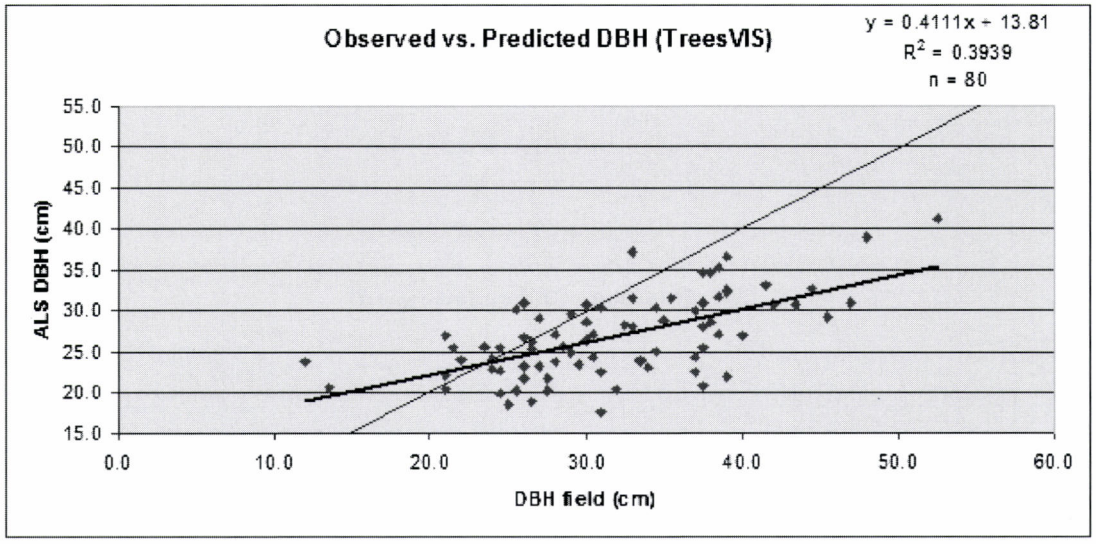

Fig. 9 Tree height and DBH estimations following the method by TreesVIS.

Running ForestGALES with Tree Lists

Tree lists were generated for all plots with the Tree Height and DBH parameters derived from the three algorithms. The ForestGALES model outputs the Critical Wind Speed (CWS) and the probabilities for both Overturning and Breakage. Likewise, the model was also run with the data obtained in the field for the 10×10m plots for a comparative analysis of the results (Fig. 10 to 12).

Overall, the three algorithms seemed to underpredict the CWS for Overturning and Breakage for trees above 30-35 cm. On the contrary, smaller trees below this threshold showed over predicted CWSs. The larger discrepancies were observed in the TreesVIS model, whereas Gougeon was more adjusted although with less number of trees detected. R^2 were generally low in all simulations, especially for tree breakage. The Gougeon method obtained better results than the other models for Overturning and Breakage.

The distribution of errors is plotted in Fig. 13. Gougeon showed a slightly better performance than the other models that were very similar to each other in their predictions for both Overturning and Breakage. These two models, in addition, showed the largest discrepancies with error values reaching $\pm 15 ms^{-1}$. The error distribution by diameter classes did not show any difference at all in each algorithm.

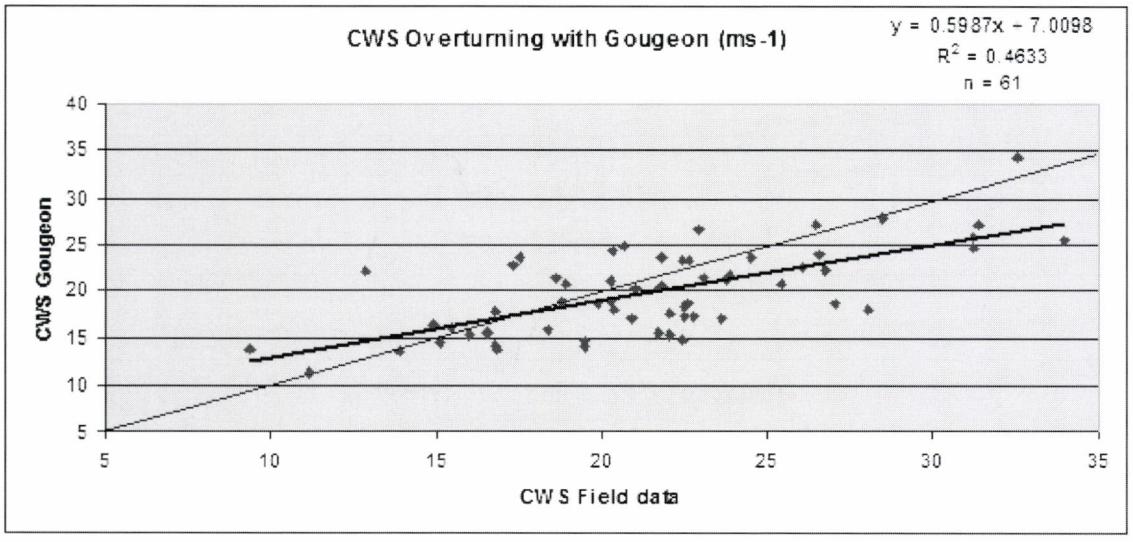

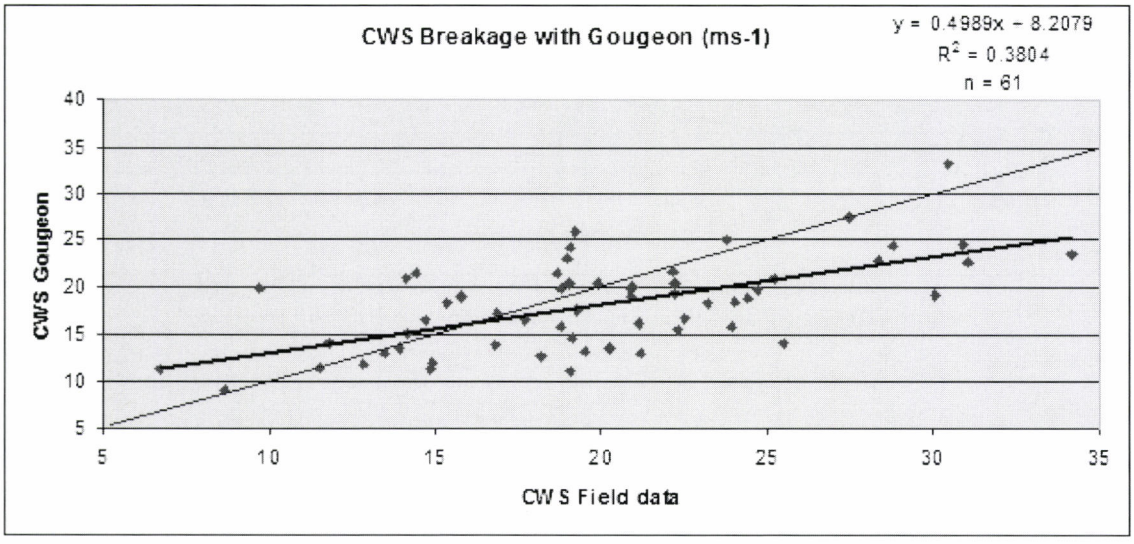

Fig. 10 Critical Wind Speeds for Overturning and Breakage estimated by Gougeon.

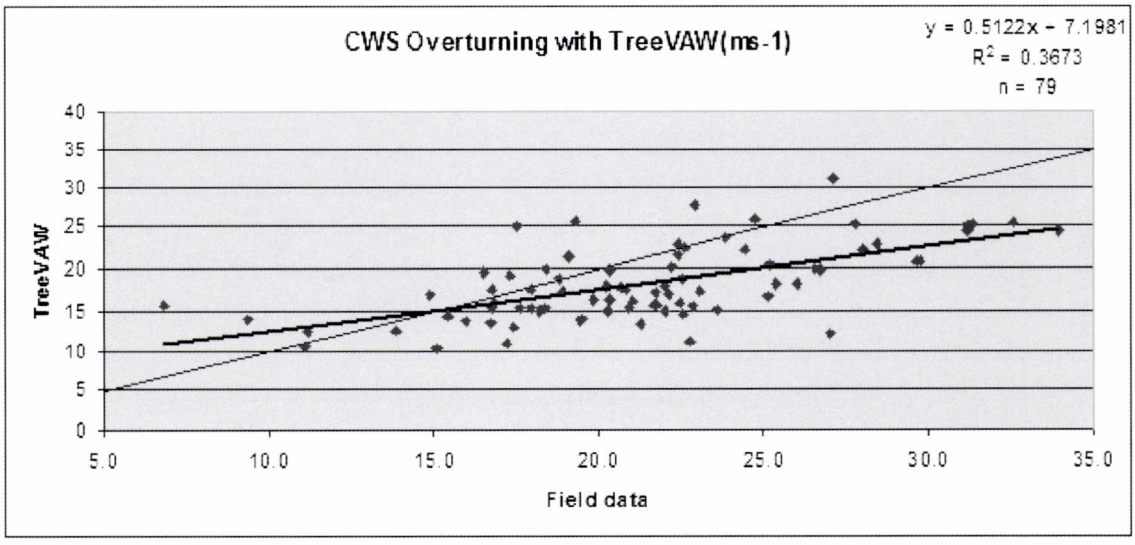

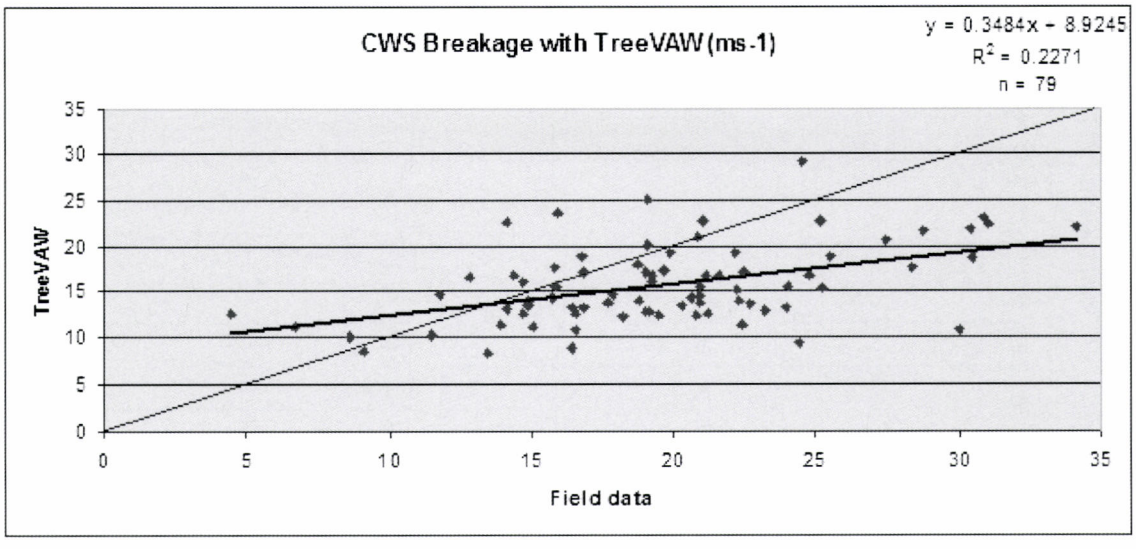

Fig. 11 Critical Wind Speeds for Overturning and Breakage estimated by TreeVAW.

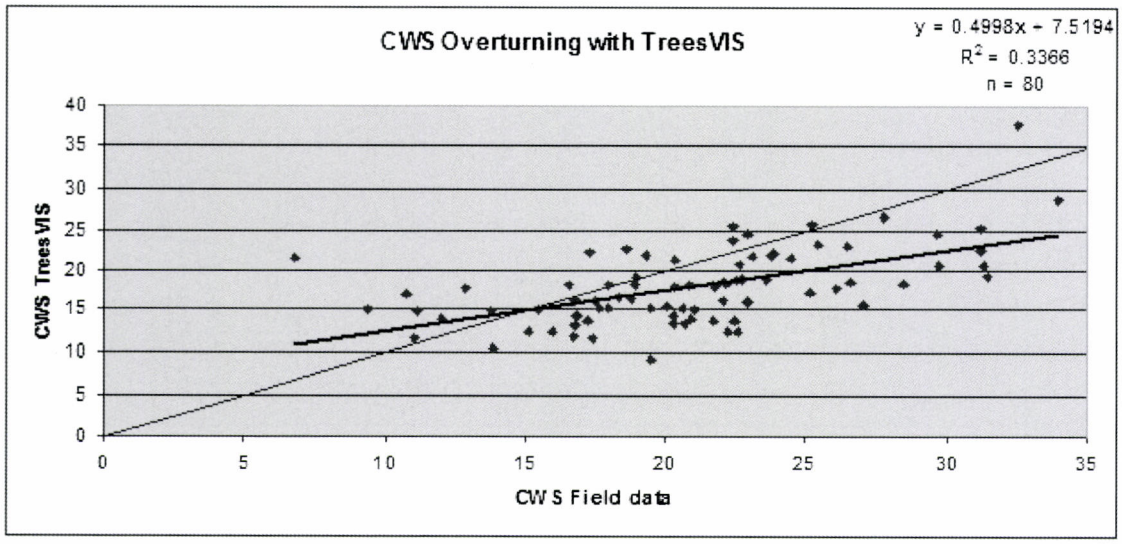

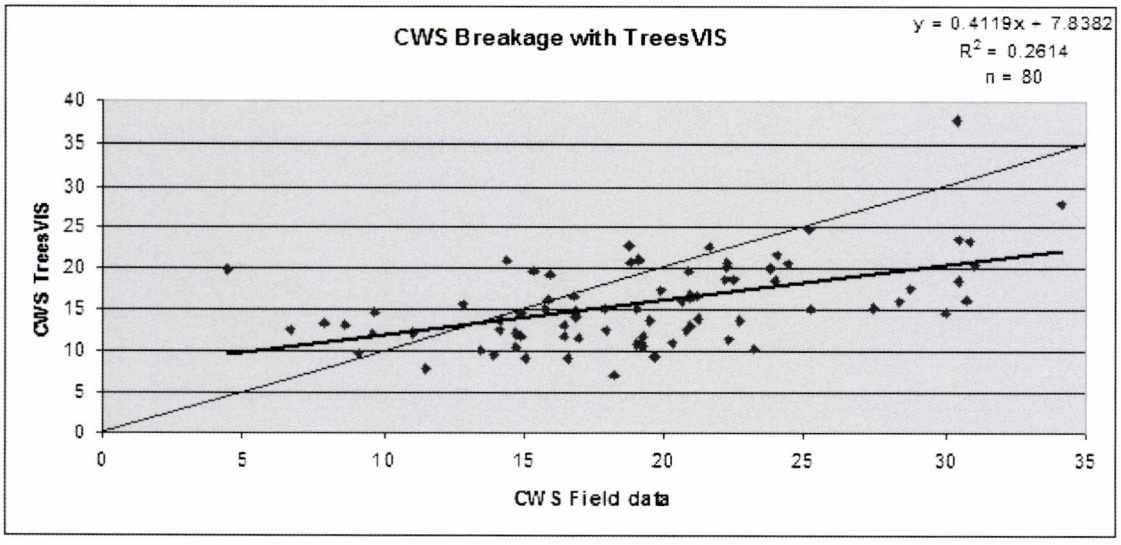

Fig. 12 Critical Wind Speeds for Overturning and Breakage estimated by TreesVIS.

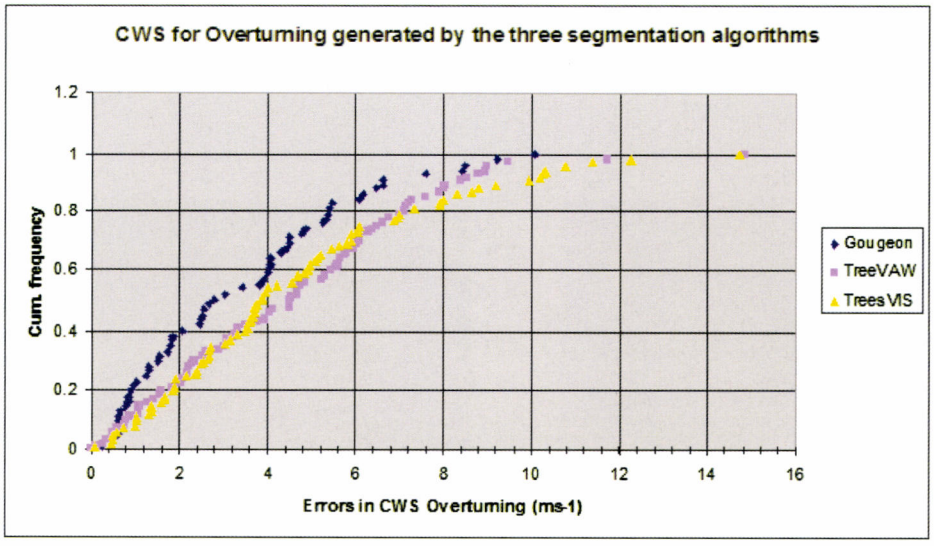

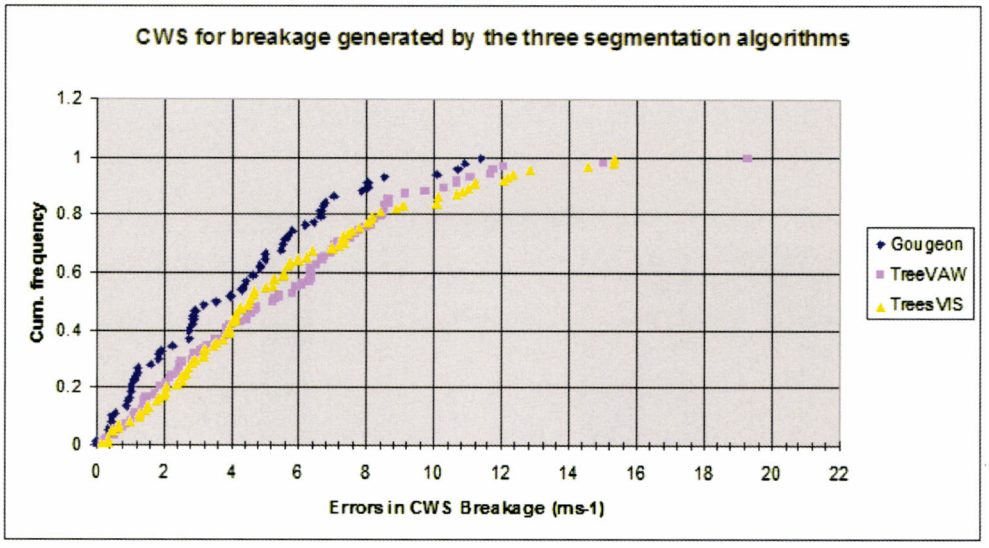

Fig. 13 Cumulative distribution of errors in the predictions of CWS for Overturning and Breakage estimated by the three models. Values expressed in $\pm$ ms^{-1}.

The Spatial Distribution of the Probability of Wind Damage

A Tree Height and DBH recovery model was derived for the three algorithms using the inverse regression models found in Fig. 7 to 9. These models were used to predict height and DBH values in the control plot (Plot 6) to generate a spatial distribution of CWSs (Fig. 14) and Return Periods for damage (Fig. 15). The use of the recovery models allowed a better fit between different diameter and height distributions, especially for the larger trees where the three models presented large underpredictions.

The spatial distribution of CWS for overturning in plot 6 is represented in Fig. 14, where the location of individual trees and crown dimensions are overlaid on top of a surface model generated from the CWS in ms^{-1} required for overturning each individual tree. The comparison between the average CWSs for overturning and breakage showed that TreesVIS provided more accurate estimations than the other two methods at stand level (Table 9). Instead, Gougeon and TreeVAW had differences between 1.2 and 1.5ms^{-1}. However, the spatial distribution of CWS in Fig. 14 showed that the results observed in TreesVIS presented large structural

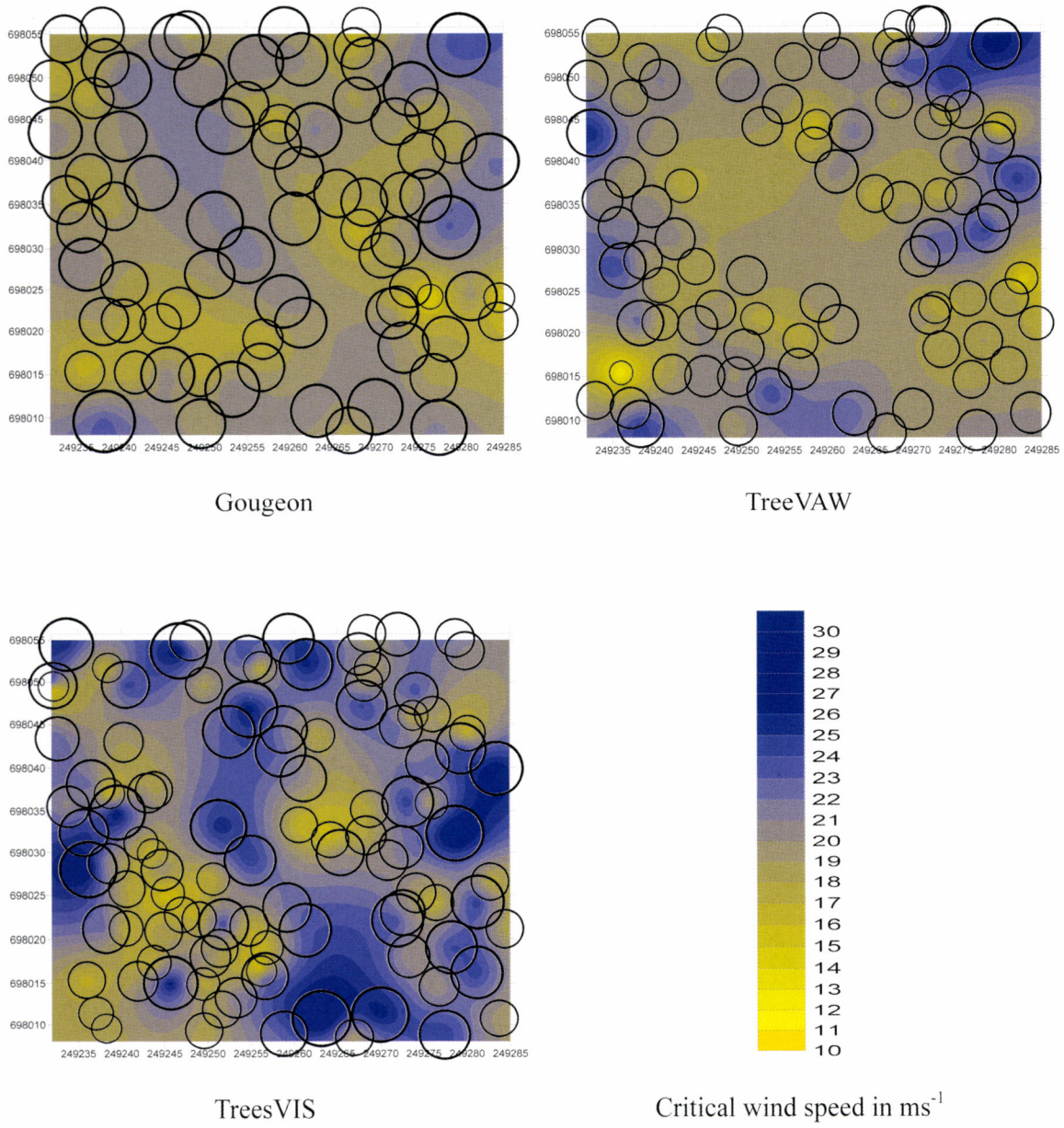

Fig. 14 CWS for Overturning as estimated by Gougeon, TreeVAW and TreesVIS models respectively. Individual crowns are represented by circles at a map scale and positioned in X and Y. Values expressed in ms^{-1}.

discrepancies, were areas that concentrated highly stable trees surrounded pockets of large instability. As a result, it seemed that default and excess errors tended to cancel each other more effectively with this model than with the other two, where the transition between stable and instable trees appeared to be smoother.

Table 9 Average CWS for overturning and breakage observed in the field and estimated by each algorithm (in ms^{-1}).

	CWS Over	CWS Break	Diff Over	Diff Break
Field	19.9	20.1	-	-
Gougeon	18.6	17.3	-1.3	-2.8
TreeVAW	18.8	17.8	-1.1	-2.3
TreesVIS	20.3	20.4	0.4	0.3

The comparisons between observations and estimations at tree level derived from the trees inside the small plots proved inconclusive for all models. The three algorithms showed similar patterns of underprediction of CWS in the larger trees and overprediction for the smaller trees (Fig. 15). Again, TreesVIS presented the largest extremes in both over prediction and under prediction observed in Fig. 14.

The distribution of risk in the three models indicates that the smaller canopies are most likely to reach unstable conditions due to lower taper values. The three models seemed to agree that more than 50% of the stand has a CWS value below $20ms^{-1}$, regarded as a stability threshold. The RMSE of predictions compared to observations in the field

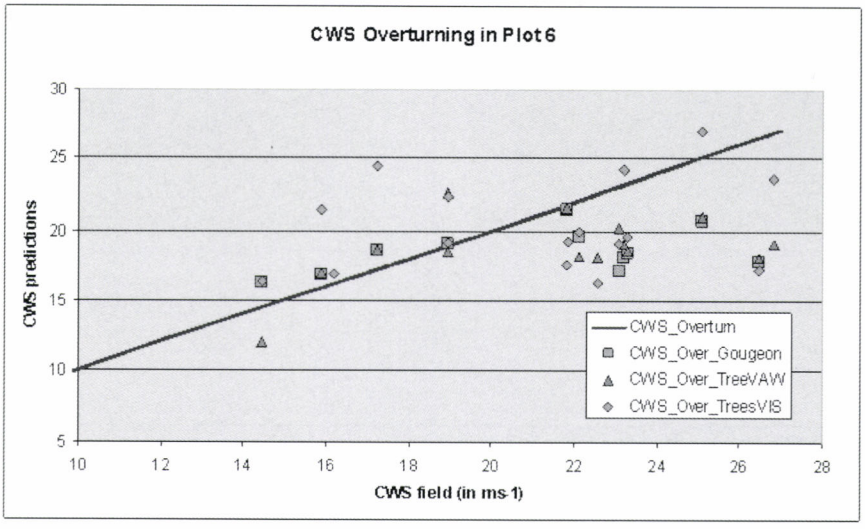

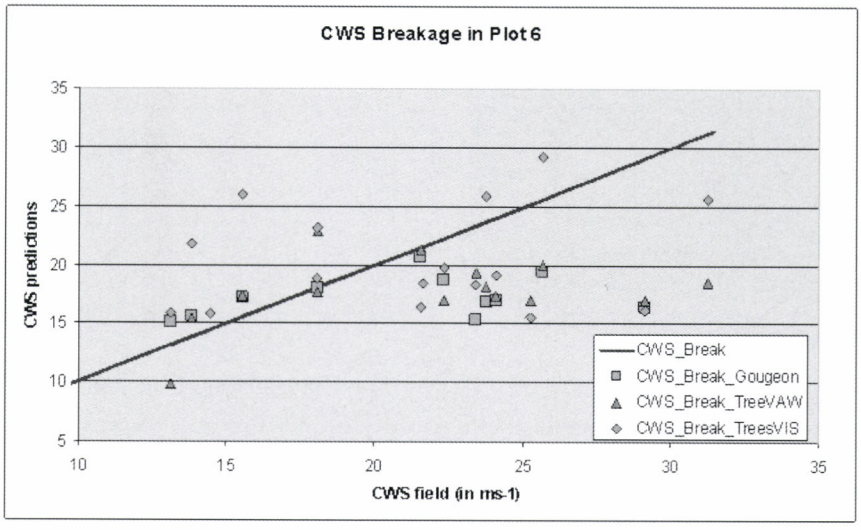

Fig. 15 CWS for Overturning and Breakage as estimated by the three algorithms compared to field measurements. Values expressed in ms^{-1}.

showed similar values (4.78ms^{-1} for Gougeon, 4.19ms^{-1} for TreeVAW and 4.11ms^{-1} for TreesVIS).

The comparison of the CWS for creating damage to the annual probability of reaching this critical value, extracted from the Weibull distribution of mean wind speed values, produced a map showing the return period for damage in Plot 6 (Fig. 15). The spatial distribution of the return period for damage (expressed in years) produced some degree of clustering in areas with trees with small diameter classes. This effect was more evident in TreesVIS, which tended to estimate more small diameter classes than the other two models.

The CWS for Breakage (not depicted in the document) followed similar spatial patterns as the ones described for Overturning. However, values were generally lower than for

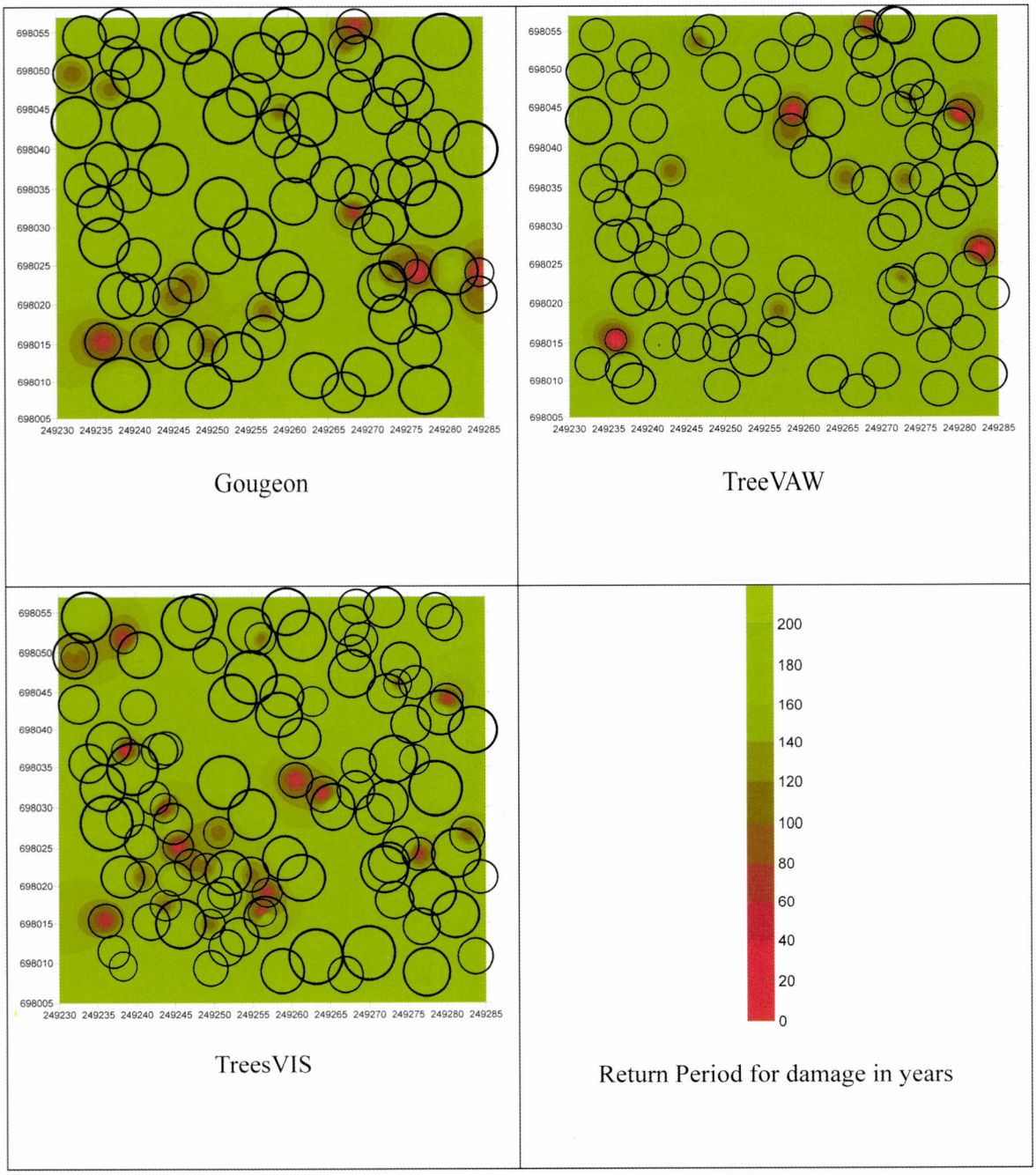

Fig. 16 Return Periods for Overturning (values expressed in years) as estimated by Gougeon, TreeVAW and TreesVIS models respectively. Individual crowns are represented by circles at a map scale and positioned in X and Y.

Table 10 Percentage distribution of the return periods for Overturning with each method aggregated by risk status classes. The Risk Status classes in ForestGALES calculate the average return period between winds strong enough to cause wind damage.

Risk Status	Probability	Return Period	Gougeon	TreeVAW	TreesVIS
1	<0.01	>100 years	78.5	85.1	78.8
2	0.01 - 0.02	50 - 100 years	15.2	9.2	9.6
3	0.02 - 0.03	33 - 50 years	3.8	2.3	7.7
4	0.03 - 0.05	20 - 33 years	2.5	2.3	3.8
5	0.05 - 0.10	10 - 20 years	0.0	1.1	0.0
6	>0.10	<10 years	0.0	0.0	0.0

Overturning. The fact that this stand is growing in a stable soil type (Brown earth) and the general underprediction of stem diameters observed in all models has created slightly lower CWS values for breakage in this simulation.

At stand level, TreeVAW presented a slightly more stable stand structure than the other two algorithms (Table 10). The return periods for damage grouped into the six risk status classes described in ForestGALES presented a more stable stand structure in TreeVAW with 85.1% of the stand in a risk status 1 class (representing a single storm in more than 100 years that is likely to create wind damage within the actual structure).

Field measurements inside the 3 10×10m plots revealed 70% of the trees in the most stable class, whereas TreeVAW estimated 85%, Gougeon was 72% and TreesVIS was 75%. The results for breakage at tree level showed a similar trend to the one described for CWS and a good proportion of trees that were in risk status 1 for overturning, now moved to risk status 2.

DISCUSSION

The comparative analysis of the three algorithms produced dissimilar results in terms of tree detection and canopy delineations. Gougeon's method produced the lowest number of canopy delineations in all the 9 stands. This algorithm, originally developed for tree counting and species classification using optical images, aggregated individual tree canopies into large segments that often grouped several crowns. Gougeon's method differed from the other two in their initial approach. The method was based on the searching for the lowest points between crowns. TreeVAW, instead, relied on a detection of tree top and a search algorithm for canopy boundaries based on allometric relationships between canopy dimensions and tree height. TreesVIS, also relied on tree top detection first and a search in all directions for the lowest limits of each canopy.

Having analysed the results produced by the three algorithms, the TreeVAW method was considered the most reliable method for canopy detection by en large. Despite TreesVIS using initially a similar approach to TreeVAW for the initial detection of tree tops, the smoothing of the NDCM with the 3×3 kernel was found to be more effective in TreeVAW for removing spurious tops than in TreesVIS.

Fig. 5 also revealed an interesting detachment between numbers of detected trees and stand structure. In this case, Gougeon's method seemed to be more in-tune with field observations than the other two methods. Both TreeVAW and TreesVIS over predicted the number of trees with smaller diameters, providing therefore a biased view of stand structure. This observation led to the conclusion that without the linking process that allowed us to associate crown delineations to real trees observed in the field, it was very difficult to gauge the operational advantages of TreeVAW or TreesVIS for mapping forest stand structures.

Fig. 5 exposed another interesting piece of information. The estimations of DBH produced by TreesVIS were similar to the predictions of Gougeon for larger trees. Somehow, the method of looking for the boundaries between canopies in those two methods proved more useful than the method implemented in TreeVAW. This draws us to the conclusion that substantial improvements in TreesVIS, in terms of tree top detection using an smoothing kernel similar to TreeVAW, can render better results in the future by eliminating noise associated to the construction of NDCM using spatial interpolation methods. Secondly, the use of allometric relationships in TreeVAW has to be revisited. Despite the fact that these relationships were constructed using information derived from permanent sample plots in the country and tuned to estimated yield class in the field, they proved limited by the fact that the plots were located in areas previously thinned. The influence of management regimes over these forest stands proved to be a dynamic factor that current models could not take into account. Finally, Gougeon's method also proved its limitations with small diameter classes. Those trees were aggregated to neighbouring crowns because they could not gather enough laser returns to produce 3-D structures with clear boundaries. These limitations were exposed in Fig. 6 with a smaller percentage of tree detections in lower diameter classes compared to the other two algorithms.

However, not all the blame had to be imposed on each method. The linking process revealed a positive correlation

between tree dimensions and its probability of being detected by any of the three methods. In LiDAR surveys, currently small canopies tend to be confused with the neighbouring ones. On the contrary, dominant and co-dominant individuals normally receive more laser hits than the smallest trees, which allow them to be more easily detected by any canopy detection algorithm. Some authors like NAESSET (1997) or MAGNUSSEN *et al.* (1999) point out the need to receive at least 6-10 returns per individual tree if a three dimensional structure is to be detected. Likewise, narrow scanning angles of less than 10 degrees help to reduce the shadowing effects of large trees over the smallest ones, increasing the probability of detecting more individuals. In our case, a scanning angle of 20 degrees seemed to limit the possibilities of being able to differentiate small tree canopies.

The estimation of DBH using a relationship between height and canopy dimensions is also problematic in the Sitka spruce stands. First of all, as already pointed out, these stands had been previously thinned which limited the validity of current models to estimate parameters hidden to ALS such as DBH. Secondly, we must consider the fact that small footprint laser scanning cannot penetrate deep into the forest canopy. The best laser returns can do is to retrieve the boundary between neighbouring tree canopies, ignoring that Sitka spruce branches can grow sideways well under the interlocking point between two crowns. This is more evident in larger trees were the linear trends seemed to depart even further in proportion from observations in the field (see DBH estimations in Fig. 7 to 9).

The estimation of individual tree parameters in detected trees such as height and diameter did not show important differences between the three algorithms. TreeVAW produced slightly better results for tree height whereas Gougeon did the same for DBH. In general, all the models consistently under predicted height and diameter values. In ALS surveys, laser returns normally hit the lowest parts of the tree crowns missing 99% of the time the apices, which produce a normal underestimation of 7-8% of the true tree tops. The fact that some heights appeared overestimated in some trees normally of medium to small dimensions may be explained by its proximity to parts of the crowns of larger trees.

The distribution of the residuals around each regression model presented the largest discrepancies in the small and medium size trees (Fig. 7 to 9). R^2 did not confirm substantial differences between the three methods in both height and DBH. TreeVAW produced a slightly better estimation of heights, whereas Gougeon, not surprisingly, manifested minor achievements in the predictions of DBH due to larger crown dimensions of the delineated polygons.

The use of tree lists generated from ALS in ForestGALES proved very useful at stand level. Despite the discrepancies in both excess and default, overall the three methods achieved similar predictions of CWS and return periods for both overturning and breakage. The best predictions were achieved with TreesVIS in the control plot using the recovery models for height and DBH derived from Fig. 7 to 9. However, the spatial analysis of the results obtained with this method verified large differences in the spatial distribution of CWSs. In this respect, evidence also gathered from Fig. 5 depicting the estimation of diameter distribution inside large plots and the minimal differences obtained in the predictions of height at individual tree level, appeared to indicate that perhaps Gougeon's method was the most reliable method of the lot.

However, this assumption could not be validated with the comparison of predictions of CWS and risk status at tree level with the observed values in the field. The comparison, possibly due to being limited to the few tree measurements collected in this plot, did not conclude a superior performance of any particular method. Quite the opposite, it showed once more that the large discrepancies observed with the TreesVIS method just managed to approximate results at stand level and did not provide a good insight into the influence of stand structure into the distribution of wind risk.

Fig. 14 and 15 presented different distributions of risk related to diverse estimations of stand structure. A common pattern was observed in all of them regarding the different role of dominance status in the distribution of wind risk. Large trees were more stable than small trees and presented higher CWS. Their favourable taper ratio made them more stable than trees with lower diameter to height relations. Also, it was found that the spatial distribution of both the CWSs and the return periods did not follow any evident clustering or inhibition process of the largest trees over the smallest. Perhaps, in the TreesVIS model it could be discerned some clustering of low CWS due to the partition of crowns into smaller individuals.

CONCLUSION

The estimation of structural parameters in forest stands such as number of individuals, DBH classes and height at tree level and its influence on tree stability, using three crown delineation algorithms on ALS data achieved good results at stand level but proved inconclusive at individual tree level.

Each model obtained partial good results when compared to the others. For instance, TreeVAW was better for estimating number of individuals and tree height. Gougeon achieved better results at modelling stand structure (diameter classes) and DBH at tree level. TreesVIS, seemed to offer better predictions of CWS required to overturn or break trees at stand level. However, none of them provided a valid indication of being able to map accurately enough the spatial distribution of tree parameters. These resulted in a confusing interpretation of the spatial distribution of wind risk in the control plot, which, at present, reduces the operational application of any canopy segmentation method.

However, the study evidenced the weaknesses and strengths of each method for future improvements. Canopy

delineations based on the location of boundaries between detected canopies seemed more effective than current allometric models in thinned forest stands. Nevertheless, this should not be the only parameter to be considered. The detection of tree tops, as proposed by TreesVIS and TreeVAW, should be a starting point in segmentation algorithms for detecting individual trees over which canopy dimensions can be associated to afterwards. At this point, TreesVIS seems a more viable option for the future.

Finally, future studies should aim at a more thorough understanding on the effects of different ALS flight configurations over the possibility of detecting individual trees and their dimensions. Most commercial configurations with low sampling density and wide scanning angles do not seem to be the optimal configuration for accurate measurements of individual tree parameters, despite their obvious advantages in terms of cost. A rigorous analysis of the effect of those flight parameters may determine cost-effective alternatives to common arrangements.

ACKNOWLEDGEMENTS

We would like to thank the Chief Executive Discretionary Fund, the Corporate Forest Services and to the European Regional Development Fund (ERDF) through the Interreg IIIB North Sea Programme STORMRISK project for the financial support that made possible this study. Also, we would like to thank the Edinburgh Earth Observatory for their enormous contribution in this work providing the expertise and the computing facilities to make possible the analysis of ALS data. Finally, we would like to thank the authors of the three algorithms tested in this study: Dr. Francois Gougeon that provided access to its ITC extension to PCI Geomatica and Geomatica Software to allowed us temporal access to their software; Dr. Sorin Popescu for his continuous advice and permission to use his method and Dr. Holger Weinacker and Prof. Barbara Koch for granting us access to TreesVIS and their support in the processing of the data.

LITERATURE CITED

BELL, P. D., QUINE, C. P. and WRIGHT, J. A., (1995): The use of digital terrain models to calculate windiness scores for the windthrow hazard classification. Scottish Forestry **49**(4): 217-225

EDWARDS, P. N. and CHRISTIE, J. M., (1981): Yield models for forest management. Forestry Commission Booklet **48**, Forestry Commission, Edinburgh

GARDINER, B. A., SUÁREZ, J. C., ACHIM, A., HALE, S. and NICOLL, B., (2004): 'ForestGALES 2.0. A PC-based wind risk model for British forests'. Forestry Commission publications. Edinburgh. ISBN 0855386320. 60 pp

GARDINER, B. A., PELTOLA., H. and KELLOMÄKI., (2000): Comparison of two methods for predicting the critical wind speed required to damage coniferous trees. Ecological Modelling **129**: 1-23

GOUGEON, F. A., (2005): 'The individual tree crown (ITC) suite.' Canadian Forest Service. Victoria, British Columbia, Canada

LECKIE, D., GOUGEON, F., HILL, D., ARMSTRONG, L. and SHREENAN, R., (2003): Combined high-density lidar and multispectral imagery for individual tree crown analysis. Canadian Journal of Remote Sensing **29**(5): 633-649

MAGNUSSEN, S., EGGERMONT, P. and LARICCIA, V. N., (1999): Recovering tree heights from airborne laser scanner data. Forest Science **45**: 407-422

NÆSSET, E., (1997): Determination of mean tree height of forest stands using airborne laser scanner data. ISPRS Journal of Photogrammetry and Remote Sensing **52**: 49-56

PERSSON, A., HOLMGREN, J. and SODERMAN, U., (2003): Detection, measurement, and species classification of individual trees for forest inventory and visualisation. (In Proceeding of the ScandLaser Scientific Workshop on Airborne Laser Scanning of Forests). Umea, Sweden: 223-234

POPESCU, S. C., (2006): TREEVAW (Tree Variable Window). http://www-ssl.tamu.edu/personnel/s_popescu/TreeVaW/. Last access: 18-02-2006

POPESCU, S. C., WYNNE, R. H. and NELSON, R. F., (2003): Measuring individual tree crown diameter with LiDAR and assessing its influence on estimating forest volume and biomass. Canadian journal of remote sensing **29**(5): 564-577

SOILLE, P., (1999): Morphological Image Analysis. Springer, Berlin, 316 pp

STACEY, G. R., BELCHER, R. E., WOOD, C. J. and GARDINER, B. A., (1994): Wind flows and forces in a model Spruce forest. Boundary-Layer Meteorology **69**: 311-334

SUÁREZ, J. C., DUNHAM, R. A., BARRETTE, J. and GARDINER, B. A., (2001): The Validation of ForestGALES. Forest Research Internal Report. 85 pp

SUÁREZ, J. C., ONTIVEROS, C., SMITH, S. and SNAPE, S., (2005): The use of airborne LiDAR and Aerial Photography in the estimation of individual tree heights in forestry. Computers and Geosciences **31**(2): 253-262

WEINACKER, H., KOCH, B., HEYDER, R. and WEINACKER, R., (2004): Development of filtering, segmentation and modelling modules for lidar and multispectral data as a fundament of an automatic forest inventory system. Proceedings of the ISPRS: Laser-Scanners for Forest and Landscape Assessment, Freiburg, Germany: 50-55

(Received 12 January 2007)
(Accepted 6 May 2007)

Article

Estimation of Biophysical Parameters of Individual Tree Stands derived from LiDAR and Digital Matrix Camera Image

Takahiro Endo[*1], Tatsuya Nawamura[*2], Hitoshi Taguchi[*1], Pranab Jyoti Baruah[*3], Masahiro Setojima[*4], Toru Katsura[*5] and Yoshifumi Yasuoka[*1]

ABSTRACT

The aim of this study is to examine the performance of a numerical ellipsoid modeling methodology to estimate tree structural characteristics in mixed forest using airborne Light Detection And Ranging (LiDAR) data along with airborne Digital Matrix Camera (DMC) image. In three-dimensional numerical analysis using points cloud of LiDAR data, ellipsoid model has the potential to simultaneously estimate tree top position, diameter and shape of individual tree crown. A Japanese cedar plantation with randomly mixed pine trees was chosen in this study as this type of forest, which is typical of Japanese cedar plantation in Japan. We developed a methodology consisting of both tree species classification and estimation of characteristics of tree structure with the followings steps: (1) classification of area of cedar and pine trees in the mixed plantation by using ortho-DMC image, (2) estimation of number of trees and estimation of tree top location in horizontal plane by standard ellipsoid model for each species, derived from Crown Height Model (CHM) and based on random selections of points clouds on each of the classified areas, (3) estimation of tree top height and realistic shape of individual tree by using a truncated cone shape model and LiDAR points cloud in respective classified areas. The study area is a cedar plantation forest in Northern Japan. LiDAR measurements with a density of 14.65 pulses/m^2 and DMC imagery with a spatial resolution of 10cm are used in this study For validation, ground truth data of tree species, geographic tree position and tree height were measured at the study site. The developed methodology could correctly identify a total of 73 out of 89 cedar trees in the areas classified as cedar, and 12 out of 29 pine trees in areas classified as pine. Validation of estimated tree height resulted in coefficient of determination (R^2) of 0.72 and 0.78 for pine and cedar respectively. This study indicates that fitting the ellipsoid model and the truncated cone shape model to LiDAR points cloud is able to simultaneously estimate tree top position, crown shape and diameter of individual tree crown.

Keywords: mixed forest, Japanese cedar, crown shape, ellipsoid model, truncated cone shape model.

INTRODUCTION

It is important to monitor and investigate forest attributes such as species, stand density, tree height, tree crown diameter and diameter-at-breast-height (DBH) for efficient forest management. Traditional forest inventory is very time-consuming and expensive. However, recently, high-resolution airborne laser scanning data and high spatial resolution multi-spectral image has been increasingly available and used for forest assessment and inventory. Previous studies have shown that number of trees, tree height and timber volume in specific area can be estimated by airborne laser scanning data. (NILSSON, 1996; NÆSSET, 1997; MEANS *et al.*, 2000; NÆSSET *et al.*,

Corresponding author: Takahiro Endo

[*1] Institute of Industrial Science, The University of Tokyo, Ce-508, 4-6-1 Komaba, Meguro-ku, Tokyo 153-8505 Japan

[*2] Central Japan Railway Campany, 2-1-85 Kounan, Minato-ku, Tokyo 108-8204 Japan

[*3] Integrated Research System for Sustainability Science (IR3S), The University of Tokyo, 7-3-1 Hongo, Bunkyo-ku, Tokyo 113-8654 Japan

[*4] Japan Association of Surveyors, Sokuryokaikan, 1-3-4 Koishikawa, Bunkyo-ku, Tokyo 112-0002 Japan

[*5] Mitsubishi Paper Mills Co. Ltd., 3-4-2, Marunouchi, Chiyoda-ku, Tokyo 100-0005 Japan

2001; NÆSSET, 2002; NÆSSET *et al.*, 2002; HYPPÄ *et al.*, 2001; PERSSON *et al.*, 2002; PATENAUDE *et al.*, 2004; TAKAHASHI *et al.*, 2004). However, most of the previous researches were in homogeneous forests or plantations. Heterogeneous forest consists of areas of different species which have to be classified correctly with appropriate methodology before estimation of biophysical variables of each species (POPESCU *et al.*, 2004; PERSSON *et al.*, 2004, HOLMGEN *et al.*, 2004).

In this study, we demonstrate a methodology to effectively detect the tree shape (crown shape), tree position as well species in a heterogeneous plantation for precise forest assessment and inventory. Tree shape is related to other biophysical variables, such as basal area, volume and dry biomass (NELSON, 1997), and is valuable for estimation of light condition on the forest floor as inputs to ecological models. Some previous studies have carried out reconstruction of crown shape in coniferous species. SHENG *et al.*, (2001) reconstructed conifer crown surface from high-resolution aerial images. HAYASHI *et al.*, (1997) carried out modeling of canopy structure of Sugi (*Cryptomeria japonica*) and Hinoki (*Chamaecyparis obtuse*) based on numerical simulation along with ground survey.

We took into consideration the fact that, point cloud of LiDAR data has the potential to reconstruct tree crown shape. Based on this fact, if one would find an appropriate model to approximate individual tree crowns from LiDAR points cloud, then tree top position and crown shape could be also be simultaneously estimated. In this study, we demonstrate an effective methodology to estimate tree structure variables, namely, tree top position, crown shape of individual trees in a mixed forest of Japanese cedar and Japanese red pine by synergetic use of LiDAR data and DMC imagery. To achieve our objective, classification of areas of individual species were done using DMC imagery and tree top position in horizontal plan was estimated using numerical ellipsoid model. Tree crown shape and height were extracted using a numerical truncated cone shape model.

MATERIALS

Study Area

The study area is a plantation forest managed by Mitsubishi Paper Mills Co., Ltd. The area is located in north of Honshu Island, Japan (lat. 40°39' N, long. 141°5' E). The ground elevation is between 190-240m above sea level. The dominant tree species are Japanese cedar (*Cryptomeria japonica*) and Japanese red pine (*Pinus densiflora*). Mixing rate of cedar and pine in the area is about 75.4% and 24.6% respectively according to field sampling. Thus, the forest is a cedar plantation with randomly mixed pine trees. Fig. 1 shows site location and Fig. 2 shows an example of DMC image subset of the study area.

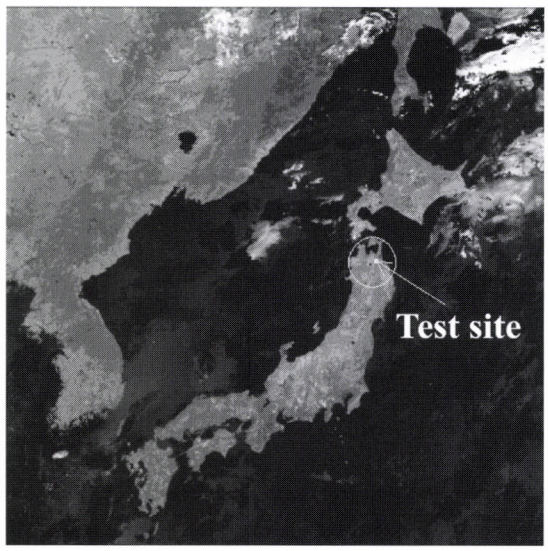

Fig. 1 Site location at northern part of Honshu Island, Japan

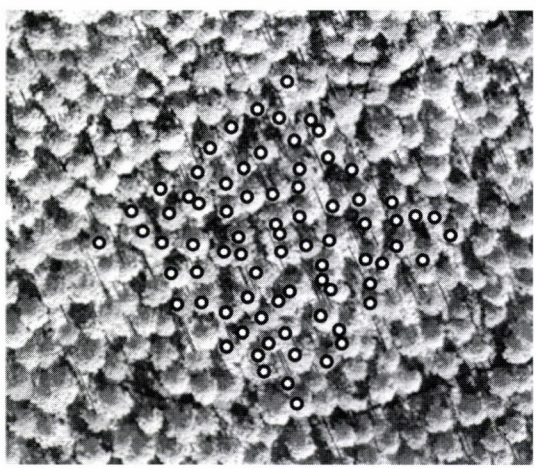

Fig. 2 A DMC image subset of the study area
Black circle stands for geographic position of tree from field survey.

Digital Matrix Camera and LiDAR Data

DMC imagery and LiDAR data for the study area was acquired under relatively clear skies. The DMC is an aerial sensor using CCD array. The main camera body is assembled with four high-resolution panchromatic camera heads and four multi-spectral camera heads. Output image size of panchromatic and color images are 7,000×4,000 and 3,000×2,000 pixels, respectively. In a DMC imagery, integration of arrayed CCDs, the global positioning system, a gyro and an inertial navigation unit contributes to increased accuracy of photogrammetric measurements. DMC data was acquired on 11th August, 2004 with a 60% overlapping and side lapping.

The spatial resolution at the ground level was 0.1 meter. LiDAR data was acquired on 11th and 12th August, 2004 using an airborne laser scanner at a cruising speed of 110kt and at a height of 1,830meters. Scan rate, pulse rate and scanning width were 39.0Hz, 46.0kHz, and 647meters respectively. Average footprint size was 0.47meters. The scanner was ALS50, a product of Leica Geosystems, that has horizontal accuracy and vertical accuracy of + 30cm and + 15cm respectively. The average density of laser reflection was 14.65 pulses per square meters.

Field Data

A field survey was conducted in the first week of August 2004. Precise geographic position of every tree top was measured using a GPS (DL4, NovAtel inc.) and a beacon receiver (MBX-3S, CSI Wireless) for differential GPS positioning. Height of individual trees was acquired with a portable laser measurement device (LaserAe300, MDL). DBH and tree species for all trees were recorded. Table 1 shows the characteristic of the study plot.

Table 1 Characteristics of study plot

Area (ha)	0.16
Number of trees	118
Number of trees per hectare	732
Year of planting	1955
Average tree height (m)	21
Average DBH (cm)	26.5

METHODOLOGY

The methodology to estimate tree species, crown shape, tree height and tree top position consisted of three major steps: (1) pre-processing of LiDAR and DMC raw data, (2) classification of areas of each specie by using DMC ortho-image, (3) creating standard ellipsoid models for cedar and pine derived from CHM, (4) fitting each of the standard models to CHM at corresponding classified areas in order to identify individual tree top position in horizontal plane, and finally (5) fitting a truncated cone shape model to points cloud at the estimated tree top position in horizontal plane in order to estimate tree top height and crown shape. The procedure developed for determination of tree shape is summarized in Fig. 3. The methodology consisted of following detail steps: (1) Digital Surface Model (DSM) of 1.0m grid, Digital Elevation Model (DEM) of 1.0m grid and CHM of 1.0m grid were created from the smoothed LiDAR data by nearest neighbor method, (2) DMC raw data was orthorectified by using DSM and collinearity equation, (3) pine and cedar areas in the orthorectified DMC image were extracted by unsupervised classification, (4) standard ellipsoid models suitable for each species were created from CHM based on random sampling at corresponding classified areas, (5) CHM and the classified image were overlaid, and individual CHM data corresponding to each species was identified, (6) individual tree top positions in horizontal plane for pine in pine areas were estimated by correlation between the standard ellipsoid model and CHM, (7) crown shape and tree height of pine at the estimated tree top position in horizontal plane were calculated by truncated cone shape model (Fig. 5), (8) individual tree top positions in horizontal plane for cedar in cedar areas were estimated by correlation between the standard ellipsoid model and CHM, and finally, (9) tree shape and height at the estimated tree top

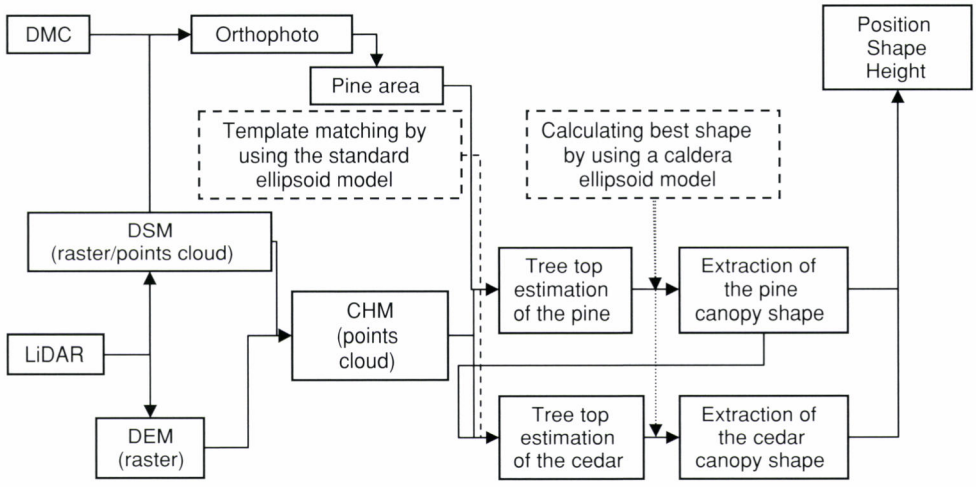

Fig. 3 Flow chart describing the estimation of tree shape from LiDAR and DMC raw data

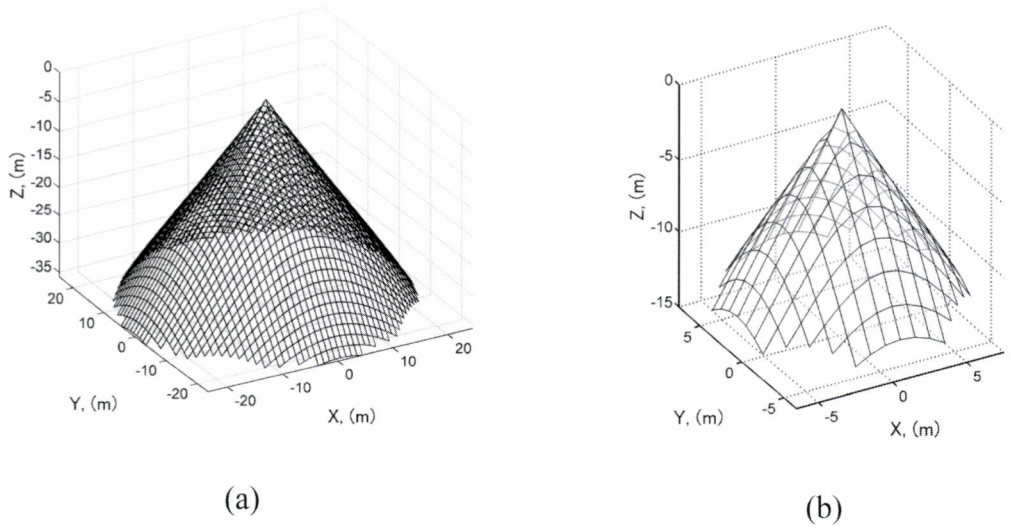

Fig. 4 The standard ellipsoid models for pine (a) and cedar (b)

position in horizontal plane were calculated by a truncated cone shape model.

Orthophoto Image

DMC image was used for classification of species in this study. DMC raw image can discriminate small objects with its high spatial resolution of 10cm. However, DMC imagery is strongly affected by terrain relief which is one of the distortions. In this study, ground control points for geometric correction could not be used, because of closed canopy and scarcity of open space in our site. In view of this situation, ortho-rectified DMC image was mapped to LiDAR imagery as LiDAR had a reliable positional accuracy. The methodology employed in registration is technically similar to PERSSON *et al.*, (2004), except the fact that, PERSSON *et al.*, (2004) mapped LiDAR imagery to DMC imagery.

Numerical Ellipsoid Model

Tree crown of conifer was represented as an ellipsoid model after SHENG et al., (2001). An ellipsoid model is shown in Eq. 1.

$$\frac{(Z+ch-cz)^{cc}}{ch^{cc}}+\frac{((X-X_t)^2+(Y+Y_t^2))^{cc/2}}{cw^{cc}}=1 \qquad (1)$$
$$cz-ch \le Z \le cz$$

where, (X_t, Y_t) is the 2-D coordinates of the crown top, cz is tree height, (X, Y, Z) is a point on the crown surface, cw is crown width, ch is the crown height, and cc is crown curvature.

Classification of Tree Species and Estimation of Tree Top Position in Horizontal Plane

Classification between cedar and pine area and estimation of individual tree top position in horizontal plane were carried out by the following steps. As a first step, the cedar and pine areas in the orthorectified DMC image were classified by an unsupervised classification method. The pine areas, which had higher radiance than the cedar, could be easily visually interpreted and this interpretation was used for validation of classification. In second step, tree top positions in horizontal plane for pine in pine area were calculated using correlation between CHM and the standard ellipsoid model. Correlation map was calculated by the standard ellipsoid model at all pixels of CHM corresponding to the classified pine area. The location of pixels with high correlation became tree top positions in horizontal plane of the individual pine trees. Similarly, tree top positions in horizontal plane for cedar were estimated for cedar areas using the methodology in second step above.

Fig. 4 shows the standard ellipsoid models of pine and cedar, respectively. In standard ellipsoid model, tree crown shapes were defined with, cw=4.9m, ch=3.6m, cc=1.0 for pine, and cw=1.5m, ch=1.3m, cc=1.0 for cedar (Fig. 4), which were based on random sampling in CHM in individual species and validated using ground truth data.

Identifying Optimum Tree Shape by a Truncated Cone Shape Model

LiDAR points generally didn't fall on the true crown top and points cloud around tree top generally had an irregular distribution. Due to this fact, in this study, we used a truncated cone shape model to effectively approximate the tree shape

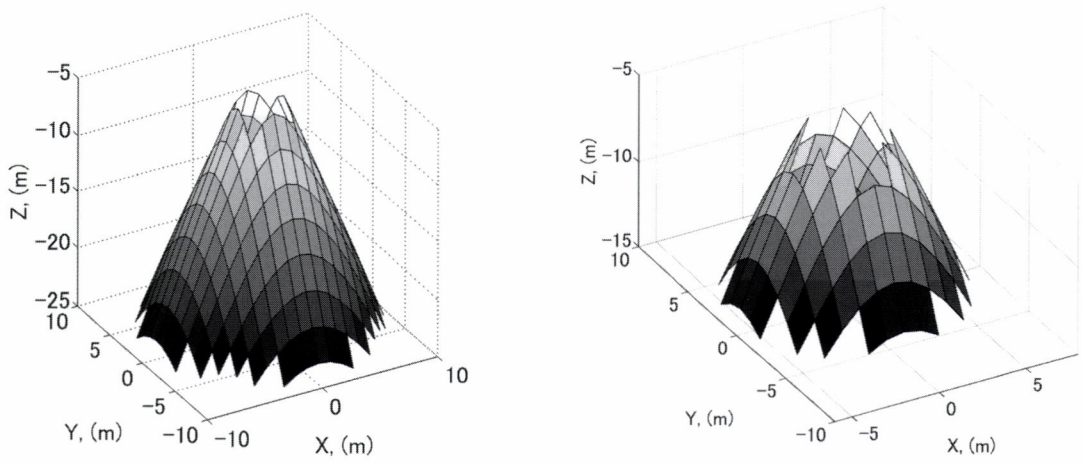

(a) (b)

Fig. 5 The truncated cone shape model of pine (a) and cedar (b)

and tree top position in vertical plane. Fig. 5 shows a sample of a truncated cone shape model.

Fitting accuracy was evaluated by standard deviation (S.D.) between the model and points cloud of individual tree. The model could avoid the effect of irregular distribution of points cloud around tree top area. Overall accuracy of the method was validated based on tree height only since we didn't have any data on crown surface owing to the difficulty of such measurement.

We carried out the search for the optimum tree shape in following way: after the estimation of tree top position in horizontal plane, optimum crown shapes were determined by an optimum combination of *cw* and *cz*, by varying *cw* at 0.2 intervals from 1.5 to 4.5m for pine and 1.1 to 2.9m for cedar, and by varying *cz* at 0.3m intervals from 0 to 0.6m for both species. Here in Equation (1), *ch* was fixed at 2.5m and *cc* was fixed at 1.0 for pine, and *ch* was fixed at 1.5m and *cc* was fixed at 1.0 for cedar. This was done in order to remove the upper 2.5m and 1.5m of tree crown in pine and cedar canopies respectively.

RESULTS AND DISCUSSION

The tree extraction results for each species are shown in Fig. 6, Fig. 7 and Table 2. The center positions of gray circles in Fig. 6 stands for estimated individual tree top positions and the size of a circle represents the diameter of estimated crown shape. The × and + marks show cedar and pine geographic positions by GPS measurement, respectively. The number of correctly indentified trees was 12 out of 29 and 73 out of 89 for pine and cedar respectively, resulting in an identification accuracy of 41% and 82% for pine and cedar respectively. At the same time, the methodology erroneously identified 14 pine trees as cedars. This is probably because those pine trees were of small sizes, but the algorithm required them to have bigger crowns to be correctly extracted. Regarding the trees not extracted at all, it might be due to their lower heights compared to the surrounding trees. Another reason might be the high density causing nearby crowns to pose as one crown in LiDAR points cloud. A total of 3 pine and 16 cedar trees could not be detected at all by the methodology.

The estimated tree heights of both species were validated with ground truth data for evaluating the usefulness of the truncated cone shape model. The scatter plot between the estimated height and the measured height is shown in Fig. 8. The coefficient of determination (R^2) for pine and cedar were 0.72 and 0.78 respectively. The estimated height was underestimated for both species. However, we concluded that, the truncated cone shape model was not responsible for the underestimation and it was a valid choice. This conclusion is based on the fact that, the relationship between the estimated and the measured height was linear. We inferred that, the underestimation was due to overestimation of DEM, which was confirmed from comparison of estimated DEM with measured ground elevation DEM from DGPS. In case of a closed canopy forest like the one in our study area, an accurate DEM was practically difficult to achieve and accuracy improvement would have needed a more robust interpolation methodology.

To solve the remaining problems in this study, future works will focus on an improved classification method from DMC imagery, improved DEM generation and improved extraction of crown shape from LiDAR data by the truncated cone shape model. Contextual analysis used for classification may increase the accuracy, since spatial resolution of DMC imagery is quite high. In case of a closed canopy forest, DEM with higher accuracy is needed for the methodology. Here, the extracted crown shape could be regarded as the closest

possible representative conical shape of the real tree crown, as in reality tree crowns were edgy with irregular shapes. Thus, a truncated cone shape model modified to more closely represent a real tree shape would increase the overall accuracy.

Structural variables derived from more realistic tree shapes estimated from LiDAR data, would be useful not only for forest research but also for various other numerical prediction model.

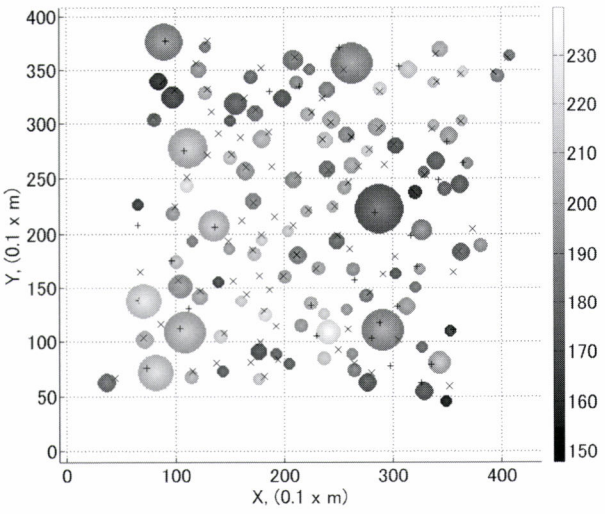

Fig. 6 Estimation of tree top poison, tree height and crown diameter of pine and cedar
× and + marks show cedar and pine geographic positions by GPS measurement.

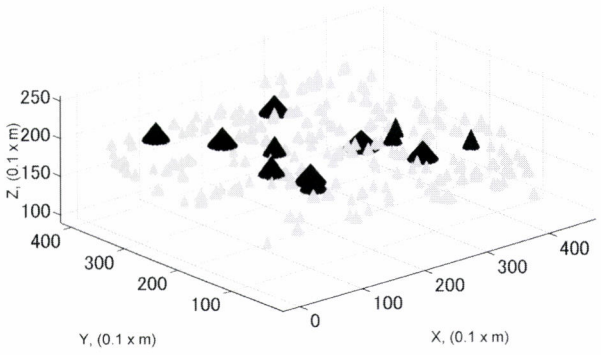

Fig. 7 Bird view eye of estimation of tree top position and crown shape of cedar and pine
Black and gray color conical shapes are pine and cedar.

Table 2 Classification accuracy of pine and cedar by using each standard ellipsoid model

	Matching process for cine	Matching process for cedar	Total	Ground truth	Non detected
Classified pine area	12 (41%)	14 (48%)	26 (90%)	29	3
Classified cedar area	0 (0%)	73 (82%)	73 (73%)	89	16

unit: number (percentage)

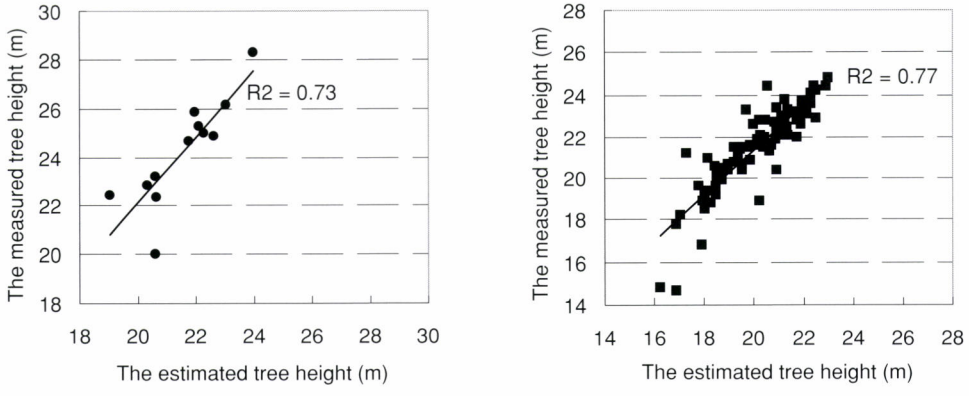

(a) (b)

Fig. 8 Comparison between the measured tree height and the estimated tree height. (a) stands for pine and (b) stands for cedar

CONCLUSIONS

In this study, a new methodology was examined for simultaneous estimation of tree structural variables derived from tree crown shape in a high density and mixed forest area with two species from DMC and LiDAR data. Classification of areas with pine and cedar trees was done using DMC imagery and unsupervised classification. Through the standard ellipsoid model fitting to CHM in corresponding classified areas of cedar and pine, each tree top position in horizontal plane was estimated. It was possible to estimate crown shape and tree height of cedar and pine by a truncated cone shape model fitting technique. As the relationship between the estimated and the measured height for cedar and pine was linear, we concluded the fitted models to be valid. The underestimation in tree height was inferred to be primarily due to overestimated DEM used in this study. Our study demonstrated that, forest structural variables along with crown shapes in a complex mixed forest canopy could be estimated effectively by synergetic use of LiDAR and multi-spectral high-resolution imagery. However, there are few remaining solvable problems in the methodology. One way to improve the overall accuracy could be adopting contextual analysis classification of areas of each species. Estimation accuracy of tree height and crown shape could be improved by using a DEM with higher accuracy and modification of the truncated cone shape model for more realistic representation of the crown shape.

LITERATURE CITED

HAYASHI, S. and TAKAHASHI, Y., (1997): On the modeling of tree's figure - case of *Cryptomeria japonica* and *Chamaecyparis obtuse* -. J. Jpn. For. Soc. **79**(4): 222-228

HOLMGEN, J. and PERSSON, Å., (2004): Identifying species of individual trees using airborne laser scanner. REMOTE SENS. ENVIRON. **90**: 415-423.

HYYPPÄ, J., KELLE, O., LEHIKOINEN, M. and INKINEN, M., (2001): A segmentation-based method to retrieve stem volume estimates from 3-d tree height models produced by laser scanners. IEEE Transactions on Geoscience and Remote Sensing **39**: 969-975

KOUKOULAS, S. and BLACKBURN, G.A., (2005): Mapping individual tree location, height and species in broadleaved deciduous forest using airborne LIDAR and multi-spectral remotely sensed data. International Journal of Remote Sensing **26**(3): 431-455

MEANS, J.E., ACKER, S.A., FITT, B.J., RENSLOW, M, EMERSON, L. and HENDRIX, C.J., (2000): Predictiong forest strand characteristics with airborne scanning lidar. Photogrammetric Engineering and Remote Sensing **66**(11): 1367-1371

NÆSSET, E., (1997): Estimating timber volume of forest stands using airborne laser scanner data. Remote Sens. Environ. **61**: 246-253

NÆSSET, E., (2002): Predicting forest stands characteristics with airborne scanning laser using a practical two-stage procedure and field data. Remote Sens. Environ. **80**: 88-99

NÆSSET, E. and BJERKNES, K-O., (2001): Estimating tree heights and number of stem in young forest stands using airborne laser scanner data. Remote Sens. Environ. **78**: 328-340

NÆSSET, E. and ØKLAND, T., (2002): Estimating tree height and tree crown properties using airborne scanning laser in a boreal nature reserve. Remote Sens. Environ. **79**: 105-115

NELSON, R.,(1997): Modeling forest canopy heights: The effects of canopy shape. Remote Sens. Environ. **60**: 327-334

PATENAUDE, G., HILL, R.A., MILNE, R., GAVEAU, D.L.A., BRIGGS, B.B.J. and DAWSON, T.P., (2004): Quantifying forest above ground carbon content using lidar remote sensing. Remote Sens. Environ. **93**: 368-380

PERSSON, Å, HOLMGREN, J. and SÖDERMAN, U., (2002): Detecting and measuring individual trees using an airborne laser scanner. Photogrammetric Engineering and Remote Sensing **68**(9): 925-932

PERSSON, Å, HOLMGREN, J., SÖDERMAN, U. and OLSSON, H, (2004): Tree species classification of individual tree in Sweden by combining high resolution laser data with high resolution near infrared digital image. International Archives of Photogrammetry, Remote Sensing and Spatial Information Sciences **XXXVI - 8/W2**: 204-207

POPESCU, C.S. and WYNNE, R.H., (2004): Seeing the trees in the forest: Using lidar and multispectral data fusion with local filtering and variable window size for estimating tree height. Photogrammetric Engineering and Remote Sensing **70**(5): 589-604

SHENG, Y., GONG, P. and BLGING, G.S., (2001): Model-based conifer-crown surface reconstruction from high-resolution aerial images. Photogrammetric Engineering and Remote Sensing **67**(8): 957-965

TAKAHASHI, T., YAMAMOTO, K., SENDA, Y. and TSUZUKU, M., (2004): Estimating individual tree heights of sugi (*Criptomeria Japonica* D. Don) plantations in mountainous area using small-footprint airborne LiDAR. J. For Res. **10**: 135-142

(Received 12 January 2007)
(Accepted 14 November 2007)

Article

Quantifying Variances of Line-Intercept-Sampling Estimators of Percentage Cover

Kaiguang Zhao*1, Sorin Popescu*1 and Ross Nelson*2

ABSTRACT

The line-intercept sampling (LIS) method has found important applications in such areas as forest and wildlife, ecological and biological sciences, and crop and agriculture fields. LIS is a sampling technique to make observations along line transects in order to make inferences of area properties. The placement of transects can be chosen in many different manners, i.e., randomly or systematically. The motivation of this study is to use LIS to infer regional information of forestry biophysical parameters based on the linear transects measurements of a profiling LiDAR system. However, there is no optimum method to properly derive a reasonable measure to the uncertainty of LIS estimates. As such, the study first developed a theoretical framework to describe the LIS estimation in two settings, one with fixed landscape configuration, and another with random configuration. The subsequent simulation of transect observation is realized for two categorical maps: the artificial one simulated by SIMMAP, and the real one classified from Landsat ETM+ multispectral imagery. The simulated samples were used to test four estimators. The methodology employed in this study provides a good starting point for practically implementing the quantification of variance estimates with LIS.

Keywords: line-intercept sampling, line-intersect sampling, profiling LiDAR, estimator, Monte Carlo

INTRODUCTION

The line-intercept method is a quite effective sampling technique, and it has found extensive applications in natural resource disciplines, such as the characterization of landscape pattern and the inventory of forestry tracts. Instead of intensive sampling over the whole study area, Line-Intercept Sampling (LIS) only measure samples along linear transects; the placement of transects over study sites can be done either randomly or systematically, with fixed or varying length for each transect, or sometimes in a prescribed configuration. Basically, LIS is used to observe a region consisting of randomly distributed particles or items by only sampling the particles intercepted by transects. According to the settings of applications, the particles may represent different entities, i.e., shrubs, tree crowns, dens, lakes, plants, roads and signs, or patches in a landscape. The particles can be geometrically arbitrary-shaped. Many estimators have been developed so far to extend the line transect observation into the inference of area properties of particles, e.g., estimating the percentage cover of certain patch type based on the length proportion of transect intercepted with the given type of patch (KAISER, 1983; BUTLER and MCDONALD, 1983).

LIS technique has a long history and it can be roughly dated back as early as 1868 when CROFTON (1868) discussed the local probability of straight lines drawn at random in a plane. CANFIELD (1941) first successfully introduced this technique to sample range vegetation and employed the random placement of transects and used the proportion of the sampled transect intercepted by the vegetation as an estimate of the ratio of the vegetation area to the whole study area. BAUER (1943) then compared the relative efficiency of the transect and quadrate methods of sampling vegetation for statistical analysis based on a series of simulated plant communities of known composition, and he showed that the transect sampling gave more accurate results than quadrate methods in the cases he investigated. In 1953, MCINTYRE further developed the LIS technique by using line transects to

Corresponding author: Kaiguang Zhao
*1 Spatial Sciences Lab., Dept. of Forest Sciences, Texas A&M University, College Station, TX 77801, USA
*2 Biospheric Sciences Branch Code 614.4 NASA's Goddard Space Flight Center Greenbelt, Maryland USA 20771

estimate plant density, say, the number of plants (particles) per unit area. Later, WARREN and OLSEN (1964) proposed a LIS-based estimator for the volume of logging waste and documented the first use of LIS in forestry applications. Instead of naming it line-intercepting sampling, the authors coined it as line-intersect sampling. The unbiasedness of their estimator was proved to be true under certain assumptions later by VAN WAGNER (1968). The theoretical work by KAISER (1983) presented two generic estimators for LIS and his theory tended to unify all the LIS results up to that time. He used geometrical probabilities to prove the unbiasedness of the proposed estimators, and provided examples in which his estimators degenerated to the commonly known estimators. KAISER's paper (1983) proved to be one of the most appreciated works in the literature of LIS. Recently, extensive applications of LIS have been seen in such areas as forest and wildlife, ecological and biological sciences, and crop and agriculture fields (e.g., KELLER *et al.*,2004; KEANE *et al.*, 2005; NELSON *et al.*, 2005). Recent progress of LIS sampling theory can also be witnessed in the work of AFFLECK *et al.* (2005), among others.

With this study, the authors are interested in developing an on-the-fly portable airborne laser profiling system for forest inventory, based on an existing system called Portable Airborne Laser System (PALS) developed by NELSON *et al.* (2003). The proposed system is a profiling laser altimeter or LiDAR (Light Detection And ranging). A laser profiler usually emits laser pulses at near-nadir direction (without scanning) and collects the returned pulses. The round-trip travel time of the laser pulse can be converted to ranging information based on the speed of light. As shown in Fig. 1, the profiling LiDAR can measure the forest canopy height profiles along a transect (NELSON, 1984). The schematic in Fig. 1.a suggests that two profiles are involved to characterize the stand structure: the top one depicting the profile of top canopy surface, and the bottom one describing the terrain topography. Studies found that the forest stand characteristics and biophysical parameters can be derived from this profiling measurement (MACLEAN and KRABILL, 1986). Transects flown over a study site in Fig. 2 illustrate the basic idea on how a profiler collects samples and what the placement of transects looks like. Unlike most current commercially available scanning LiDAR systems capable of continuously sampling the study area (LEFSKY *et al.*, 2002; POPESCU *et al.*, 2002; POPESCU *et al.*, 2003), the proposed profiler can produce only data along transects which are typically almost parallel and 2-4km apart.

In order to infer information on the area-based variables, LIS needs to analyze the profiling transect data. However, before applying LIS, relevant information should be able to be extracted from profiler altimeter data along transects, preferably by some automatic data processing algorithms. These may include but not be limited to such algorithms as those for reconstructing ground topography, deriving canopy height profiles, and stratifying the canopy height profiles into segments with respect to the types of land cover. Central to

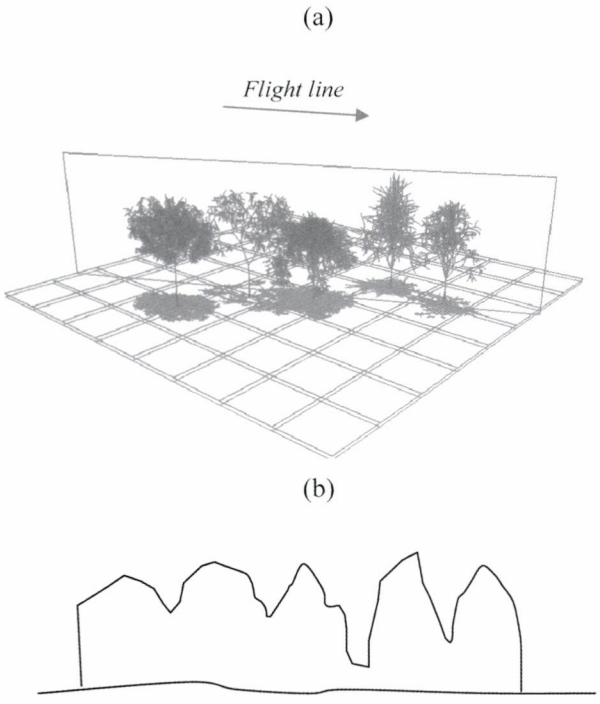

Fig. 1 An example of a forest canopy profile which might be obtained via a laser profiling instrument (see also Nelson et al., 1984)

Fig. 2 Parallel transects flown by a profiling LiDAR (profiler) over a study site: the dark lines are the flight lines of the laser profiler, the background is a false-color QuickBird image.

this study, the stratification of profiling transects is essentially important for the purpose of estimating percentage cover of each land cover. To achieve this, advanced signal processing techniques such as wavelet analysis is effective in designing automatic algorithms. No elaboration on these aspects is made in this paper, and details on the implementation of relevant algorithms is planned to appear in a future publication.

Airborne profiling measurements have been used to inventory forestry resources with LIS sampling techniques, particularly over large areas. NELSON *et al.* (2005) exploited the possibility of using over 1,300km of systematic profiling transect measurements acquired over the State of Delaware, USA, to do state-level multiple resources inventory by the LIS method, and their estimates of merchantable volume fell into the 21% of US forest service estimates at the county level , and 1% statewide. Total above-ground dry biomass estimates were within 22% of USFS estimates at the county level and with 16% statewide. They also used profiling measurements to estimate the area percentage of impervious and open water area for three counties of Delaware, and found that results were comparable to estimates from other sources. By using the same dataset, NELSON *et al.* (2005) again utilized the LIS method to help estimate the extent of Delmarva Squirrel Fox habitat. Their results have demonstrated the feasibility of profiling laser measurements for regional resources inventory. However, although their estimations are accurate enough to be comparable to the known estimates by other means, their report on the variance of the LIS estimates only provides an approximation to the true variance; also, they claimed that such estimated variance gives an upward conservative estimation of the true value (NELSON *et al.*, 2005).

Because the variance or standard error of an estimator is an indicator of the accuracy or, on the other hand, the uncertainty of the estimator; without good knowledge of the estimator variance, estimates will be less valuable. KAISER (1983) gave for his estimators a definition formula of the variance which includes two components, namely the variance term and the covariance term. He mentioned that even in simple cases the formula is mathematically intractable mostly due to the unknown form of the covariance component. He finally suggested obtaining a number (m) of independently and identically distributed estimates based on m independently chosen transects of certain length L, then pooling these m estimates by arithmetic averaging as a final estimate and taking the sample variance as the estimated variance. In terms of the intractability of the formula for covariance, DEVRIES (1986) had the same argument, and he offered a similar formula to evaluate the variance in the cases of varying transect length, where the length of transect is used as weighting in the calculation. NELSON *et al.* (2005) restated a successive difference estimator based on the study of LINDEBERG (1926); and he also envisioned relying on a large Monte Carlo experiment to obtain a valid estimate of the estimator's variance for the systematic airborne LiDAR samplings. As such, this paper attempts to investigate the uncertainty of LIS estimates by quantifying its variance, which will serve as a crucial step in appropriately analyzing and interpreting profiling LiDAR measurements.

Specifically, the paper will use both the computer-simulated landscape and the real land cover map classified from a Landsat ETM+ image to simulate transect observations in a systematic manner. From a series of simulated data, four estimators for cover percentage of certain patch type are tested and their variances are also constructed. The paper simplifies the demonstration by only considering a binary landscape, i.e., background and patches of interest for the computer-generated landscape, and forestry/non-forestry for the land cover map. Furthermore, for practical conveniences, the following discussion will term pixels of value 1 as forestry and 0 as non-forestry in both the artificial and real landscape maps. The results can be easily generalized to the multiple-type cases. Also, this paper formulates a theoretical framework to evaluate estimator variances under certain assumptions.

METHODS

Computer-simulated Landscape

A landscape simulation package SIMMAP, which implemented a modified random simulation method (SAURA and MARTÍNEZ-MILLÁN, 2000), was utilized to generate a categorical landscape map with 2 patch types and an extent of 900 × 900 pixels (Fig. 3). The default values for initial probability and neighborhood criteria were used, and the minimum patch size was set to 90 pixels. The forest cover percentage is the main metric of inference interest.

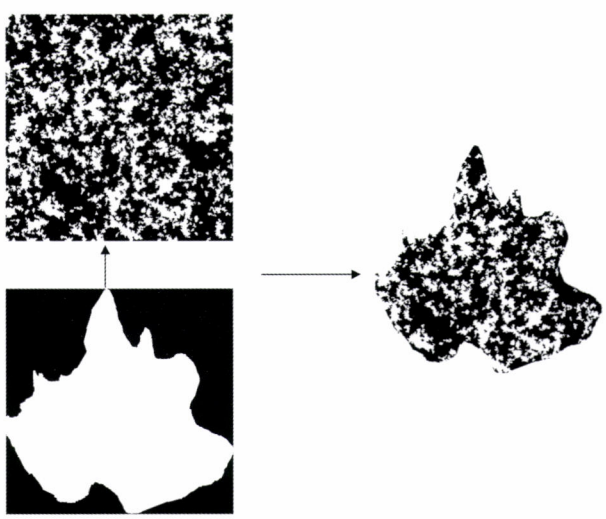

Fig. 3 The computer-generated categorical map and a mask of the boundary of study area, and the resulting landscape after applying the mask to the original square region.

Usually, the shape of the study region, i.e., a county or state, may be arbitrary. Hence, in order to mimic reality, a mask was arbitrarily delineated on-screen in ENVI (ITT Visual Information Solutions, Inc.) and used to clip out the region of interest, as shown in Fig. 3.

Classified Map From Remotely Sensed Data

A Landsat ETM+ multispectral image over Huntsville, East Texas, USA, was used for this study. The unsupervised ISO-DATA algorithm was used to classify the image into 7 classes, which were then grouped into two categories: forest and non-forest. Because the inference of interest does not depend on the exact type of classification and the absolute true value of relative to the real landscape is of no interest in this study, the step of accuracy assessment was ignored. Likewise, a mask was applied to discard the pixels out of a delineated boundary in order to mimic a natural shape of study area. The resulting map is depicted in Fig. 4.

Calculating the Total Area of a Given Class

To simplify the illustration, again it is assumed that the landscape contains only two categorical classes, i.e., non-forest and forest. The interest is in estimating the total forested area. In practice, when a profiler system is flown, the flight direction is typically set and fixed; the sampling transects are parallel and spaced almost equally. A coordinate system was chose such that the x axis is perpendicular to the direction of sampling transects and the y axis is selected as the tangent to the left-most boundary (Fig. 5). For a given transect at x, its length $l(x)$ is equal to the distance between the upper and lower boundary points connecting the transect, excluding the portion that may lie outside the study area, if any (i.e., the second transect from the left in Fig. 5); and the proportion of it intercepted by forest patches is denoted as $r(x)$. Note that a transect may intercept many patches. Then, the total area of all forest patches can be evaluated by:

$$a = \int_0^s r(x)\, l(x)\, dx \tag{1}$$

where s represents the span of study area along x axis.

To clarify notations, lowercase letters will denote variables or functions that are fixed or prescribed, while the uppercase is used to denote a random variable or function.

Estimators when the Configuration of Landscape is Fixed yet Unknown

Before investigating a study site, its extent is usually known by referring to archived data source, most likely a GIS database. In addition, suppose that the orientation of all sampling transects are the same and already determined. Typically, this is the case for the profiling LiDAR survey. Hence, $l(x)$ is known and can be calculated. However, the $r(x)$, which is the proportion of transect intercepted by the patches of a certain type, e.g., forest, is fixed for a given study site, but remains unknown to investigators. If the placement of transects is uniformly random over the x-direction span [0, s] and the property of $r(x)$ is unknown, the following estimator $\hat{a}_1$ can be effective:

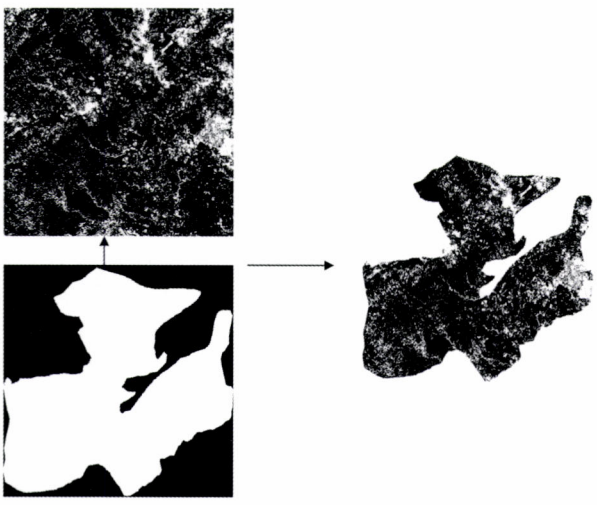

Fig. 4 The classified Landsat ETM+ image with two classes (green for forest and black for non-forest), and a mask of the study area boundary, and the resulting landscape after applying the mask to the original square region.

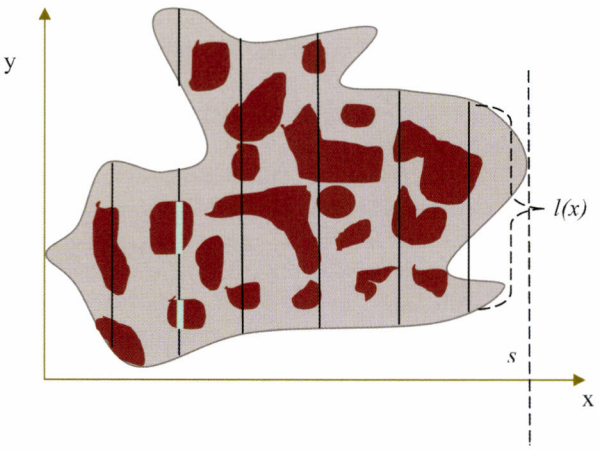

Fig. 5 A hypothetical region of study where the black solid lines are transects for LIS and will be used to infer information on the colored patches, i.e., the cover percentage. The transect at x touches the upper and lower boundary points of the region, and has a length of l(x); the transect intercepts with patches, and denote the proportion intercepted to its total length is r(x).

$$a = s\int_0^s r(x)\, l(x)\, \frac{1}{s}\, dx \Rightarrow \hat{a}_1 = s\,\frac{\sum_{i=1}^{n} r(x_i)\, l(x_i)}{n} \tag{2}$$

where n is the number of transects observed, and the variance is given as,

$$\begin{aligned} Var\,[\hat{a}_1] &= \frac{s^2}{n}\, Var_{\frac{1}{s}}[r(X)\, l(X)] \\ &= \frac{1}{n}\left[s\int r^2(x)\, l^2(x)\, dx - \left(\int r(x)\, l(x)\, dx\right)^2 \right] \end{aligned} \tag{3}$$

where $Var_{1/s}[r(X)l(X)]$ means the variance of $r(X)l(X)$ when assuming X is uniformly distributed, i.e., $X \sim 1/s$. Since the above variance formula requires evaluating $r(x)$ over [0, s], it cannot be used directly. Alternatively, the sample values of $r(x)$ at the observed transect should be substituted to calculate the sample variance of $r(x)l(x)$ as the estimated variance, that is,

$$\hat{Var}_{nm}[\hat{a}_1] \approx \frac{s^2\sum_{i=1}^{n}[r(x_i)\, l(x_i) - \overline{r(x)\, l(x)}]^2}{n(n-1)} \tag{4}$$

where $\overline{r(x)\, l(x)} = \sum[r(x_i)\, l(x_i)]/n$ is simply the sample mean.

Intuitively, the longer $l(x)$, the more contribution to the total area it is supposed to bring. Rather than being randomly placed, transects can be located by the probability of $l(x)/m$, where m is the total area of the whole study region. This means that there are more transects placed over x's with larger $l(x)$. According to such a design, a natural estimator should be,

$$a = m\int_0^s r(x)\frac{l(x)}{m}\, dx \Rightarrow \hat{a}_2 = m\,\frac{\sum_{i=1}^{n} r(x_i)}{n} \tag{5}$$

where m, again, is the total area of the whole landscape such that $m = \int_0^s l(x)\, dx$ and the corresponding variance will be,

$$\begin{aligned} Var\,[\hat{a}_2] &= \frac{m^2}{n}\, Var_{\frac{l(x)}{m}}[r(X)] \\ &= \frac{1}{n}\left[m\int r^2(x)\, l(x)\, dx - \left(\int r(x)\, l(x)\, dx\right)^2 \right] \end{aligned} \tag{6}$$

where $Var_{l(x)/m}[r(X)]$ is the variance of $r(X)$ by assuming $X \sim l(x)/m$. Similarly, the observed samples of r(x) can be used to obtain an approximation to the true variance, and it follows that,

$$\hat{Var}\,[\hat{a}_2] \approx \frac{m^2\sum_{i=1}^{n}[r(x_i) - \overline{r(x)}]^2}{n(n-1)} \tag{7}$$

Estimators when the Configuration of Landscape is Supposed to be Random

In contrast to the aforementioned setting, here the configuration, i.e., $r(x)$, is supposed to be an unknown yet random function of x and was denotes as $R(x)$. Consequently, the total area of forest cover (patch type of interest) is a random variable instead of an unknown constant. It can be computed by the counterpart to Eq. 1,

$$A = \int_0^s R(x)\, l(x) \Rightarrow \mu_A = E[A] = \int_0^s \mu_R(x)\, l(x)\, dx \tag{8}$$

where $\mu_R(x)$ is the mean function of $R(x)$, and in most cases may be not a constant function. Of particular note is that mathematically $R(x)$ cannot be a Gaussian random function because for any x, $R(x)$ is bounded over [0, 1]; however, for practical convenience, $R(x)$ may be approximately gaussian.

In this random setting of landscape configuration, the corresponding parameter of interest is $E[A]$, i.e., the mean of A. To simplify, assuming that $R(x)$ has a mean μ_R independent of x, the $E[A]$ and $Var[A]$ then can be obtained respectively by:

$$\mu_A = \mu_R\int_0^s l(x)\, dx = m\,\mu_R \tag{9}$$

$$Var\,(\mu_A) = \int_0^s\int_{-x_1}^{s-x_1} C_R(x)\, l(x+x_1)\, l(x_1)\, dx dx_1 \tag{10}$$

where $C_R(x)$ is the covariance function of $R(x)$, and Eq. 10 holds if and only if $R(x)$ is widely-sense stationary, which, in most cases, should not be too rigid a requirement. By further assuming the mean-ergodicity of $R(x)$, a reasonable estimator of μ_A can be expressed as,

$$\hat{\mu}_{A,1} = m\,\hat{\mu}_R = \frac{m\sum_{i=1}^{n} R(x_i)}{n} \tag{11}$$

and its variance is,

$$Var\,[\hat{\mu}_{A,1}] = \frac{m^2}{n^2}\, 1' \cdot \sum_R \cdot 1 \tag{12}$$

where again, m is the area of whole landscape, $R(x_i)$'s are the sampled value at n transects that can be either systematically or randomly placed; and Σ_R is the variance-covariance matrix of $R(x_i)$, and can be constructed from $C_R(x)$ which, for the (i,j) entry of Σ_R, gives $C_R(|x_i - x_j|)$. Unfortunately, the structure of $C_R(x)$ is usually unknown; therefore, in practice prior knowledge about $C_R(x)$ may be entailed.

Another estimator of μ_A is given in Eq. 11, and Eq. 12 is for the associated variance.

$$\hat{\mu}_{A,2} = s\,\frac{\sum_{i=1}^{n} R(x_i)\, l(x_i)}{n} \tag{13}$$

$$\begin{aligned} &Var\,[\hat{\mu}_{A,2}] \\ &= \frac{s^2}{n^2}[l(x_1), l(x_2), \ldots, l(x_n)]\sum_R [l(x_1), l(x_2), \ldots, l(x_n)]' \end{aligned} \tag{14}$$

The unbiasedness of $\hat{\mu}_{A,2}$ depends on both the properties of $R(x)$ and the sampling schemes of x_i. For instance, if $R(x)$ assumes a constant mean, $\hat{\mu}_{A,2}$ is unbiased when x_i's are randomly sampled; conversely, suppose that $\mu_R(x)$ is dependent on x, $\hat{\mu}_{A,2}$ is biased when transects are observed at fixed locations x_i's.

Simulation Schemes

First, systematic samples of transects, which are observed in a manner similar to the profiling LiDAR, are drawn randomly. The spacing between adjacent transects are purposely designed to be randomly distributed around the average spacing since the flight lines of profiling LiDAR are not exactly equally spaced. However, randomly sampled transects are employed to obtain more appropriate Monte Carlo estimates of uncertainty; specifically, for each of the computer-generated landscape and classified categorical map, a range of transect numbers are used; and at a given number of transects, 30 realizations are simulated. The sample variance of each 30 realizations is calculated to be compared with those obtained by the proposed variance formula.

RESULTS

The proportion of transects intercepted by forest patches, $r(x)$, is plotted against x in Fig. 6a and 6b respectively for the artificial landscape generated by computer and the real landscape created from ETM+ imagery. The curves suggested that in both cases, the $r(x)$ appears to be randomly fluctuating and there exists some spatial correlation to a certain degree as also shown in Fig. 7a and 7b which show the sample covariance function calculated from the corresponding $r(x)$'s. It is clearly seen that the correlation monotonically decreases as the lags increase. These two sample covariance functions were plugged as $C_R(x)$ into the formula in Eqs. 10, 12, and 14 developed above, to compute the sample variance of the estimators.

Fig. 8 shows the forest cover percentage estimated by four different estimators, at different choices of transect number. The forest cover percentage is simply the ratio of estimated forest area to the total area. The four estimators are respectively the one used by NELSON *et al.* (2005), and three of the four discussed above except the second one. They are respectively denoted by "Nelson" or "N", "a1", "A1" and "A2" as labeled in the legends of Fig. 8-11. The plotted values of estimates in Fig. 8 and 10 only represent one randomly selected realization out of 30. The true forest percentages are 0.3684 and 0.2281 for the simulated artificial and classified real landscape maps, respectively. In both cases, the estimated values tend to come closer to the true value as more transects are observed. Moreover, an overall trend of overestimation is observed for all the four estimators (Fig. 8a) in the case of simulated landscape, although occasionally the estimates are lower than the true value at some transect numbers, and the estimator of "N" and "A1" seem to consistently give the estimation closest to the true value. On the other hand, an opposite trend was noticed for the classified ETM+ image where overall, all four estimators were apt to underestimate the percentage cover.

A way of calculating estimator variance is to take the

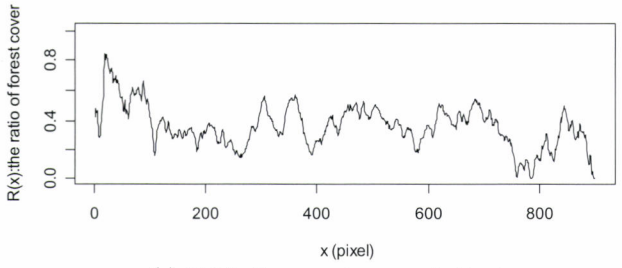

(a) R(x) for the computer-generated landscape

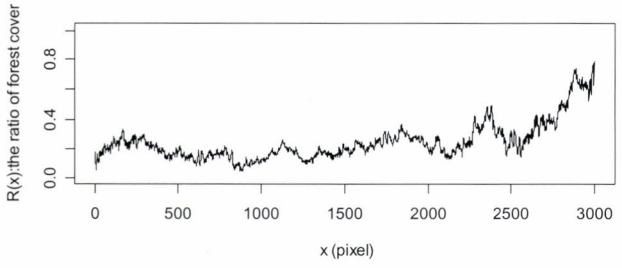

(b) R(x) for the classified Landsat ETM+ Image

Fig. 6 The proportion of transects intercepted by forest patches, $r(x)$, is plotted against x (pixels) in Fig. 5a and 5b respectively for the artificial landscape generated by computer and the real landscape created from ETM+ imagery.

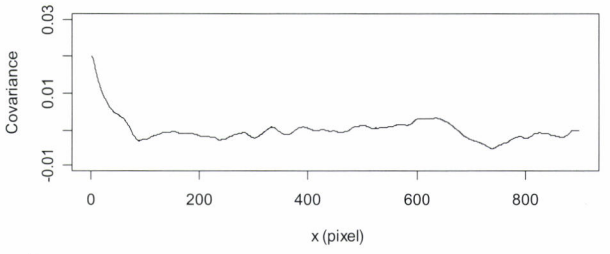

(a) Sample covariance function for the computer-generated landscape

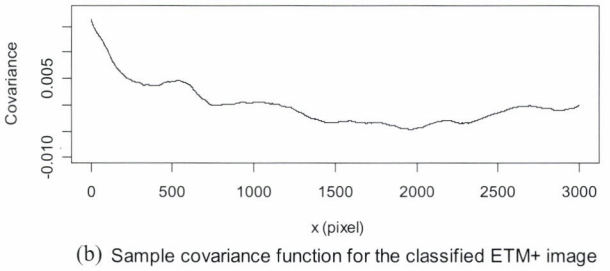

(b) Sample covariance function for the classified ETM+ image

Fig. 7 *The sample* covariance function calculated from the $r(x)$'s of Fig. 5, respectively for the artificial landscape (a), and the classified land cover map (b).

sample variance of 30 realizations. This is quite often employed in Monte Carlo simulation and supposed to offer a quite reasonable approximation to the true variance inherent in the sampling design. Fig. 9 suggests that for both landscapes the variances of four estimators almost coincide; but, to be more precise, for the simulated landscape, the estimated standard errors (SE) from the simulation with "Nelson" estimator is the lowest with "a1" and "A2" providing the highest estimates, while for the classified image, the estimated SE of "Nelson" and those of "a1" and "A2" are very close especially at a large number of transects. In addition, another way to calculate the estimator variance is to directly use the aforementioned formula which is derived under certain assumptions, with results given in Fig. 10. As with the Monte Carlo simulated estimates, the SEs calculated with variance formula appear to follow a similar trend except that "a1" and "A2" have different estimates due to the difference in assumptions. Moreover, in contrast to the decreasing variance with more transects for Nelson's estimator and a1, A1 and A2 exhibit an almost invariant pattern.

To further compare the two ways of computing variance, the ratio of the formula-derived SE to the estimates by Monte Carlo simulation is presented in Fig. 11. Assuming that the simulation-derived sample variance is a more reasonable estimate, the closer to 1 the ratio approaches, more valid the formula for variances is, or a more reasonable assumption is made as to $r(x)$. As shown in Fig. 11, the resulting plots reveal that in the case of simulated landscape, the ratios fluctuated

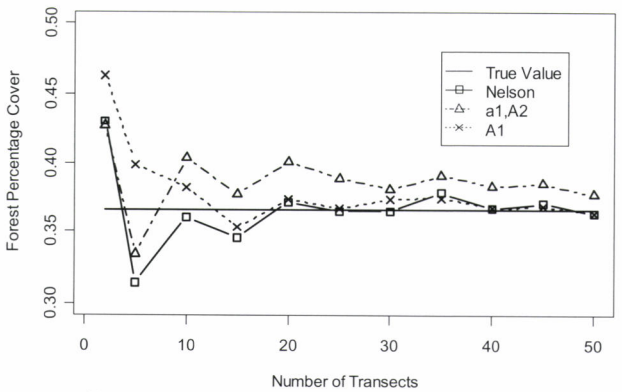

(a) Estimated percentage cover for simulated landscape

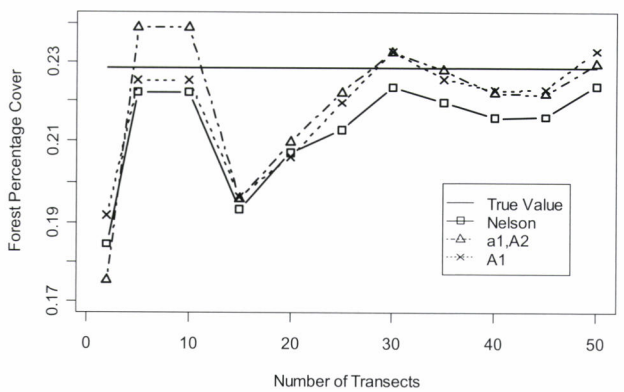

(b) Estimated percentage cover for ETM+ image

Fig. 8 The forest cover percentage estimated by four different estimators as a function of the number of transects used. The four estimators are the ones used by NELSON *et al.* (2005), the first estimator a1 discussed in "*Estimators when the configuration of landscape is fixed yet unknown*", and the two estimators A1 and A2 discussed in "*Estimators when the configuration of landscape is supposed to be random*". (a) is the case for artificial landscape, and (b) for the classified remote sensing imagery.

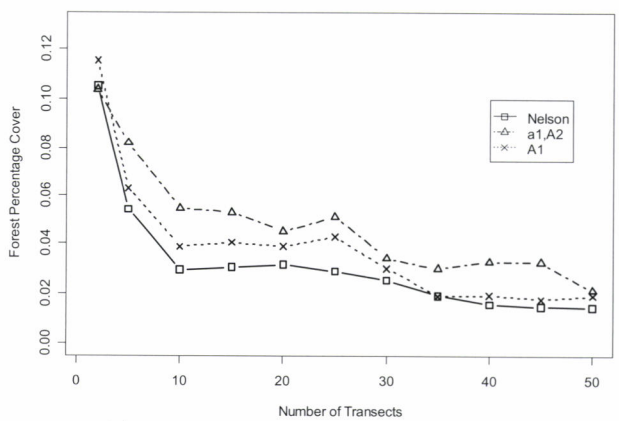

(a) **Estimated standard error by Monto Carlo simulation for simulated landscape**

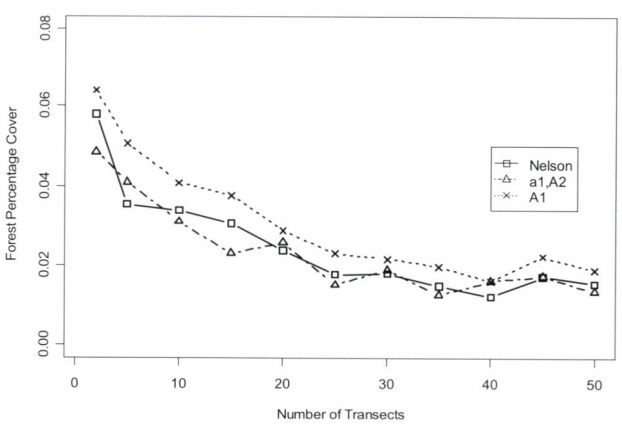

(b) **Estimated standard error by Monto Carlo simulation for ETM+ image**

Fig. 9 The estimated variance by sample variance of the simulation: (a) is the case for artificial landscape, and (b) for the classified remote sensing imagery.

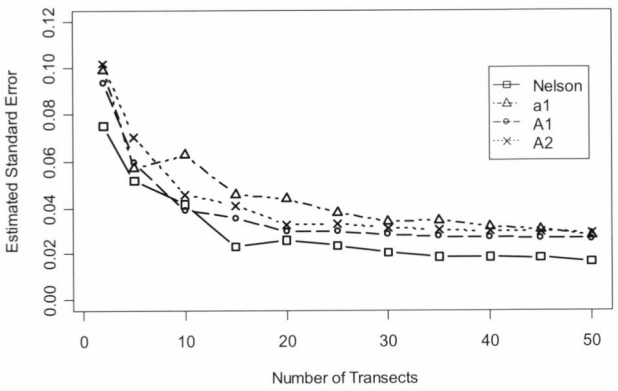

(a) Estimated standard error by Variance Formula for simulated landscape

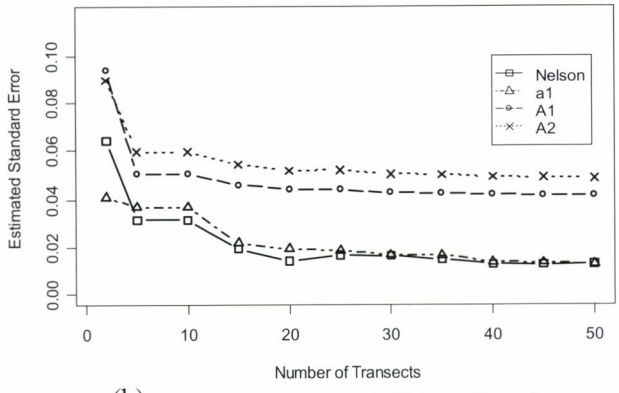

(b) Estimated standard error by Variance Formula for ETM+ image

Fig. 10 The estimated variance calculated by the variance formula: (a) is the case for artificial landscape, and (b) for the classified remote sensing imagery.

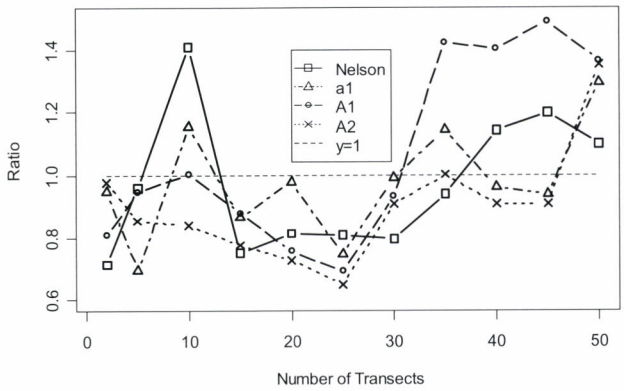

(a) Ratios of SE between formula and Monte carlo for simulated landscape

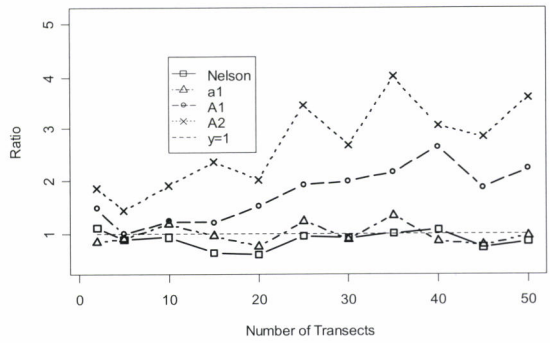

(b) Ratios of SE between formula and Monte carlo for ETM+ image

Fig. 11 The ratio of the formula-derived variance (shown in Fig. 9) to the sample variance of simulation (shown in Fig. 8) as a function of number of transects used. The closer to 1 the ratio is, the more valid the variance formula is. (a) is the case for artificial landscape, and (b) for the classified remote sensing imagery.

around 1.0 for all four variance estimators, e.g., with a range from 0.72 to 1.41 for the Nelson's estimator; However, for the real landscape of classified image, "A1" and "A2" provided inflated estimates relative to reference values of Monte carlo simulation, with "A2" producing the most upward estimates and "A1" following next. In contrast, Nelson's estimator and "a1" have fluctuating ratios more closer to 1, which suggests that in this case these two estimators offer more realistic estimates of variance.

DISCUSSIONS AND CONCLUSION

By mimicking the way a profiling LiDAR collects linear transect observations, the simulation of random realizations supposes to offer the possibility of examining the variability of simulated samples as well as quantifying the variance of a given estimator for a certain quantity. In this study, estimators for the percentage cover of given classes is tested, more importantly, the variance of these estimates are obtained by either taking sampling variance of the simulation or using the proposed formula as expressed in Eqs. 4, 7, 12 and 14.

Two settings for deriving the estimator and variance formula are assumed, when the landscape configuration is fixed and unknown, or random. Instead of using geometrical probability as in KAISER (1983), in this study, Monte carlo integration approach is refereed to for developing estimators of percentage cover; and the basic ideas are illustrated by Eqs. 1, 2, 5 and 8. The estimator ($\hat{a}_1$ or a1) of the first setting appear to be quite similar to the one used by NELSON *et al.* (2005), but difference exists that $\hat{a}_1$ is an estimator for area of interested patches which must be divided by the already known value of total area to obtain percentage cover, while the estimator in NELSON *et al.* (2005) directly provides estimates of percentage cover. The estimators for the random setting, however, tend to have a much more inflated variance that's much larger than the reference value of sample variance obtained by simulation; and this may either be caused by treating the systematical

sampling as random when evaluating the variance, or be an artifact of introducing randomness to depict the fixed but unknown landscape, i.e., $r(x)$. Furthermore, in practice the inference of the second setting can be only made for the mean since $R(x)$ in itself is assumed to be random. As such, the simulation of drawing transects from a fixed landscape is not too methodologically rigorous; but this appeared not to be a problem as demonstrated by the results for the simulated landscape.

In fact, the apparent disparity between the formula-based and simulation-based variance estimates for "A1" and "A2", as indicated in Fig. 11. b for the classified image, can be most likely attributed to the departure of $R(x)$ from the underlying assumptions made for deriving the variance estimators. It becomes clear that a drift is present in $r(x)$, as depicted in Fig. 6. b, which shows a high tail at large x; as a result, the incorporation of this overall trend into the calculation may mislead the estimation of covariance function as in Fig. 7.b since covariance function is supposed to capture only the random components of underlying stochastic process. Consequently, the inappropriate knowledge about covariance function will result in unreasonable variance estimates, as also noted for the variance estimator in KAISER (1983). In this study, estimates of covariance function were computed from $r(x)$. However, in practice, $r(x)$ remains unknown and is of inference interest based on the available samples observed at transects. Because of the limited number of transects, it is less possible to do estimation on covariance function using only these few samples. This prevents the effective use of variance estimators corresponding to the random setting. A possible remedy is to fit a parametric covariance model of known form to the available observation; specifically, the parameter relevant to the magnitude is simply estimated by the sample variance of $r(x_i)$'s, and parameters relevant to effective correlation distance may be inferred by analyzing the observations along the transect direction (i.e., the y axis in Fig. 5), due to continuous measurements available in this direction. However, the development of an efficient and reliable fitting procedure needs further investigation in future studies.

In our derivation, it is assumed that the geometry of study areas is known, which means that given a direction, $l(x)$ can be calculated. This is typically the case as GIS layers about study areas are often readily available prior to the flight mission. By changing the observation direction, not only $l(x)$ but also $r(x)$ changes; therefore, the orientation of transects has great influence on the properties of relevant estimation; and also there may exist a preferable direction for high-precision estimates. For example, an extreme scenario is hypothesized in Fig. 12 where the dotted half of the square region represents forested area. If a single vertical transect is randomly observed (the left of Fig. 12), the sampled percentage can take either 1 or 0 with equal probabilities; however, when observed horizontally, the true value 1/2 is always observed. To this end, prior knowledge, if available, can be used to guide the selection of appropriate direction; otherwise, the direction that could minimize the variability of $l(x)$ may be an option. In fact, when $l(x)$ is constant, all the four estimators as well as the one used in Nelson et al. (2005) essentially produce the same estimates, but they do have varying variance estimates due to the different assumptions. In deriving the LIS estimate or the corresponding variance estimator such as $\hat{a}_1$ and $\hat{\mu}_2$, only the transect length at observed locations is used. To compensate this, the primary author suspects that incorporating all information on $l(x)$ should increase the precision of estimates.

As a final note, although the aforementioned derivation is based on binary categorical landscapes, the proposed estimators can be equally applied to estimate percentage cover for landscapes with multiple categories without any modification. Moreover, they can also be extended for estimating the mean value of variable that varies continuously across the study area, e.g., regional biomass. To illustrate this point, suppose that the variable is a spatial-explicit function denoted by $f(x, y)$; then, by assuming the same geometry as in Fig. 1, the mean value of the variable averaged over the study area is simply obtained by an integration as follows,

$$\bar{f} = \frac{1}{m}\int_0^s \int_{y_l(x)}^{y_u(x)} f(x, y)\, dydx = \frac{1}{m}\int_0^s f_y(x)\, l(x)\, dx \qquad (15)$$

where $f_y(x) = \int_{y_l(x)}^{y_u(x)} f(x, y)\, dy$. $y_l(x)$ and $y_u(x)$ are the y coordinates respectively for the lower and upper boundary points at x, and m is the size of study area. In eq. 15, $f_y(x)$ plays the same role as the $r(x)$ in eq. 1. Hence, after the samples of $f_y(x)$ are observed at a number of transects that are parallel to y, $\bar{f}$ can be estimated by using the same estimators as previously discussed.

The logic to formulate the estimators for LIS is a little different from the mostly used geometrical probability approach by KAISER (1983). Hence, it still remains undetermined whether a logically sound reasoning line is followed to deal with the LIS problems in this study, or not. Nevertheless, the attempt to rely on Monte carlo integration random simulation for evaluating LIS estimators points a bright direction towards the ease of practical implementation of LIS schemes other than the mathematical intractability.

Fig. 12 An extreme hypothetical landscape of square shape where the dotted half represents forested area, for the purpose of demonstrating the effects of transect orientation : vertically-placed transects (the left) and horizontally-placed transects (the right).

LITERATURE CITED

AFFLECK, D. L. R., GREGOIRE, T. G. and VALENTINE., H. T. (2005): Design unbiased estimation in line intersect sampling using segmented transects. Environmental and Ecological Statistics **12**(2): 139-154

BAUER, H. L., (1943): The statistical analysis of chaparral and other plant communities by means of transect samples. Ecology **24**: 45-60

BUTLER, S. and MCDONALD, L. L., (1983): Unbiased systematic sampling plans for the line intercept method. Journal of Range Management **36**: 463-8

CANFIELD, R. H., (1941): Application of the line interception method in sampling range vegetation. Journal of Forestry **39**: 388-394

CROFTON, M. W., (1868): On the theory of local probability, applied to straight lines drawn at random in a plane. Philosophical Transactions of the Royal Society of London **158**: 181-199

KAISER, L., (1983): Unbiased estimation in line-intercept sampling. Biometrics **39**: 965-976

KEANE, R. E., REINHARDT, E. D., SCOTT, J., GRAY, K. and REARDON, J., (2005): Estimating forest canopy bulk density using six indirect methods. Can. J. For. Res. **35**: 724-739

KELLER, M., PALACE, M., ASNER, G. P., PEREIRA, R. and SILVA, J. N. M., (2004): Coarse woody debris in undisturbed and logged forests in the eastern Brazilian Amazon. Global Change Biol. **10**: 784-795

LEFSKY, M. A., COHEN, W. B., PARKER, G. G. and HARDING, D. J., (2002): Lidar remote sensing for ecosystem studies. Bioscience **52**: 19-30

LINDEBERG, J. W., (1926): Zur Theorie Derr Linientaxierung. Acta Forestalia Fennica **31**(6): 3-9

MACLEAN, G. A. and W. B. KRABILL, (1986): Gross-merchantable timber volume estimation using an airborne LIDAR system. Canadian Journal of Remote Sensing **12**(1): 7-18

MCINTYRE, G. A., (1953): Estimation of Plant Density Using Line Transects. Journal of Ecology **41**: 319-330

NELSON, R., KELLER, C. and RATNASWAMY, M., (2005): Locating and estimating the extent of Delmarva fox squirrel habitat using an airborne LiDAR profiler. Remote sensing of environment **96** (3-4): 292-301

NELSON, R. F., KRABILL, W. B. and MACLEAN, G. A., (1984): Determining forest canopy characteristics using airborne laser data.Remote Sensing of Environment **15**: 201-212

NELSON, R. F., KRABILL, W. B. and TONELLI, J., (1988): Estimating forest biomass and volume using airborne laser data. Remote Sensing of Environment **24**: 247-267

NELSON, R., PARKER, G. and HOM, M., (2003): A portable airborne laser system for forest inventory. Photogrammetric Engineering & Remote Sensing **69** : 267

NELSON, R., SHORT, A. and VALENTI, M., (2004): Measuring biomass and carbon in Delaware using airborne profiling LiDAR. Scand. J. For. Res. **19**: 500-511

POPESCU, S. C., WYNNE, R. H. and NELSON, R. F., (2002): Estimating plot-level tree heights with lidar: local filtering with a canopy-height based variable window size. Com Elect Agr **37**: 71-95

POPESCU, S. C., WYNNE, R. H. and NELSON, R. E., (2003): Measuring individual tree crown diameter with LiDAR and assessing its influence on estimating forest volume and biomass. Canadian Journal of Remote Sensing.

SAURA and MARTÍNEZ-MILLÁN, (2000): Landscape patterns simulation with a modified random clusters method. Landscape Ecology **15**(7): 661-678

VAN WAGNER, C. E., (1961): The line intersect method in forest fuel sampling. Forest Science **14**(1): 20-26

WARREN, W. G. and P. F. OLSEN., (1964): A line intersect technique for assessing logging waste. Forest Science **10**: 267-276

(Received 13 January 2007)
(Accepted 6 May 2007)

Article

Stemwood Volume Estimates for a Mixed Temperate Forest using Satellite LiDAR

Jacqueline Rosette[*1], Peter North[*2] and Juan Suárez[*3]

ABSTRACT

Data from the Geoscience Laser Altimeter System (GLAS) aboard the Ice Cloud and Land Elevation Satellite (ICESat) were used to explore the potential of satellite LiDAR for the estimation of forest parameters such as vegetation height and stemwood volume. This was carried out for the Forest of Dean, Gloucestershire, UK, a semi-ancient, highly mixed, temperate forest. Previous research suggests use of Waveform Extent (the difference of alternate model fit Signal Begin and Signal End) and a Terrain Index (maximum minus minimum elevations from a 7×7 matrix, 10m resolution DTM) to provide the most robust estimate of maximum canopy height. These waveform-based maximum vegetation height estimations were used to investigate the potential of satellite LiDAR for the estimation of stemwood volume for the tallest species within each footprint. Relationships were established with predictions of stemwood volume calculated from Forestry Commission yield models. These equations succeeded in explaining 68% of variance with 88.7m³/ha RMSE for coniferous species and R^2 of 0.65 with 68.2m³/ha RMSE for broadleaf species. The ability of satellite LiDAR waveforms to account for stemwood volume within mixed composition stands was also investigated. Area under the waveform canopy return, maximum canopy height, dominant canopy height and height of cumulative energy percentiles were considered. The height of the 90th percentile of cumulative energy was found to best represent the weighted stemwood volume of heterogeneous stands producing R^2 of 0.57, 92.3m³/ha RMSE and R^2 of 0.59, 67.5m³/ha RMSE for stands dominated by coniferous and broadleaf species respectively. The results of this local study indicate the potential for similar methods to be applied to regional or national scales.

Keywords: ICESat, GLAS, stemwood volume, vegetation height, satellite LiDAR

INTRODUCTION

The necessity of quantifying and monitoring changes in carbon stock has been recognised in international agreements such as the Kyoto Protocol to the United Nations Framework Convention on Climate Change 1997 (UNFCCC, 2007; FOREST RESEARCH, 2006). Estimating this requires prior knowledge of carbon dispersal and, as an effective carbon sink, understanding distribution of vegetation volume.

For the purposes of forest management, quantifying timber volume is of importance for commercial viability and assessing stand processes such as regeneration. Additionally, height is an important input parameter for yield model estimates (EDWARDS and CHRISTIE, 1981; FORESTRY COMMISSION, 2006).

Earth observation plays a significant role in contributing to the knowledge of vegetation distribution and its biophysical properties. Optical remote sensing has been shown to provide indirect associations using reflectance

Corresponding author: Jacqueline Rosette
[*1] Swansea University, Climate and Land-Surface Systems Interaction Centre (CLASSIC), Department of Geography, Swansea, SA2 8PP, United Kingdom. ggrosette@swansea.ac.uk
[*2] Swansea University, Climate and Land-Surface Systems Interaction Centre (CLASSIC), Department of Geography, Swansea, SA2 8PP, United Kingdom. p.r.j.north@swansea.ac.uk
[*3] The Forest Research Agency of the Forestry Commission Great Britain, Northern Research Station, Roslin, Midlothian, EH25 9SY, United Kingdom.
juan.suarez@forestry.gsi.gov.uk

properties for Normalised Difference Vegetation Index (e.g. DEFRIES and TOWNSHEND, 1994; LOS *et al.*, 1994; SELLERS *et al.*, 1994) and Leaf Area Index (e.g. LOS *et al.*, 2000; MYNENI *et al.*, 2002) although there are difficulties associated with use of reflectance alone (NORTH, 2002). More direct assessment using the physical properties of vegetation and interactions between canopy structure and photons detected by the sensor have been demonstrated through radiative transfer modelling (NORTH, 1996; NI-MEISTER *et al.*, 2001; KOTCHENOVA *et al.*, 2003).

Active instruments have been exploited to estimate vegetation height and volume using radar (BALTZER *et al.*, 2003; GAVEAU *et al.*, 2003; TANSEY *et al.*, 2004; BALZTER *et al.*, 2007) and more recently LiDAR (Light Detection and Ranging) systems.

Potential for biophysical parameter estimation at local scales has been shown for discrete return airborne laser scanning (e.g. HYYPPÄ *et al.*, 2001; NÆSSET, 2002; PATENAUDE *et al.*, 2004) and waveform recording devices (LEFSKY *et al.*, 1999a; LEFSKY *et al.*, 1999b; HARDING *et al.*, 2001; DRAKE *et al.*, 2002; DRAKE *et al.* 2003). The benefits of combining spectral data/ aerial photography and airborne lidar data have also been shown (e.g. HILL and THOMPSON, 2005; SUÁREZ *et al.*, 2005). Additionally, NELSON *et al.* (2004) and NELSON *et al.* (2006) have shown the potential for USA State-wide documentation of commercially viable volume and total above ground biomass using first return airborne LiDAR profiling. Discussions relating to full waveform, satellite LiDAR systems are provided by BUFTON (1989), GARDNER (1992), HARDING *et al.* (1994), BRENNER *et al.* (2003) and HESE *et al.* (2005).

An important limitation of remote sensing estimates is that direct account is only taken of above ground biomass whilst root systems would make a substantial contribution to carbon storage. However, JENKINS *et al.* (2003) have shown a means to overcome this using USA-wide allometric equations for estimating above ground biomass for broad species classes and have found generalised relationships accounting for vegetation component biomass (root, foliage, stem bark and stemwood). This potential has also been demonstrated by FANG *et al.* (1998) who have related stem volume density (m^3/ha) to stand biomass (Mg/ha) comprising both above and below ground biomass.

The objectives of this study are therefore to explore the use of ICESat/GLAS data for forest inventory and to develop straightforward, repeatable methods for estimating vegetation height and stemwood volume that can be applied to regional and national scales. In particular, we examine how existing methods for stemwood volume estimation based on yield models compare with estimates derived from satellite LiDAR. We assume a sample of height data is available to calibrate LiDAR height estimates.

METHOD

Study Site

The Forest of Dean, Gloucestershire, UK (Fig. 1; left) is a semi-ancient, heterogeneous, temperate forest, bordering Wales and extending over an area of approximately 11,000 hectares (ROYAL FOREST OF DEAN, 2006). The Forest is managed by the Forestry Commission of Great Britain a

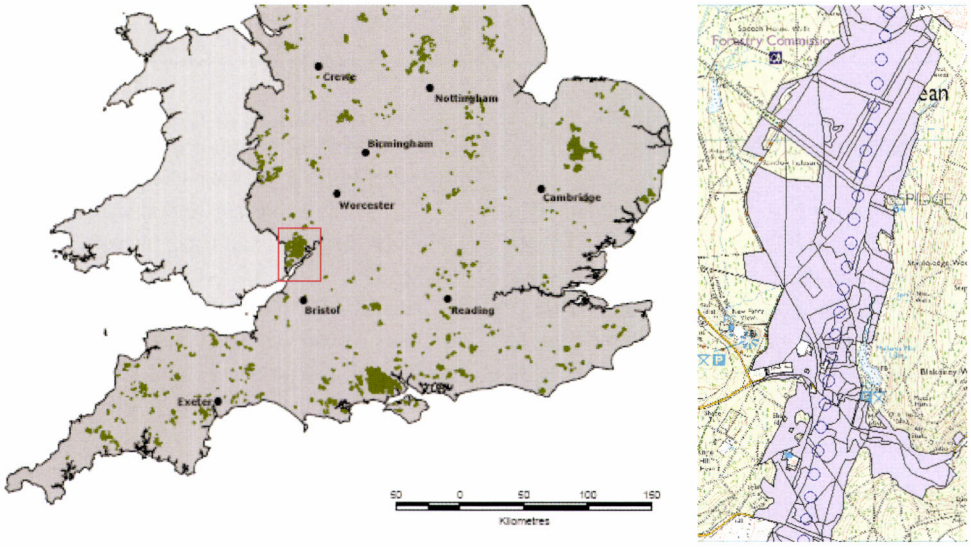

Fig. 1 (left) Map of Forestry Commission Woodland in central and southern England with the Forest of Dean indicated. Source: MAGIC (2007). (right) 1:25,000 scale map of the Forest of Dean overlaid by Forestry Commission sub-compartments and representation of a section of ICESat footprints. North is orientated to the top of the image (2km × 4km area shown). Source: ORDNANCE SURVEY (2006)

division of which, Forest Enterprise, maintains a sub-compartment database of management units throughout the area. These sub-compartments (Fig. 1; right) are comprised of discrete, irregularly distributed components with known species, physical conditions and management criteria (FORESTRY COMMISSION, 2006). Thus for each footprint location, the associated sub-compartment and constituent components permit reference to be made to relevant yield models (EDWARDS and CHRISTIE, 1981). This enables prediction of vegetation growth for the given conditions.

The ICESat ground-track crossed the Forest between latitude 51.74° N and 51.88° N and longitude 2.54° W and 2.51° W. Of the stands sampled by ICESat/GLAS footprints, the most commonly occurring species were Norway Spruce (*Picea abies*), mixed broadleaf species, Oak (*Quercus* spp), Corsican Pine (*Pinus nigra var maritima*), Douglas Fir (*Pseudotsuga menziesii*), Scots Pine (*Pinus sylvestris*) and European Larch (*Larix decidua*). Vegetation was predominantly still in leaf at the time of GLAS data acquisition. Only footprints falling within the contents of the Forestry Commission sub-compartment database were studied and additionally, those footprints which partially traversed urban developments were excluded as surface features would contribute to waveform structure and could not be isolated. This resulted in a total of 69 waveforms analysed.

Yield Models

Forestry Commission yield models were used to calculate stemwood volume coincident with ICESat footprints. The yield models are empirically-derived and estimate growth over time accounting for habitat conditions and consequently differing growth characteristics between and within species groups. Initial spacing of individuals, species, yield class (defined as an annual increment in m^3/ha/year) and management (e.g. thinning regime) are used for each model to estimate vegetation parameters which comprise top height, individual tree volume, volume per hectare and mean diameter at breast height by age.

Stemwood volume is defined by EDWARDS and CHRISTIE (1981) as living tree over-bark volume (m^3/ha) which, for coniferous species, includes main stem timber of 7cm diameter or greater. This was estimated for sub-compartments sampled by each ICESat footprint making reference to the sub-compartment database and relevant yield models. Two measures of stemwood volume are used in this study:

Single species stand volume

The first uses yield model stemwood volume calculated for the tallest species within each footprint, determined from the sub-compartment database. Using one species, identifiable from the waveforms (maximum canopy height estimations), aims to indicate the potential for stemwood volume estimation within pure stands. Footprints were then distinguished according to whether the tallest species was broadleaf or coniferous to determine whether this would result in an improved correlation with waveform parameters (described in "Waveform estimators of stemwood volume" section).

Mixed stand stemwood volume

Only six footprints crossing the Forest of Dean sample sub-compartments containing a single species and furthermore several footprints cross more than one sub-compartment. Therefore the second measure represents mixed stands and uses a weighted stemwood volume calculation, taking account of the percentage composition of species within all components of each sub-compartment covered by footprints. Footprints were differentiated according to whether broadleaf or coniferous species formed the greatest percentage cover. Relationships with the waveform parameters discussed above were then calculated.

ICESat/ GLAS Data

The Ice Cloud and land Elevation Satellite (ICESat) carries the Geoscience Laser Altimeter System (GLAS) and provides near global coverage of between ±86° latitude. Lasers are operated intermittently, typically three times per annum during February-March, May-June and October-November. ICESat orbits at an altitude of 600km and simultaneously emits 1,064nm and 532nm wavelength pulses at 40Hz. This produces a series of elliptical footprints with 64m average equivalent circular area diameter and 172m intervals between consecutive footprint centres. Further information regarding the mission is discussed by ZWALLY *et al.* (2002), BRENNER *et al.* (2003), KICHAK (2003), ABSHIRE *et al.* (2005), SCHUTZ *et al.* (2005) and NSIDC (2006).

Data from GLAS release V026; level 1A product GLA01 (Global Altimetry data) and level 2 products GLA06 (Global Elevation data) and GLA14 (Global Land Surface Altimetry data) captured on 22nd October 2005 at 8:28am (ZWALLY *et al.* 2006), were used for this study. These products provide respectively the raw waveform, geographical co-ordinates of footprint locations and a model fit to the waveform using the sum of six Gaussian peaks (Fig. 2b). Near infrared waveforms have been used for the study discussed in this paper. The GLAS Visualizer Tool (10th April 2006 version) was used to explore the waveform, as well as to identify and export relevant parameters.

LiDAR waveforms consist of the returned energy from intercepted surfaces at and above ground level within the area illuminated by the laser pulse. The time for energy from the emitted pulse to be returned to the sensor enables elevations of above-surface features within the footprint to be calculated.

For vegetated areas of significant relief, signals from ground and vegetation elevations may be combined within the returned waveform. This is a particular challenge for broader footprints where the likelihood is increased. Footprints

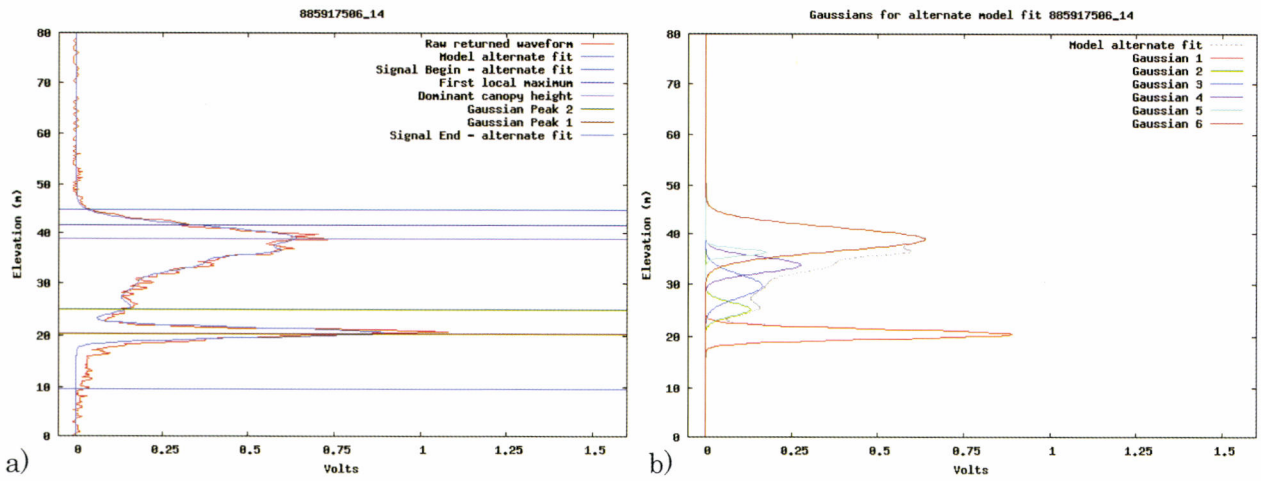

Fig. 2 a) A bimodal waveform typical of vegetated footprints, illustrating key waveform parameters. b) Alternate model fit decomposition; the sum of six Gaussian peaks.

containing vegetation overlying a ground surface of low relief are expected to produce a bimodal LiDAR waveform consisting of a narrow peak pertaining to topography and a broader, more complex return determined by responses from vegetation (Fig. 2). The waveform structure relating to the vegetation return may be considered a function of vegetation volume (surface area of canopy elements) as well as reflectivity at the scattered wavelength.

The work presented in the paper aims firstly to identify an appropriate means of estimating maximum canopy height from satellite LiDAR waveforms. This estimate is then used to identify the region of the waveform attributable to the vegetation. Several methods of estimating stemwood volume from GLAS waveforms are subsequently explored and compared with Forestry Commission yield model predictions.

GLAS Waveform Parameters

Canopy height

Key features within waveforms can be identified with the aim of facilitating interpretation (Fig. 2). Signal Begin and Signal End positions are assigned where a background noise threshold is exceeded and represent respectively, the highest canopy surface and lowest ground elevations within the footprint. The distance between these limits is referred to as Waveform Extent (HARDING and CARABAJAL, 2005; LEFSKY *et al.*, 2005).

Adapted from LEFSKY *et al.* (2005), a Terrain Index for each footprint location was calculated. For the purposes of this study, this consisted of the difference in metres between the highest and lowest elevations within a 7×7 matrix of a 10m resolution DTM (ORDNANCE SURVEY, 2006) about the footprint centre.

Field tree height measurements at nineteen footprint locations were conducted in June 2006. These comprised eight inclinometer measurements of the tree with largest diameter at breast height, one within each 45° segment of 35m radius about the footprint centre.

Removal of the effect of topography from the Waveform Extent is anticipated to provide an estimate of maximum canopy height within a footprint. Waveform Extent and Terrain Index were therefore used to establish a relationship with the greatest of the eight tree height measurements for each footprint.

Previous work (ROSETTE *et al.* in press) demonstrated significant correlation between waveform estimates of maximum canopy height using Waveform Extent (*WE*) and Terrain Index (*TI*) with field measurements (*H*) taken at footprint locations.

Equation (1) was found to explain 90% of variance and produced RMSE of 2.86m for the Forest of Dean.

$$H = 1.0208 * WE - 0.7310 * TI \quad (1)$$

Estimated maximum canopy heights resulting from this multiple regression equation are hereafter referred to as R_{WT}.

HARDING *et al.* (1998) and NI-MEISTER *et al.* (2001) note issues associated with allocation of the Signal Begin position due to the characteristics of the waveform Leading Edge (representing uppermost canopy variability). Research presented by LEFSKY *et al.* (2005) succeeded in improving correlation with maximum field height when additionally incorporating the waveform Leading Edge parameter, increasing R^2 from 0.59 to 0.69 and decreasing RMSE from 4.85 to 4.21m for sites within the Great Smoky Mountains National Park, Tennessee, USA.

As part of this current study, the waveform leading edge and upper canopy variability were calculated to determine whether either may improve on the estimation of this

maximum canopy height based on methods reported by LEFSKY *et al.* (2005). For the Forest of Dean, neither the uppermost height difference between Signal Begin and the first local waveform maximum, nor the upper canopy height variability between Signal Begin and the position of the maximum canopy peak resulted in statistically significant coefficients.

Therefore results using equation 1, substituting Waveform Extent and Terrain Index values for each footprint, were subsequently taken to be the most robust maximum canopy height estimations (R_{WT}) and are used in later methods of estimating stemwood volume and identifying waveform parameters.

Waveform estimators of stemwood volume

Several waveform parameters were explored as potential indicators of stemwood volume:

- Maximum canopy height

Use of maximum canopy height estimations (R_{WT}) described above were examined. The square of these values $(R_{WT})^2$ were also considered as an improved relationship had been previously achieved by LEFSKY *et al.* (2005).

- Height of cumulative energy percentiles

The waveform estimate of maximum canopy height (R_{WT}) was used to locate the portion of the waveform representing the vegetation return. Within this region of the waveform, percentiles of cumulative energy (adapted from HARDING *et al.*, 2001) were calculated and the heights at which the 50th, 75th, 80th, 90th and 95th percentiles occurred were used to estimate stemwood volume.

- Dominant canopy height

The height above the ground surface to the canopy return peak was named the dominant canopy height and was calculated by multiple regression using the Terrain Index presented in "canopy height" section and the elevation difference between the Signal End position and the elevation of the canopy return peak.

- Canopy waveform area

An alternative means of attributing waveform structure to volume of intercepted vegetation was investigated using the area under the canopy return. This was achieved by removing the ground surface contribution from the waveform. Two methods were explored, the first of which used the location of the ground peak represented by either Gaussian Peak 1 or 2, whichever demonstrated greatest amplitude (ROSETTE *et al.* submitted). If the ground peak was allocated to Gaussian Peak 1, the sum of the areas beneath Peaks 2-6 was assumed to represent canopy volume, whilst volume was estimated as the total area of Gaussian Peaks 3-6 if Peak 2 was designated the ground return (Fig. 2b). The second method calculated the area beneath the waveform between the alternate fit signal begin position to the upper limit of the Terrain Index elevation.

RESULTS

Tallest Species Stemwood Volume Estimates

Regression analysis was carried out using the parameters described in "Waveform estimators of stemwood volume" section with yield model stemwood volume estimates ("single species stand volume" section). These results are shown in Table 1.

Table 1 Tallest species stemwood volume estimates

Waveform parameter	Tallest species	R^2	Intercept	Coefficient	RMSE (m^3/ha)	Number
Maximum canopy height (R_{WT})	Coniferous	0.68	NS	13.8	88.7	55
	Broadleaf	0.65	NS	8.27	68.2	18
	Combined	0.60	NS	12.8	98.7	69
$(R_{WT})^2$	Coniferous	0.63	80.0 $p > 0.001$	0.39	96.0	55
	Broadleaf	0.57	NS	0.31	80.0	18
	Combined	0.55	73.7 $p > 0.001$	0.37	104.4	69
Height of 90th percentile cumulative energy	Coniferous	0.50	NS	17.4	105.3	52
	Broadleaf	0.64	NS	10. 5	71.0	16
	Combined	0.46	NS	16.2	111.2	65

Comparison of tallest species stemwood volume with estimation results using waveform parameters. Groups include common footprints classified as un-vegetated. The number of footprints used differs due to missing values, discrepancies between Waveform Extent and estimated maximum height or anomalies such as 'negative' energy within height bins. Coefficients and intercepts are statistically significant ($p < 0.001$) except where stated. NS indicates not significant.

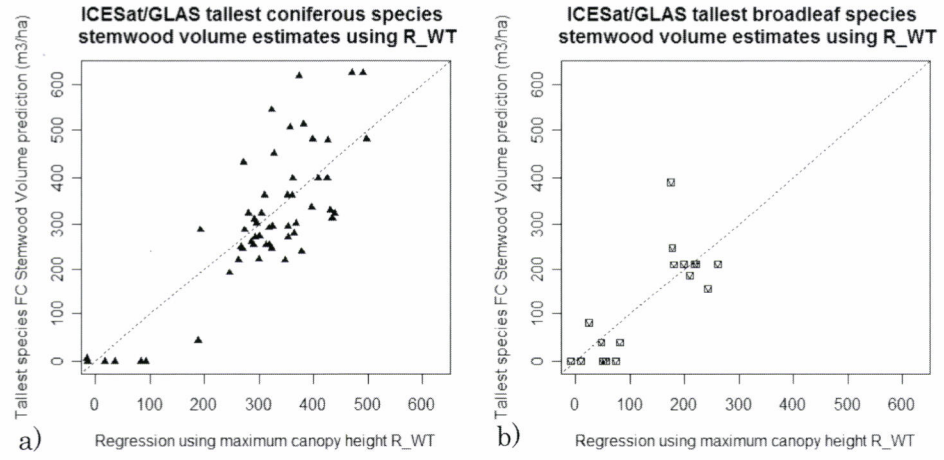

Fig. 3 Relationship between Forestry Commission (FC) stemwood volume predictions and volume estimates using Maximum Canopy Height R_{WT}, for (a) coniferous species, RMSE 88.7m³/ha and (b) broadleaf species, RMSE 68.2m³/ha.

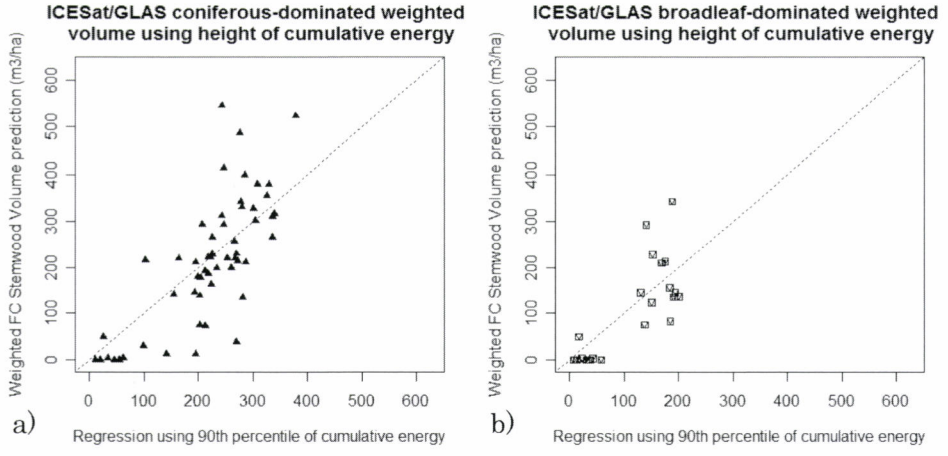

Fig. 4 Relationship between weighted stemwood volume predictions and volume estimates using height of the 90th percentile of cumulative energy for footprints with greatest percentage cover by: (a) coniferous species, RMSE 92.3m³/ha and (b) broadleaf species, RMSE 67.5m³/ha. Please refer to Table 2.

Table 3 Additional correlation ranges

Waveform parameter	R^2 range	RMSE range m³/ha
Dominant canopy height	0.05 - 0.34	100.2 - 143.4
Waveform canopy area (Gaussian peaks)	0.08 - 0.19	98.9 - 149.7
Waveform canopy area (to upper terrain index limit)	0.05 - 0.24	93.4 - 140.1

Parameters shown were not found to be statistically significant or produced weak correlations. Ranges stated are for both stemwood volume methods.

Estimated maximum canopy height (R_{WT}) produced the best estimate of stemwood volume for the tallest species within footprints with R^2 of 0.60 and RMSE of 98.7m³/ha.

Differentiating between broadleaf and coniferous species improved the correlation to R^2 of 0.65, RMSE of 68.2m³/ha and R^2 of 0.68, RMSE of 88.7m³/ha respectively. These relationships are illustrated in Fig. 3.

Neither heights of cumulative energy percentiles nor the square of maximum canopy height improved these stemwood volume estimates. Other waveform parameters used did not produce statistically significant results or showed weak correlations (Table 3).

Table 2 Mixed stand stemwood volume estimates

Waveform parameter	Predominant species	R^2	Intercept	Coefficient	RMSE (m^3/ha)	Number
Maximum canopy height (R_{WT})	Coniferous	0.52	NS	9.83	98.1	58
	Broadleaf	0.48	NS	5.69	74.7	24
	Combined	0.40	NS	8.90	105.9	69
$(R_{WT})^2$	Coniferous	0.50	NS	0.36	101.2	58
	Broadleaf	0.45	NS	0.21	76.8	24
	Combined	0.37	46.0 $p > 0.05$	0.26	108.8	69
Height of 90th percentile cumulative energy	Coniferous	0.57	NS	12.8	92.3	55
	Broadleaf	0.59	NS	8.69	67.5	21
	Combined	0.49	NS	11.9	94.9	65

Comparison of weighted stemwood volume calculations with waveform parameter estimations. Groups include common footprints classified as un-vegetated and those with no dominant vegetation type. The number of footprints used differs due to missing values, discrepancies between Waveform Extent and estimated maximum height or anomalies such as 'negative' energy within height bins. Coefficients and intercepts are statistically significant ($p < 0.001$) except where stated. NS indicates not significant.

Mixed Stand Stemwood Volume Estimation

Using the same waveform parameters, regression analysis was repeated for the mixed stand weighted stemwood volume estimates ("Mixed stand stemwood volume" section). Correlation was found to be lower for estimates of mixed stand stemwood volume than for the single species estimates discussed in "Tallest species stemwood volume estimates" section.

The height of the 90th percentile of cumulative energy produced the best relationship with R^2 of 0.49, RMSE 94.9m^3/ha for all footprints sampled.

Footprints were then distinguished according to whether the predominant vegetation cover consisted of broadleaf or coniferous species. This produced respectively R^2 of 0.59, RMSE 67.5m^3/ha for broadleaf species and R^2 of 0.57, RMSE 92.3m^3/ha for conifers. These relationships are shown in Fig. 4 whilst the results of all waveform parameter analyses are outlined in Tables 2 and 3.

DISCUSSION

A number of waveform-derived parameters were considered with respect to their ability to estimate stand stemwood volume as defined by independent estimates derived from yield models.

Previous work (Rosette *et al.* in press) has shown the ability for maximum canopy height to be extracted from GLAS waveforms over this study site. This enabled an assessment to be made of stemwood volume estimates for the corresponding tallest tree species within footprints.

Maximum canopy height is, by its nature, determined by little foliage of one or few trees within the stand. Therefore positions within and characteristics of the waveform canopy return were explored as, particularly for mixed stands, they are anticipated to better represent the combined contribution of the canopy elements for the diverse species present within footprints.

However, in some cases little relationship is seen which may be a result of these factors varying considerably between species e.g. the elevation of greatest returns from within the canopy is determined by species canopy structure which will also affect laser penetration. The validity of the methods using waveform canopy area are dependent on the degree to which reflectance between species differs at the measured wavelength (1,064nm) in addition to the effects of canopy profile on multiple scattering events and their representation within waveforms. The weak correlation with weighted stemwood volume suggests that, for such highly mixed stands, if a relationship does exist with area under the waveform or dominant canopy height, the broad distinction between broadleaf and coniferous coverage is insufficient or that values are inconsistent due to variation in species structure or reflectivity. However, the highest correlation for mixed stand stemwood volume estimates was provided by relative positions within the canopy return produced using percentiles of cumulative energy.

Forestry sub-compartments that were listed by the Forestry Commission but classified as unpopulated (i.e. zero anticipated stemwood volume) were included in comparisons and the incorporation of these lower values has resulted in improved correlation.

Due to expected deviation in relationships between coniferous and broadleaf species, these groups were first analysed together as a sample forest population before being considered in isolation. Nelson *et al.* (2004) found estimates of

volume and biomass using their Portable Airborne Laser System (PALS) to be significantly more accurate for conifers than for their hardwood grouping (i.e. deciduous trees). This paper shows only minor differences in correlation between coniferous and broadleaf species, whilst RMSE is seen to be lower for broadleaf-dominated footprints. However, mean values of stemwood volume for vegetated stands are 327.7m³/ha and 174.7m³/ha for coniferous and broadleaf species respectively and therefore a lower RMSE would be anticipated for the latter as a result of this alone. The results of this study suggest that differentiation may be necessary between coniferous and broadleaf species in order to use generalised relationships for broader scale stemwood volume estimates.

Dispersion among smaller volume values is observed and may be attributable to unmanaged re-growth or the effect of the 5 ns emitted pulse width producing an artificial minimum elevation difference of 1.5m even for flat surfaces. An initial investigation suggests that, in most cases, GLAS waveforms are representing actual above surface features such as individual trees, shrubs or buildings.

Several waveform-based parameters within this study use the maximum canopy height estimated from the multiple regression equation using Waveform Extent and a Terrain Index with field measurements taken within 19 footprints. These estimates are dependent on the accuracy of the field measurements (LARSEN *et al.* 1987) in addition to how representative the selected footprints are of the complete pass. Future work will explore methods of estimating stemwood volume solely from waveform parameters.

Deviations from actual stand volumes are anticipated due to errors inherent in yield model predictions as individual stands may not perform in accordance with the models. If stand performance and management treatments differ from the yield model assigned, long-term forecast production for an individual stand may vary from actual production by 20% (EDWARDS and CHRISTIE, 1981). However, the sub-compartment database is updated annually to contain details of current conditions. Recent work conducted by the Forestry Commission at a stand level using yield model estimates calibrated with field measurements, produced vegetation height accuracy of 98% whilst, in the course of this study, a comparison of greatest field height measurements within 21 footprints with corresponding yield model estimates of Top Height for the tallest species revealed R^2 of 0.94.

Since top height is used within yield models they may be anticipated to provide a reasonable indication of the vegetation present. However sources of error are known and for coniferous stands, yield models have been found to overestimate actual volume. Furthermore, the Forestry Commission yield models are not dynamic and therefore do not account for mortality or species competition, assuming that stand composition remains that of the time of planting.

A further simplification made in this study is that the weighted stemwood volume calculation for mixed stands assumes a regular distribution of components within sub-compartments. Nevertheless, these yield models offer the best available estimate of current conditions, are widely used in forest management and provide useful data in order to explore GLAS volume estimates.

LiDAR stemwood volume estimates with accuracy in excess of 60-70% are anticipated to be welcomed by forestry practitioners to contribute to national inventory. The results of this study suggest that for homogeneous sites, this can be achieved; however to reach this threshold for areas with more complex species composition would require greater refinement.

It is recognised that differences in relationships between maximum canopy height or percentiles of cumulative energy and stemwood volume within both coniferous species and broadleaf species groups are likely to contribute to a proportion of the variation observed. Investigation of a more homogenous site may reveal improved correlation and a possible significant contribution of other waveform parameters. Future work will also explore exploitation of the full waveform signal through radiative transfer modelling (NORTH 1996).

CONCLUSION

For a highly diverse, temperate forest, waveform-based calculations from maximum height estimations using ICESat/GLAS Waveform Extent and Terrain Index were compared with yield model estimates of stemwood volume. The results succeeded in estimating stemwood volume of the tallest species within coniferous stands with R^2 of 0.68 and RMSE of 88.7m³/ha whilst for broadleaf stands, R^2 of 0.65 and RMSE of 68.2m³/ha were produced.

An analysis of stemwood volume accounting for the mixed composition of stands contained within footprint areas was additionally carried out. A distinction was drawn between footprints dominated by coniferous or broadleaf species. Relationships using height of the 90th percentile of cumulative energy explained 57% of variance, RMSE 92.3m³/ha, for footprints in which coniferous species are prevalent. Footprints with greatest cover formed by broadleaf species were found to produce R^2 of 0.59 and RMSE of 67.5m³/ha.

The results suggest the potential for satellite LiDAR estimates of volume to be extended to regional and national scales and that a similar broad distinction between broadleaf or coniferous species may be sufficient to quantify vegetation for the requirements of forest inventory.

ACKNOWLEDGEMENTS

This research is funded by the UK Natural Environment Research Council (NERC), forming part of the objectives of the Climate and Land-Surface Systems Interaction Centre

(CLASSIC).

Recognition is given to the Forestry Commission GB for their assistance with this work; in particular to Peter Burnett, staff at the Forest of Dean District Office and Genevieve Patenaude. Thanks are given to Sietse Los and Mike Barnsley of Swansea University plus Heiko Balzter, University of Leicester. Speakers at Silvilaser 2006 are also acknowledged for the insight into their related work, amongst whom are Michael Lefsky, Ross Nelson, Sorin Popescu, Guoquing Sun and Hayato Tsuzuki. Thanks are also due to the anonymous reviewer for the helpful comments and advice.

LITERATURE CITED

ABSHIRE, J., SUN, X., RIRIS, H., SIROTA, J., MCGARRY, J., PALM, S., YI, D. and LIIVA, P., (2005): Geoscience Laser Altimeter System (GLAS) on the ICESat Mission: On-orbit measurement performance. Geophysical Research Letters **32**: L21S02

BALZTER, H., ROWLAND, C. S. and SAICH, P., (2007): Forest canopy height and carbon estimation at Monks Wood National Nature Reserve, UK, using dual-wavelength SAR interferometry. Remote Sensing of Environment **108**: 224-239

BALZTER, H., SKINNER, L., LUCKMAN, A. J. and BROOKE, R., (2003): Estimation of tree growth in a conifer plantation over nineteen years from multi-satellite L-band SAR. Remote Sensing of Environment **84**: 184-191

BRENNER, A., ZWALLY, H., BENTLEY, C., CSATHÓ, B., HARDING, B., HOFTON, M., MINSTER, J.-B., ROBERTS, L., SABA, J., THOMAS, R. and YI, D., (2003): Derivation of Range and Range Distributions From Laser Pulse Waveform Analysis for Surface Elevations, Roughness, Slope, and Vegetation Heights. Algorithm Theoretical Basis Document V4.1. Available online at: http://www.csr.utexas.edu/glas/pdf/Atbd_20031224.pdf (accessed March 2005)

BUFTON, J., (1989): Laser Altimetry Measurements from Aircraft and Spacecraft. Proceedings of the IEEE **77**: 463-477

DEFRIES, R. S. and TOWNSHEND, J. R. G., (1994): NDVI-derived land cover classifications at a global scale. International Journal of Remote Sensing **15**(17): 3567-3586

DRAKE, J. B., DUBAYAH, R. O., CLARK, D. B., KNOX, R. G., BLAIR, J. B., HOFTON, M. A., CHAZDON, R. L., WEISHAMPEL, J. F. and PRINCE, S. D., (2002): Estimation of tropical forest structural characteristics using large-footprint LiDAR. Remote Sensing of Environment **79**: 305-319

DRAKE, J. B., KNOX, R. G., DUBAYAH, R. O., CLARK, D. B., CONDIT, R., BLAIR, J. B. and HOFTON, M. A., (2003): Above-ground biomass estimation in closed canopy Neotropical forests using LiDAR remote sensing: factors affecting the generality of relationships. Global Ecology and Biogeography **12**: 147-159

EDWARDS, P. N. and CHRISTIE, J. M., (1981): Yield Models for Forest Management, Booklet 48. Edinburgh, The Forestry Commission

FANG, J.-Y., WANG, G. G., LIU, G.-H. and XU, S.-L., (1998): Forest Biomass of China: An estimate based on the Biomass - Volume Relationship. Ecological Applications **8**(4): 1084-1091

FOREST RESEARCH, (2006): UK Forest Carbon Inventory. Available online at: http://www.forestresearch.gov.uk/website/forestresearch.nsf/By Unique/INFD-62XH5R (accessed June 2006)

FORESTRY COMMISSION, (2006): Operational Guidance Booklet Number 6, Survey Handbook. Edinburgh, The Forestry Commission

GARDNER, C., (1992): Ranging Performance of Satellite Laser Altimeters. IEEE Transactions on Geoscience and Remote Sensing **30**: 1061-1072

GAVEAU, D. L. A., BALZTER, H. and PLUMMER, S., (2003): Forest woody biomass classification with satellite-based radar coherence over 900 000km² in Central Siberia. Forest Ecology and Management, **174**: 65-74

HARDING, D., BUFTON, J. and FRAWLEY, J., (1994): Satellite Laser Altimetry of Terrestrial Topography: Vertical Accuracy as a Function of Surface Slope, Roughness and Cloud Cover. IEEE Transactions on Geoscience and Remote Sensing **32**: 329-339

HARDING, D. and CARABAJAL, C., (2005): ICESat waveform measurements of within-footprint topographic relief and vegetation vertical structure. Geophysical Research Letters **32**: L21S10

HARDING, D. J., BLAIR, J. B., RABINE, D. R. and STILL, K., (1998): SLICER: Scanning LiDAR Imager of Canopies by Echo Recovery. Instrument and Product Description

HARDING, D. J., LEFSKY, M. A., PARKER, G. G. and BLAIR, J. B., (2001): Laser altimeter canopy height profiles; Methods and validation for closed-canopy, broadleaf forests. Remote Sensing of Environment **76**: 283-297

HESE, S., LUCHT, W., SCHMULLIUS, C., BARNSLEY, M., DUBAYAH, R., KNORR, D., NEUMANN, K., RIEDEL, T. and SCHROTER, K., (2005): Global biomass mapping for an improved understanding of the CO_2 balance - the Earth observation mission Carbon-3D. Remote Sensing of Environment **94**: 94-104

HILL, R. A. and THOMSON, A. G., (2005): Mapping woodland species composition and structure using airborne spectral and LIDAR data. International Journal of Remote Sensing **26**(17): 3763-3779

HYYPPÄ, J., KELLE, O., LEHIKOINEN, M. and INKINEN, M., (2001): A Segmentation-based Method to Retrieve Stem Volume Estimates from 3-D Tree Height Models Produced by Laser Scanners. IEEE Transactions on Geoscience and Remote Sensing **39**(5): 969-975

JENKINS, J., CHOJNACKY, D., HEATH, L. and BIRDSEY, R., (2003): National-Scale Biomass Estimators for United States Tree Species. Forest Science **49**(1): 12-35

KICHAK, R., (2003), Chairman's Executive Summary, Technical Report. Independent GLAS Anomaly Review Board, Available online at: http://icesat.gsfc.nasa.gov/docs/IGARB.pdf (accessed June 2005)

KOTCHENOVA, S., SHABANOV, N., KNYAZIKHIN, Y., DAVIS, A., DUBAYAH, R. and MYNENI, R., (2003): Modeling LiDAR waveforms with time-dependent stochastic radiative transfer theory for remote estimations of forest structure. Journal of Geophysical Research **108**, ACL 12: 1-13

LARSEN, D., HANN, D. and STEARNS-SMITH, S., (1987): Accuracy and Precision of the Tangent Method of Measuring Tree Height. Western Journal of Applied Forestry **2**(1): 26-28

LEFSKY, M., HARDING, D., KELLER, M., COHEN, W., CARABAJAL, C., DEL BOM ESPIRITO-SANTO, F., HUNTER, M., DE OLIVEIRA Jr., R. and DE CAMARGO, P., (2005): Estimates of forest canopy height and aboveground biomass using ICESat. Geophysical Research Letters **32**: L22S02

LEFSKY, M. A., HARDING, D., COHEN, W. B., PARKER, G. and SHUGART, H.

H., (1999a): Surface LiDAR Remote Sensing of Basal Area and Biomass in Deciduous Forests of Eastern Maryland, USA. Remote Sensing of Environment **67**: 83-98

LEFSKY, M. A., COHEN, W. B., ACKER, S. A., PARKER, G. G., SPIES, T. A. and HARDING, D., (1999b): LiDAR Remote Sensing of the Canopy Structure and Biophysical Properties of Douglas-Fir Western Hemlock Forests. Remote Sensing of Environment **70**: 339-361

LOS, S. O., COLLATZ, G. J., SELLERS, P. J., MALMSTRÖM, C. M., POLLACK, N. H., DEFRIES, R. S., BOUNOUA, L., PARRIS, M. T., TUCKER, C. J. and DAZLICH, D. A., (2000): A Global 9-yr Biophysical Land Surface Dataset from NOAA AVHRR Data. Journal of Hydrometeorology **1**(2): 183-199

LOS, S. O., JUSTICE, C. O. and TUCKER, C. J., (1994): A global 1° by 1° data set for climate studies derived from the GIMMS continential NDVI data. International Journal of Remote Sensing **15**(17): 3493-3518

MAGIC, (2007): GIS Digital Boundary Datasets Forestry Commission Woodland. Available online at: http://www.magic.gov.uk/staticmaps/national.htm (accessed January 2007)

MYNENI, R. B., HOFFMAN, S., KNYAZIKHIN, Y., PRIVETTE, J.L., GLASSY, J., TIAN, Y., WANG, Y., SONG, X., ZHANG, Y., SMITH, G. R., LOTSCH, A., FRIEDL, M., MORISETTE, J.T., VOTAVO, P., NEMANI, R. R. and RUNNING, S. W., (2002): Global products of vegetation leaf area and fraction absorbed PAR from year one MODIS data. Remote Sensing of Environment **83**: 214-231

NÆSSET, E., (2002): Predicting forest stand characteristics with airborne scanning laser using a practical two-stage procedure and field data. Remote Sensing of Environment **80**: 88-99

NELSON, R., NÆSSET, E., GOBAKKEN, T., STÅHL, G. and GREGOIRE, T., (2006): Regional forest inventory using an airborne profiling LiDAR. Proceedings of the International Conference Silvilaser 2006, 7th-10th November 2006, Matsuyama, Japan

NELSON, R., SHORT, A. and VALENTI, M., (2004): Measuring Biomass and Carbon in Delaware Using an Airborne Profiling LIDAR. Scandinavian Journal of Forest Research **19**: 500-511

NI-MEISTER, W., JUPP, D. L. B. and DUBAYAH, R., (2001): Modeling LiDAR Waveforms in Heterogeneous and Discrete Canopies. IEEE Transactions on Geoscience and Remote Sensing **39**: 1943-1958

NORTH, P. R. J., (1996): Three-dimensional forest light interaction model using a Monte Carlo method. IEEE Transactions on Geoscience and Remote Sensing **34**(4): 946-956

NORTH, P. R. J., (2002): Estimation of fAPAR, LAI and vegetation fractional cover from ATSR-2 imagery. Remote Sensing of Environment **80**: 114-121

NSIDC, (2006): The Attributes for ICESat Laser Operations Periods. Available online at: http://nsidc.org/data/icesat/data.html (accessed June 2006)

ORDNANCE SURVEY, (2006): OS Land-Form PROFILE DTM 1:10000 and 1: 25,000 Colour Raster ©Crown Copyright/database right 2006. An Ordnance Survey/EDINA supplied service

PATENAUDE, G., HILL, R., MILNE, R., GAVEAU, D., BRIGGS, B. and DAWSON, T., (2004): Quantifying forest above ground carbon content using LiDAR remote sensing. Remote Sensing of Environment **93**: 368-380

ROSETTE, J., NORTH, P. and SUÁREZ, J., (in press): Vegetation Height Estimates for a Mixed Temperate Forest using Satellite Laser Altimetry. International Journal of Remote Sensing, 3D Forestry Special Issue

ROYAL FOREST OF DEAN, (2006): History. Available online at: http://www.visitforestofdean.co.uk/history.htm (accessed February 2006)

SCHUTZ B., ZWALLY, H., SHUMAN, C., HANCOCK, D. and DIMARZIO, J., (2005): Overview of the ICESat Mission. Geophysical Research Letters **32**: L21S01

SELLERS, P. J., TUCKER, C. J., COLLATZ, G. J., LOS, S. O., JUSTICE, C. O., DAZLICH, D. A. and RANDALL, D. A., (1994): A global 1 degree by 1 degree NDVI data set for climate studies. Part 2: The generation of global fields of terrestrial biophysical parameters from the NDVI. International Journal of Remote Sensing **15**(17): 3519-3545

SUÁREZ, J., ONTIVEROS, C., SMITH, S. and SNAPE, S., (2005): Use of airborne LiDAR and aerial photography in the estimation of individual tree heights in forestry. Computers and Geosciences **31**: 253-262

TANSEY, K.J., LUCKMAN, A.J., SKINNER, L., BALZTER, H., STROZZI, T. and WAGNER, W., (2004): Classification of forest volume resources using ERS tandem coherence and JERS backscatter data. International Journal of Remote Sensing **25**: 751-786

UNFCCC, (2007): Kyoto Protocol. Available online at: http://unfccc.int/kyoto_protocol/items/2830.php (accessed April 2007)

ZWALLY, H., SCHUTZ, B., ABDALATI, W., ABSHIRE, J., BENTLEY, C., BRENNER, A., BUFTON, J., DEZIO, J., HANCOCK, D., HARDING, D., HERRING, T., MINSTER, B., QUINN, K., PALM, S., SPINHIRNE J. and THOMAS, R., (2002): ICESat's Laser Measurements of Polar Ice, Atmosphere, Ocean and Land. Journal of Geodynamics **34**: 405-445

ZWALLY, H.J., SCHUTZ, R., BENTLEY, C., BUFTON, J., HERRING, T., MINSTER, J., SPINHIRNE, J. and THOMAS., R. (2006): GLAS/ICESat L1A Global Altimetry Data and L2 Global Elevation Data and Global Land Surface Altimetry data V026. Boulder, CO: National Snow and Ice Data Center. Digital media.

(Received 13 January 2007)
(Accepted 3 August 2007)

Article

Forest Habitability for Wildlife as Evaluated by Airborne Laser Profiling

Sayoko Ueda[*1,2], Hayato Tsuzuki[*1] and Tatsuo Sweda[*1]

ABSTRACT

With an objective of evaluating forest habitability for wildlife in terms of forest structure, wildlife abundance was observed using automated infrared sensor cameras while forest structure of the habitat was quantified with airborne laser profiling in three study areas of 400ha each set up around Mt. Ishizuchi-san, Mt. Myoujin-ga-mori, and Mt. Takanawa-san in Ehime Prefecture, Japan. Two parameters derived from airborne laser profiling, i.e. mean and standard deviation of standing timber stock in each study area, were used as structural indexes of forests, while the richness of fauna was quantified as the number of inhabitant species and their frequency of being captured by the automated camera. Of the four possible combinations of the forest and faunal parameters, only the one between the photographic capture frequency and standard deviation of standing timber stock revealed strong negative correlation. Thus it was reasoned that the variability in timber stock has resulted from altitude variability within a given study area which tends to be more pronounced in higher and more remote areas, leading to a conclusion that what is really correlated with wildlife abundance is the proximity to the human domain.

Keywords: forest habitability for wildlife, airborne laser profiling, standing timber volume, infrared sensor camera

INTRODUCTION

Forest structure should be associated with its habitability for wildlife in some way. Young regenerating forest stands with their foliage layers close to the ground mean easy availability of food for herbivores, while their openness allows easy sighting by predators to result in less security. On the other hand, old mature stands have opposite pros and cons for feeding and nesting. What makes the regional evaluation of habitability for wildlife difficult is the complexity which innumerable forest stands of different species, age, area etc. create. This is the very reason why the airborne laser profiling was introduced in this study to characterize forest structure of extensive study areas. Should any relationship be found between the forest structure and abundance of wildlife, airborne laser profiling would prove to be a versatile tool for quantitatively estimating not only timber resources but also wildlife habitat over an extensive range.

As a matter of fact NELSON *et al.* (2005) suggested relationship between the habitat of Delmarva fox squirrels (*Sciurus niger cinereus*) and tree height and canopy closure recorded using airborne laser profiling. In our study the mean and standard deviation of standing timber stock were chosen to represent forest structure of a given study area since they are readily measurable by airborne laser profiling and that they seem to be associated with welfare for wildlife in terms of food availability and security.

METHOD

A study area of approximately 400ha was set up each around Mt. Ishizuchi-san (1,982m a.s.l.), Mt. Myoujin-ga-mori (1,216m) and Mt. Takanawa-san (986m) in Ehime prefecture, Japan (Fig.1). At mean altitude of 1,300m the Ishizuchi study area is the highest with vegetation ranging from dwarf stands of such sub-alpine species as birch (*Betula ermanii*) on and near the ridges to lush and tall stands of deciduous broadleaved species and plantation of cedar (*Cryptomeria*

Corresponding author: Sayoko Ueda
[*1] Faculty of Agriculture, Ehime University. 3-5-7 Tarumi, Matsuyama, Ehime, 790-8566, Japan
Phone/ Fax: +81-89-946-4876/+81-89-946-9879
E-mail: [1] dhole@agr.ehime-u.ac.jp,
[2] zzukky@agr.ehime-u.ac.jp,
[3] sweda@agr.ehime-u.ac.jp
[*2] present address : Faculty of Bioscience and Biotechnology, Tokyo Institute of Technology 2-12-1 Ookayama, Meguro-ku, Tokyo, 152-8551, Japan
Phone/ Fax: +81-3-5734-3383/+81-3-5734-2946
E-mail: ueda.s.ab@m.titech.ac.jp,

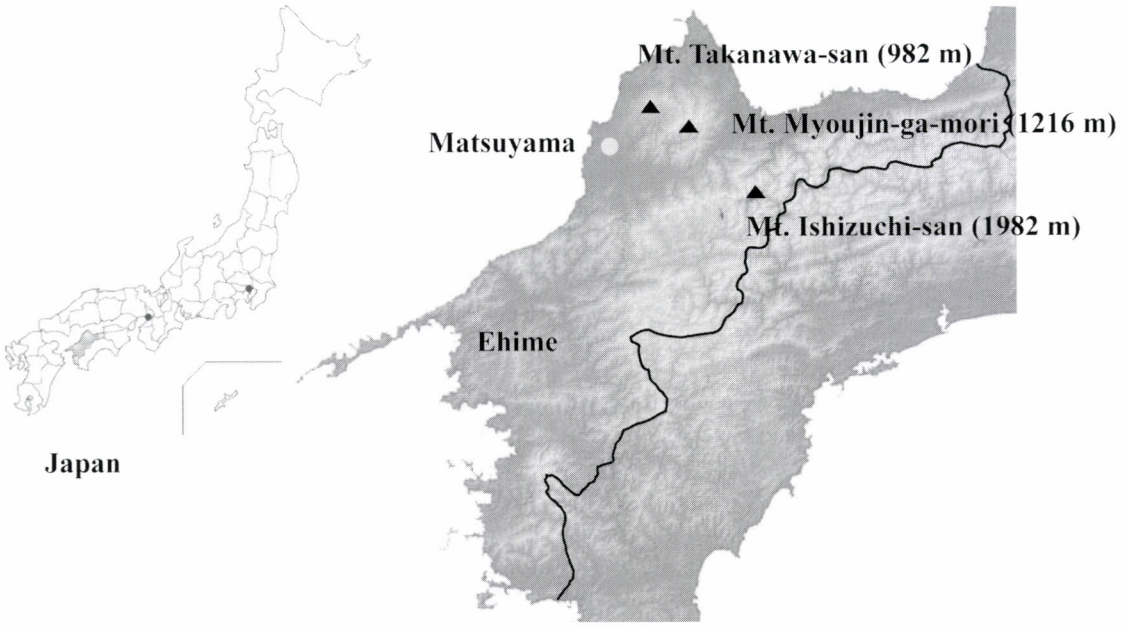

Fig. 1 Study area: Three mountain of Ehime prefecture and these altitudes

japonica) and cypress (*Chamaecyparis obtusa*) on lower slopes toward the valley bottom. It is also the remotest from the heavily populated area of the Matsuyama Plain. At mean altitudes of 800m and 500m respectively, the Myoujin and Takanawa study areas are not only lower in elevation but also closer in this order to Matsuyama, the capital of the prefecture. Both the areas are basically covered by plantation-forest of ceder and cypress with some remnants of such natural vegetation as beech (*Fagus crenata*) and hemlock (*Tsuga sieboldii*) on upper slopes and ridges with increasing dominance of fir (*Abies firma*), chinquapin (*Castanopsis* spp.) and evergreen oak (*Quercus* spp.) down the slope with sporadic mixture of tiny cultivated lands along the lower valley bottom.

The standing timber stock was estimated by airborne laser profiling flown for approximately 4km through each study area (Fig. 2). These data constitute a parts of the nadir laser altimetry dataset acquired in September 2005 using the NASA's Portable Airborne Laser System (PALS) over the entire Ehime prefecture along 23 transects totaling 1360km. The mission was flown 200m above the ground at a nominal cruising speed of 180km/hr with an altimetry data retrieval frequency of 400 Hz to result in the altimetry interval of 0.13m horizontally along the flight track. However, with the steep terrain slowing both the uphill and downhill flights, the final altimetry interval turned out to be 0.08m horizontally along the flight track. The primary data include reflections both from the canopy and the ground. A continuous ground profile was estimated by interpolating ground reflections, which subsequently was subtracted from the canopy profile to obtain the vegetation profile $h(x)$. Standing timber volume V (m³/ha) was estimated on a basis of its correlation with the area $\bar{S}$ (m²/m) under the vegetation profile per unit fight distance (TSUZUKI, 2004; TSUZUKI *et al.*, 2006), i.e.

$$V = a \cdot \bar{S} = a \cdot \frac{\int h(x)\,dx}{\int dx} \approx a \cdot \frac{\sum \Delta x \cdot h_i}{\sum \Delta x} = a \cdot \bar{h} \qquad (1)$$

where

x: distance along the flight track (m),

a: constant (m²/ha), and

$\bar{h}$: mean vegetation height (m).

The constant a = 31.9m²/ha is obtained as a ratio of vegetation profile area S to the standing timber volume actually measured in 34 sample plots of 100-700m² each laid out randomly directly under the fight path (TSUZUKI *et al.* in prep.). However, the value is tentative since this ground truth survey is still under way for final target count of 200 plots, and it would take some time to finalize. To obtain the standard deviation of standing timber stock along with the mean and total, the stock estimation was conducted for each 10m segments of vegetation profile.

The wildlife observation was conducted with automated infrared sensor cameras from August 2005 till October 2006, but the actual duration and intensity of observation varied by study area. The most intensive observation was made in the Myoujin area (MM, Fig. 2-b) with five automated cameras deployed alternately at 16 different localities within the study area for the entire period of observation. For Ishizuchi (MI, Fig. 2-a) three cameras were deployed at 15 localities but with an interruption from December 2005 to June 2006 due to winter closure of the access road. To compensate for the loss, similar automated photographic observation by YAMAMOTO *et*

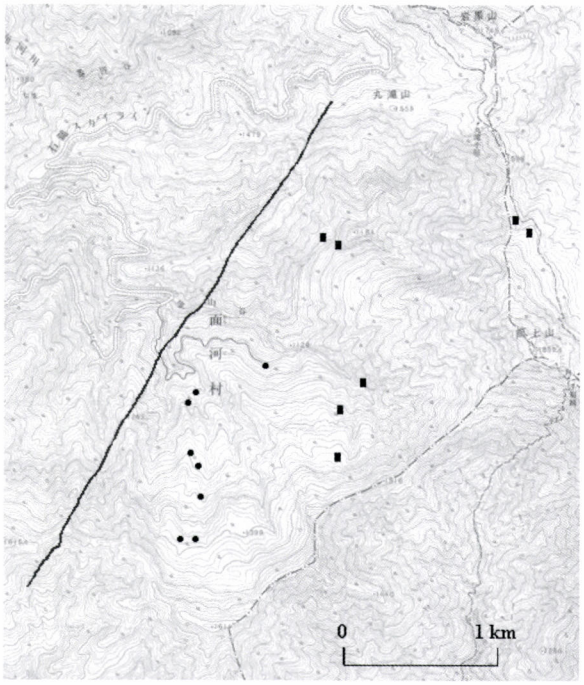

a: Ishizuchi

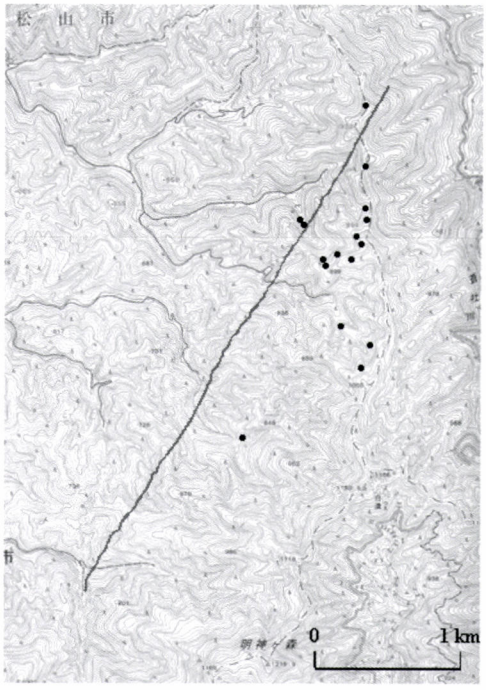

b: Myoujin

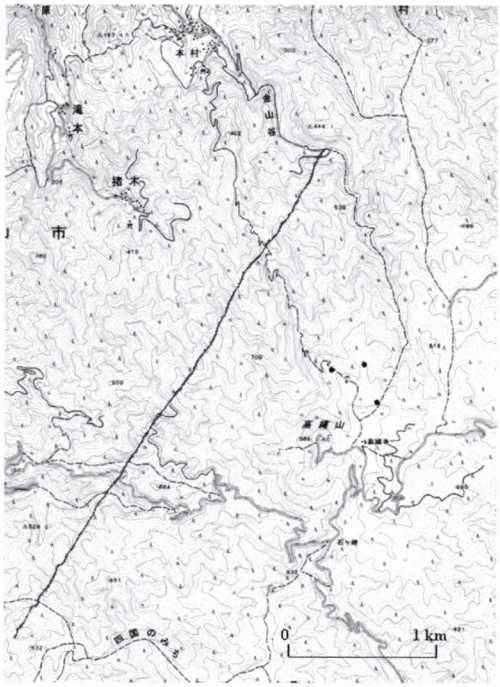

c: Takanawa

Fig. 2a-c Laser profiling transect and camera locality of study area
a, b and c figures study areas of Ishizuchi, Myoujin and Takanawa respectively.
Lines indicate the airborne laser profiling transects.
Dots indicate observation camera locality (● by this study, ■ by YAMAMOTO *et al.* (2006)).

al. (2006) during the snow-free period of May to November in 2004 and 2005 was also used. With only two cameras at three localities from July to October 2006, observation in Takanawa (MT, Fig. 2-c) was the shortest and least intensive.

The cameras were set up focusing on animal trails in a wide variety of topography and vegetation without any bait, but in the observation by YAMAMOTO *et al.* (2006) such bait as honey and wine had been used. In both cases the cameras used are 35-mm focal length "Field Note I" and "Field Note II" (Marif.Co.Ltd) equipped with an infrared motion sensor to trigger the shutter automatically. ASA 400 films of 36 exposures were exchanged along with batteries in one to three months before they are exhausted. The cameras were wrapped in waterproof film and plastic case, and fixed on nearby trees by clamp.

The target fauna consists of 16 species, and include such carnivores as red fox (*Vulpes vulpes japonica*), raccoon dog (*Nyctereutes procyonoides viverrinus*), masked palm civet (*Paguma larvata*), badger (*Meles meles anakuma*), Japanese marten (*Martes memlampus memlamous*) and J. mink (*Mustela itatsi*); such hoofed mammals as shika deer (*Cervus nippon nippon*) and wild boar (*Sus scrofa leucomystax*); such other mammals as J. macaque (*Macaca fuscata fuscata*), J. hare (*Lepus brachyurus brachyurus*), J. squirrel (*Sciurus lis*), flying squirrel (*Pteromys momonga*) and mice (*Apodemus* spp.), and such avian species as ural owl (*Strix uralensis*), copper pheasant (*Phasianus Sommerringii intermedius*) and J. night heron (*Gorsachius goisagi*). Bats and canopy-feeding small birds, also very common in Ehime prefecture and captured by our camera as well, were discounted in this study since they normally do not feed on the ground and their capture seems rather accidental. Richness of the fauna with those 16 species was evaluated by the number of species and their frequency of appearance as they were photographed in a given study area. The appearance frequency F was quantified as exposure frequency per day per camera without any regard to animal individuality, i.e.

$$F=\frac{\sum M_i}{\sum D_i}, \qquad (2)$$

where

M_i: total number of wildlife photographed by the ith camera, and

D_i: total number of observation days made by the ith camera.

RESULT

The results are shown in table 1. In terms of mean standing timber stock, the forest structure of the three study areas tuned out to be almost the same, but were significantly different in terms of standard deviation. This difference in standard deviation may be best explained by the variability in altitude within each study area. In the Ishizuchi area, the contrast between the bushy vegetation even sporadically devoid of woody species on the ridge and lush growth of conifer plantations and remnant broadleaved deciduous stands near the valley bottom contributed to the large standard deviation. On the other hand, relatively less altitude variability in the Myoujin and Tankanawa areas did to lessen standard deviation.

In wildlife observation, the automated cameras captured target animals totals of 209, 549 and 49 times respectively in Ishizuchi, Myoujin and Takanawa. When adjusted for the difference in observation period and number of cameras deployed, the mean sighting frequency per day per camera respectively translates to 0.13, 0.21 and 0.37 times and in strong negative correlation (Fig. 4-a) with standard deviation of standing timber stock ($r = -0.921$, $p>0.05$).

As for the number of resident wildlife, all the 16 target species were identified by the automated camera in the Myoujin area (Fig. 3), while it was only 11 species in Ishizuchi with fox, deer, flying squirrel, owl and heron being absent, and 10 species in Takanawa with fox, mink, squirrel, flying squirrel, owl and heron absent. The observed numbers of resident species may well represent the reality for Myoujin and Ishizuchi where the gross observation intensity exceeds 1500 camera·days each. However, this may not be the case for Takanawa where the observation intensity was significantly weak at only one fifteenth of the former two areas, and considering its highest wildlife sighting frequency, there is a good possibility that further observation may reveal all the 16 target species.

Fig. 4-a shows the correspondence between the wildlife

Table 1 Wildlife richness and forest strucre

	Study Area	MI	MM	MT
Wildlife	Observation days	574	435	84
	Cumulative camera days	1,663	2,648	134
	Total number of photographic capture	209	549	49
	Appearance frequency (/ day/ camera)	0.13	0.21	0.37
	Number of species identified	11	16	10
Forest Structure (Standing timber stock)	Mean (m^3/ha)	202.5	199.7	204.0
	Standard deviation (m^3/ha)	93.7	76.3	68.6

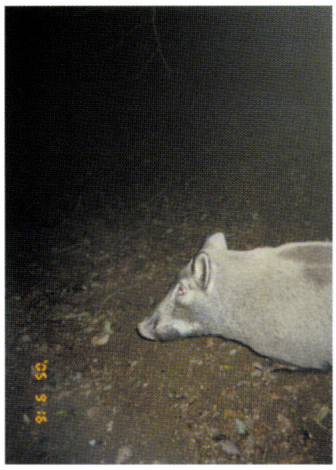

a): Wild boar

b): Shika deer

c): Red fox

d): Raccoon dog

e): Bagger

f): Japanese marten

Fig. 3 Observed fauna (All of them were observed at the Myoujin area.)

g): J. mink

h): Masked palm civet

i): J. macaque

j): J. hare

k): Flying squirrel

l): Mouse

Fig. 3 continue

m): J. squirrel

n): Ural owl

o): Copper pheasant

p): J. night heron

Fig. 3 continue

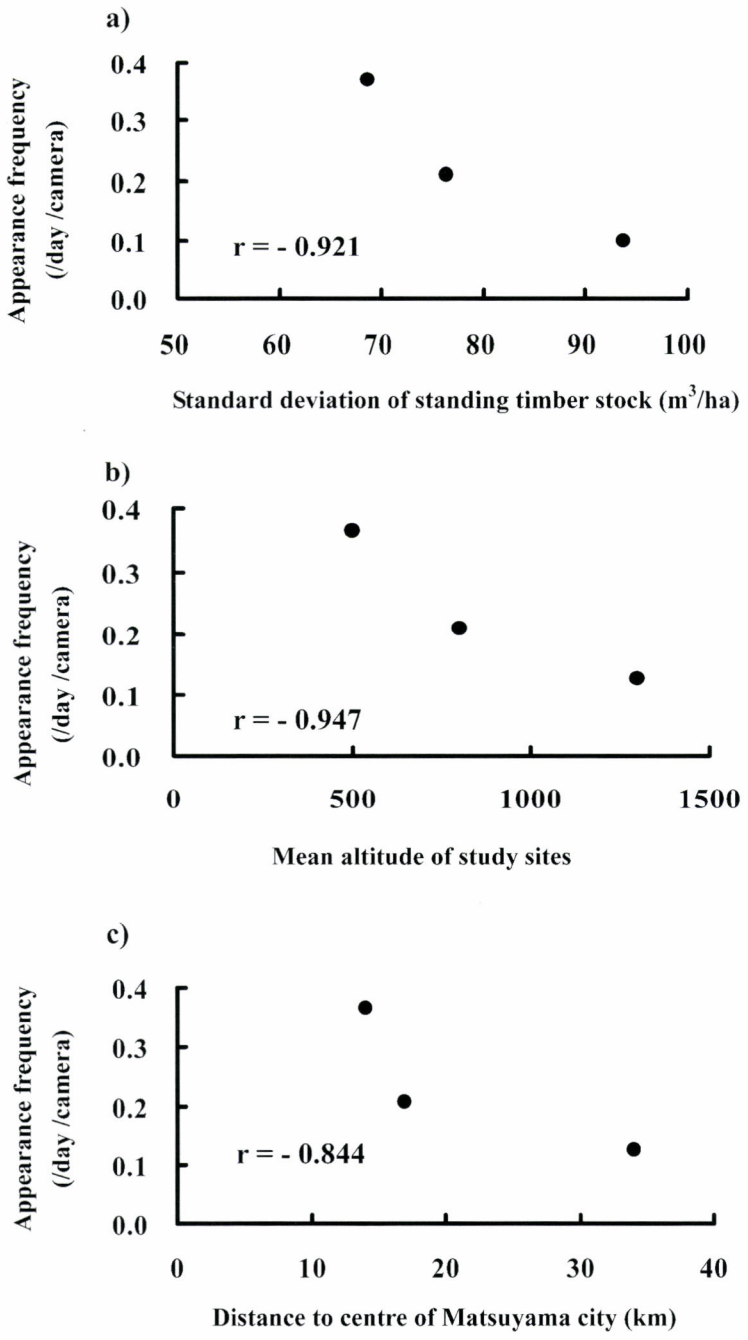

Fig. 4 Relation between appearance frequency of wildlife and standard deviation of standing timber stock (a), mean altitude of study sites (b) or distance to centre of Matsuyama city (c)

appearance frequency and standard deviation of standing timber stock, which is the only relationship found seemingly significant in the present analysis between forest structure and wildlife richness. However, the negative correlation in Fig. 4-a is rather hard to explain from wildlife ecology point of view since with higher availability of food in younger stands and more places to hide in older stands, greater variability in standing timber stock should be more favorable for wildlife welfare. Thus, considering the aforementioned fact that the variability in standing timber stock is associated with altitude variability, which in turn is further associated with the absolute altitude of the study area and its remoteness from the human domain, it is more reasonable to conclude that the negative correlation in Fig. 4-a is simply apparent with hidden but true

correlation existing between wildlife abundance and proximity to the human domain. As a matter of fact, the wildlife appearance frequency is equally well and negatively correlated with altitude of the study sites and their distances from the local population center of Matsuyama (34km to Ishizuchi, 17km to Myoujin, and 14km to Takanawa) as shown in Figs. 4-b ($r=-0.947$, $p>0.05$) and 4-c ($r=-0.844$, $p>0.05$).

In a closer look into the correlation by species, the affinity to the human domain remained the same for herbivores and omnivores, but not for carnivores, i.e. the correlation between appearance frequency and standard deviation of standing timber stock (and equivocally site altitude and distance from Matsuyama) was negative for herbivores (deer, hare, and mouse) and omnivores (raccoon dog, masked palm civet, macaque, boar and pheasant) but positive for carnivores (marten and bagger) with exception of fox, mink, squirrel, flying squirrel, night heron and owl which were absent in one or two sites and the specific correlation analysis was not possible. This misanthropic tendency of carnivores can also be seen in their absolute frequency of appearance. The top two wildlife in Ishizuchi are J. marten and bagger while they are wild boar and masked palm civet in Myoujin and deer and raccoon dog in Takanawa.

DISCUSSION

With the limitation of only three study sites, even apparently strong correlations between wildlife and forest structure/location variables did not turn out to be significant statistically. Thus the following discussion is limited to the one on the tendency, but two patterns seem to be obvious, i.e., while herbivores and omnivores have strong affinity to the human domain, carnivores namely the weasel family tend to be misanthropic.

Three reasons are conceivable for herbivores and omnivores. Firstly, their natural habitat ranges from mountains to plains, with the latter now under human domination (KOMIYA, 2002; EHIME pref., 2003 ; IMAIZUMI and HIRANO, 2004). Additionally they are not misanthropic, and their sighting even in urban area is not rare. Secondly, with widespread orchard and farmland, more food is available closer to the human domain. In addition, abandoned orchard and farmland increasing over the past decades in the neighborhood of forested areas are much easier to graze and vandalize. Finally, the declining hunter population of the prefecture is making approach to the vicinity of human domain safer and easier. According to the MINISTRY of the ENVIRONMENT (2004), issue of hunting license in the prefecture decreased by ten percent in six years from 1998 to 2004 with rapidly increasing proportion of old and dormant license holders.

The misanthropic reasons for weasels are less obvious because such a strong tendency is found only in J. marten while J. mink is well known for their appetite for domestic fowl. The possibility is that being a competing carnivore, weasels tend to be repelled by dogs and cats around the human domain.

In conclusion, no direct correspondence was found between wildlife abundance and forest structure against the original objective and expectation of the present study. However, present finding that wildlife richness is much less associated with forest structure than with proximity of forests to the human domain was made possible only by the airborne laser profiling which enables us quick, accurate and expedient quantification of extensive forested area.

LITERATURE CITED

EHIME pref., Environment division, (2003): Red Data Book, EHIME. Ehime pref., 447pp (in Japanese)

IMAIZUMI, T. and HIRANO, M., (2004): Encyclopedia of Animal Tracking. Tokyodoshuppan, (8) + 309pp (in Japanese)

KOMIYA, T., (2002): Mammals in Japan. Field Best Encyclopedia 12, Gakken, 256pp (in Japanese)

MINISTRY of the ENVIRONMENT, Wildlife division, Nature conservation Bureau, "yachouju kankei toukei" (2004): Online, Internet, http://www.sizenken.biodic.go.jp/wildbird/sim-ple/toukei/guide.html (in Japanese)

NELSON, R., KELLER, C. and RATNASWAMY, M., (2005): Locating and estimating the extent of Delmarva fox squirrel habitat using an air borne LiDAR profiler. Remote Sensing of Environment **96**: 292-301

TSUZUKI, H., (2004): Long-range Estimation of Standing Timber Stock and Biomass in Boreal Forest Using Airborne Laser Altimetry. Ph.D. Diss., Ehime Univ., Ehime, Japan (in Japanese)

TSUZUKI, H., KUSAKABE, T. and SWEDA, T., (2006): Long-range Estimation of Standing Timber Stock in Western Boreal Forest of Canada Using Airborne Laser Altimetry. J. Jpn. For. Soc. **88**: 103-113 (in Japanese with English abstract)

TSUZUKI, H., NELSON, R. and SWEDA, T.: Timber Stock Estimate by air borne Laser Profiling for entire Ehime Prefecture, Japan. (in preparation for J. Forest Planning)

YAMAMOTO, T., MIYAUCHI, F., MIYAMOTO, T., FURUKAWA, M., YANO, S., KANAZAWA, B., YACHIMORI, S. and KANESHIRO, Y., (2006): An automatic photographing of Ishizuchi Range, Shikoku, Japan, Bulletin of Omogo Mountain Museum **2**: 37-44 (in Japanese)

(Received 15 January 2007)
(Accepted 8 May 2007)

Article

Analysis of Canopy Structure in Beech (*Fagus crenata*) Secondary Forests using an Airborne Laser Scanner

Ai Nishikami[*1,3], Yukihiro Chiba[*1], Yoshio Awaya[*1] and Yoshitaka Kakubari[*2]

ABSTRACT

Airborne Light Detection and Ranging (LiDAR) is a useful tool for scaling up physiological processes from an individual tree to the landscape level, because it can measure parameters that are related to canopy structure. The objectives of this study were (1) to calculate the canopy and stand parameters that characterize the heterogeneity of beech canopies and stands from LiDAR data and (2) to examine the applicability of these parameters by comparing them with field census measurements. A total of eight census plots with various stand structures were set up in beech forests on the Appi plateau (Iwate Pref., northern Japan) and on Mt. Naeba (Niigata Pref., central Japan). LiDAR data was used to calculate several parameters for describing canopy structure: gap ratio; mean canopy height; standard deviation (SD) and coefficients of variance (CV) of canopy height models (CHMs); canopy and stand surface area derived from the CHMs and digital surface models. The gap ratios and CVs of the CHMs were closely related to basal area (BA), and it may be possible to use them to quantify this variable when factors such as low gap ratio and topographic condition are considered. The CV tended to increase with the gap ratio. In contrast, canopy surface area was not strongly related to the canopy structure parameters. Consequently, the gap ratio and the CVs of the CHMs are the preferable parameters for representing structural properties of beech stands. Further analyses are needed to understand uncertainties in the relationships (*inter alia*) between, gap sizes, canopy height and individual tree size.

Keywords: Beech forests, gap ratio, canopy surface area, CV of CHM

INTRODUCTION

Scaling up physiological processes from an individual tree to the landscape level requires quantitative knowledge of the relationships between canopy structures and the architectural development of forest trees. It is essential to understand forest structure in a large area. However, information about forest structure has not been sufficiently described by linking ordinary field census measurements with passive optical remote sensing, because the field census data is conducted on too small of an area for the two-dimensional remote sensing data. Airborne Light Detection and Ranging (LiDAR) has proved to be a useful tool for measuring canopy structures at an appropriate large scale. Using this technique, the three-dimensional canopy structure can be analyzed in more detail than by either ordinary field census or passive optical remote sensing.

Various analyses of forest structure, using airborne LiDAR data, have been reported: e.g., detecting individual tree crowns in deciduous forests (Brandtberg *et al.*, 2003), estimating canopy profile, leaf area index (LAI), and the aboveground biomass of broad-leaved forests (Lefsky *et al.*, 1999; Lovell *et al.*, 2003; Parker and Russ, 2004; Riaño *et al.*, 2004). In further studies, Riaño *et al.* (2004) found that the percentage of 'canopy hits' was the best LiDAR-derived estimator of canopy properties in oak forests, while Parker and Russ (2004) related the standard deviations of canopy height to LAI in Tulip poplar forests. However, additional effort is needed to develop more reliable and useful LiDAR method for the purpose of scaling physiological processes. Some of the architectural parameters derived from LiDAR methods, such as canopy shape, canopy surface and canopy

Corresponding author: Ai Nishikami
[*1] Forestry and Forest Products Research Institute, Tsukuba, Ibaraki 305-8687, Japan
[*2] Fucluty of Agriculture, Shizuoka University, Shizuoka, Shizuoka 422-8017, Japan
[*3] Present address: Colorado State University, Fort Collins, Colorado 80523-1472, USA

gaps, might provide desirable information related to canopy structure and particularly the amount of leaves and branches; these foliage measurements are necessary to scale-up ecophysiological processes. These parameters are not directly related to the quantity of foliage and branches, therefore we will compare LiDAR measurements with the properties of canopy structure obtained from ordinary field census in forest stands.

Scaling-up physiological processes is required to evaluate carbon sequestration and growth response of forest stands under climate change, particularly in natural forests such as the beech forests commonly found in cool-temperate regions of Japan. Compared to artificial conifer forests, natural broadleaved forests tend to be more heterogeneous in terms of both species composition and the spatial patterns of canopy structure. The heterogeneity of broadleaved forests makes it difficult to describe their canopy and stand structures. LiDAR methods, however, can be used to evaluate larger beech forest area and accomplish the objectives of our study which are (1) to calculate the canopy and stand parameters that characterize the heterogeneity of beech canopies and stands and (2) to examine the applicability of the parameters by comparison with stand structures measured by field census.

MATERIALS AND METHODS

Study Site and Field Measurement

The beech forests sites are located on the Appi plateau, Iwate Pref., northern Japan, (140°56′E; 40°00′N; 825m a.s.l.) and Mt. Naeba, Niigata Pref., central Japan (138°44′-138°46′E; 36°51′-36°56′N; 550 - 1,500m a.s.l.) (Fig. 1). Appi beech forests can be separated into two types: secondary forests that have comparatively uniform canopy structures; and selectively cut forests, which have a more heterogeneous structure. The stand age of Appi beech forests is about seventy years. The Appi beech forests grow on a gentle slope of 6°. Three census plots (Appi-1 to -3) were established in secondary forest, and Appi-4 was in an area of selective cutting.

At Naeba there are four census plots, each at a different altitude: Naeba-1 is at 550m a.s.l., Naeba-2 and -4 at 900m a.s.l., and Naeba-3 at 1,500m a.s.l. Naeba-1, -2 and -3 are on gentle slopes, but Naeba-4 is in a depression. The ages of the stands at Naeba-1, -2 and -3 are about 150-200, 80-90 and 190-260 years, respectively (KUBOTA *et al.*, 2005; KAKUBARI, 1975).

The topographic position and DBH (diameter at 1.3m above the ground) of all trees with DBH ≥ 5cm were measured in each census plot. Except for Appi-4 and Naeba-4, tree heights were also measured. Naeba-1, -2 and -3 plots were delimited in the 1960s and the DBH of all stems in their plots have been measured periodically since then. The stand characteristics of the census plots are shown in Table 1.

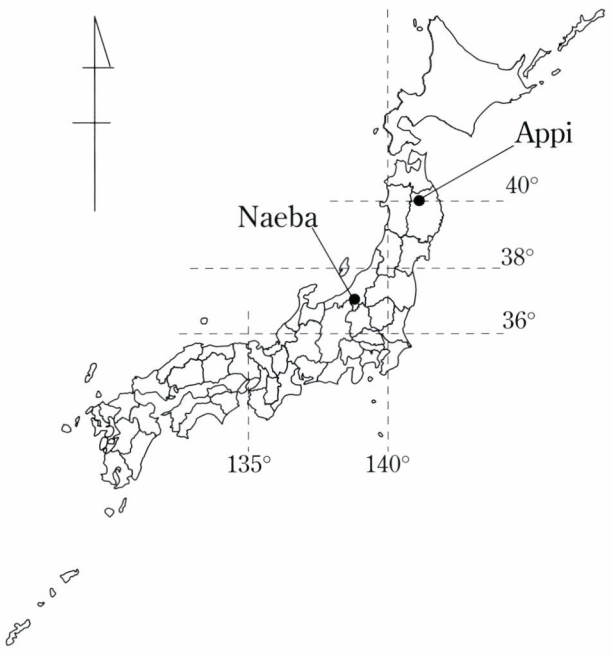

Fig. 1 Location of study sites

Table 1 Stand characteristics

Plot name	Stand density (stem no./ha)	Mean DBH (cm)	Mean Height (m)	Stand Basal Area (m^2/ha)	Plot size (m^2)	Stand age	Note
Appi-1	2,208	14.7	14.1	46.6	610	70	Appi secondary forest
Appi-2	1,244	19.9	14.2	50.8	2500	70	Appi secondary forest
Appi-3	802	22.0	15.6	40.8	935	70	Appi secondary forest
Appi-4	127	32.3	-*1	14.3	2965	-*1	Appi selectively cut forests
Naeba-1	265	38.0	23.7	40.4	2000	150 - 200*2	Mt. Naeba 550m a.s.l.
Naeba-2	1,033	23.2	18.3	48.3	600	80 - 90*2	Mt. Naeba 900m a.s.l.
Naeba-3	450	24.7	13.0	30.4	1000	190 - 260*2	Mt. Naeba 1,500m a.s.l.
Naeba-4	362	32.1	-*1	32.5	1545	-*1	Mt. Naeba 900m a.s.l.

*1: not measured
*2: referred to KUBOTA *et al.* (2005) and KAKUBARI (1975)

LiDAR Measurement

The airborne LiDAR data from the Appi beech forests were acquired in September 2001 over a 1km × 1km area, using an Asahi Laser Mapping System (Aero Asahi Co., Japan) deployed on a helicopter. The data acquisition in Naeba, using the same set-up, was undertaken in July and August 2003 over 400m × 400m area for all plot sites. At Appi, the flying height was 200-300m above the ground, the flight speed was 13.9 m/s, the beam divergence of the laser was 1.2 mrad, and the laser sampling density was 14 to 17 points/m^2. At Naeba, the flying height was 500-600m above the ground, the speed was 19.4m/s, the beam divergence of the laser was 0.2 mrad, and the laser sampling density was 8 to 11 points/m^2. The scan angles were at ±20 degrees and the pulsing frequency was 25,000Hz at both sites. Both the first and last return pulses were recorded.

The data sets obtained from the LiDAR measurement data include a digital terrain model (DTM), digital surface model (DSM), and canopy height model (CHM) calculated by subtracting DTM from DSM for each site. Each data set was described using three coordinates: horizontal east-west, horizontal north-south, and vertical. The horizontal coordinates were at 0.5m intervals.

Parameters Derived from LiDAR

In order to compare the canopy status with the stand structure of the census plots, we employed seven parameters calculated from LiDAR measurements: i.e., gap ratio, mean canopy height, standard deviation (SD) and coefficient of variance (CV) of CHM for canopy, SD of CHM for stand, canopy surface area and stand surface area. All the parameters can be calculated from the CHMs and DSMs. The SD and CV of CHM for canopy or stand represent the variations in the canopy or stand surface. The gap ratio denotes the ground cover ratio of gap area to stand area of the forest. The canopy surface area over the corresponding ground area reflects the roughness of the canopy surface, which may relate to the stand leaf areas because most leaves tend to aggregate towards the canopy surface. The stand surface area would depend on the roughness of the stand including both the canopy surface and the ground area where there is no canopy layer. Grid squares of 50m × 50m were set up in each study site (54 grid squares in total), in order to compare the relationship between the canopy parameters: gap ratio, CV of CHM and canopy surface area.

The SDs of stand and the stand surface area were calculated using all CHM and DSM data in each census plot area. To determine canopy surface areas from LiDAR data, the discrimination between canopy level and non-canopy level was needed. Hence, the following criteria of CHM and DSM value were adopted. CHM values less than 5m were regarded as shrubs and/or the ground surface, since most trees in the census plots were ≥ 5m. In order to judge whether the CHM values of neighboring grids belong to a continuous canopy surface or not, the threshold for the vertical maximum difference between neighboring DSM grids was set to 3.5m. The 3.5m threshold was determined by measuring the crown shape of isolated beech trees: i.e. the vertical difference of crown surface over a horizontal distance of 0.5m was less than 3.5m for beech trees. Areas where CHM < 5m and neighboring DSM values differed in elevation by more than 3.5m were classified as gap areas. The gap ratio of the site was then the gap area divided by the entire study area.

RESULTS AND DISCUSSION

Stand Structure from the Field Census

The stand density in the Appi secondary forests (Appi-1, -2 and -3) ranged from 802 to 2,208 trees/ha; this was much higher than the 130 trees/ha in the Appi selectively cut forest (Appi-4). The mean DBH of the Appi secondary forest was 14.7-22.0cm, while that of the Appi-4 was 32.3cm (Table 1). The mean DBH in each Naeba census plot was larger than those in the Appi secondary forests (Table 1). The stand density was low, 265-450 trees /ha, and the stand basal area (BA) was moderate, 30.4-40.4 m^2/ha, in Naeba-1, -3, and -4 (Table 1). In Naeba-2, the stand density was higher than in the other plots on Mt. Naeba. At all of the census plots, mean DBH tended to decrease with stand density. A large number of relatively small trees were present in the Appi secondary forests and in Naeba-2, while large trees were sparsely distributed in the selectively cut forests at Appi and in the other plots at Naeba.

It is difficult to determine the successional stage of a forest from diameter distribution and mean DBH data without additional information, since stand structure is influenced by a range of factors (e.g. soil conditions and topography) besides tree size and stand density. However, Naeba-1 and -3 appeared to be more mature than the Appi secondary forests (Appi-1, -2 and -3) and Naeba-2 because these sites have older (KUBOTA *et al.*, 2005; KAKUBARI, 1975) and larger trees (Fig. 2). Of all the study plots, it was most difficult to determine the successional stage of Naeba-4 and Appi-4 because of topographic conditions and the selectively cutting, respectively.

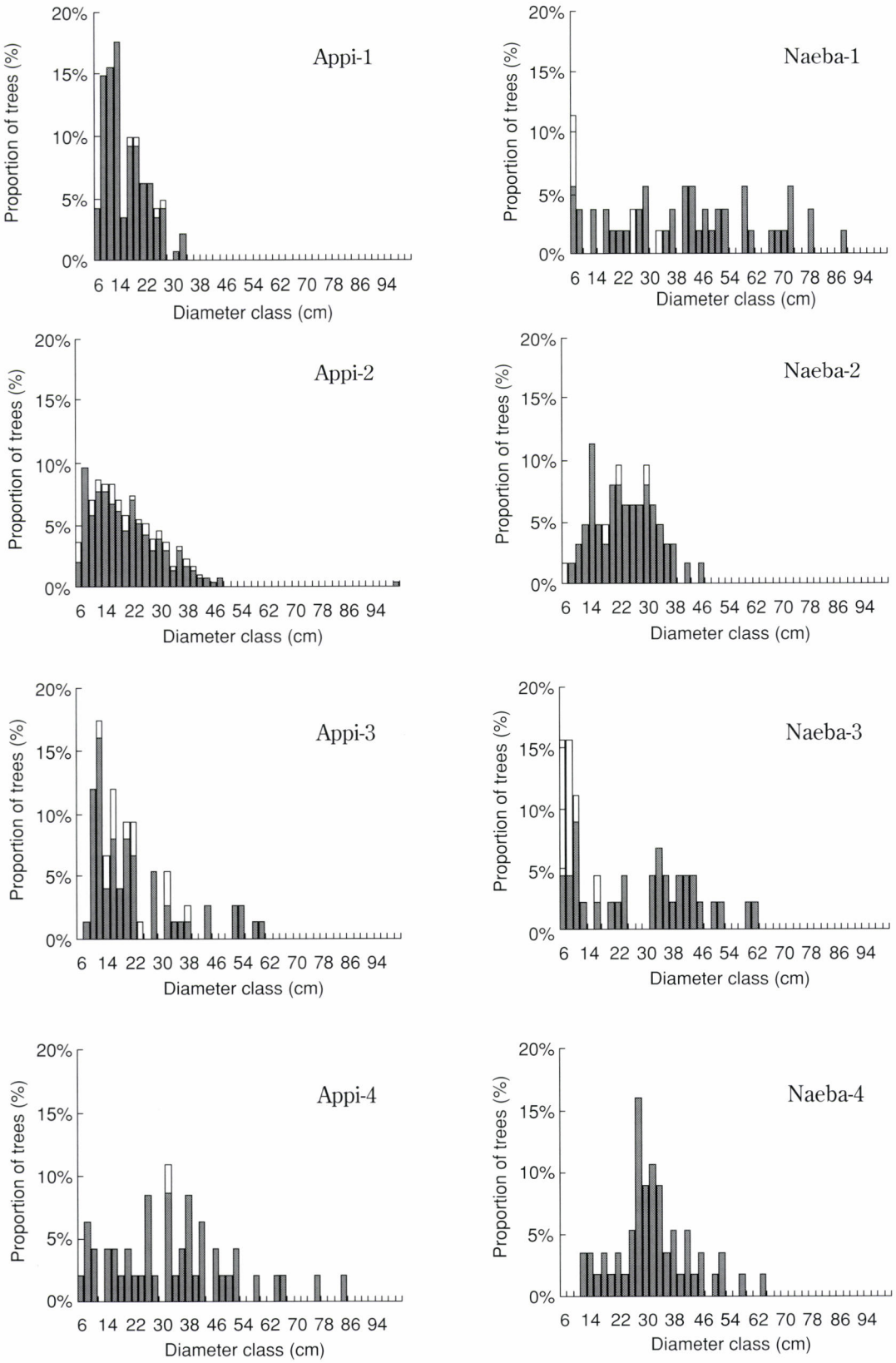

Fig. 2 Diameter distribution in census plots
*White columns indicate species other than beech.

Comparison of Stand Structures Determined by Field Census and LiDAR Derived Canopy Parameters

The gap ratio, mean canopy height, SD and CV of CHM for canopy, SD of CHM for stand, and canopy and stand surface area were calculated from CHMs and DSMs for each field census plot (Table 2). The gap ratios in Appi-1, -2 and -3, Naeba-2, and Naeba-4 were the lowest (1-3%) suggesting completely closed canopy, while those in Appi-4, Naeba-1 and Naeba-3 were relatively high (53%, 17%, and 38%, respectively). Artificial selective cutting was the cause of the high gap ratio in Appi-4, whereas the high ratios in Naeba-1 and -3 were ascribed to mortality of tall trees around 10-20 years ago. NAKASHIZUKA (1984) recorded a gap ratio of 20.5% for beech forests with stands that were more mature than those at our study sites.

Mean canopy heights calculated from CHMs were higher than the mean tree heights measured during the field census (Table 1 and 2), though many studies show mean height from LiDAR data being lower than field census (e.g. COOPS *et al.*, 2007; NÆSSET, 1997). The reason would be we count all trees with DBH ≥ 5cm in field census, whereas the canopy heights estimated by LiDAR data were based on the "canopy" criteria as mentioned before.

The SD and CV of the CHMs for canopy and the SD for stand in Appi-1, -2 and -3 and Naeba-2 were smaller than those in Appi-4, Naeba-1, -3, and -4. The SD of the canopy height, calculated from laser altimetry data, was found to increase with the successional stage of Tulip poplar forests in Maryland, USA (PARKER and RUSS, 2004), which corresponded to our results. However, the parameter of canopy surface area did not vary so much between the census plots: approximately 2.0 ha/ha in each plot. But the stand surface area varied considerably 2.0-6.1 ha/ha (Table 2). In the secondary and primary forests in French Guiana, the ratios of canopy surface area to ground surface area of 1.2 and 2.1 have been recorded (BIRNBAUM, 2001). These values are comparable with our results, although slight differences existed in the methods for measuring and calculating the parameter. The values tended to differ according to the successional stage in the range of 2.0-2.4 and 3.9-5.0 in younger forests (Appi secondary forests and Naeba-2) and more mature forests (Naeba-1 and -3), respectively.

The stand density was compared with the following canopy parameter: the gap ratio, canopy surface area and the CVs of the CHMs (Fig. 3). The gap ratio is the most basic parameter and is highly correlated with the SD for stand and stand surface area. The canopy surface area and CVs of the CHMs are expected to describe canopy condition. In Appi-1, -2 and -3 and Naeba-2 the stand densities were higher than 800 trees/ha, the gap ratios and the CV of the CHM were lower than 5% and 10%, respectively (Fig. 3 (A) and (B)). The high stand density resulted in high canopy closure, thus the gap ratios and CVs were low. Appi-4, Naeba-1 and -3 exhibited comparatively low tree densities, and the values of the gap ratio and the CVs of the CHMs appeared to be higher than the other stands (Fig. 3 (A) and (B)). It should be noted, however, that the gap ratios and the CVs of the CHMs were not closely related to the stand densities. For example, although the stand density at Naeba-4 was low, the gap ratio was also unexpectedly low. This exception presented by Naeba-4 could be explained by the topographic properties of low-lying depressions with fewer trees than the surrounding area although the canopy covered the whole area of Naeba-4. The canopy surface areas of the stands with lower gap ratios were about 2 ha/ha; this might be a minimum value for canopy surface area. Canopy surface areas of all stands decreased modestly with the stand density (Fig. 3 (C)).

We also examined the relationships between BA and the canopy parameters (Fig. 4) because BA is often used as an indicator for canopy closure and stand biomass. In the stands with comparatively higher gap ratio and lower density (Appi-4, Naeba-1 and -3), the gap ratio decreased with the BA (Fig. 4 (A)). A similar tendency was found in the relationship between

Table 2 Canopy parameters from LiDAR data

Plot name	Gap ratio (%)	Mean canopy height (m)	SD*1 of CHM for canopy (m)	CV *2 of CHM for canopy (%)	SD*1 of CHM for stand (m)	Canopy surface area (ha/ha)	Stand surface area (ha/ha)
Appi-1	1	17.3	0.9	5	0.9	2.09	2.17
Appi-2	2	17.1	1.6	9	1.7	2.23	2.39
Appi-3	2	17.8	1.7	10	1.8	2.13	2.23
Appi-4	53	14.7	4.9	33	6.9	2.57	6.09
Naeba-1	17	26.0	2.6	10	6.1	2.03	3.93
Naeba-2	3	19.9	1.2	6	1.9	1.70	2.01
Naeba-3	38	17.0	2.8	17	6.4	2.48	4.98
Naeba-4	2	22.1	2.1	9	2.1	1.88	2.00

*1: SD: standard deviation
*2: CV: coefficient of variance

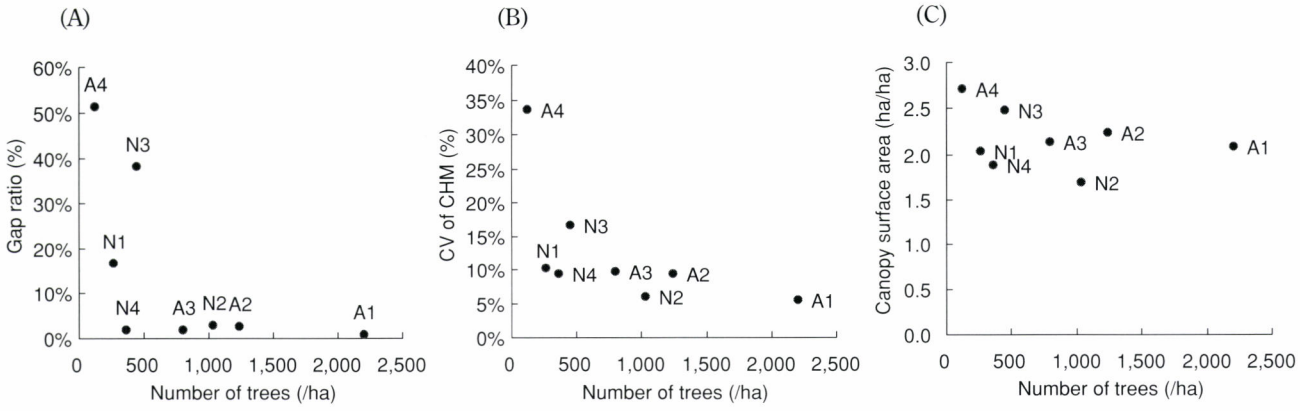

Fig. 3 Relationship between canopy parameters and stand density
(A): gap ratio vs stand density, (B): CV of CHM vs stand density, (C): canopy surface area vs stand density
*A1 to 4 and N1 to 4 correspond to Appi-1 to Appi-4 and Naeba-1 to Naeba-4, respectively.

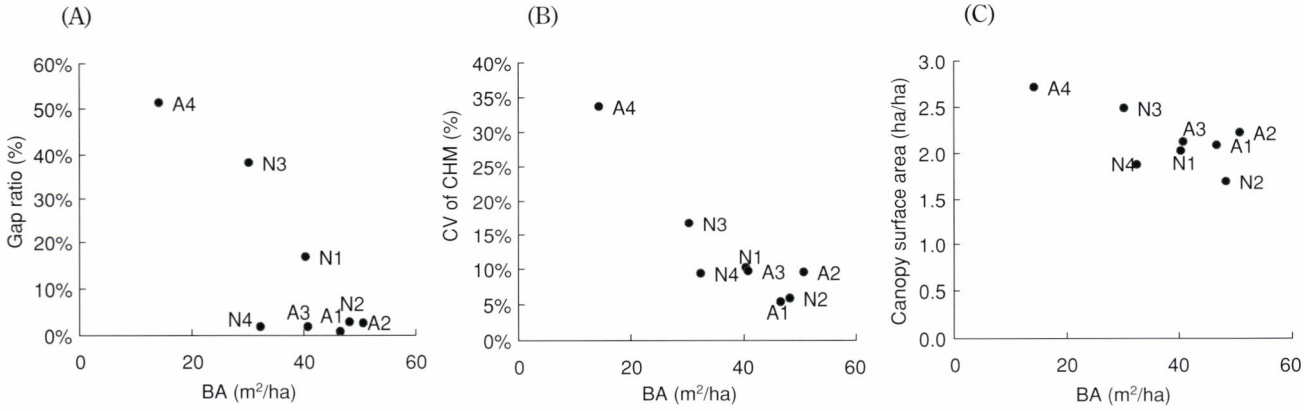

Fig. 4 Relationship between canopy parameters and BA
(A): gap ratio vs BA, (B): CV of CHM vs BA, (C): canopy surface area vs BA
*A1 to 4 and N1 to 4 correspond to Appi-1 to Appi-4 and Naeba-1 to Naeba-4, respectively.

the CV of the CHM and BA (Fig. 4 (B)). In the stands with high gap ratio, canopy closure advanced with BA which is closely related to foliage mass, therefore the gap ratio and CV decreased with BA. On the other hand, the gap ratio and CV of the CHM did not change with BA in the stands with lower gap ratio, Appi-1, -2, -3, Naeba-2 and -4 (Fig. 4 (A) and (B)). However, the parameters have potential to estimate BA when factors such as low gap ratio and topographic condition are considered because these parameters tended to decrease with BA using all census plot data. The canopy surface area of the stands with lower gap ratios did not change along with BA, however, the canopy surface area of all the stands tended to decrease with BA. This is similar to the relationship between the canopy surface areas and stand density.

The results suggest that parameters obtained from LiDAR data correspond to the successional stage and may provide information about structural heterogeneity or roughness of canopy surface. The structural heterogeneity may principally be caused by the extent of stand development as expressed by stand density, tree height, canopy layering etc. Furthermore, interrelationships between the different canopy parameters were identified and examined in the following section.

Relationships between Canopy Parameters in 54 Grid Squares

The interrelationships between the canopy parameters (i.e., the gap ratio, CVs of the CHMs and canopy surface area) observed at 54 grid squares in the Appi and Naeba areas were examined. The gap ratios varied widely ranging from 1to 68%, and the CVs of the CHMs varied between 5 and 51%. In comparison with these two parameters, the canopy surface areas did not vary so much (1.7 - 2.8 ha/ha) among the grid squares. The CV tended to be positively correlated with gap ratio (Fig. 5 (A)).

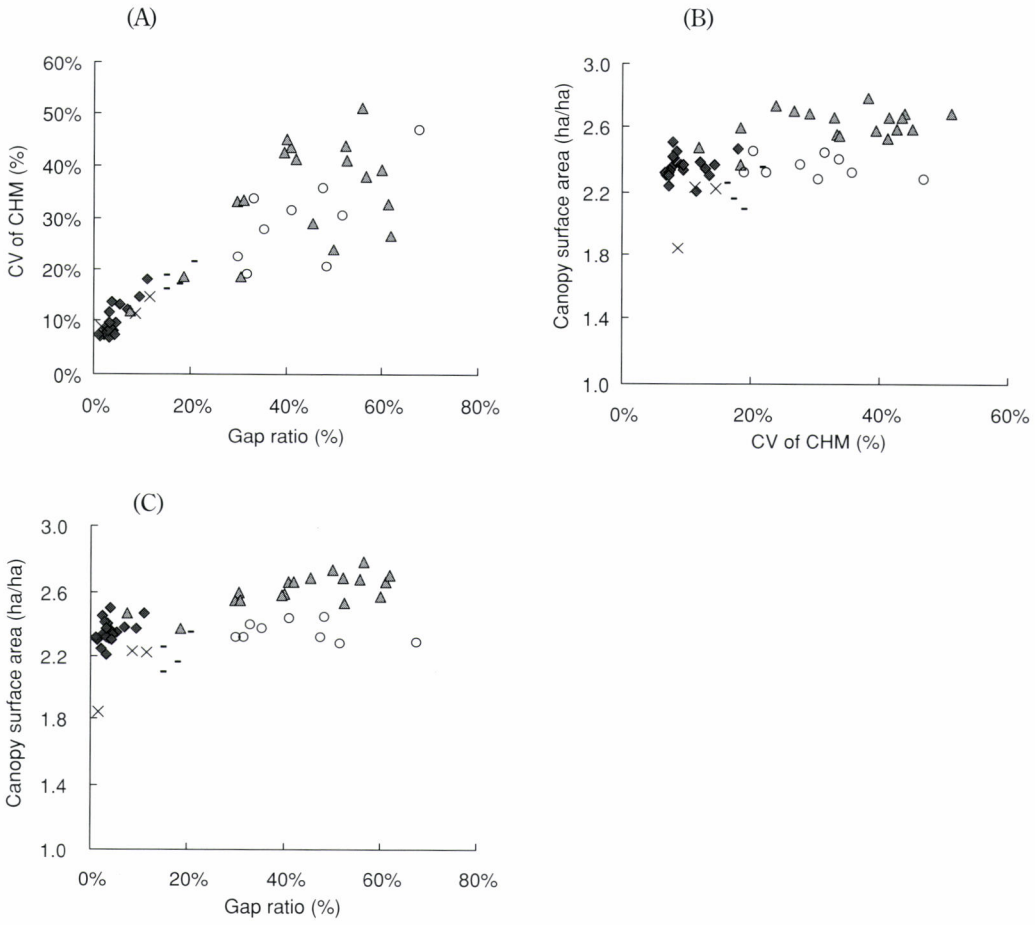

Fig. 5 Relationships between canopy parameters
(A): CV of CHM vs gap ratio, (B): canopy surface area vs CV of CHM, (C): canopy surface area vs gap ratio
◆: Appi secondary forests ▲: Appi selectively cut forests
×: Mt. Naeba at 550m a. s. l. -: Mt. Naeba at 900m a. s. l. ○: Mt. Naeba at 1500m a. s. l.

After gap formation in the canopy, the understory and sub-canopy trees will grow rapidly as a result of the improved light conditions. However, vegetation recovery in any gap area will be affected by the canopy structure, species composition and site conditions as well as light environment. This may lead to an increase in the variability of the canopy surface. Resultantly, we could obtain the positive relationship between the CVs of the CHMs and gap ratios as shown in Fig. 5 (A).

The canopy surface areas increased slightly with the gap ratio and CVs of CHMs (Fig. 5 (B) and (C)), showing weak correlations with canopy structure and spatial heterogeneity. The stands with low gap ratio had approximately 2 ha/ha canopy surface area and 5 - 10% CV (Fig. 5 (B) and (C)), which had similar values of lower gap ratio stands regardless of stand density and BA as discussed previously. These findings suggest that the canopy surface, which effectively functions as an interface between the atmosphere and the foliage layer, remains similar, irrespective of the crown shape and roughness of the forest canopy.

CONCLUSION

In this study we analyzed canopy parameters easily derived from LiDAR data, aiming to estimate canopy structure parameters and elucidate the heterogeneity in extensive beech forests. Our results indicate that the gap ratio and CVs of the CHMs may be preferred parameters for describing stand structure and its relationship to canopy structure. In the studied forests there was some variation with respect to gap ratio and roughness of canopy surface. Since the parameters derived from LiDAR data involve structural aspects of broadleaved forests, further study is needed to relate canopy architecture to structural heterogeneity: e.g., the relationships between gap size, canopy height, individual tree size and other factors.

REFERENCES

BRANDTBERG, T., WARNER, T.A., LANDENBERGER, R.E. and MCGRAW, J.B., (2003): Detection and analysis of individual leaf-off tree crowns in small footprint, high sampling density lidar data from the eastern deciduous forest in North America. Rem. Sens. Environ. **85**: 290-303

BIRNBAUM, P., (2001): Canopy surface topography in a French Guiana forest and the folded forest theory. Plant Ecol. **153**: 293-300

COOPS, N.C., HILKER, T., WULDER, M.A., St-ONGE, B., NEWNHAM, G., SIGGINS, A. and TROFYMOW, J.A., (Tony) (2007): Estimating canopy structure of Douglas-fir forest stands from discrete-return LiDAR. Trees **21**: 295-310

KAKUBARI, Y., (1975): Change of biomass and productivity in beech forests at different stand age. Proceedings of the Kanto Conference of the Japanese Forest Society **27**: 1-2 (in Japanese)

KUBOTA, M., TENHUNEN, J., ZIMMERMANN, R., SCHMIDT, M., ADIKU, S. and KAKUBARI, Y., (2005): Influences of environmental factors on the radial profile of sap flux density in *Fagus crenata* growing at different elevations in the Naeba Mountains, Japan. Tree Physiol. **25**: 545-556

LEFSKY, M.A., HARDING, D., COHEN, W.B., PARKER, G. and SHUGART, H.H., (1999): Surface lidar remote sensing of basal area and biomass in deciduous forests of eastern Maryland, USA. Rem. Sens. Environ. **67**: 83-98

LOVELL, J.L., JUPP, D.L.B., CULVENOR, D.S. and COOPS, N.C., (2003): Using airborne and ground-based ranging lidar to measure canopy structure in Australian forests. Can. J. Rem. Sens. **29**(5): 607-622

NÆSSET, E., (1997): Determination of mean tree height of forest stands using airborne laser scanner data. J. Photogramm. Rem. Sens. **52**: 49-56

NAKASHIZUKA, T., (1984): Regeneration process of climax beech (*Fagus crenata* blume) forests IV. Gap formation. Jap. J. Ecol. **34**: 75-85

PARKER, G.G. and RUSS, M.E., (2004): The canopy surface and stand development: assessing forest canopy structure and complexity with near-surface altimetry. For. Ecol. Manag. **189**: 307-315

RIAÑO, D., VALLADARES, F., CONDÉS, S. and CHUVIECO, E., (2004): Estimation of leaf area index and covered ground from airborne laser scanner (LiDAR) in two contrasting forests. Agric. For. Meteorol. **124**: 269-275

(Received 15 January 2007)
(Accepted 15 November 2007)

Article

Estimation of Stand Structure in the Deciduous Broad-leaved Forest using Multi-temporal LiDAR Data

Yasuteru Imai[*1], Masahiro Setojima[*1], Manabu Funahashi[*1], Toshio Katsuki[*2] and Masahiro Amano[*3]

ABSTRACT

In this study, we tried to estimate the stand structure of deciduous broad-leaved forest and mixed forest using multi-temporal LiDAR data, and it was compared with field survey result and photo interpretation result. As a result, there is the consistency in LiDAR data obtained the same period and the reproducibility of the DSM is high. In deciduous broad-leaved forest, the amount of changes in the DSM around the defoliation allows us to understand the stand structure such as the covering situation of sub tree and shrub and floor plant. In mixed forest, the multi-temporal LiDAR data is effective for the evergreen tree/deciduous tree classification.

Keywords: LiDAR, DSM, deciduous broad-leaved forest, mixed forest, stand structure

INTRODUCTION

The development of the LiDAR techniques is making progress in recent years, and many attempts have been made to estimate the ground height and the tree height, as well as to extract crowns (PERSSON *et al.*, 2002) and estimate LAI. And there are some reports on new applications in order to understand the stand structure of the forest (SETOJIMA *et al.*, 2003), estimate the snow depth, and classify vegetation etc. Especially, the stand structure of the forest provides useful information that can be used for evaluation of the situation of plantation management, habitat environment of wildlife, and biodiversity.

In this study, we obtained the LiDAR data in multiple periods. And we calculated the difference in the DSMs (Digital Surface Model) in multiple periods (hereinafter referred to as the "difference method") to understand the stand structure of deciduous broad-leaved forest and mixed forest with different tree species and management conditions. Furthermore, the result of tree height estimation was used to classify the types of stand structures.

Corresponding author: Yasuteru Imai
[*1] Kokusai Kogyo Co.,Ltd. 2-24-1 Harumicho, Fuchu City, Tokyo, 183-0057, JAPAN
(yasuteru_imai, masahiro_setojima, manabu_funahashi)@kkc.co.jp
[*2] Forestry and Forest Products Research Institute. Matsunosato 1, Tsukuba City, Ibaraki, 305-8687, JAPAN
katsuki@ffpri.affrc.go.jp
[*3] Waseda University. 2-579-15 Mikajima, Tokorozawa City, Saitama, 359-1192, JAPAN
amano@waseda.jp

METHOD

Study Area

Target area was set to Tama Forest Science Garden in Tokyo, Japan. And three forests with different tree species and management conditions were selected as the verification areas (see Fig. 1).

- Area A: Well-managed cherry (*Prunus yedoensis*) forest
- Area B: Zelkova (*Zelkova serrata*) forest in natural state
- Area C: Mixed forest

LiDAR Data Acquisition

The LiDAR data used in this study are shown in Table 1. The LiDAR data collected in four periods by a fixed wing airplane were used in this study. The footprint was about 66 cm, and the point density was 0.25 point/m² in all periods.

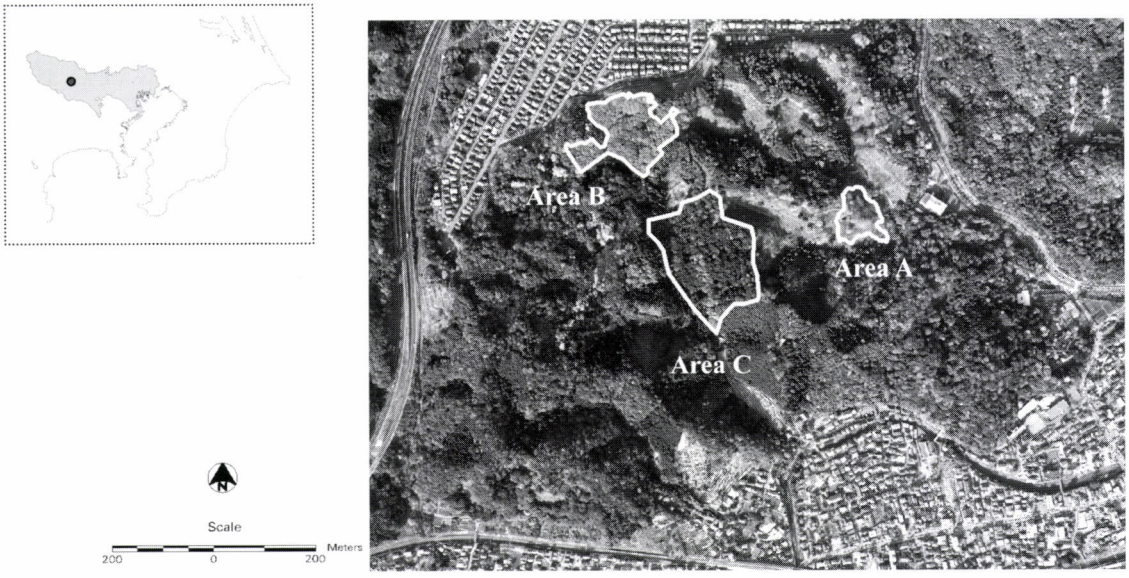

Fig. 1 Study sites of this study (Tama Forest Science Garden)

Table 1 LiDAR data used for this study

Date	Flight Altitude (m)	FOV (degrees)	Scan Rate (Hz)	Swath (m)	Density (points/m^2)
2000.10.11	2500	15	20	658	0.25
2001.02.12	2500	16	19.5	703	0.25
2001.12.03	2500	20	24	882	0.25
2002.10.04	2590	15	20	682	0.25

Analysis

Examination of reproducibility of DSM

The difference method focuses on the change in the DSMs accompanying the leaf fall from autumn to winter. It is necessary to confirm that the DSMs of the same season reflect almost the same crown surface (reproducibility). We tried to compare the point clouds in the DSMs obtained two seasons before leaf fall (October 11, 2000 and October 4, 2002) to examine the reproducibility of the DSM.

The point clouds in the DSMs were prepared by extracting only the 1st return pulses from the random points and resampling the points at 2m intervals after interpolation by the TIN (triangulated irregular network).

Estimation of tree height based on DSM before leaf fall and DEM after leaf fall

We prepared the DSM grid in 2m mesh before leaf fall (October 11, 2000) and the DEM (Digital Elevation Model) grid in 2m mesh after leaf fall (February 12, 2001), and the DHM (Digital Height Model) was made after differentiation of the two grids.

The DHM was compared with the result of field survey, which had been obtained in Area A and a mixed forest similar to that in Area C, to confirm the tree height estimation accuracy.

Understanding the stand structure based on difference in DSMs

We prepared the DSM grids in 2m mesh collected before leaf fall (October 11, 2000), during leaf fall (December 3, 2001), and after leaf fall (February 12, 2001) to find the change in the DSM in each period after differentiation. The DSM change from October to December is called "ΔDSM_1", the DSM change from December to February is called "ΔDSM_2" and the DSM change from October to February is called "ΔDSM_3". Every ΔDSMs corresponds to the amount of change in the crown height in each period. After that, we tried to understand the vertical structure (stand structure) in three areas.

Approach to stand structure type classification using DHM and ΔDSM

To achieve the objective classification of stand structures, we attempted to quantitative classify the types of stand structures using both ΔDSM_3 and DHM by thresholding the values.

RESULTS AND DISCUSSION

Examination of Reproducibility of DSM

Table 2 shows the result of examination of the reproducibility of the DSM.

In Area A, the correlation coefficient between the two DSMs with 4,025 points was 0.970, the RMSE (Root Mean Square Error) was 1.334m, and the standard deviation of height difference was 1.327m.

In Area B, the correlation coefficient with 11,010 points was 0.959, the RMSE was 1.546m, and the standard deviation of height difference was 1.493m.

In Area C, the correlation coefficient with 16,936 points was 0.986, the RMSE was 1.417m, and the standard deviation of height difference was 1.399m.

The correlation coefficient was very high in three areas, suggesting that the variation patterns of the DSMs in the two periods were similar. The RMSE and standard deviation of height difference were about 1.5m, which is far smaller than the range of the value of every ΔDSMs. It is considered that the reproducibility of the DSM before leaf fall is high, representing almost the same height (crown height).

Estimation of Tree Height based on DSM before Leaf Fall and DEM after Leaf Fall

Fig. 2 shows the DHM based on the difference between the DSM before leaf fall (October 11, 2000) and the DEM after leaf fall (February 12, 2001). It is assumed that Area B has many high trees of more than 20m in height, Area A has comparatively low trees of 15m in height, and Area C has high and low trees mixed together.

Table 2 shows the result of comparison between the DSM, DEM, DHM and actually measured values. It was found that the RMSE of the DSM was about 1.5-2m, the RMSE of the DEM was about 0.5m, and the RMSE of the DHM was about 1.5m. This result suggested that the DHM includes a difference about 1.5m with respect to the actually measured tree height.

Understanding the Stand Structure based on Difference in DSMs

Fig. 3 shows the ΔDSMs in three periods from before leaf fall till after leaf fall. Since the DHM includes an error of about 1.5m as shown in Table 2, it was considered that the canopy condition didn't change where the ΔDSMs was less than 2m.

Table 2 The evaluation result on the reproducibility of the DSM and the height accuracy of the DHM

	Reproducibility of the DSM				Height accuracy of the DHM					
					DSM		DEM		DHM	
	N	C.C	RMSE	S.D	N	RMSE	N	RMSE	N	RMSE
Area A	4,025	0.970	1.334	1.327	20	1.434	526	0.486	20	1.489
Area B	11,010	0.959	1.546	1.493	-	-	-	-	-	-
Area C	16,936	0.986	1.417	1.399	-	-	-	-	-	-
Mixed Forest	-	-	-	-	15	2.051	314	0.669	15	1.493

N: Number of points, C.C: Correlation Coefficient, RMSE: Root Mean Square Error (m)
S.D: Standard Deviation of height difference of two DSMs (m)

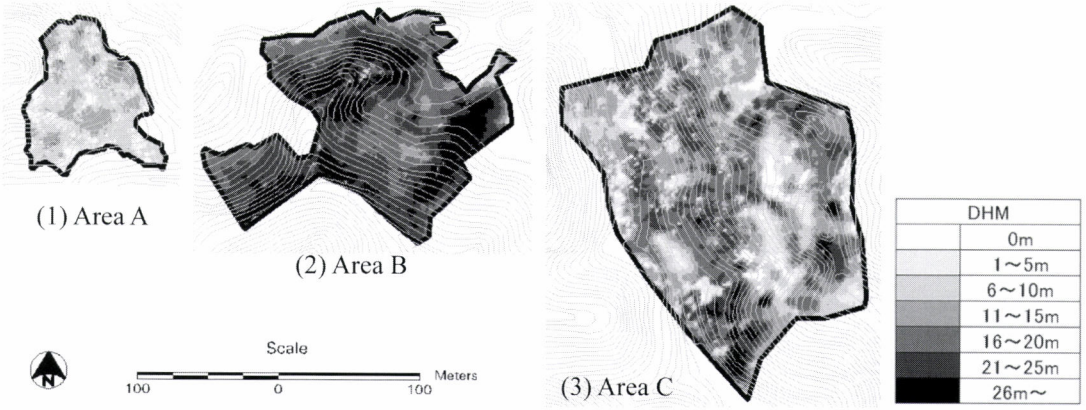

Fig. 2 The DHM of three areas

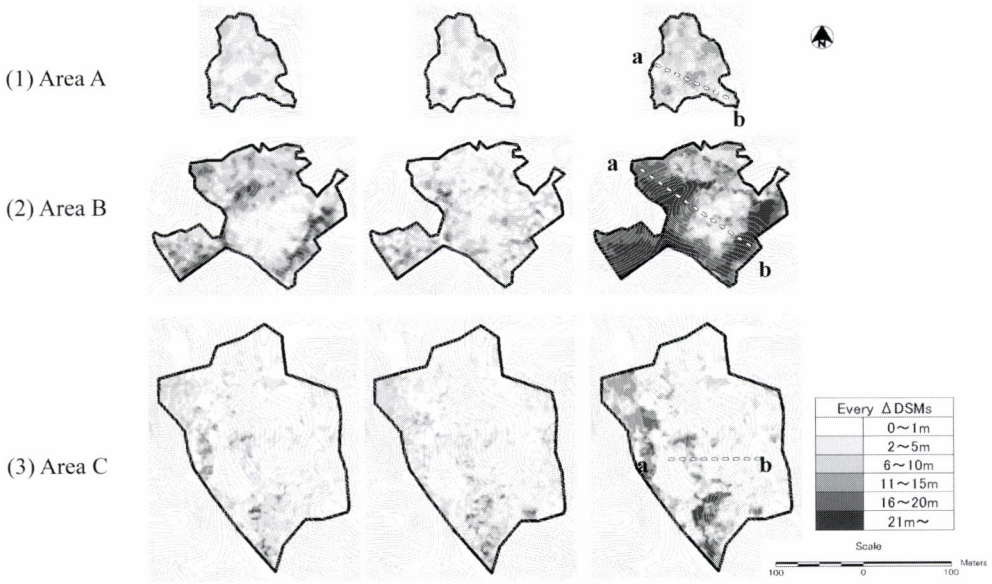

ΔDSM_1 (Oct. ~ Dec.) ΔDSM_2 (Dec. ~ Feb.) ΔDSM_3 (Oct. ~ Feb.)

Fig. 3 ΔDSMs in three periods (before leaf fall till after leaf fall)

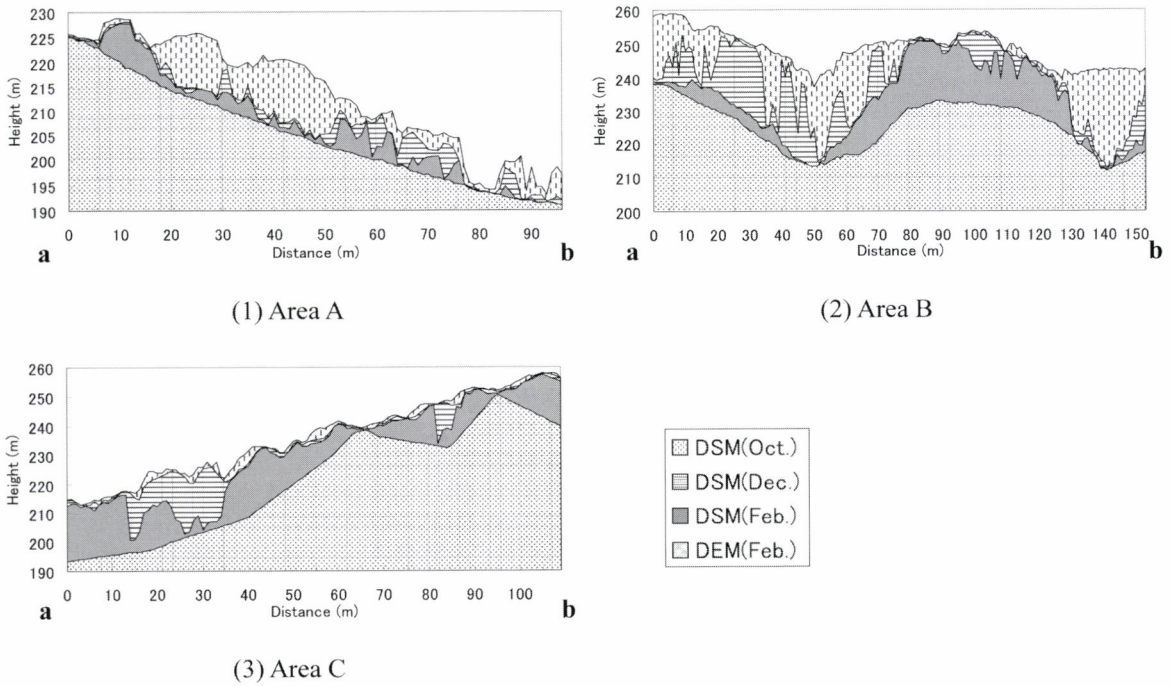

Fig. 4 Cross sectional drawing of change in DSMs during the defoliation period

In Area A, the ΔDSM_1 was less than 10m from October to December. From December to February, the ΔDSM_2 was less than 10m in some places, but the number of these places was less composed to that of October to December.

In Area B, the DSM change areas from October to December were observed in all areas except the central area, and the amount of change exceeded 20m in some areas. From December to February, the DSM change areas were few compared with October to December.

In Area C, many areas were no change, but the DSM change areas were found in patches in three periods.

As a result, it is considered that the ΔDSM_1 corresponds

to cherry trees and zelkova trees that shed leaves early.

Fig. 4 shows the cross section of the change in the DSMs from before leaf fall till after leaf fall (Refer to Fig. 3 for the cross sectional location). It visually shows the condition of low trees and forest floors in the interior of a deciduous broadleaved forest, permitting estimation of the stand structure. In forests where evergreen trees and broad-leaved trees coexist like Area B and Area C, the ΔDSM_3 permits clear classification of the boundary between evergreen trees and broad-leaved trees.

Approach to Stand Structure Type Classification using DHM and ΔDSM

We tried to classify the stand structure types using DHM and ΔDSM_3 by thresholding the values.

Table 3 shows the concept of type classification. Based on the DHM, the dominant tree height was classified. Taking into consideration the error of the DHM, 0-1m, 1-5m, 5-10m, and more than 10m were regarded as the "road and herb", "shrub", "sub-high tree", and "high tree".

Based on the ΔDSM_3, the condition of the lower layer was classified. Areas where the ΔDSM_3 is 0-1m were regarded as the "evergreen forest" because the seasonal change of the DSM was almost nothing, and the other areas were regarded as the "deciduous forest." In the deciduous forest, the areas where the same category of the DHM and the ΔDSM_3 were regarded as "no lower layer," the areas where the difference in the two classes were 1-5m were regarded as "herbs in lower layer," and the difference was 5-10m were regarded as "shrubs in lower layer."

Fig. 5 shows the result of type classification.

Area A was mostly composed of deciduous high sub-high trees, and the lower layer had nothing or herbs only.

Area B was mostly composed of deciduous high trees, having nothing in the lower layer except the central and northern parts. The central and northern parts were composed of evergreen trees.

Area C was mostly composed of evergreen high/sub-high trees, and deciduous high/sub-high trees were distributed in columns and patches. In the lower layer, nothing or herbs were growing at the bottom of slopes, while herbs or shrubs were growing at the top of slopes.

To validate the result, field survey was conducted and the

Table 3 Concept of type classification of stand structure using DHM and ΔDSM_3

		DHM			
		0～1m	1～5m	5～10m	10m～
ΔDSM_3	0～1m	road and herb	U : shrub (e) L : indistinctness	U : sub-high tree (e) L : indistinctness	U : high tree (e) L : indistinctness
	1～5m	–	U : shrub (d) L : none	U : sub-high tree (d) L : herbs	U : high tree (d) L : shrubs (e)
	5～10m	–	–	U : sub-high tree (d) L : none	U : high tree (d) L : herbs
	10m～	–	–	–	U : high tree (d) L : none

U: upper layer, L: lower layer, (e): evergreen, (d): deciduous

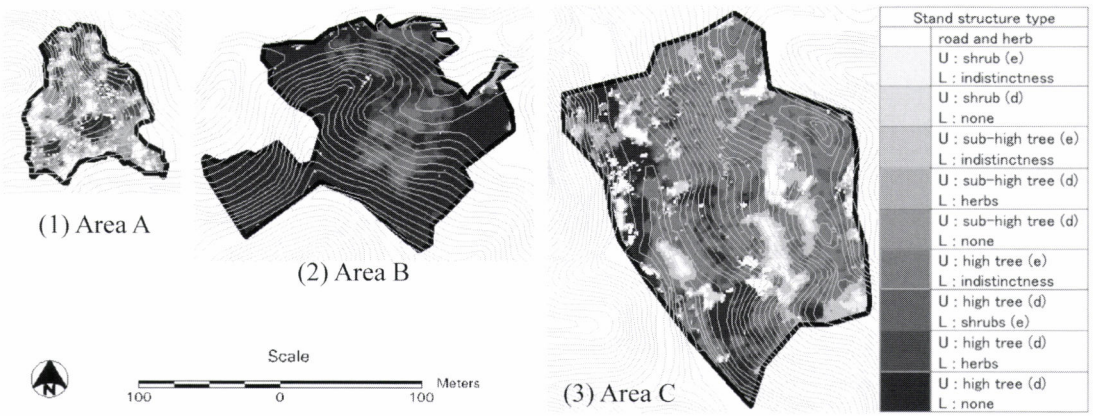

Fig. 5 The result of type classification of stand structure

above result was compared with the cross section (see Fig. 4). As a result, the type classification was almost satisfactory, although the area with "no lower layer" was slightly larger in the classification. In mixed forest, the evergreen/deciduous classification of the high tree layer was correct, and the identification of deciduous broad-leaved trees was comparatively correct.

CONCLUSION

This study was intended to understand the stand structure of deciduous broad-leaved forest and mixed forest based on LiDAR data obtained in four periods. It is also intended to classify the types of stand structures with the help of the information about tree height.

As a result, it was found that there is consistency in the LiDAR data obtained the same period and the reproducibility of the DSM is high; the amount of changes in the DSM allows us to understand the stand structure of the interior of deciduous broad-leaved forest, as well as type classification; In mixed forest, LiDAR data collected in multiple periods are effective for classification of evergreen trees and deciduous trees.

However, the verification is insufficient at present, and it is necessary to collect the height information of high trees, shrubs, and herbs by field measurement and aerial photogrammetry to conduct quantitative verification of the results of the method described in this paper.

LITERATURE CITED

PERSSON, A. *et al.*(2002): Detecting and measuring individual trees using an airborne laser scanner. Photogrammetric Engineering and Remote Sensing **68**: 925-932

SETOJIMA, M. *et al.* (2003): Basic study of tree height measurement in Satoyama Coppice Forests and identification of the distribution of deciduous broadleaf trees using airborne laser scanner data before and after defoliation. Journal of the Japanese Institute of Landscape Architecture **66**(5): 503-508

(Received 15 January 2007)
(Accepted 17 Janurey 2008)

Article

Estimating Mean Height and Stand Volume in Broad Leaved Forest Stands using LiDAR

Eiji Kodani[*1] and Yoshio Awaya[*2]

ABSTRACT

Forest stand variables (mean height, stand volume, and mean diameter breast height (DBH), tree density) were estimated in evergreen and deciduous broad leaved forest stand using LiDAR. LiDAR data were acquired along 12km and 28km transects with 1 pulse per square meter and small foot print (20cm). We set plots in evergreen and deciduous broad leaved forest stands from small to large on the transect and measured forest stand variables (mean DBH: 3.4-41.2cm; mean H: 3.1-17.4m; V: 25.1-854m^3; N: 295-9,507ha^{-1}; n=18). Laser pulses of digital canopy height model were extracted in each plot and LiDAR indexes were calculated: average, maximum, 90, 75, 50, 25 percentiles, standard deviation, and coefficient of variation. A linear regression analysis was performed between LiDAR indexes and forest stand variables. Mean height had the highest relationship with the LiDAR index 75 percentile (r^2=0.79); stand volume with the LiDAR index average (r^2=0.79), mean DBH with the LiDAR index 75 percentile (r^2=0.56), and tree density with LiDAR index 75 percentile (r^2=0.52).These results showed that low density LiDAR was useful for forest stand variable and would be useful for update and modification of forest base map and forest register.

Keywords: stand volume, mean height, deciduous broad leaved forest stand, evergreen broad leaved forest stand, LiDAR

INTRODUCTION

Estimating spatial forest stand variables (e.g. mean height, stand volume, mean diameter breast height DBH, and tree density) is important for forest management. Air photo interpretation and optical satellite remote sensing are generally used in both study and practice. However there are some problems with these methods: air photo interpretation requires a technical professional and much effort, and the accuracy of optical satellite remote sensing is relatively poor (Fransson *et al.*, 2004). Recent studies show that small footprint area LiDAR (Light Detecting And Ranging) is useful for estimating forest stand variables. Small footprint LiDAR can be acquired with high and low density. Laser pulses of 5 or more per square meter are irradiated from platform (i.e. airplane or helicopter) to ground in high density LiDAR (Hyyppä *et al.*, 2001), while laser pulses of 1 or less per square meter in low density LiDAR (Næsset, 1997a, b). High density LiDAR is used for each tree variable, while low density LiDAR is used for forest stand variable. Low density LiDAR can estimate forest stand variables in a large area at low cost, while high density LiDAR can obtain more detailed information.

Forest stand variables have been estimated with low density LiDAR and various reports have been published especially in North America and Europe. Species surveyed with low density LiDAR have included Norway spruce (*Picea ablies* Karst.), Scots pine (*Pinus sylvestris* L.) and birch (*Betula pubescens* Ehrh.) in northern Europe (Næsset, 1997a; 1997b; 2002; 2004; Næsset and Bjerknes, 2001; Nilsson, 1996; Holmgren, 2004), and Douglas-fir (*Pseudotsuga menziesii* Franco) in North America (Magnussen and Boudewyn, 1998; Means *et al.*, 2000).

In laser profiling LiDAR, laser pulses are measured at the point just under the airplane and line data are acquired as the airplane moves. Although there is a difference between area LiDAR and laser profiling in acquiring dimensions (i.e. area or line), there are similarities in that the objective scale is forest stand and the LiDAR index for estimating forest stand

Corresponding author: Eiji Kodani
[*1] Forestry and Forest Products Research Institute, Shikoku Research Center, Kochi 780-8077, Japan.
[*2] Forestry and Forest Products Research Institute, Tsukuba 305-8687, Japan.

variables is calculated from many laser pulse data statistically. Pine plantation and naturally occurred hardwood forests in the Delaware Peninsula (MACLEAN and KRABILL, 1986), pine plantation (NELSON *et al.*, 1988), 6 land-cover biomass in Delaware USA (NELSON *et al.*, 2004), Canadian boreal forest (TSUZUKI *et al.*, 2006) and Siberia forest (KUSAKABE *et al.*, 2006) were surveyed with this method.

Forests in Japan are mainly manmade coniferous forest (Sugi: *Cryptomeria japonica*, hinoki cypress: *Chamaecyparis obtusa* and Japanese larch: *Larix kaempferi*) and natural forest (evergreen broad leaved forests and deciduous broad leaved forests, NUMATA *et al.*, 1975). The objective of this study was to estimate evergreen and deciduous broad leaved forest stand variables (mean height, stand volume, mean DBH and tree density) using small footprint and low density LiDAR.

METHOD

LiDAR Specification

We set up two transects of 12km and 28km long and 100m wide which traverse the western part of Shikoku island (Fig. 1). The 28km transect (T1) is located in the Ishizuchi Mountains, and an additional 500m square (S1) is located near T1 in the Ishizuchi Mountains. The 12km transect (T2) is located in Ashizuri cape. LiDAR data were acquired along the transects with an Optec ALTM 1255DC on 14 and 25 September 2002 before leaves turned yellow and on the square with an Optec ALTM 1255 on 25 May 2004 after leaf flushing finished. Asahi-koyo Corporation observed all area. Most of the area was national forest. Flight height was 1000m above the ground, LiDAR density was 1 pulse m^{-2}, footprint was approximately 20cm, and the first and last pulses were recorded. A digital terrain model (DTM) was generated by Asahi-koyo using the last pulse data.

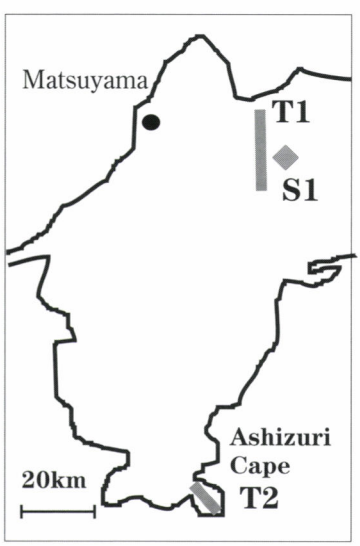

T1: Transect of deciduous broad leaved forest stand (28km)
S1: Square of deciduous broad leaved forest stand (500m)
T2: Transect of Evergreen broad leaved forest stand (12km)

Fig. 1 Map of the transects and the square in the western part of Shikoku island

There are three types of methods of estimating DTM from LiDAR data: 1) ground surface points are calculated from minimum elevation of LiDAR pulse data in the local area, 2) curved surfaces of the ground are estimated from LiDAR pulse data using statistical methods, and 3) LiDAR pulse data are divided using the segment method and segments of the ground surface are extracted (MASAHARU, 2006). Asahi-koyo used a roller method, which is a type of minimum elevation method (YOKOTA *et al.*, 2006): LiDAR pulse data in a stripe are plotted on a y-z distribution graph, a roller of diameter R is moved along the laser pulse data touching the minimum elevation data, and LiDAR pulse data touched by the roller are selected as ground surface elevation.

The processes of calculating DTM in this article were as follows: 1) Outlier data with atmospheric dust were removed. 2) The roller method was used for selecting LiDAR last pulse data and the first step DTM was generated. 3) The first step DTM was plotted and outlier pulse data were excluded manually. 4) LiDAR pulse data were selected again as ground surface elevation and DTM was generated with the kriging method using selected LiDAR pulse data in a 20-m circle. The digital canopy height model (DCHM) was generated using the differences between laser pulse data and DTM.

Field Survey

We set plots on the two transects and the square. The plots included both small and large of evergreen broad-leaved forest stand in Ashizuri cape and deciduous broad-leaved forest stand in the Ishizuchi Mountains. Major species were *Machilus thunbergii*, *Quercus glauca*, *Quercus acuta*, and *Castanopsis sieboldii* in the evergreen broad-leaved forest transect and *Fagus crenata*, *Quercus crispula*, *Betula ermanii*, *Acer sieboldianum*, and *Lindera triloba* in the deciduous broad-leaved forest area.

The plot size was 15m wide and 15-40m long, depending on the tree density. Circle plots of 20m long diameter were used for the 2 young forest stands. A square plot of 5m was used for one young and high density stand. Thirty to forty meter square plots were used for two low density forest stands. We measured DBH with a tape measure and height with VERTEX (Haglof Inc., Sweden). Tree volume was calculated with DBH, H and volume table (Forest Planning Division of Japanese Forest Agency, 1970). The plots data rage was as follows (mean DBH: 3.4-41.2cm; mean H: 3.1-17.4m; V: 25.1-854m^3; N: 295-9,507ha^{-1}). One or two points on the plots were surveyed with differential GPS Trimble Pathfinder Pro (Trimble Inc., USA) or Mobile Mapper (Thales Inc, USA) for more than 10 minutes. Eighteen plots were surveyed from autumn 2004 to winter 2005. The time difference between the acquisition of field data and LiDAR data will not be significant, because most surveyed stands were old and slow growing.

LiDAR Analysis

We estimated forest stand variables using regression analysis: calculating the correlation coefficients between forest stand variables and LiDAR indexes, selecting the best LiDAR index, and calculating the slope and the intercept of the regression line. The following LiDAR indexes were calculated according to previous studies: average, maximum, 90, 75, 50, 25 percentiles, standard deviation, and coefficient of variation (ALDRED and BONNOR, 1985; NELSON *et al.*, 1988; NÆSSET, 1997a, b; 2002; 2004; NÆSSET and BJERKNES, 2001; TSUZUKI *et al.*, 2006).

LiDAR indexes were calculated as follows. The first pulses laser data of DCHM were extracted from each plot and indexes of maximum, average, standard deviation and coefficient of variation were calculated. The quantiles corresponding to the 25, 50, 75, and 90 percentiles were calculated from a cumulative histogram of LiDAR DCHM in each plot. It should be noted with this method that low density LiDAR cannot detect individual trees, while forest stand variables are calculated from measuring individual trees in field plots. Although there is not a direct relationship between LiDAR indexes and forest stand variables, there is an indirect relationship between them, according to allometrical relationship and sampling theory (SPURR, 1960; MACLEAN and KRABILL, 1986; TSUZUKI *et al.*, 2006).

RESULTS AND DISCUSSION

A linear regression analysis was performed between LiDAR indexes and forest stand variables (Table 1). Mean height had the highest relationship with the LiDAR index 75 percentile (r^2=0.79, p=0.000); stand volume with the LiDAR index average (r^2=0.79, p=0.000), mean DBH with the LiDAR index 75 percentile (r^2=0.56, p=0.000) and tree density with the LiDAR index 75 percentile (r^2=0.52, p=0.001). LiDAR indexes of the highest relationship and forest stand variable were plotted, separating evergreen and deciduous forest stands (Fig. 2-a to d). Fig. 2-a to d show all data were roughly on one regression line, therefore we estimated them with that regression line.

Although the r^2 between tree density and LiDAR index coefficient of variation was high, plot no. 61 (P61) affected much the r^2 (Fig. 2-d). P61 was only the young forest stand in all plots that had lots of naturally regenerated small trees. When removing the outlier p61, it was more difficult to

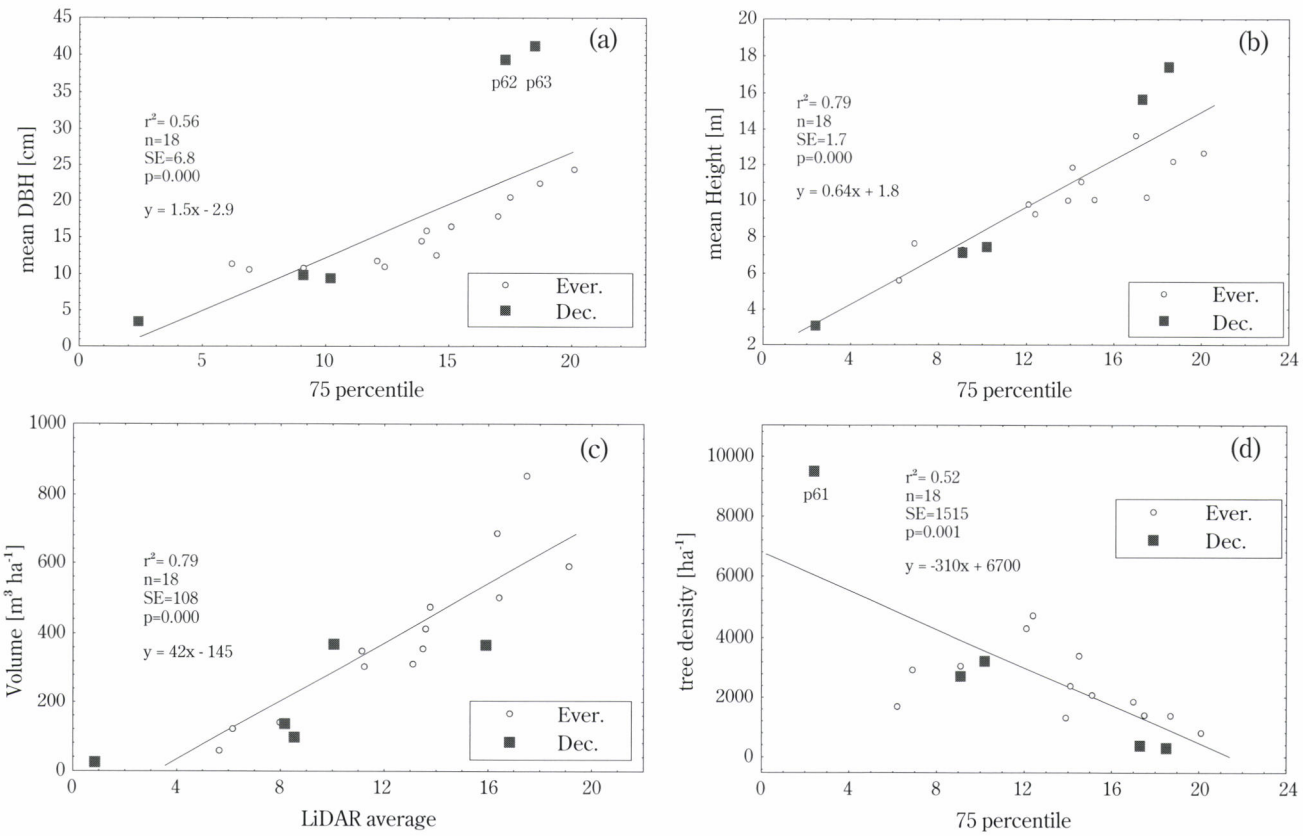

Fig. 2 The relationship between forest stand variables and the LiDAR indexes of highest linear relationship (a: mean diameter breath height DBH; b: mean height; c: stand volume; d: tree density; Ever.: Evergreen broad leaved forest stand; Dec.: Deciduous broad leaved forest stand)

Table 1 r^2 between forest stand variables and LiDAR indexes and the statistical significance of the relationships (p)

	Average	Max	Percentile 25	50	75	90	Standard Deviation	Coefficient of Variation
DBH [cm]	0.31 p=0.016	0.32 p=0.014	0.31 p=0.017	0.51 p=0.001	0.56 p=0.000	0.53 p=0.001	0.34 p=0.011	0.02 p=0.531
H [m]	0.60 p=0.000	0.50 p=0.001	0.58 p=0.000	0.77 p=0.000	0.79 p=0.000	0.74 p=0.000	0.17 p=0.094	0.17 p=0.094
V [m^3 ha^{-1}]	0.79 p=0.000	0.47 p=0.002	0.77 p=0.000	0.78 p=0.000	0.76 p=0.000	0.70 p=0.000	0.00 p=0.847	0.26 p=0.032
N [ha^{-1}]	0.45 p=0.002	0.40 p=0.005	0.40 p=0.005	0.50 p=0.001	0.52 p=0.001	0.50 p=0.001	0.08 p=0.245	0.45 p=0.002

(n=18)

estimate tree density than height and volume (r^2=0.33, p=0.016). Plot no. 62 and 63 (P62, P63) were over the regression line in Fig. 2-a, because P62 and P63 stands included only upper story trees, while other stands included upper and middle story trees. The forest canopy condition and the DBH distribution affected mean DBH value. When removing the outliers p62 and p63, mean DBH had highest relationship with LiDAR index 25 percentile (r^2=0.88, p=0.000). Comparing 4 forest stand variables, the correlation coefficients were higher, there were little outside data and most data were nearly on the regression line in the mean height and the stand volume. These results had an advantage, because stand volume and mean height are more important for forest management.

CONCLUSION

Forest stand variables are important information for forest practice (i.e. silvicultural management and harvesting). In Japan, a forest resource information system has been constructed with a forest base map and forest register that includes forest stand variables. However, more precise data and surveying methods are needed in view of the growing importance of estimating forest carbon stock. Forest resource information is surveyed, modified and updated using aerial photo interpretation and satellite optical remote sensing. This article showed that low density LiDAR was useful for estimating broad leaved forest stands variables and would be a valid third method for such surveys.

There are two problems for estimating forest resources in a large area using LiDAR: the high cost of acquiring data, and the many field surveys required. The Forest Agency of Japan has been building a national forest resource inventory system since 1999 and permanent plots in 4-km mesh are surveyed every five years. LiDAR data in low density are acquired by the Geographical Survey Institute and by the Ministry of Land, Infrastructure and Transport, and the data cover a large area of Japan. Forest resources could be estimated using LiDAR at lower cost from these existing data, and methods of analyzing low density LiDAR are becoming more important.

LITERATURE CITED

Aldred, A. H. and Bonnor, G. M., (1985): Application of airborne lasers to forest surveys. Information Report PI-X-51 Petawawa National Forestry Institute, Canada, 62pp

Forest Planning Division of Forest Agency, (1970): Two-way volume tables for western Japan. Japan Investigation Committee, Tokyo, 319pp (in Japanese)

Fransson, J.E.S., Magnusson, M. and Holmgren J., (2004) Estimation of forest stem volume using optical SPOT-5 satellite and laser data in combination, IEEE IGARSS 2004 symposium proceedings: 1-5

Holmgren, J., (2004): Prediction of tree height, basal area and stem volume in forest stands using airborne laser scanning. Scandinavian Journal of Forest Research **19**(6): 543-553

Hyyppä, J., Kelle, O., Lehikoinen, M. and Inkinen, M., (2001): A segmentation-based method to retrieve stem volume estimates from 3-d tree height models produced by laser scanners. IEEE Transactions on Geoscience and Remote Sensing **39**: 969-975

Kusakabe, T., Tsuzuki, H. and Sweda, T., (2006): Long-range estimation of Leaf Area Index using airborne laser altimetry in Siberian boreal forest. Journal of Japanese forest society **88**(1): 21-29 (in Japanese)

Maclean, G. A. and Krabill, W. B., (1986): Gross-merchantable timber volume estimation using an airborne lidar system. Canadian Journal of Remote Sensing **12**(1): 7-18

Magnussen, S. and Boudewyn, P., (1998): Derivations of stand heights from airborne laser scanner data with canopy-based quantile estimators. Canadian Journal of Forest Research **28**(7): 1016-1031

Masaharu, H.(2006): a review of filtering methods of airborne laser scanner data for generating DTM*. Journal of Japan Society of Photogrammetry and Remote Sensing **45**(4): 5-8 (in Japanese)

Means, J. E., Acker, S. A., Fitt, B. J., Renslow, M., Emerson, L. and Hendrix, C. J., (2000): Predicting forest stand characteristics with airborne scanning LiDAR. Photogrammetric Engineering & Remote Sensing **66**(11): 1367-1371

Næsset, E., (1997a): Determination of mean tree height of forest stands using airborne lidar scammer data. ISPRS Journal of Photogrammetry and Remote Sensing **52**: 49-56

Næsset, E., (1997b): Estimating timber volume of forest stands using

airborne laser scanner data. Remote Sensing Environment **61**(2): 246-253

NÆSSET, E., (2002): Predicting forest stand characteristics with airborne scanning laser using a practical two-stage procedure and field data. Remote Sensing of Environment **80**(1): 88-99

NÆSSET, E. (2004): Practical large-scale forest stand inventory using a small-footprint airborne scanning laser. Scandinavian Journal of Forest Research **19**(2): 164-179

NÆSSET, E. and BJERKNES, K. O., (2001): Estimating tree heights and number of stems in young forest stands using airborne laser scanner data. Remote Sensing of Environment **78**(3): 328-340

NELSON, R., KRABILL, W. and TONELLI, J. (1988): Estimating forest biomass and volume using airborne laser date. Remote Sensing Environment **24**: 247-267

NELSON, R., SHORT, A. and VALENTI, M., (2004): Measuring biomass and carbon in Delaware using ana airborne profiling LIDAR. Scandinavian Journal of Forest Research **19**: 500-511

NILSSON, M., (1996): Estimation of tree heights and stand volume using an airborne lidar system. Remote Sensing of Environment **56**(1): 1-7

NUMATA, M., YOSHIOKA, K. and KATO, M., (ed.) (1975): Studies in conservation of natural terrestrial ecosystems in Japan Part I: Vegetation and its conservation, 157pp, Japanese committee for the International Biological Program (IBP), University of Tokyo press, Tokyo

SPURR, S.H., (1960): Photogrammetry and photo-interpretation (Second edition). Ronald Press, New York, 472pp

TSUZUKI, H., KUSAKABE, T. and SWEDA, T., (2006): Long-range estimation of standing timber stock in western boreal forest of Canada using airborne laser altimetry Journal of Japanese forest society **88**(2): 103-113 (in Japanese)

YOKOTA, H., NAKAZIMA, T. and TAMINO, T., (2006): Introduction of roller method for filtering LiDAR data*. Journal of Japan Society of Photogrammetry and Remote Sensing **45**(4): 18-21 (in Japanese)

*The titles were tentative translations from original Japanese title by the authors of this article.

(Received 17 January 2007)
(Accepted 15 November 2007)

Article

Land-cover Classification of Ehime Prefecture, Japan using Airborne Laser Altimetry

Yoshiko Maeda[*1], Hayato Tsuzuki[*1], Ross Nelson[*2] and Tatsuo Sweda[*1]

ABSTRACT

Airborne laser profiling of mainland Ehime Prefecture, Japan was conducted to develop an entirely new method of land-cover classification, partly in preparation for the post-Kyoto national carbon budget accounting, and partly for correction of the existing government land-use statistics, which should constitute the very basis of the impending national carbon budget accounting of the Kyoto Protocol. The altimetry data was obtained by using NASA's Portable Airborne Laser System (PALS) along 23 parallel flight lines 4km apart from each other covering the whole mainland portion of the prefecture. Based on the resulting surface profile representing topography and structures on the ground with some reference to laser return intensity and nadir video images, land cover along the flight line was classified into "forest", "farmland", "residential and urban", and "others" using PALSA (PALS Analyzer), a software developed for this particular purpose. This line evaluation was then developed into area statistics by simply multiplying by the distance between the flight lines, i.e. 4km. The resultant land-cover estimates not only differed from the existing government statistics as much as the latter does within itself, but also helped to identify the causes and sources of discrepancy quantitatively. Thus it was concluded that coordinated use of this new method with the existing system of land-use statistics would improve the overall credibility of the land-use/land-cover statistics of the prefecture and the nation.

Keywords: airborne laser altimetry, land-cover classification, Ehime Prefecture, discrepancy with government statistics, abandoned farmland

INTRODUCTION

As one of its prerequisites for national carbon budget accounting, the Kyoto Protocol demands accurate and consistent land-cover/land-use statistics from the Annex I countries. This is particularly important for a country like Japan which intends to utilize its forests as carbon sink to offset emission from other sources. However, as far as the existing land-use statistics are concerned, Japan does not seem to be capable of coping with this requirement of consistency due to contradicting figures among the statistics from different ministries, departments and agencies. Some of the discrepancies are identifiable as arising from difference in the definition of land-use categories. However, they still leave considerable discrepancies, the source of which is either unidentifiable or can only be guessed at best, degrading the confidence in all the statistics involved.

As recommended by the Intergovernmental Panel on Climate Change (IPCC, 2003), the best tool for correcting such discrepancies of or renewing the existing statistics is remote sensing due to its capabilities of covering large areas to the remotest corners and of providing spatially explicit information repeatedly. Most probably being too new and too advanced, the airborne laser altimetry is not included in the IPCC list of means of remote sensing, but it can provide much better defined and more precise land classification than the conventional means of remote sensing as NELSON *et al.* (2003) has demonstrated for the state of Delaware, U.S.A. The present work was conducted to develop a new method of land classification for Japan using airborne laser altimetry for more consistent and accurate statistics in response to the impending Kyoto Protocol carbon budget reporting as well as in preparation for the post-Kyoto greenhouse gas inventorying. To be reasonably practical for countrywide application in not

Corresponding author: Yoshiko Maeda
[*1] Faculty of Agriculture, Ehime University, 3-5-7, Tarumi, Matsuyama, Ehime 790-8566 Japan
[*1] 923/Biospheric Sciences Branch, NASA-Goddard Space Flight Center, Greenbelt, MD, USA

too distant future, Ehime Prefecture, one of the 47 prefectures of Japan, was chosen as the test area. The completely independent land-cover statistics thus created by airborne laser altimetry alone was compared with the existing government figures.

EXISTING GOVERNMENT LAND-USE STATISTICS

The two most comprehensive land-use statistics on Ehime Prefecture available today are the one on the Land Use Control bacK-up sYstem (LUCKY) from the Ministry of Land (LAND and WATER BUREAU, MINISTRY of LAND) and another from the prefectural statistics office (EHIME PREFECTURE STATISTICAL OFFICE (EPSO), 2005). The former is accompanied with a map while the latter is not. Of the numerous discrepancies between the two, the first to be mentioned is the 3.8% difference in total land area of the prefecture, i.e. 5,677km² by LUCKY against 5,247km² by EPSO. The exact agreement of the former with the figure from the most authoritative Geographical Survey Institute (GSI) does not necessarily mean its accuracy since the statistical discrepancies are adjusted for the total land area from the GSI.

The discrepancies between the national and prefectural statistics arise partly from the difference in definition of land-use categories and partly from accuracy in data collection and compilation. As shown in Fig. 1 categorization of "Road", "Water" and "Rangeland" is explicitly different between the two. Implicit but more significant difference in definition exists in handling of agricultural land and forest reserve. The former is the area actually cultivated in the national statistics, while it is the area legally registered as such in the prefectural statistics. The latter is as a part of "Forest" in the national statistics, but it is a part of "Others" in the prefectural statistics.

These discrepancies are difficult to be resolved due to rather unaccountable difference in some of the actual figures, which in turn distort the entire proportion of the statistics. A typical example is "Forest", which appears 21.5% more in national statistics than in the prefectural. A small part of this disagreement can be accounted for by the difference in definition mentioned above, but the rest is beyond any other explanation than by what has been traditionally called "the stretched measure", which results in smaller figures than what really is. This was rather common when the modern land registration system was introduced a century ago partly due to under declaration of land area on the side of owners to evade tax, and partly due to lack of exact and efficient means of surveying on the side of government. The correction seems to have been almost completed by today for residential and agricultural lands due to their limited size and accessibility, but the measure seems still stretched for forests due to their vastness and inaccessibility. Relatively small difference between the national and prefectural statistics in the total land area as compared with that in "Forest" area, indicates possible distortion in the areas of other land uses.

Prefectural (PSO)	National (LUCKY)		
Forest	Forest		
	National forest	Private forest	
Paddy	Farmland		
Field	Paddy	Field	Rangeland
Urban and Built-up	Urban and Built-up		
	Residential	Other residential	Industrial
Pond / Marsh	Water	River	Canal
Range- and Wasteland	Wasteland		
Others	Road		
	Forest	Agricultural	General
	Others		

Fig. 1 Existing land-use classification of Ehime

AIRBORNE LASER PROFILING OF EHIME PREFECTURE

The airborne laser altimetry was flown in September 2005 in cooperation with the NASA using its Portable Airborne Laser System (PALS) onboard a Bell Jet Ranger domestically hired from Akagi Helicopter Co. By this mission, the entire Ehime Prefecture excluding the islands off the mainland was covered with a total of 23 straight line transects 4km apart from each other as shown in Fig. 2. By eliminating overlaps and approach flights to the transects, the total length of the flight lines used for land-cover classification and biomass estimation was 1,358km. PALS is a nadir ranging system with laser beam emission frequency of 2,000Hz, but only every five ranging data was retrieved along with return intensity resulting in a recording frequency of 400Hz. Nadir video picture was also taken for reference in later analysis.

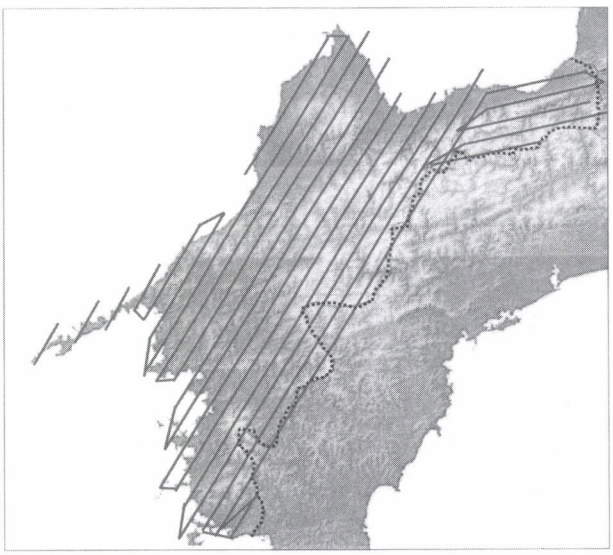

Fig. 2 Airborne laser altimetry Flight passage

CLASSIFICATION SOFTWARE

A software named PALSA (PALS Analyzer) was developed for convenience and ease of land-cover classification with the PALS data. It displays surface profile and laser return intensity graphically along with video movie in coordination with each other on the computer screen. Classification has to be done manually by the operator by delimiting a continuous portion of the same land cover and specifying its type. Then the segment changes its color according to the prescribed land-cover color code while the corresponding original altimetry records are flagged behind the screen according to the prescribed flag code for later statistical processing.

LAND-COVER CLASSIFICATION

With altimetry and return intensity recorded for every 17cm along the flight track, detailed land-cover classification is possible with the PALS data. However, in the present analysis only four major categories were distinguished, i.e.: "Forest" where trees are growing including newly harvested areas where continued forestry use is obvious; "Agricultural" which includes paddy, cropland and orchard; "Residential and Urban" which cover all the buildup areas including industrial areas, airports, parking lots etc.; and "Others" which include all the other areas as golf courses not covered by the preceding categories. Roads were included in the category surrounding them. So were inland water surfaces since their extent is more or less negligible in mountainous Ehime Prefecture.

Classification was conducted in two steps with transect length of 20m as a yardstick, i.e. when a given land cover continued for more than 20m it was classified as such, but otherwise it was temporarily classified as "Mosaic" for more detailed classification later on. Theoretically, there are 11 ways of combination in choosing two or more cover categories out of the four major categories, but the actual mosaics encountered were only three kinds, i.e. Forest + Residential, Forest + Agriculture, and Agriculture + Residential. Being relatively little, the first two mosaic transects were simply reclassified. In the last category, however, only the sample sections of 2.3km were reclassified into detail and the resulting proportion was applied to the remaining 19.1km of mosaic segments. The cover classification results along the flight line were then converted into area statistics by simple rectangular approximation, i.e., by multiplying the flight-line length of a given cover category by the distance of 4km between the flight lines.

RESULTS AND DISCUSSION

In spite of this seemingly very rough method of conversion into area, the total land area of the prefecture turned out to be 5,435km², which is only 0.4% less than the GSI figure of 5,455km². Considering the fact that the GSI figure for the mainland Ehime was obtained as the grand prefecture total less the area of islands over 1km², the actual discrepancy could be even smaller. On the other hand as shown in Fig. 3, the laser-based cover classification looks as contradicting with the existing statistics as the latter is within. However, the following detailed analysis leads to some consistency among the three estimates of land-cover/land-use classification.

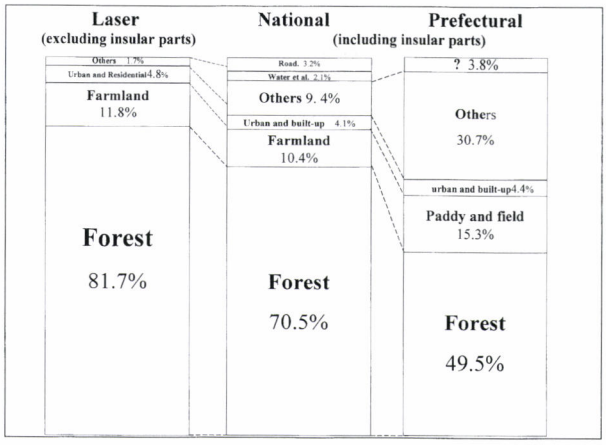

Fig. 3 Result of airborne laser altimetry land-cover classification as compared with national and prefecture statistics. (The areas of bar graph are not exactly to the percentage figures given due to space limitation)

Firstly, of the discrepancies in "Agricultural" land areas, the one between the laser estimate and the national statistics can be best explained by the fallow area, which amounts to 1% of the prefectural land area according to the 2005 Agro-forestry Census (EHIME PREFECTURE STATISTICAL OFFICE, 2005). Unable to distinguish between them, the laser estimate of "Farmland" (11.8%) may well includes the fallows in addition to the actually cultivated "Farmland" (10.4%) given by the national statistics, to result in the remaining discrepancy of only 0.4%. The further discrepancy of 3.5% with the "Paddy and Field" area (15.3%) of the prefectural statistics can be best accounted for as the farmlands abandoned decades ago and forested now but still registered as farmland. As a matter of fact, more and more agricultural lands have been abandoned and reclaimed by forests as the primary industry of the nation dwindled and isolated communities in remote areas were evacuated over the past decades. Some of them have been artificially reforested, but the majority seems to have been just left aside to natural reforestation. What makes the matter worse in this prefecture is the rapidly collapsing orange farming. The abandoned orchards turn more easily into bush to make the government statistics hard to catch up.

The farmlands supposedly reclaimed by forests not only resolve the discrepancies among the three estimates in "Agricultural" land area but also ease those in "Forest" area.

Consider the laser estimate of 81.7% and the national figure of 70.5% for "Forest", and leave aside the prefectural figure of 49.5%, which is heavily distorted by the stretched measure explained earlier. By discounting the reforested farmland, the laser estimate of "Forest" area reduces to 78.5%, easing the overall discrepancy. The remaining imbalance of 7.7% can be explained as an underestimation in the national statistics, the forest area of which is cited from the National Forest Inventory (NFI). According to MATSUMOTO (2003), a verification against actually measured forestland area revealed an average of 6.7% underestimation in the NFI figures. Involving only 40 or so sub-compartments totaling only 150ha, the credibility of this result is limited but it makes ends meet almost completely.

On the other hand, the laser estimate is neither free from errors. Two sources of errors are conceivable. One is associated with cover classification along the flight line, and the other with the two-dimensional expansion of the line classification into area by multiplying the distance between the two adjacent flight lines. In this study, the first source of error can be considered negligible since the cover classification was made at every point of altimetry, i.e. at an interval of 17cm along the flight line. Thus the only source of error in this study is the distance between the two adjacent flight lines, which happened to be four km. The closer the adjacent flight lines, the less the error would be, but it is difficult to quantify the latter as a function of the former in the present study. Thus, it would be fair to attribute the final discrepancy of 6.7% equally to the laser estimate and to the national statistics.

The discrepancies in the "Urban" and "Others" areas among the laser, national and prefectural estimates are less serious than in the "Agriculture" and "Forest" areas. The discrepancies in the "Urban" area are negligible at 4.8, 4.1 and 4.4% of the prefectural land area respectively in the laser, national and prefectural statistics. Large discrepancies in the "Others" area may seem serious, but the value of 9.4% of the prefectural land area in the national statistics can be explained as simply inflated in adjustment of its internal imbalance to the authoritative figure of the GSI, while the over-inflated figure of 30.7% in the prefectural statistics is simply a compensation for the reduction in "Forest" area due to the stretched measure.

CONCLUSION

Two conclusions can be drawn from the result above. Firstly, the airborne laser profiling proved to be a prospective method of consistent and objective land-cover classification. With its cover classification along the flight line as precise as 17cm, its overall accuracy depends on the distance between two adjacent flight lines. With only 0.4% discrepancy with the most authoritative GSI figure on the total land area of the prefecture, the present spacing of 4km between the flight lines should be satisfactory enough for the areas as large as a prefecture, but finer spacing would improve the accuracy of land-cover statistics since each cover category occupies only a part of the prefecture.

Secondly, our land-cover classification by airborne laser profiling revealed some of the problems in the existing government land-use statistics primarily based on legal land registration and aerial photography. It also helped to ensure the credibility of the existing land-use statistics by identifying quantitatively the causes and sources of discrepancies between them as well as with the laser-based classification. Coordinated use of the airborne laser altimetry with the existing statistics would certainly improve the overall quality of land-use/land-cover statistics of the prefecture and the nation. The most urgent and important task for such coordination is establishment of common definition and terminology.

LITERATURE CITED

EHIME PREFECTURE STATISTICAL OFFICE, (2005): Statistical yearbook of Ehime prefecture. Ehime statistical assoc., Matsuyama, Ⅵ + 370pp (in Japanese)

GEOGRAPHICAL SURVEY INSTITUTE, (2006): National municipality aerial statistics. http://www.gsi.go.jp/KOKUJYOHO/MENCHO/200510/ichiran.htm (in Japanese)

INTERGOVERNMENTAL PANEL on CLIMATE CHANGE, (2003): Good practice guidance for land use, land-use change and forestry. Institute for Global Environmental Strategies (IGES) for the IPCC, Hayama, Ⅴ + 588pp

LAND and WATER BUREAU, MINISTRY of LAND,: Land use control back-up system. http://lucky.tochi.mlit.go.jp/whats.html (in Japanese)

MATSUMOTO, M., (2003): Forest information to meet the demands of the Kyoto protocol and Marrakech accords. Proc. Forest Planning Soc.**407**: 15-24 (in Japanese)

NELSON, R., SHORT, A. and VALENTI, M., (2004): Measuring biomass and carbon in Delaware using an airborne profiling LiDAR. Scandinavian Journal of Forest Research **19**(6): 500-511

(Received 17 January 2007)
(Accepted 20 October 2007)

Article

Comparison of Different Sampling Density Data for Detecting and Measuring Individual-trees in a Mountainous Coniferous Forest using Small-footprint Airborne LiDAR

Tomoaki Takahashi[*1], Kazukiyo Yamamoto[*2,3] and Yoshimichi Senda[*4]

ABSTRACT

This study investigated the effects of laser-sampling density on individual-tree detection and tree height estimation changing the sampling density by overlapping three flight data in a mountainous coniferous forest. The LiDAR system used in this study was mounted on a fixed-wing aircraft. The study area was closed-canopy, middle-aged Japanese cedar (*Cryptomeria japonica*) plantation in Japan. We prepared three sets of single flight data (3.2 points/m^2), three sets of double-overlapping data (6.5 points/m^2) consisted of two single flight data, and one set of triple-overlapping data (9.7 points/m^2) consisted of three single flight data within this study plot. Namely, a total of seven datasets were used in the analysis. The numbers of detected same trees among same laser-sampling density datasets were different and increased with the increase of the density. The detection rate of same trees among all datasets was approximately 55%, and the detected trees belonged to dominant and co-dominant trees within the plot. In all datasets, we found that if a given field tree has relatively lower treetop-elevation and smaller crown radius than that of the nearest field tree, and these trees are close to each other, the lower tree is difficult to detect in mountainous coniferous forest. But the number of detected small trees between 10m and 18m height increased with the increase of laser-sampling density. LiDAR-derived median and mean tree heights were slightly greater than that of field measured tree height in this study site. Although there were significant differences between field measured and LiDAR-derived tree heights for all datasets ($p < 0.01$), the difference between maximum and minimum RMSE for tree height estimates was only 0.17m and the maximum RMSE was 1.02m. All results of this study indicate that although greater laser-sampling density data can provide information of more varying tree size, 3 or 4 points/m^2 of laser-sampling density data would provide accurate individual-tree detection of upper-storey trees and tree height estimates, given as RMSE, is approximately 1m in middle-aged Japanese cedar forests in mountainous areas.

Keywords: LiDAR, laser, sampling density, individual-tree, coniferous forest

INTRODUCTION

Airborne light detection and ranging (LiDAR) is a useful and powerful tool for estimating forest parameters. Especially, many researchers have previously shown that individual-tree height in some coniferous forests with flat and steep slope terrain can be estimated accurately with high-density small-footprint airborne LiDAR data (HYYPPÄ *et al.*, 2001; PERSSON *et al.*, 2002; TAKAHASHI *et al.*, 2005a). Some researchers have focused on the effects of laser-sampling density on estimation of individual-tree parameters using small-footprint LiDAR for the purpose of reducing costs of data acquisition in recent years (NILSON and HOLMGREN, 2003; HIRATA, 2004; YU *et al.*,

Corresponding author: Tomoaki Takahashi
[*1] Forestry and Forest Products Research Institute, 1, Matsunosato, Tsukuba, Ibaraki, 305-8687, Japan
[*2] Graduate School of Bioagricultural Sciences, Nagoya University, Furo-cho, Chikusa, Nagoya, Aichi, 464-8601, Japan
[*3] Japan Science and Technology Agency/CREST, Kawaguchi 332-0012, Japan
[*4] Nakanihon Air Service Co., Ltd., 2, Tonogama, Ho-jo-aza, Toyoyamatyo-oaza, Nishikasugai, Aichi, 480-0202, Japan

2004). In general, when the sampling density decreases, not only the number of detected trees would decrease (ZIMBLE *et al.*, 2003), but also the accuracy of tree height estimates would deteriorate because of missing treetops (GAVEAU and HILL, 2003). Tree height estimates with small-footprint airborne LiDAR data would be principally calculated by subtracting digital terrain model (DTM) from digital surface model (DSM). Therefore it is considered that not only the accuracy of the DSM, but also the accuracy of the DTM would significantly affect individual-tree height estimates.

Although KRAUS and PFEIFER, (1998) indicated that the steeper the slope angle become and the lower the number of laser pulses that hit the ground surface become, the accuracy of DTM would be lower. Our previous study showed that the root mean square error (RMSE) of the LiDAR-derived tree height estimates was less than 1m in a mountainous coniferous forest with steep slope in Japan when using a helicopter-borne scanning LiDAR which produced high-density data (e.g., more than 8 to 10 points/m^2) by single flight (TAKAHASHI *et al.*, 2005a). In order to acquire high-density laser data, researchers may select two ways, one is application of helicopter-borne scanning LiDAR systems with lower flight speed and altitude by single flight, and the other is application of LiDAR systems mounted on fixed-wing aircrafts with higher flight speed and altitude by several repeat flights. While these ways have both merits and demerits in terms of cost, quality of the acquired data, and measurement time, the former way seem to be able to provide higher quality data and the latter way seem to be more suitable for the measurement for wide area in terms of cost, respectively. Although we found that the helicopter-borne LiDAR could provide good estimates of individual-tree heights in a mountainous coniferous forest in Japan, the relationship between the laser-sampling density and the accuracy of LiDAR-derived tree height estimates when using fixed-wing airborne LiDAR remains unknown.

For the purpose of reducing costs of LiDAR data acquisition maintaining a preferable accuracy of the estimates of forest parameters in mountainous forests with steep slopes, we should investigate the effects of laser-sampling density on the estimation of individual-tree parameters in such forests. Therefore in this study, we investigated the effects of laser-sampling density on individual-tree detection and tree height estimation changing the density by overlapping three flight data acquired by a fixed-wing airborne LiDAR in a mountainous coniferous forest in Japan.

MATERIALS AND METHODS

Ground Reference Data

The study area was the Nagoya University experimental forest located in Aichi Prefecture in central Japan (lat. 35° 12' N, long. 137° 33' E, 930m asl). Even-aged (49-year-old) closed-canopy coniferous plantation was chosen for this study. We established a square plot (approximately 50×50m) in the plantation, and the terrain slope within the plot ranged from 11.4 to 47.8 degrees. The plot mainly consisted of planted Japanese cedar (*Cryptomeria japonica*) (235 trees); however, planted hinoki cypress (*Chamaecyparis obtusa*) (21 trees), Japanese red pine (*Pinus densiflora*) (2 trees), fir (*Abies homolepis*) (2 trees), and sawara cypress (*Chamaecyparis pisifera*) (2 trees) were also mixed in. The forest floor was covered with litter, and the understorey vegetation that had not been weeded mainly consisted of kumazasa (*Sasa veitchii*) and shiromoji (*Lindera triloba*) with a height less than approximately 2m. Because there were two trees whose crown shape was distorted, a total of 260 trees were used for the analysis in this study.

During fall and winter of 2003, i.e., after the growth season had ended, tree measurements were completed. Static GPS surveys were used to determine the accurate position of a reference point in an open area near the plot; subsequently, the tree positions were surveyed in relation to the reference point as follows. The positions of the center of all tree stems were measured using a compass with an accuracy of 1° and a portable laser distance measurement with an accuracy of 1mm (DISTO4, Leica Geosystems, Heerbrugg, Switzerland), thus making corrections for each stem diameter at the height at which the laser beam was incident. Then, tree heights and diameters at breast heights (1.3m above ground level) of all individual-trees were measured using a dendrometer with an accuracy of 1cm (Ledha-Geo, Jenoptik laser, Jena, Germany) and a diameter tape, respectively. Subsequently, the projected on-ground crown radii at a height of 1.3m above ground level (eight directions) were measured using a measuring tape.

Although it was only one year, there was a gap between the acquisition time of the LiDAR data (fall 2004) and the ground truth data (fall and winter 2003). Because we mainly address individual-tree height estimation by LiDAR, field measured tree height values in 2003 should be corrected in some degree. To ascertain the one-year increment in tree height, we used the results of stem analysis for three sampled trees (Japanese cedar) that had been used for estimating past tree heights as of 2001 in our previous study (TAKAHASHI *et al.*, 2005a). Richards growth function (RICHARDS, 1958) was used to predict the height as of 2004 (H(t)) for each sampled tree as follows:

$$H(t) = M(1\text{-}e^{at})^b \quad (1)$$

where M, a, and b are parameters and t is age. These three parameters were estimated with the results of the stem analysis for each sampled tree. The predicted height increments between 2003 and 2004 for each sampled tree are shown in Table 1. In this study, the arithmetic mean value of the height increments was added to field measured tree height values as of 2003 for each standing tree within the plot. Subsequently, the corrected tree heights and uncorrected

Table 1 Predicted parameters (*M*, *a*, and *b*) of Richards growth function for three sampled trees and tree height increments between 2003 and 2004

	Stem 1	Stem 2	Stem 3	Mean
M	28.485	36.923	22.041	
a	-0.047	-0.020	-0.050	
b	1.654	1.046	1.365	
Increment	1.009	1.013	1.007	1.010

Richards growth function is shown in Eq.(1) in the text.

Table 2 Summary of plot reference data

	Range	Mean ±SD[c]
Diameter at breast height (cm)[a]	8.2–49.0	25.7±7.7
Tree height (m)[b]	9.0–29.8	19.3±3.5
Crown radius (m)[a]	0.4– 3.4	1.6±0.5

[a]Measured data as of 2003

[b]Predicted data as of 2004

[c]SD denotes standard deviation

DBH and crown radius were used as reference data in the analysis. A summary of the plot reference data is shown in Table 2. Hereafter, trees identified in the field are called "field tree" in this study.

LiDAR Data Collection

The LiDAR data acquisition was performed on 4th November 2004 using a fixed-wing airborne laser scanner (Optech ALTM 2050) operated by Nakanihon Air Service Co., Ltd., Japan. In this study, the position of the reflecting object was determined from the first and last pulse. Laser measurements were made on three parallel flight lines, hereafter, referred to as S_1, S_2, and S_3. The settings of the LiDAR system for each flight were almost same. The beam divergence was 0.19 mrad, giving a footprint diameter of approximately 0.2m with the flight altitude of approximately 1,080m above ground level, and the aircraft's speed was approximately 70m/s. The scan mirror frequency, laser pulse frequency, and the scan width were 70Hz, 50,000Hz, and ± 4.9°, respectively. By these specifications, the theoretical average distance between footprints was approximately 0.5m along the scan line and approximately 1.0m along the flight line for each flight. We firstly prepared three sets of single flight data, i.e., S_1, S_2, and S_3, then three sets of double-overlapping data (D_{12}, D_{13}, and D_{23}) consisted of S_1 and S_2, S_1 and S_3, and S_2 and S_3, respectively. Finally, one set of triple-overlapping data (T_{123}) consisted of all three single flight data was prepared. So a total of seven datasets were used in this analysis. The details of incident angle of laser pulses and actual laser-sampling density for each single flight data within the plot are shown in Table 3.

Processing LiDAR Data, Detecting Individual-tree Crowns and Estimating Tree Heights

Parameter settings in processing data were not changed for all datasets. The methods for preprocessing each dataset and creating a digital surface model (DSM), digital terrain model (DTM), and canopy height model (CHM) within the plot were the same as reported in TAKAHASHI *et al.* (2005a). Firstly, the unevenly distributed laser reflection point data was converted into two raster layers with a pixel size of 0.5m because theoretical laser-sampling density was approximately 3.2 points/m² for single flight data. The first raster layer, referred to as DSM_{raw}, was assigned the height value of the highest laser reflection point within each pixel using only first pulse data. The second raster layer, referred to as DTM_{raw}, was assigned the lowest laser reflection point within each pixel using both first and last pulse data. Then both DSM_{raw} and DTM_{raw} were refined by removing noise and interpolated for null-pixels. The interpolation methods used in this study were spline interpolation for DTM (MAGNUSSEN and BOUDEWYN, 1998; RIAÑO *et al.*, 2003), and inverse distance weighting method that does not change the original value for DSM (POPESCU *et al.*, 2002). Subsequently, CHM was computed by subtracting DTM from DSM.

Individual-tree crowns were identified using our software named LiDAS (LiDAR Data Analysis System), which has functions to identify individual canopy gaps and segment tree crowns (TAKAHASHI *et al.*, 2005b). Similar algorithms of segmenting tree crowns based on both the extraction of local maxima (WULDER *et al.*, 2000) and region growing were shown in HYYPPÄ *et al.* (2001) and MALTAMO *et al.* (2003). In order to locate trees, local maxima which are considered to be treetops were searched by 3×3 moving window in low-pass filtered (i.e., smoothed) DSM, and then used for region growing segmentation. This system requires the determination of an important threshold value, which is the difference between the height of the crown base within the smoothed DSM and the ground surface height of canopy gaps within the smoothed DSM. The best threshold value was determined by trial and error, and 8m was selected as the threshold value in this study. After generating individual-tree crown outlines by LiDAS for the smoothed DSM, they were laid over CHM. LiDAR-derived individual-tree heights were computed as the maximum value of CHM within each segmented crown (MALTAMO *et al.*, 2004).

Evaluation Method for Detected Tree Crowns and Estimates of Tree Heights

As mentioned before, LiDAR-derived tree heights were directly derived from CHM which was calculated by subtracting DTM from DSM in this study. Therefore, before evaluating both detection of individual-tree crowns and

measurement of tree heights, the statistics of DSM and DTM were investigated for each dataset. Also, we incidentally investigated the relationships between two single flight datasets among three flight lines (S_1, S_2, and S_3) concerning the elevation of DSM and DTM to assess reproducibility of DSM and DTM derived from different single flight lines.

Each LiDAR-detected tree crown had to be identified at the location of field tree for all datasets. If one field tree existed within a segmented crown, the detection was considered to be correct. If several field trees existed within a segmented crown, the field tree with the highest treetop-elevation was identified as the segmented crown, and the remaining unidentified field trees were defined as undetected trees. For calculating individual-treetop-elevation, we used field tree heights and ground elevations surveyed in the field. The tree matching process is based on the fact that dominant and co-dominant trees are more likely to detect than intermediate or suppressed trees in Japanese cedar plantations in a mountainous forest by LiDAR measurements as shown in our previous study (TAKAHASHI *et al.*, 2005). In order to ensure the accuracy of the tree matching process, we assessed the differences between horizontal location of field tree with the highest treetop-elevation and local maximum pixel within individual crown segment. In this assessment, the detected same trees among all datasets were targeted. Then, to investigate the characteristics of detected and undetected trees, we mainly focused on mean crown radius and tangent ($\tan\theta$) consisted of horizontal distance and viewing angle (depression or elevation angle) from a given field treetop to the closest field treetop (see Fig. 1) referencing a method in PERSSON *et al.*, (2002). In this study, we denoted that the depression and elevation angle have negative and positive value, respectively.

For the evaluation of tree height estimates, the detected same trees among seven datasets were mainly targeted. We firstly assessed the statistical significant difference of average such as mean and median tree heights among groups, including filed data and seven datasets. In this study, Friedman test (HOLLANDER and WOLFE, 1973) and the Scheffe procedure as a post hoc test were applied in the statistical tests. Next, RMSE for LiDAR-derived tree height estimates was computed for each dataset as follows:

$$\mathrm{RMSE}=\sqrt{\frac{\sum_{i=1}^{n}(h_{L(i)}-h_{f(i)})^2}{n}} \quad (2)$$

where h_L and h_f are LiDAR-derived and field measured tree height, respectively. Finally, we investigated the relationships between LiDAR-derived and field measured tree heights by regression analysis, in which models were fitted to the data using the least-squares method. Only for the regression analysis, the detected same trees among same laser-sampling density datasets were targeted.

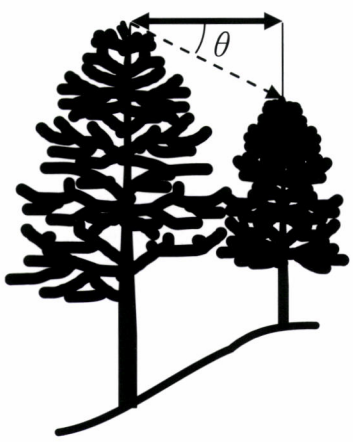

Fig. 1 Horizontal distance (solid arrow) and viewing angle (θ) from a given field treetop (left tree) to the closest field treetop (right tree)
In the case of this figure, θ represents depression angle.

RESULTS

The statistics of DSM and DTM for each dataset are shown in Table 3. Five statistics, i.e., minimum, maximum, mean, standard deviation, and coefficient of variation of the elevation were almost same among all datasets for DSM and DTM. Table 4 shows that the differences between two single flight datasets among three flight lines (S_1, S_2, and S_3) concerning the elevation of DSM and DTM. Although mean errors of DSMs and DTMs were almost zero, RMSEs of DSMs were grater than that of DTMs. Fig. 2 shows that the example of scatter plots for the relationship between two single flight datasets (S_1 and S_2) concerning the elevation of DSM and DTM. Many outliers exist in the relationship between two DSMs, on the contrary, there are few outliers in the relationship between two DTMs.

The differences between locations of field tree and local maximum within each crown segment for detected same trees among all datasets are shown in Table 5. In this table, dx and dy denote the mean differences for easting and northing, respectively, and they were computed by subtracting the position coordinate of local maxima from that of the corresponding field tree for each direction. They had negative values and their magnitude of the values was small for all datasets. RMSEs for the differences were slightly grater than the resolution of raster data used in this study for all datasets except S_2.

The number of detected trees for each dataset is shown in Table 6. The detection rates were almost same among all datasets. But the numbers of detected same trees among same laser-sampling density datasets were different and increased with the increase of the density. The detection rate of same trees among all datasets was approximately 55%. Both Table 7 and Fig. 3 show the characteristics of detected and undetected same trees among all datasets. Also, trees which were either

Table 3 Actual laser-sampling density and incident angle within plot, and statistics of DSM and DTM for each dataset

		S_1[a]	S_2[a]	S_3[a]	D_{12}[b]	D_{13}[b]	D_{23}[b]	T_{123}[c]
Sampling density (points/m^2)		3.3	3.3	3.1	6.6	6.4	6.4	9.7
Incident angle (degree)		0.5–3.7	0.0–2.2	0.0–3.3				
DSM	Min	938.50	938.46	938.52	938.46	938.50	938.52	938.52
	Max	997.98	997.97	997.54	997.98	997.98	997.97	997.98
	Mean	967.58	967.62	967.63	967.79	967.76	967.81	967.95
	SD[d]	14.05	14.05	14.04	14.09	14.08	14.08	14.08
	CV (%)[e]	1.45	1.45	1.45	1.46	1.45	1.46	1.46
DTM	Min	938.56	938.65	938.52	938.54	938.57	938.60	938.53
	Max	978.80	978.73	979.24	978.67	979.10	979.06	979.07
	Mean	952.89	952.87	952.89	952.84	952.86	952.85	952.82
	SD[d]	9.57	9.58	9.62	9.59	9.60	9.59	9.59
	CV (%)[e]	1.00	1.01	1.01	1.01	1.01	1.01	1.01

[a] Three sets of single flight data, i.e., S_1, S_2, and S_3

[b] Three sets of double-overlapping data (D_{12}, D_{13}, and D_{23}) consisted of S_1 and S_2, S_1 and S_3, and S_2 and S_3, respectively

[c] One set of triple-overlapping data (T_{123}) consisted of all three single flight data

[d] SD denotes standard deviation

[e] CV denotes coefficient of variation

Table 4 Differences between two single flight data concerning DSM and DTM

	DSM			DTM		
	S_1[a]–S_2[a]	S_1[a]–S_3[a]	S_2[a]–S_3[a]	S_1[a]–S_2[a]	S_1[a]–S_3[a]	S_2[a]–S_3[a]
Mean error (m)	-0.04	-0.05	-0.02	0.01	-0.01	-0.02
RMSE (m)	1.64	1.63	1.67	0.24	0.28	0.22

[a] Three sets of single flight data, i.e., S_1, S_2, and S_3

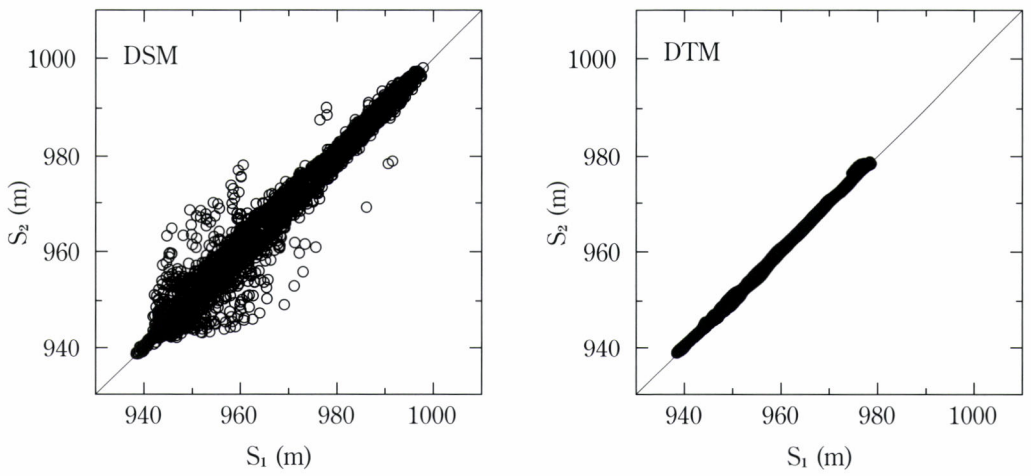

Fig. 2 The relationship between two single flight data (S_1 and S_2) concerning the elevation of DSM (left) and DTM (right)
The line in each graph indicates 1 : 1 correspondence. The number of data in each graph coincides with the number of pixels within study area.

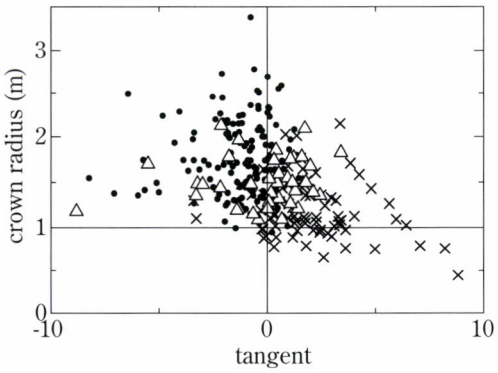

Fig. 3 Characteristics of detected and undetected trees for the same trees among all datasets, and trees which were either detected or undetected among different datasets
We denoted such trees as "ambivalently detected trees". This figure shows the relationship between mean crown radius and tangent (tanθ) consisted of horizontal distance and viewing angle (depression or elevation angle) from a given field treetop to the closest field treetop (see Fig. 1). *Black dots, crosses,* and *white triangles* denote detected, undetected, and ambivalently detected trees, respectively.

detected or undetected among different datasets were shown in Table 7 and Fig. 3, and we denoted such trees as "ambivalently detected trees". We can see most of the detected trees have depression angles and their crown radii are larger than that of undetected trees. On the contrary, most of the undetected trees have elevation angles. Moreover, many ambivalently detected trees exist around the border between detected and undetected trees, although some of them exist beyond the border in Fig. 3.

Table 8 shows the results of the statistical significant difference for the average of tree heights among groups, including filed data and seven datasets. There were significant differences between h_f and h_L for all datasets ($p < 0.01$). But there were not significant differences among same laser-sampling density datasets ($p > 0.05$). Moreover, some pairs among different laser-sampling density datasets had significant difference. In Table 7, we can see LiDAR-derived median and mean tree height and RMSE for the estimates increase slightly with the increase of laser-sampling density, but the differences are small. Then, there was a strong liner relationship between h_L and h_f for all datasets as shown in Fig. 4. As seen in this figure, there is no outlier in the

Table 5 Differences between locations of field tree and local maximum within each crown segment for detected same trees among all datasets

	S_1[a]	S_2[a]	S_3[a]	D_{12}[b]	D_{13}[b]	D_{23}[b]	T_{123}[c]
dx[d]	-0.30	-0.22	-0.25	-0.24	-0.26	-0.25	-0.25
dy[d]	-0.12	-0.02	-0.14	-0.09	-0.14	-0.09	-0.12
RMSE[e]	0.58	0.47	0.53	0.53	0.54	0.51	0.52

[a] Three sets of single flight data, i.e., S_1, S_2, and S_3

[b] Three sets of double-overlapping data (D_{12}, D_{13}, and D_{23}) consisted of S_1 and S_2, S_1 and S_3, and S_2 and S_3, respectively.

[c] One set of triple-overlapping data (T_{123}) consisted of all three single flight data.

[d] *dx* and *dy* denote the differences for easting and northing, respectively.

[e] RMSE means two-dimensional distance between the corresponding trees.

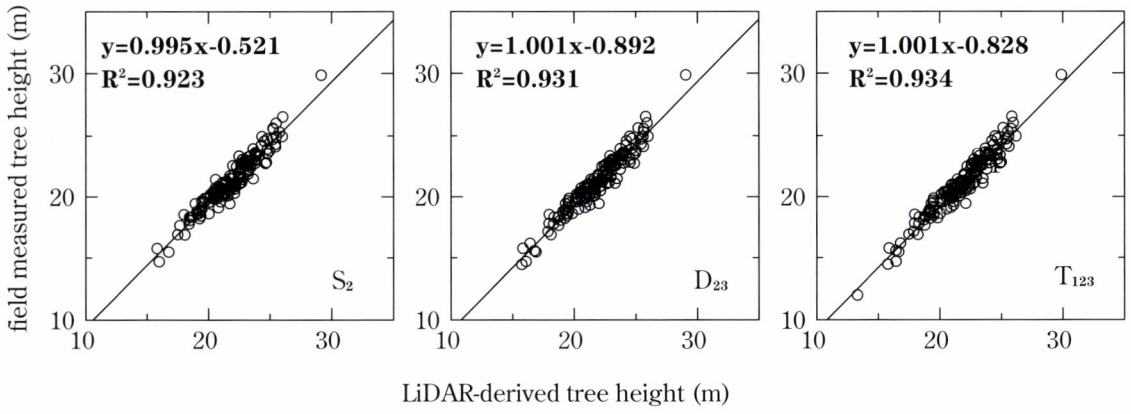

Fig. 4 The relationship between LiDAR-derived and field measured tree heights for one single flight data (S_2), one double-overlapping data (D_{23}), and one triple-overlapping data (T_{123})
S_2, D_{23}, T_{123} are described in the text.

relationship between h_L and h_f for all datasets.

DISCUSSION AND CONCLUSION

Although there were seemingly no differences among all datasets for DSM and DTM judging from Table 3 and 4, spatial localization of each pixel within DSM and DTM was not actually considered in the statistics. In fact, Fig. 2 shows many outliers exist in the relationship between two DSMs. Most of the pixels of the outliers are considered to be edge pixels of individual-tree crowns. Because the location of each laser measurement point by one flight does not always correspond to that of another flight, there is no telling that either the measurement point data around crown edges will belong to crown pixels or ground pixels (i.e., gap pixels) for each flight data. Moreover, the effects of both displacement and selection of point data within each pixel around crown edges would not be ignored during conversion point data into raster data, especially when the laser sampling density is low. On the other hand, there are few outliers in the relationship between two DTMs in Fig. 2 and both mean errors and RMSEs for the differences between two DTMs were smaller than that of DSMs as shown in Table 4. The cause was considered to be much less variation between adjacent pixels within DTM than that of DSM, and indeed field ground surface generally have much less variation than canopy surface above the ground. But we should know that the number of null-pixels which had been interpolated within DTM was much more frequent than that of DSM in closed-canopy Japanese cedar forests (TAKAHASHI *et al.*, 2006), and the effects of the interpolation would also cause such less variation between adjacent pixels within DTM.

As reported by ZIMBLE *et al.*, (2003), local maxima within DSM or CHM do not always correspond to treetops, especially when the laser sampling density is low. Therefore, we applied the tree matching approach based on crown segment because this approach was considered to be less mismatching than an approach which is based on using only local maxima. Table 5 shows the accuracy of the tree matching process used in this study. The results in this table indicate that the tree matching was considered as reasonable and proper. Moreover, we found an interesting tendency that both *dx* and *dy* had negative values for all datasets, thus indicating that LiDAR-detected local maxima were off to southwest from locations of stems. This is because even coniferous tree stems are not always upright on steep slops and the treetops are likely to tilt toward the valley side (HEURICH *et al.*, 2003; TAKAHASHI *et al.*, 2005a). In fact, the study area was southwestern slope as shown in our previous study (TAKAHASHI *et al.*, 2005a). The effects of this tendency on tree height estimation will be discussed later on.

Although the detection rates of tree were not so different among all datasets, the variation of the number of detected trees among double-overlapping datasets was smaller than that of single flight datasets as shown in Table 6. This indicates that if the laser-sampling density increase, the stability to detect trees would rise. Also, the number of detected same trees among same laser-sampling density datasets increased with the increase of the density, thus indicating that the probability to detect same trees would rise by the grater laser-sampling density. Therefore, greater laser-sampling density would be

Table 6 Detection rates of trees, tree height estimates, and root mean square errors (RMSEs) between field measured and LiDAR-derived tree heights

	Single flight[a]			Double-overlapping[b]			Triple-overlapping[c]	
	S_1	S_2	S_3	D_{12}	D_{13}	D_{23}	T_{123}	Field data[d]
Number of detected trees for each dataset	160	168	163	163	162	164	160	
Detection rates of trees for each dataset (%)	62	65	63	63	62	63	62	
Number of detected same trees among same laser-sampling density datasets	145	145	145	154	154	154	160	
Detection rates of same trees among same laser-sampling density datasets (%)	56	56	56	59	59	59	62	
Number of detected same trees among all datasets	142	142	142	142	142	142	142	
Detection rates of same trees among all datasets (%)	55	55	55	55	55	55	55	
Median tree heights for detected same trees among all datasets (m)	22.0	22.0	22.0	22.2	22.2	22.1	22.2	21.1
Mean tree heights detected same trees among all datasets (m)	21.9	22.0	22.0	22.1	22.1	22.1	22.2	21.4
[e] RMSE of tree height estimates for detected same trees among all datasets (m)	0.85	0.90	0.90	0.97	0.95	0.96	1.02	

[a] Three sets of single flight data, i.e., S_1, S_2, and S_3

[b] Three sets of double-overlapping data (D_{12}, D_{13}, and D_{23}) consisted of S_1 and S_2, S_1 and S_3, and S_2 and S_3, respectively.

[c] One set of triple-overlapping data (T_{123}) consisted of all three single flight data.

[d] The numbers of field tree were 260 within the plot.

[e] RMSEs were computed using Eq. 2 in the text.

better for both the stability and reproducibility of detecting individual-tree crowns. However, we should note that the relationships between laser incident angle (Table 3) and the detection rate of trees for single flight datasets (Table 6). The acuter the incident angle became, the greater the detection rates became in this study site, although the magnitude of incident angle was fairly small for flight data. HOLMGREN *et al.*, (2003) simulated the effects of laser scanning angle on tree height estimation, and they showed that laser height percentiles and proportion of canopy returns changed with by increasing scanning angle within 20m × 50m simulated forest plots. Similar simulations and results were found in LOVELL *et al.*, (2005). Considering these reports, detection rates of trees whose treetop-elevation is low would be decreased with the increase of scanning angle. Therefore, not only the effect of laser-sampling density, but also the effect of flight direction of LiDAR systems, laser incident angle, terrain slope angle, and slope aspect on the detection of individual-tree crowns would be crucial in mountainous forests. These effects should be investigated in detail in the future.

As shown in Table 7, the detection rate of same trees among all datasets was 54.6%, and rates of ambivalently detected trees and undetected trees were 14.6% and 30.8%, respectively. Both Table 7 and Fig. 3 indicate that if a given field tree has relatively lower treetop-elevation and smaller crown radius than that of the nearest field tree, and these trees are close to each other, the lower tree is difficult to detect in mountainous coniferous forests. Similar tendency for the detection of individual-trees seems to be found in boreal coniferous forests with flat terrain (PERSSON *et al.*, 2002). Conversely, it is indicated that most of the dominant and co-dominant trees would detect accurately in middle-aged Japanese cedar plantations in mountainous forests by the laser-sampling density of 3 or 4 points/m^2 as shown in Fig. 3. Many ambivalently detected trees existed around the border between detected and undetected trees in Fig.3, but some of them whose tangent were small existed beyond the border. Although it is not known the exact reason, such trees might be surrounded another neighbor trees with higher treetop-elevation. Moreover, we should note that trees whose crown radius with smaller than 1m can hardly detect. This is considered to be essentially the limitation of detection by 3 × 3 local maximum filtering for DSM whose resolution was 0.5m.

LiDAR-derived median and mean tree heights for the detected same trees were slightly greater than that of field measured tree heights in this study site (Table 6). As shown in Table 8, there were significant differences between h_f and h_L for all datasets ($p < 0.01$). One of the reasons for the differences might be insufficient correction for field individual-tree heights measured in 2003. However, it would be difficult to determine each tree height growth of all standing trees within the plot exactly because even the sampled trees had variations in height growth as shown in Table 1. Instead, we should note another possible reason, for example, the horizontal positional error between the field treetop and the stem as mentioned before. In fact, the results in Table 5 indicate that LiDAR-detected local maxima tilted toward the valley side (i.e., southwestern) from locations of stems. LiDAR-derived tree heights calculated with a distance between local maximum on DSM and DTM just below the local maximum would be overestimates in forests with steep slopes (HIRATA, 2004; TAKAHASHI *et al.*, 2005a). Moreover, the magnitude of overestimates increased with the increase of laser-sampling density (Table 6). According to GAVEAU and HILL (2003), the failure of sampling treetops because of an insufficient laser-sampling density is likely to occur in coniferous woodlands where crown shape is more conical than in broadleaf woodlands where crowns are more rounded. NÆSSET and ØKLAND (2002) concluded that the observed standard deviations in tree height residuals in LiDAR data for a forest

Table 7 Characteristics of detected, ambivalently detected, and undetected trees

	Detected[a]	Ambivalently detected[c]	Undetected[b]
Rate (%)[d]	54.6	14.6	30.8
Crown radius (m)[e]	2.2	1.5	1.2
Tangent[f]	-1.2	-0.2	2.0
Horizontal distance (m)[f]	2.4	1.9	1.7
Vewing angle (degree)[f]	-31.5	3.9	45.9

[a] Detected same trees among all datasets

[b] Undetected same trees among all datasets

[c] Trees which were either detected or undetected among different datasets

[d] Percentage of the number of detected, ambivalently detected, and undetected trees

[e] Mean crown radius

[f] Tangent ($\tan\theta$) consistes of horizontal distance and viewing angle (depression or elevation angle) from a given field treetop to the closest field treetop (see Fig. 1). Depression and elevation angle have negative and positive value, respectively.

dominated by Norway spruce (*Picea abies*) could be improved by increasing laser-sampling density. Considering these reports, the phenomenon that the errors of overestimations were increasing with the increase of laser-sampling density is not surprising.

Fig. 4 indicates that the accuracy of LiDAR-derived individual-tree heights was really high for all datasets. We should note that the number of detected small trees between 10 m and 18m height are increasing with the increase of laser-sampling density, and such trees fit correctly each regression line in this figure. According to the regression analysis, the intercepts of all regression equations did not significantly differ from zero ($p > 0.05$), thus indicating that the mean error of the regression equations was not significant. Moreover, the slopes for all regression equations could be statistically regarded as one ($p > 0.05$), thus indicating that the error between h_L and h_f was independent of tree size. Furthermore, the difference between maximum and minimum RMSE for tree height estimates was only 0.17m, and the maximum RMSE was 1.02m in this study site (Table 6). This accuracy was almost the same as we previously reported that we used a helicopter-borne LiDAR system in the same site for individual-tree height estimation (TAKAHASHI *et al.*, 2005a). Therefore, all results of this study indicate that although greater laser-sampling density data can provide information of more varying tree size, 3 or 4 points/m² of laser-sampling density data would provide accurate individual-tree detection of upper-storey trees and tree height estimates, given as RMSE, is approximately 1m in middle-aged Japanese cedar forests in mountainous areas.

Table 8 Statistical significant difference for the average of tree heights tested by Friedman test and Scheffe procedure

Group 1	Group 2	Chi-square statistic	*P* value	
Field tree height	S_1	31.8597	0.0000	**
Field tree height	S_2	86.5352	0.0000	**
Field tree height	S_3	48.3386	0.0000	**
Field tree height	D_{12}	140.3292	0.0000	**
Field tree height	D_{13}	109.5211	0.0000	**
Field tree height	D_{23}	130.7418	0.0000	**
Field tree height	T_{123}	210.5640	0.0000	**
S_1	S_2	13.3809	0.0634	
S_1	S_3	1.7113	0.9741	
S_1	D_{12}	38.4601	0.0000	**
S_1	D_{13}	23.2400	0.0015	**
S_1	D_{23}	33.5217	0.0000	**
S_1	T_{123}	78.6127	0.0000	**
S_2	S_3	5.5217	0.5966	
S_2	D_{12}	6.4701	0.4861	
S_2	D_{13}	1.3521	0.9870	
S_2	D_{23}	4.5446	0.7153	
S_2	T_{123}	27.1273	0.0003	**
S_3	D_{12}	23.9460	0.0012	**
S_3	D_{13}	12.3386	0.0900	
S_3	D_{23}	20.0851	0.0054	**
S_3	T_{123}	57.1268	0.0000	**
D_{12}	D_{13}	1.9067	0.9648	
D_{12}	D_{23}	0.1696	1.0000	
D_{12}	T_{123}	7.1009	0.4184	
D_{13}	D_{23}	0.9390	0.9958	
D_{13}	T_{123}	16.3668	0.0220	*
D_{23}	T_{123}	9.4654	0.2209	

* $P < 0.05$; ** $P < 0.01$

[a] Three sets of single flight data, i.e., S_1, S_2, and S_3

[b] Three sets of double-overlapping data (D_{12}, D_{13}, and D_{23}) consisted of S_1 and S_2, S_1 and S_3, and S_2 and S_3, respectively.

[c] One set of triple-overlapping data (T_{123}) consisted of all three single flight data.

LITERATURE CITED

GAVEAU, D. L. A. and HILL, R. A., (2003): Quantifying canopy height underestimation by laser pulse penetration in small-footprint airborne laser scanning data. Can. J. Remote Sens. **29**: 650-657

HEURICH, M., SCHNEIDER., T. and KENNEL., E., (2003): Laser scanning for identification of forest structures in the Bavarian Forest National Park. Proceedings of ScandLaser, 2-4 September, Umeå, Sweden 97-106

HIRATA, Y., (2004): The effects of footprint size and sampling density in airborne laser scanning to extract individual-trees in mountainous terrain. Int. Arc. Photogramm. Remote Sens. and Spatial Info. Sci. **36**: part8/w2

HYYPPÄ, J., KELLE, O., LEHIKOINEN, M. and INKINEN, M., (2001): A segmentation-based method to retrieve stem volume estimates from 3-D tree height models produced by laser scanners. IEEE Trans. Geosci. Remote Sens. **39**: 969-975

HOLLANDER, M. and WOLFE, D. A., (1973): Nonparametric statistical inference. New York: John Wiley & Son. 139-146

HOLMGREN, J., NILSSON, M. and OLSSON, H., (2003) Simulating the effects of lidar scanning angle for estimation of mean tree height and canopy closure. Can. J. Remote Sens. **29**: 623-632

KRAUS, K. and PFEIFER, N., (1998): Determination of terrain models in wooded areas with airborne laser scanning data. ISPRS J. Photogramm. Remote Sens. **53**: 193-203

LOVELL, J. L., JUPP, D. L. B., NEWNHAM, G. J., COOPS, N. C. and CULVENOR, D. S., (2005): Simulation study for finding optimal lidar acquisition parameters for forest height retrieval. For. Ecol. Man. **214**: 398-412

MAGNUSSEN, S. and BOUDEWYN, P., (1998): Derivations of stand heights from airborne laser scanner data with canopy-based quantile estimators. Can. J. For. Res. **28**: 1016-1031

MALTAMO, M., EERIKÄINEN, K., PITKÄNEN, J., HYYPPÄ, J. and VEHMAS, M., (2004): Estimation of timber volume and stem density based on scanning laser altimetry and expected tree size distribution functions. Remote Sens. Environ. **90**: 319-330

NÆSSET, E. and ØKLAND, T., (2002): Estimating tree height and tree crown properties using airborne scanning laser in a boreal nature reserve. Remote Sens. Environ. **79**: 105-115

NILSON, M. and HOLMGREN, J., (2003): Prediction of forest variables using LIDAR measurements with different footprint size and measurement densities. Proceedings of ScandLaser, 2-4 September, Umeå, Sweden: 124-132

PERSSON, A., HOLMGREN, J. and SODERMAN, U., (2002): Detecting and measuring individual-trees using an airborne laser scanner. Photogramm. Eng. Remote Sens. **68**: 925-932

POPESCU, S. C., WYNNE, R. H. and NELSON, R. F., (2002): Estimating plot-level tree heights with lidar: local filtering with a canopy-height based variable window size. Com. Elect. Agr. **37**: 71-95

RIAÑO, D., MEIER, E., ALLGÖWER, B., CHUVIECO, E. and USTIN, S.L., (2003): Modeling airborne laser scanning data for the spatial generation of critical forest parameters in fire behavior modeling. Remote Sens. Environ. **86**: 177-186

RICHARDS, F., (1958): A flexible growth function to empirical use. J. Experi. Bot. **10**: 290-300

TAKAHASHI, T., YAMAMOTO, K., SENDA, Y. and TSUZUKU, M., (2005a): Estimating individual-tree heights of sugi (*Cryptomeria japonica* D. Don) plantations in mountainous areas using small-footprint airborne LiDAR. J. For. Res. **10**: 135-142

TAKAHASHI, T., YAMAMOTO, K., SENDA, Y. and TSUZUKU, M., (2005b): Predicting individual stem volumes of sugi (*Cryptomeria japonica* D. Don) plantations in mountainous areas using small-footprint airborne LiDAR. J. For. Res. **10**: 305-312

TAKAHASHI, T., YAMAMOTO, K., MIYACHI, Y., SENDA, Y. and TSUZUKU, M., (2006): The penetration rate of laser pulses transmitted from a small-footprint airborne LiDAR: a case study in closed-canopy, middle-aged pure sugi (*Cryptomeria japonica* D. Don) and hinoki cypress (*Chamaecyparis obtusa* Sieb. et Zucc.) stands in Japan. J. For. Res. **11**: 117-123.

WULDER, M., NIEMANN, K. O. and GOODENOUGH, D. G., (2000): Local maximum filtering for the extraction of tree locations and basal area from high spatial resolution imagery. Remote Sens. Environ. **73**: 103-114

YU, X., HYYPPÄ, J., HYYPPÄ, H. and MALTAMO, M., (2004): Effects of flight altitude on tree height estimation using airborne laser scanning. Int. Arc. Photogramm. Remote Sens. and Spatial Info. Sci. **36**: part8/w2

ZIMBLE, D. A., EVANS, D. L., CARLSON, G. C., PARKER, R. C., GRADO, S. C. and GERARD, P. D., (2003): Characterizing vertical forest structure using small-footprint airborne LiDAR. Remote Sens. Environ. **87**: 171-182

(Recceived 17 January 2007)
(Accepted 28 October 2007)

Article

Estimating Timber Stock of Ehime Prefecture, Japan using Airborne Laser Profiling

Hayato Tsuzuki[*1], Ross Nelson[*2] and Tatsuo Sweda[*1]

ABSTRACT

The timber stock of mainland Ehime prefecture was estimated using airborne laser profiling data. Our provisional analysis revealed that: 1) at 5,435km^2, the laser estimate of land area obtained as a simple product of flight path length and its 4km width was fairly consistent with the figure of 5,455km^2 by the Geographical Survey Institute, considered the most reliable of the government statistics; 2) on the other hand, at 176 million m^3 for the entire prefecture our estimate of standing timber stock turned out to be twice as much as the government figure of 87 million m^3; 3) judging from the precision in land-area estimation and results from other research, our estimate is considered more likely to represent the actual timber stock than the government figure; 4) thus airborne laser altimetry would provide more accurate national forest carbon budget for the Kyoto Protocol than does the existing national forest inventory; 5) at the present density of laser profiling transects, 4km apart from each other, however, no reasonable accuracy is expected at the municipality level.

Keywords: timber stock, airborne laser profiling, prefecture-wide inventory, Ehime prefecture, Kyoto protocol

INTRODUCTION

Japan is now determined to base its forest carbon budget accounting of the Kyoto Protocol on the Forest Inventory Book (FIB), an original system of inventorying the nation's forest resources by sub-compartments as tiny as one-tenth of a hectare. However, the FIB is reputed for its inaccuracy due partly to its obsolescent bookkeeping system and partly to lack of field checks in recent decades, and without major reform it may not survive long beyond the first commitment period of the Protocol. This study was intended to develop a new system of national forest inventory using airborne laser altimetry with particular aims of: 1) developing a prefecture-wide laser altimetry inventory system; 2) assessing prefectural forest carbon budgets using multi-temporal airborne laser profiling at 2-year intervals, and 3) comparing the resulting inventory and carbon sequestration estimates with the corresponding official figures of the government. In this paper the first outcome of the project, i.e. an estimate of prefectural forest inventory resulting from the term-head airborne laser profiling and its comparison with the existing government statistics are reported.

Corresponding author: Hayato Tsuzuki
[*1] Faculty of Agriculture, Ehime University
3-5-7 Tarumi, Matsuyama 790-8566 Japan
[*2] Biospheric Sciences Branch, NASA-Goddard Space Flight Center
Greenbelt, MD 20771 USA

MATERIALS AND METHODS

Study Area and Laser Profiling

Ehime (5,677.12km^2) is one of the 47 prefectures of Japan, comprising of mainland (5,455.38km^2) and numerous small islands (221.74km^2) to the north and west in the Seto Inland Sea (Fig. 1). The terrain is rugged especially along the Ishizuchi (1,982 m a.s.l.) Range, which constitutes the border with Kochi prefecture to the south. According to the government statistics 71% of the prefecture or 3,870km^2 is forested, of which approximately 3/5 is plantations primarily of *Cryptomeria japonica* and *Chamaecyparis obtusa* and the remaining 2/5 is secondary natural forests of mainly broadleaved species (Ochi *et al.*, 2006). Approximately 10% of the forested land is nationally owned and managed directly by the Forestry Agency (Shikoku Regional Forest Office, 2006).

The term-head laser profiling mission with NASA's Portable Airborne Laser System (PALS, Nelson *et al.*, 2003), mounted on-board a Bell 206 helicopter was flown September

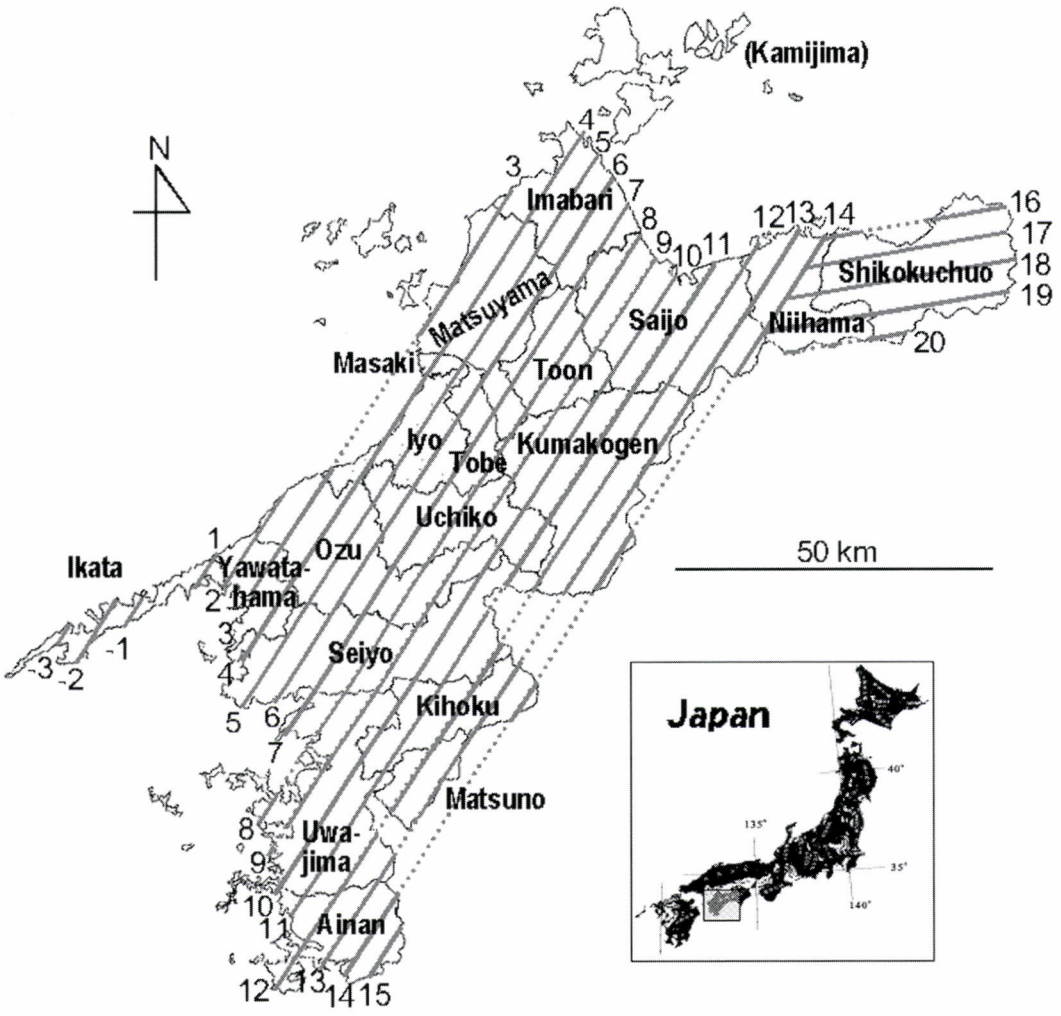

Fig. 1 Study area of Ehime prefecture and profiling transects

10-17, 2005 over the mainland Ehime in a series of 23 parallel flight lines four kilometer apart, totaling 1,358.7km (Fig. 1). The helicopter was flown 200m above ground at a target ground speed of 180km/hr with an alternating first/last pulse altimetry data retrieval frequency of 400Hz. However, slow climb-ups and -downs over the steep terrain reduced the nominal data retrieval interval of 12.5cm along the flight track to an overall average of 8.5cm with a local minimum as short as 3cm.

Land-area Estimation

As a way of assessing the accuracy of timber stock estimation by laser profiling, laser-based land area was also estimated and compared with corresponding government figures from the Geographical Survey Institute (GSI, http://www.gsi.go.jp). The laser estimates were obtained as a simple product of flight length and width of 4km between the flight lines. For a fair comparison, insular areas totaling 221.74km² were discounted in the government figures. Only the islands equal to or larger than 1km² are accounted for in the insular total, but the remaining error was deemed negligible.

Timber Stock Estimation

The standing timber stock was estimated on a basis of its correlation with the area of vegetation profile induced from airborne laser profiling data as a difference between canopy and topographic profiles (TSUZUKI, 2004; TSUZUKI *et al.*, 2006), i.e. according to a regression of standing timber stock V (m³/ha) on cross sectional area S (m²/m) of vegetation profile $f(x)$,

$$V = aS = a\int f(x)\,dx \qquad (1)$$

The coefficient a in the above equation was determined

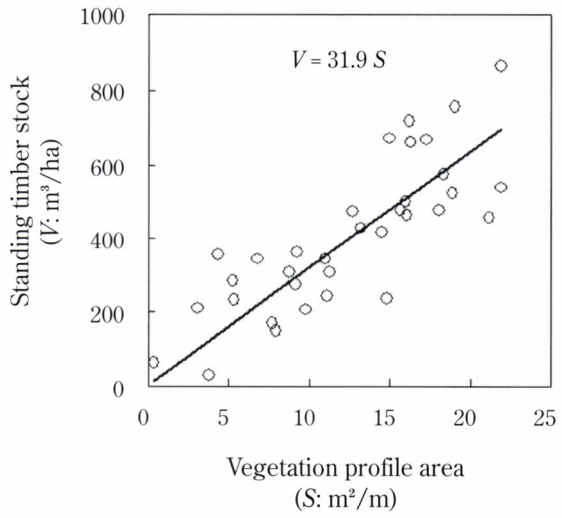

Fig. 2 Regression of standing timber stock on vegetation profile area

by the regression of actual standing timber stock measured on the ground on the vegetation profile area calculated from the laser altimetry data as shown in Fig. 2.

Timber stock measurement was made in sample plots established directly under the laser profiling flight path. A total of 34 sample plots were established, one each in 16 stands of *Cryptomeria japonica*, 12 of *Chamaecyparis obtusa* and six of mixed broadleaved species. The plot size varied from 21 to 829m² depending on the stand height but was made greater than the area of a square with its side length equal to stand height. In each plot stem diameter at breast height (dbh) was censused and then converted to stem volume by allometric volume equations made from a total of 219 sample trees consisting of 58 *C. japonica*, 79 *C. obtusa*, 23 *Pinus densiflora* and 59 broadleaved species, felled in and around the sample plots and measured for stem volume. Rather than differentiating by species, only two volume equations, i.e., one for conifer and the other for broadleaves were used since no significant difference was found among the coniferous species.

Eventually, the coefficient a turned out to be 31.9 (dimensionless) as has been shown in Fig. 2. The validity of the coefficient was tested then by: 1) dividing the sample plots randomly into equal halves of 17 plots each, and 2) comparing the measured timber volume of the first half against its estimate made using coefficient a determined from the other half. The process was repeated 10 times by random selection of plots. Note that the above coefficient is still a temporary figure since the plot measurement and data compilation are still under way for the ultimate total of 200 plots.

In this process of standing timber stock estimation, no prior delineation of forest area from other land use was conducted for two reasons. Firstly, with minutely fragmented land use over the past, delineation of forests from other land use is too complicated and tedious even for possible improvement in accuracy it may bring. Secondly, with the first and last returns registering the same clearance in the area devoid of vegetation, no vegetation profile is formed, and thus the other land use than forest do not virtually affect the timber estimate even if other land-use categories are included in the analysis. The only sources of possible over-estimation are small forested parks in and in the vicinity of city, shade trees along the road etc. for which 3% allowance was given in the final estimate. The timber stock estimation was tallied by municipality and compared with the corresponding government statistics.

The government estimates of timber stock used for comparison was the forest inventory book (FIB) compiled in basically the same method throughout Japan but with different yield tables specific to districts as well as to species and site quality. In Ehime prefecture, five forest districts of nearly the same area are distinguished by major watersheds. Species distinguished in each district are *C. japonica*, *C. obtusa*, *Pinus* spp., *Quercus* spp. and other broadleaves with five site quality classes for conifers and three for all the broadleaves. Based on a prefecture-wide yield survey made 40-50 years ago, the yield tables were compiled to give standard annual volumetric increment by age class of five-year interval for each species and site class. With reference to these yield tables by a mainframe, standing timber volume is routinely calculated by adding corresponding increment year after year for each sub-compartment consisting of trees of the same age and same species category. The sub-compartment timber volumes are added for the compartment totals, which then are added for municipal totals and subsequently for the prefecture total with the harvested sub-compartments reset to null according to the obligatory harvest reports from forest owners.

Widely reputed inaccuracy of the FIB is generally considered to have arisen from a multitude of causes. The most significant one of them would be complete lack of field checks in the last few decades due to declining forestry budgets and personnel to result in accumulated errors. Another could be the deviation in the yield tables made when the nation's forests were significantly younger with over representation of younger stands and under representation of mature stands.

RESULTS AND DISCUSSIONS

Validity of the Laser Estimates

The results of the validity test for the regression coefficient a and estimated timber stock by randomly halving 34 sample plots into estimation and verification groups are given in Table 1. In each round of the test repeated 10 times, timber stock of the verification group was estimated by a regression established using data from the estimation group, and then checked against measured counterparts. First of all,

Table 1 Validity tests for regression coefficient a of equation (1)

Repetition		Correlation of vegetation profile area with standing timber stock		Regression coefficient	Mean timber stock (m^3/ha)		Error $\frac{V_{est} - V_{act}}{V_{act}}$ (%)
		Correlation coefficient	Level of significance		Estimate (V_{est})	Ground measured (V_{act})	
1	obverse	0.843	<0.0001	33.538	465	437	6.6
	verso	0.767	<0.001	30.786	338	375	-10.0
2	obverse	0.858	<0.0001	32.545	384	390	-1.5
	verso	0.785	<0.0001	31.256	408	422	-3.3
3	obverse	0.773	<0.001	32.529	377	377	0.0
	verso	0.866	<0.0001	31.217	414	435	-4.8
4	obverse	0.804	<0.0001	29.054	362	437	-17.1
	verso	0.857	<0.0001	34.864	432	375	15.2
5	obverse	0.790	<0.0001	30.385	354	399	-11.4
	verso	0.853	<0.0001	33.913	448	413	8.5
6	obverse	0.872	<0.0001	31.517	374	405	-7.6
	verso	0.746	<0.001	32.432	421	407	3.5
7	obverse	0.838	<0.0001	32.039	379	393	-3.6
	verso	0.781	<0.001	31.799	414	419	-1.1
8	obverse	0.865	<0.0001	33.356	372	347	7.0
	verso	0.730	<0.001	29.876	410	465	-11.8
9	obverse	0.754	<0.001	30.459	428	458	-6.5
	verso	0.849	<0.0001	32.849	355	354	0.2
10	obverse	0.763	<0.001	30.955	396	428	-7.5
	verso	0.866	<0.0001	32.817	396	384	3.2
			Mean	31.909	396	406	
			S.D.	1.46	33	32	
			C.V.	4.56	8.4	7.9	
			S.E.	0.35	8.1	7.8	

the 20 correlation coefficients between the standing timber stock V and the vegetation profile area S calculated using 20 sets of randomly chosen halves of 17 plots were no less than 0.73 and highly significant with the level of significance no greater than 0.1%. Small standard deviation also indicates that the correlation is consistent and stable with data from as few as 17 sample plots.

The mean of 20 regression coefficients calculated using data from 20 estimation halves turned out to be 31.9 (dimensionless) with the standard error of only 0.35 (dimensionless), indicating the robustness of the regression coefficient. The difference between the observed mean standing timber stock of 17 sample plots and their estimated counterparts ranged from -75 to 57m^3/ha, or -17.1% to 15.2% in terms of relative error with an overall mean and standard error of 396 ± 8.1m^3/ha in the estimated timber stock against 406 ± 7.8m^3/ha in the observed timber stock.

On the basis of the significant correlation and robust regression indicated above, the regression coefficient of a=31.9 based on all the 34 sample plots was judged as valid for estimating the prefecture-wide timber stock.

Land-area Estimation and Comparison with Government Figures

The laser estimates of land area and standing timber stock by municipality are shown in Table 2. The total area of mainland Ehime differed from the GSI figure by only 0.38%, indicating that our rough laser estimate by rectangular area of transect length and width of 4 km should be good enough for the prefecture level area estimation. When it comes to the comparison by municipality, however, the discrepancy became much more conspicuous with estimation errors over 10% for six of 19 municipalities. The largest error was found for Ikata, where one flight line (line 0 between lines –1 and 1 in Fig. 1) had to be omitted due to flight restrictions in a 5-km bound of a nuclear power station. For more precise estimates at the municipality level, the flight lines have to be significantly closer.

Table 2 Comparison between government statistics and airborne laser estimates in land area and standing timber stock

	Land Area			Standing Timber Stock		
	Geographical Survey Inst. (km^2)	Laser (km^2)	Laser-GSI / GSI	Government (million m^3)	Laser (million m^3)	/ Gov.
Ehime	5,455	5,435	-0.38%	87.32	175.53	2.010
Shikokuchuo	420	362	-14%	8.62	12.89	1.50
Niihama	234	285	+22%	3.95	8.57	2.17
Saijo	509	511	± 0%	8.68	15.14	1.74
Imabari	286	281	-2%	2.60	6.67	2.56
Matsuyama	386	354	-8%	3.74	8.26	2.21
Iyo	194	214	+10%	1.28	5.60	4.37
Toon	211	215	+2%	3.98	6.93	1.74
Masaki	20	16	-19%	0	0.07	∞
Tobe	102	106	+4%	1.50	3.80	2.54
Ozu	432	430	-1%	6.53	14.49	2.22
Uchiko	300	299	± 0%	4.98	10.73	2.15
Yawatahama	130	128	-2%	1.52	3.29	2.16
Ikata	94	55	-42%	0.63	1.15	1.81
Seiyo	515	523	+2%	9.25	18.05	1.95
Kumakogen	584	611	+5%	13.94	26.73	1.92
Uwajima	459	455	-1%	6.44	13.31	2.07
Kihoku	242	235	-3%	4.79	9.16	1.91
Matsuno	99	113	+15%	1.75	4.27	2.44
Ainan	238	242	+2%	3.13	6.41	2.05

Timber Stock Estimation and Comparison with Government Figures

Our timber stock estimates differed unequivocally from the government counterparts, even at the prefectural level. At 176 million m^3, our estimate turned out to be twice as much as the government figure (OCHI *et al.*, 2006; SHIKOKU REGIONAL FOREST OFFICE, 2006; 2005; 2004; 2003; 2002) of 87 million m^3. Both estimates seem responsible for this disagreement but the government figure seems much less representative of the reality than the laser estimate for the following reasons. First of all, the government statistics has long been notorious for excessive under-estimation (FUJIMOTO *et al.*, 2007; MATSUMOTO, 2003; SHIRAISHI, 1999) as has already been mentioned. Secondly, in our two-way comparison of the government statistics and airborne laser estimate against actual timber cruising results for a 200 ha tract in the Tomakomai National Forest in northern Japan, the former under-estimated the reality by a factor of 0.56, whereas the latter over-estimated only by a factor of 1.09 (SWEDA and TSUZUKI, 2006). Thirdly, in the "National Forest Resource Monitoring Survey" now in progress to improve the government inventory in preparation for the Kyoto Protocol forest carbon accounting, significant under-estimation is becoming evident by the very hand of the Forestry Agency responsible for the FIB (YOSHIDA, personal communication). Taking all these factors into account and considering possible over-estimation on the side of laser estimate as will be discussed below, 70 to 80% of the discrepancy could be attributed to the government statistics with remaining 20 to 30% to the laser estimate. This leaves the most likely actual timber stock of the prefecture at around 155 million m^3 though a series of rigorous and extensive ground truthing surveys are inevitable for a more decisive conclusion.

As was the case with the area estimate, the discrepancy was more pronounced in the comparison at the municipality level. The inconsistency tended to be relatively small in the large municipalities with high standing timber stock, and more outstanding in small municipalities like Masaki, Iyo and Tobe, all adjacent to the prefectural capital Matsuyama with little standing timber stock.

Possibility of Over-estimation in Laser Estimate

As has been mentioned above, our laser-based prefecture-wide timber stock could well be over-estimating the unknown reality for four reasons. The most obvious and significant of all is counting abandoned and wooded farmland (Fig. 3) as forest. Forests have been reclaiming a considerable area of farmland over the past 40 years, as the nation's agriculture sector dwindled and the population shifted to the secondary and tertiary industries in and around cities. A considerable part of these abandoned farmlands is still registered as such, but is accounted as forest in our estimate due to their appearance. Judging from the 10% disagreement in forested area between

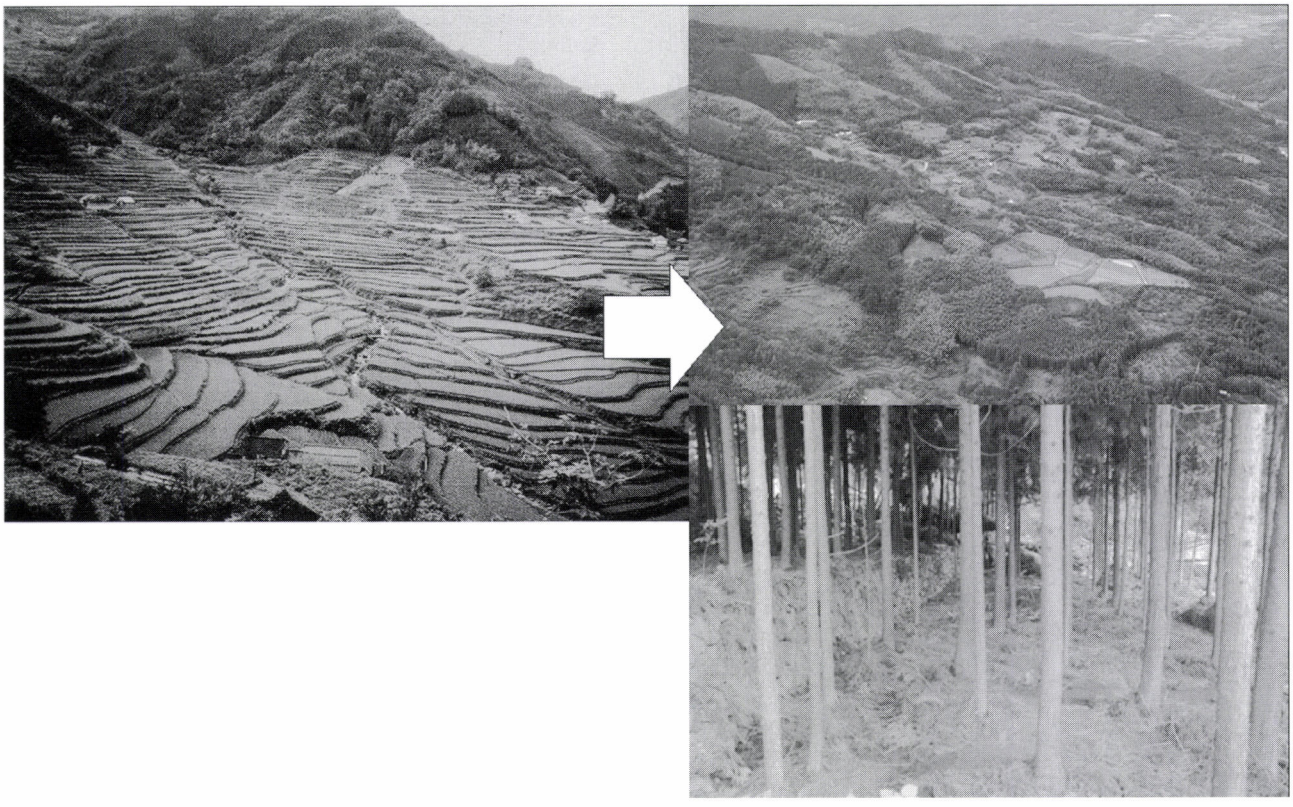

Fig. 3 Change from cropland to forest

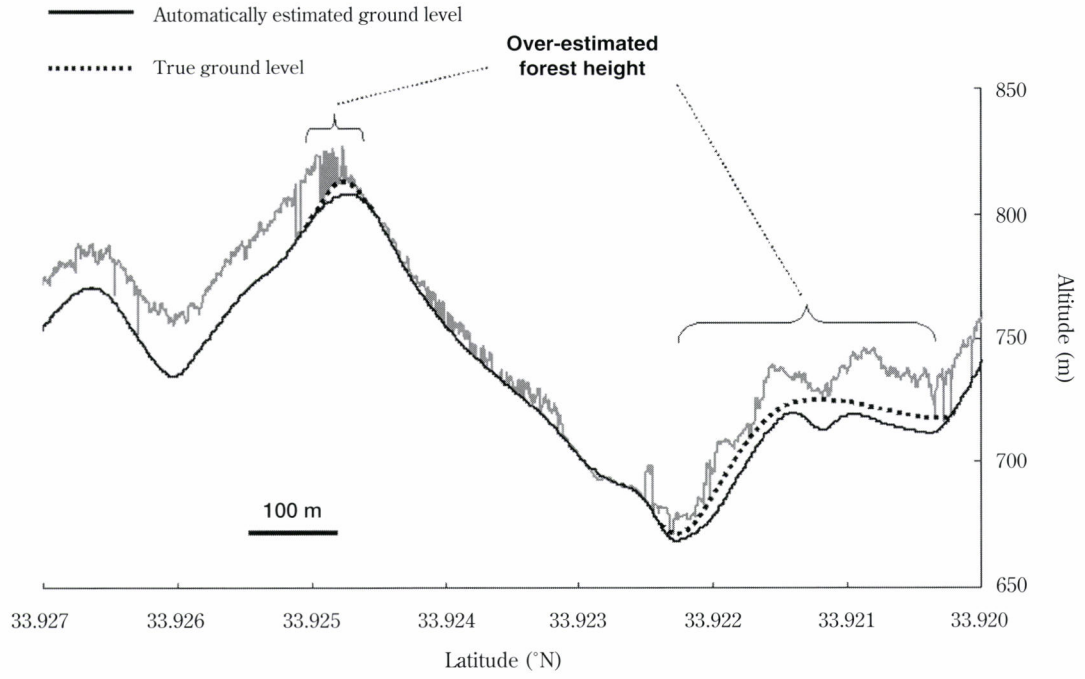

Fig. 4 Over-estimation of stand height due to poor ground level estimation

our laser estimate and the Ministry-of-Land statistics (MAEDA *et al.*, 2006), the reclaimed farmland could be as much as 10% of the prefecture. By simple proportional discounting, this accounts for 10% over-estimation in our figure of standing timber stock.

The second source of over-estimation could be attributed to local over-estimation of canopy height. This occurred partly from scarcity of ground returns in dense forests where thick foliage prevented the laser beam to penetrate down to the ground, and partly from the rigidity of spline curve used for estimating continuous ground level. The latter tends to shortcut missing ground returns to result in taller vegetation height than actually is as shown in Fig. 4. The third source could be the inherent tendency of over-estimation in our method of timber stock estimation, which was also the case in our previous work in the Tomakomai national forest mentioned above. The reason for this has yet to be resolved. The last and least likely source of over-estimation could be isolated trees in parks and farmland as well as along the road. However, urban and residential area and farmland respectively cover only 4 to 5 and 10 to 12% of the prefecture respectively (MINISTRY-OF-LAND, http://lucky.tochi.mlit.go.jp/; MAEDA *et al.*, 2006), and trees and groves sporadically scattered over the areas do not seem to affect the forested area very much.

CONCLUSION

Judging from its accuracy of land-area estimation, airborne laser altimetry can give reasonably accurate estimates of standing timber stock for an area as large as a prefecture, and therefore could well be applicable to the national forest carbon accounting for the Kyoto Protocol or for the post-Kyoto, as a transparent, consistent and accurate method. However, the present density of profiling transects, i.e. 4km apart from each other or 249 m/km² or altimetry point density of 2,930 points/km² is not sufficient for reasonable estimates at the municipality level. However the cost of increasing the transect density is minimal in comparison with the time and cost of maintaining the present system of national forest inventory.

LITERATURE CITED

FUJIMOTO, K., HUKADA, H., MIYAMA, H. and IMANISHI, T., (2007): Long-term monitoring of Shimanto forest planning region. Trans. J. For. Soc. E11 (in Japanese)

MAEDA, Y., TSUZUKI, H., NELSON, R. and SWEDA, T., (2006): Land use classification of Ehime prefecture, Japan using airborne laser altimetry. Proc. Int'l Conf. Silvilaser 2006, Matsuyama. 24-29

MATSUMOTO, M., (2003): What information about forest is demanded by Kyoto protocol / Marrakech agreement? Trans. Soc. J. For. Plan. Res. **407**: 15-24 (in Japanese)

MINISTRY-OF-LAND, (2006): LUCKY (Land use control back-up system). http://lucky.tochi.mlit.go.jp/

NELSON, R., PARKER, G. and HOM, M., (2003): A portable airborne laser system for forest inventory. Phot. Eng. Rem. Sen. **69**: 267-273

OCHI, M., ITOH, M., SHINOHARA, T., YABUKI, Y., WATANABE, A., SAKAMOTO, Y., KANAGAKI, M., OHNISHI, Y., NISHIMURA, T. and JINNO, T., (2006): Regional forest planning of Imabari and Matsuyama region. Ehime Prefecture, Matsuyama, vii+234pp (in Japanese)

SHIKOKU REGIONAL FOREST OFFICE, (2002): National-forest planning of Nanyo region. Shikoku Regional Forest Office, Kochi, iii+28pp (in Japanese)

SHIKOKU REGIONAL FOREST OFFICE, (2003): National-forest planning of Hijikawa region. Shikoku Regional Forest Office, Kochi, iii+14pp (in Japanese)

SHIKOKU REGIONAL FOREST OFFICE, (2004): National-forest planning of Chuyo Sangaku region. Shikoku Regional Forest Office, Kochi, iii+23pp (in Japanese)

SHIKOKU REGIONAL FOREST OFFICE, (2005): National-forest planning of Toyo region. Shikoku Regional Forest Office, Kochi, iii+21pp (in Japanese)

SHIKOKU REGIONAL FOREST OFFICE, (2006): National-forest planning of Imabari and Matsuyama region. Shikoku Regional Forest Office, Kochi, iii+25pp (in Japanese)

SHIRAISHI, N., (1999): States and problems of Japanese forest monitoring system. Bull. J. For. Soc. **27**: 35-37 (in Japanese)

SWEDA, T. and TSUZUKI, H., (2006): Forest carbon budget accounting and early detection of warming-induced vegetation change using laser altimetry. Proc. 28th Symposium on Remote Sensing for Environmental Sciences. 1-12

TSUZUKI, H., (2004): Long-range estimation of standing timber stock and forest biomass using airborne laser altimetry. Ph. D Thesis. v+120pp (in Japanese)

TSUZUKI, H., KUSAKABE, T. and SWEDA, T., (2006): Long-range estimation of standing timber stock in western boreal forest of Canada using airborne laser altimetry. J. Jpn. For. Soc. **88**: 103-113 (in Japanese)

(Received 17 January 2007)
(Accepted 28 September 2007)

Article

Measurement of Snow Depth Distribution in a Mountainous Watershed using an Airborne Laser Scanner

Yoshio Tsuboyama[*1], Akira Shimizu[*2], Tayoko Kubota[*1], Toshio Abe[*1], Naoki Kabeya[*1] and Tatsuhiko Nobuhiro[*1]

ABSTRACT

The distribution of snow depth in a mountainous watershed located in northern Gunma Prefecture, Japan was measured by applying an airborne laser scanner on three different occasions: an autumn period with no snow, a mid winter period with maximum snow cover, and a late winter period with a maximum rate of snowmelt. Depth of snow was estimated as the difference in elevation between the snow and the ground surface. Snow depth at the opening of the meteorological station adjacent to the outlet of the watershed was compared with automatic readings of the ultrasonic distance sensor equipped on the ground. Discrepancies between the airborne and the ground-based snow depths were within an acceptable range for both periods, while slightly larger discrepancies were observed between the values during the late winter period. Snow appeared to be deeper with increasing elevation in most of the watershed, except the highest part where it became shallower. Decrease in snow depth from the mid to the late winter periods was larger in the lower part of the watershed, suggesting higher rates of snowmelt. Overall, the airborne laser scanner could measure snow depth at the flat opening quite accurately and was useful to capture spatial and temporal patterns of snow depth over the watershed. However, it appeared that snow depth could be calculated to be negative in some cases, typically when influenced by lodging of dense vegetation such as bamboo grasses due to the weight of snow. While these results are encouraging, further research on the measurement of snow depth on steep slopes and/or under tree canopies is recommended.

Keywords: hydrology, mountainous watershed, snow depth, airborne laser scanner

INTRODUCTION

Snow is one of the most common and familiar forms of water in many climate regions. Snow cover affects the processes of exchange of water and energy between atmosphere and land surface, thus affecting catchment hydrology as well as regional climate. From the view point of water resources management of a river basin, it is important to assess the amount of snow water over a catchment scale, but this is difficult due to the spatial and temporal variability of quantitative entities of snow such as depth and water equivalent (e.g., TARBOTON *et al.*, 2000). For simplicity, the distribution of snow in a mountainous catchment is often represented using a linear relationship between elevation and snow water equivalent (e.g., YAMADA, 1943; TANI, 1996; SAITO *et al.*, 1999; MURAKAMI and YAMANOI, 2003).

A snow course survey has long been used to obtain ground-based information on the spatial distribution of snow depth and water equivalent in a mountainous watershed (e.g., YAMADA, 1943). However, it requires so much time and effort that it is difficult to apply this approach to a large-scale investigation, particularly in steep mountains with heavy snow. For larger scale information, networks of snow gauging stations are maintained in some cases (SEIDEL and MARTINEC, 2004), but the networks are often too coarse compared to the heterogeneity of topography and land cover conditions and, hence, insufficient to evaluate the spatial distribution of snow properties.

By taking advantages of wide coverage, frequency, and simultaneity of measurements, satellite remote sensing data have been used for snow cover mapping at regional to global

Corresponding author: Yoshio Tsuboyama
[*1] Forestry and Forest Products Research Institute
1 Matsunosato, Tsukuba, Ibaraki 305-8687, Japan
[*2] Kyushu Research Center, Forestry and Forest Research Institute, 4-11-6 Kurokami, Kumamoto, Kumamoto 860-0862, Japan

scales (SEIDEL and MARTINEC, 2004). Passive microwave sensors have commonly been used (ARMSTRONG and BRODZIK, 2001; PULLIAINEN, 2006; WOODHOUSE, 2006), which have advantages over optical sensors in terms of their ability to penetrate clouds, to be used during darkness, and to provide a measure of snow depth or water equivalent (PULLIAINEN, 2006). However, passive microwave sensors have some potential shortcomings as well, such as relatively low spatial resolution resulting from weak signal and long integration time (SEIDEL and MARTINEC, 2004), which may prevent evaluating the effects of rugged topography and different land covers on snow distribution at a mid to small catchment scale. The interaction of microwaves with different types of targets arranged in both horizontal and vertical directions further complicates the measurement and data interpretation processes, and so an empirical correlation based on the observed spectral brightness temperature differences may be used as an alternative to detailed quantitative descriptions of this process (WOODHOUSE, 2006). However, such an empirical approach may cause a bias in measurements in deep snow (DERKSEN *et al.*, 2005). Moreover, a fundamental limitation of satellite remote sensing techniques regarding snow cover measurements in densely forested areas remains (SEIDEL and MARTINEC, 2004). Consequently, an alternative and complementary method is necessary to obtain more detailed and accurate information on spatial distribution of snow properties.

Recently, airborne light detection and ranging (LiDAR) is increasingly used to obtain altimetric information about the ground and various land cover surfaces. Applications include forest measurement (e.g., NÆSSET and ØKLAND, 2004) and snow depth estimation (e.g., OKAMOTO *et al.*, 2004; AKIYAMA and SATO, 2006). Airborne LiDAR is considered to be a useful tool because of its high resolution and ability to distinguish the ground surface from overlying layers such as vegetation, although it is still being developed and needs to be studied for operational application (e.g., HIRATA, 2005).

With this background, this paper presents the results of using the airborne LiDAR scanner to measure the distribution of snow depth over a steep mountainous watershed and discusses some potential problems in relation to snow depth measurements.

METHOD

Study Site

This study was conducted at the Takaragawa Forest Watershed Experiment Station of the Forestry and Forest Products Research Institute. The site is located at a longitude of 139°01'E and a latitude of 36°51'N with an altitude ranging from 805 to 1945 m (Fig. 1). Although the watershed is in the northern part of the Kanto district, it experiences a Japan Sea climate characterized by heavy snow during winter due to its proximity to the divide.

Snow Depth Measurement

Airborne laser scanning over the watershed was conducted on three different occasions: an autumn period with no snow (October 24 to 26, 2003), a mid winter period with

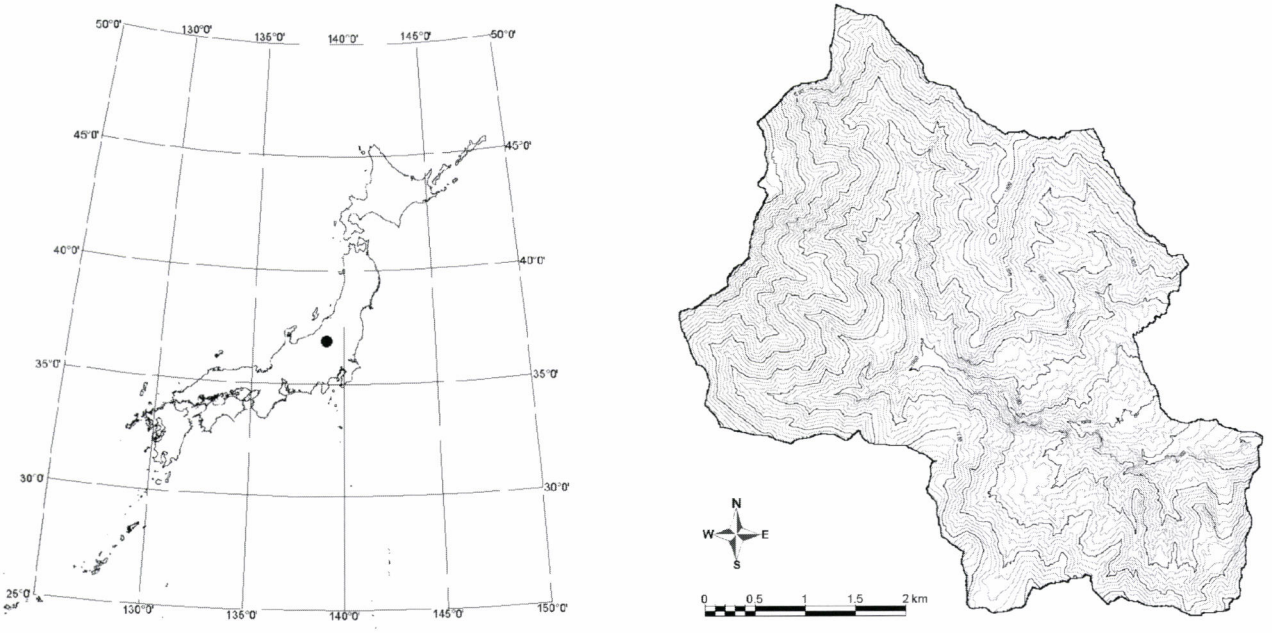

Fig. 1 Map of the study site showing its location in Japan (left) and topography (right)
The contour interval of the topographic map is 20m.

maximum snow cover (February 21 to 25, 2004), and a late winter period with a maximum rate of snowmelt (April 16 to 18, 2004). A rotary-wing Aerospatiale AS350B (JA9807) aircraft carried the Optech ALTM 1225DC laser scanning system. Flight speed ranged from 50 to 250km h^{-1}. Flying altitude ranged from 600 to 800m a.g.l. and the footprint diameter was estimated to be 0.17m at the flying altitude of 800 m a.g.l. Pulse repetition frequency was 25 kHz, scan frequency was 22 Hz, and the maximum scan angle was 15 degrees. The sampling density of the laser data approximated 1 pulse m^{-2}. The specifications and timings of laser scanning are shown in Table 1 and Fig. 2, respectively.

The laser data were pre-processed by the contractor (Aero Asahi Corporation, Japan). Planimetric coordinates and ellipsoidic heights were calculated for the last returns. Three sets of 1-m grid digital terrain models (DTMs) were generated by filtering and converting the planimetric coordinates and corresponding heights using a kriging method.

Snow depth was then estimated based on these 1-m grids as the difference in elevation between the snow and the ground surface. Frequency distribution of snow depth in relation to elevation was calculated based on these grid-based estimates, except for the grid points for which snow depth was calculated to be negative. Causes of negative values of snow depth at some points will be discussed later.

As ground information, snow depth at the opening of the meteorological station adjacent to the outlet of the watershed was monitored every 10 minutes using a combination of an ultrasonic distance sensor and a data logger (Campbell SR50 and CR10X, respectively) mounted on the meteorological tower. Snow depth at this opening was also surveyed by digging a snow pit once a month, together with measurements of vertical distribution of snow density. Because of differences in spatial and temporal coverage of the airborne and the ground-based methods, we used spatial averages of the laser pulse data within the $1m^2$ square just under the ultrasonic sensor, whereas the ultrasonic readings were averaged over the time of laser scanning, which was estimated from the time stamps of the main swaths covering this square.

Table 1 Specifications of the airborne laser scanner measurements

Pulse density	~1 pulse m^{-2}
Pulse frequency	25,000Hz
Scan angle	± 15 degrees
Scan frequency	22Hz
Flying altitude	600-800m a.g.l.
Footprint diameter	0.17m for the flying altitude of 800m a.g.l.
Flight speed	50-250km h^{-1}
Flight course interval	180m
Overlap between swaths	50%
Scanner	Optech ALTM1225DC
Platform	Aerospatiale AS 350B (JA9807)

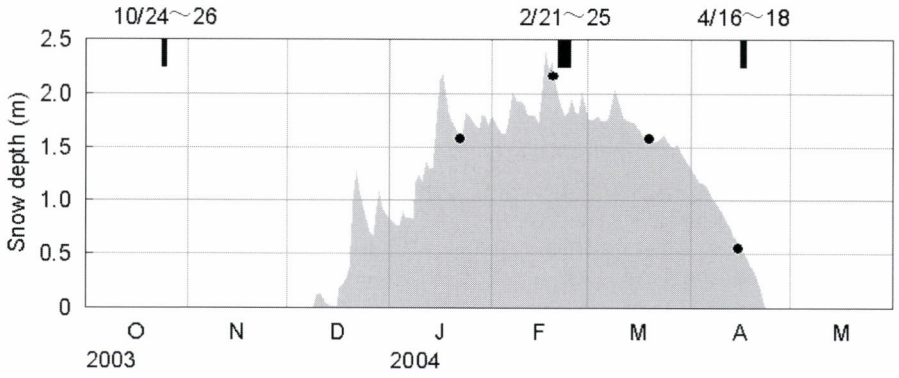

Fig. 2 Timings of measurements in comparison with seasonal variations in snow depth measured by the ultrasonic sensor
Solid circles and rectangles indicate the periods of the direct snow survey and the laser scanning, respectively.

Table 2 Comparison of the airborne and ground-based readings of snow depth

Period		Feb. 24 11:30-11:50	Apr. 16 10:50-11:00
Ultrasonic sensor	Minimum	1.96	0.52
	Maximum	1.96	0.53
	Average	1.96	0.53
Laser scanner		1.95	0.46

Unit: m

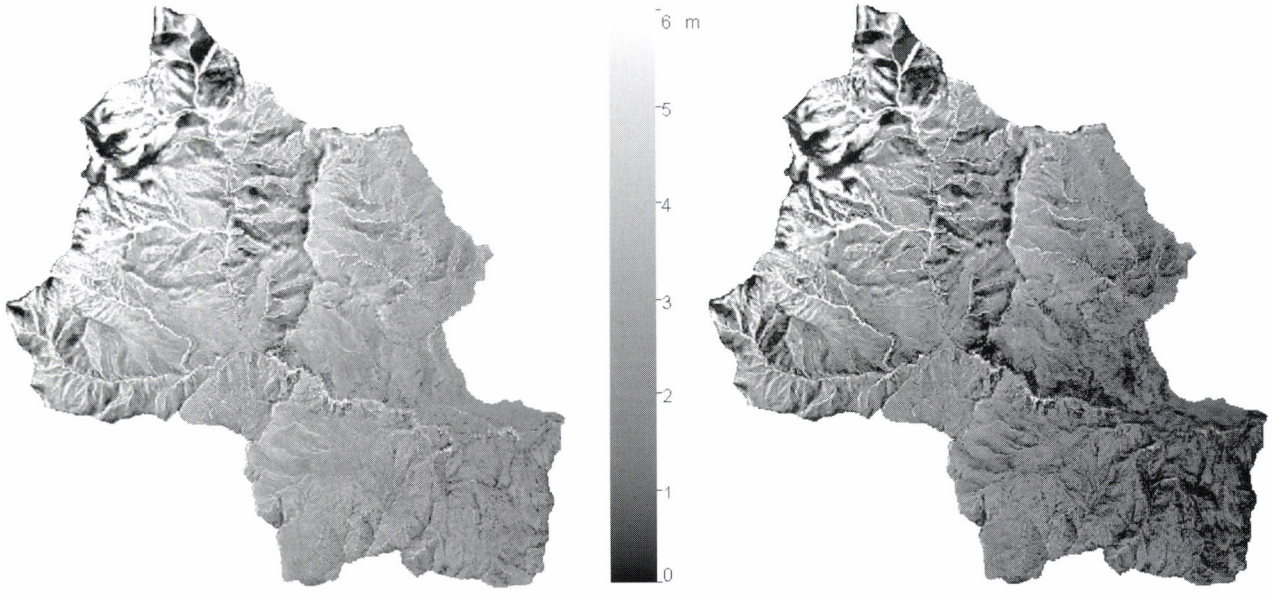

Fig. 3 Spatial distribution of snow depth during the mid (left) and the late (right) winter periods

RESULTS AND DISCUSSION

Ground Information

Snow depths calculated from the airborne laser scanning and the ground-based ultrasonic readings at the flat opening of the meteorological station are compared in Table 2. Snow depth calculated from the laser data for the site was 1.95 and 0.46m for the mid and the late winter periods, respectively, while the ultrasonic readings averaged 1.96 and 0.53m over the respective periods (Table 2). Considering that the accuracy of elevation measurement using an airborne laser scanner is ±0.15m (e.g., OKAMOTO *et al.*, 2004), discrepancies between the two methods were within an acceptable range for both periods. Slightly larger discrepancies were observed between the values during the late winter period, likely due to faster snowmelt and/or larger spatial variability of snow depth at the local scale.

Spatial Distribution of Snow Depth

The spatial distribution of snow depth estimated from laser scanner measurements during the mid and late winter periods is shown in Fig. 3. By comparing the images in Fig. 3 with the topography of the site shown in Fig. 1, it is clear that snow generally becomes deeper with increasing elevation.

The relationship between snow depth and elevation was evaluated more quantitatively by calculating the frequency distribution of snow depth for 25 m interval elevation class (Fig. 4). Fig. 4 suggests that the conventional linear relationship between elevation and snow water equivalent is a reasonable approximation, at least on an average basis, if the snow density is spatially uniform. However, it also indicates considerable deviations in both sides of these regression lines and that snow depth decreases with increasing elevation for the highest part of the watershed. Such an inverse relationship between elevation and snow depth might have been overlooked by conventional ground-based snow surveys. Although its effects on catchment-scale water balance might

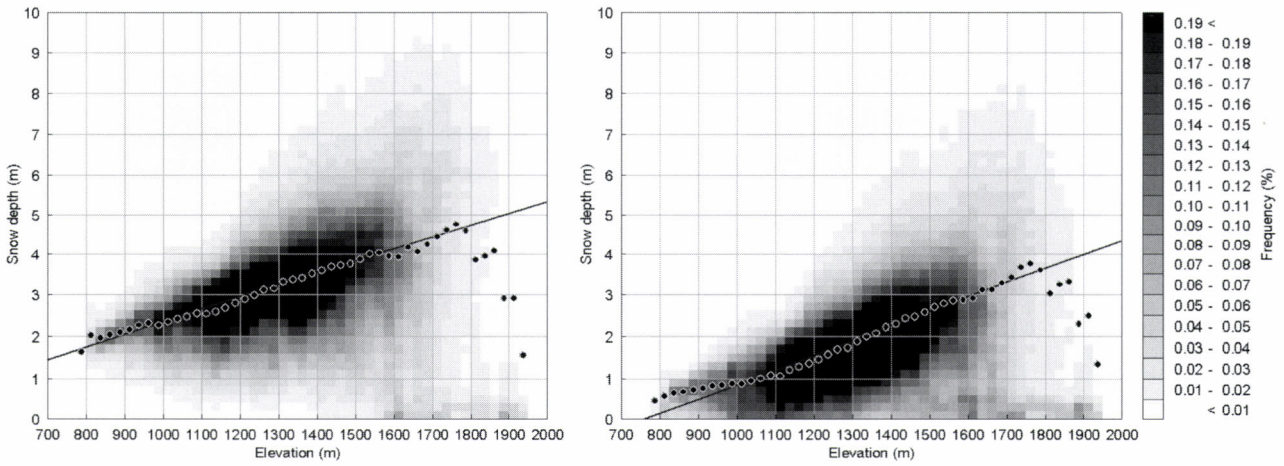

Fig. 4 Frequency distribution of snow depth during the mid (left) and the late (right) winter periods
Solid circles indicate average snow depths in each elevation class (25m interval). The solid lines represent the regression lines between snow depth and elevation.

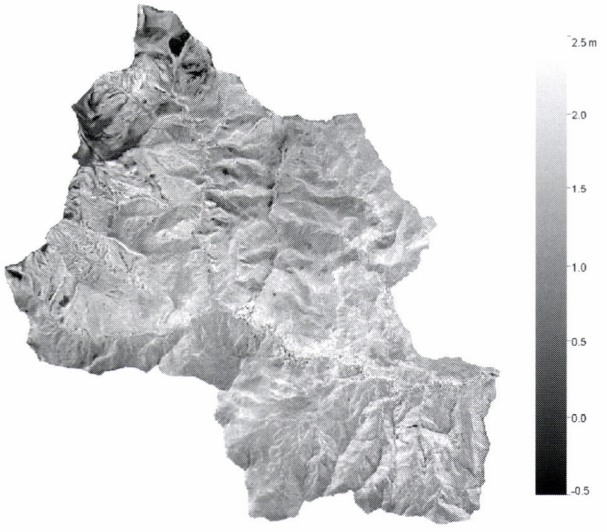

Fig. 5 Decrease in snow depth from the mid to the late winter periods

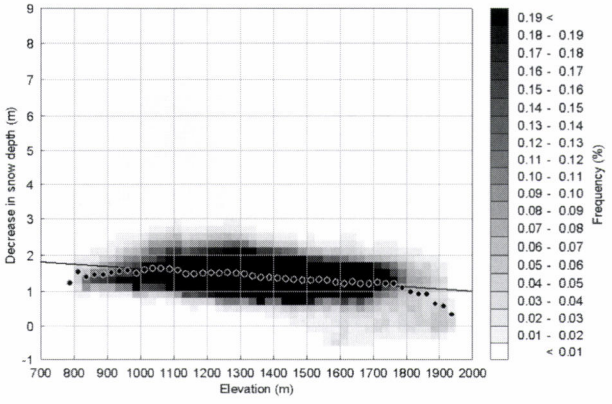

Fig. 6 Frequency distribution of decrease in snow depth from the mid to the late winter periods
Solid circles indicate average decrease in snow depth in each elevation class (25m interval). The solid line represents the regression line between decrease in snow depth and elevation.

be small due to its relatively small frequency, this inverse relationship is an important finding of this study.

Temporal Variations in Snow Depth Distribution

Figs. 5 and 6 depict spatially the difference in snow depth from the mid to the late winter periods and its frequency distribution for each elevation class, respectively. These figures clearly show that the snow depth decreased to a larger extent in the lower part of the watershed, likely reflecting higher air temperature. Fig. 5 also indicates that the largest decrease in snow depth appeared on slopes facing south, reflecting a larger amount of incoming solar radiation. While changes in snow depth should not only be associated with snowmelt because they would also reflect other factors including snow drift, avalanches, and spatially variable snowfall during the intervening period, the quantitative information presented in Figs. 5 and 6, together with Figs. 3 and 4, will greatly help us to develop and validate a distributed snowmelt model.

Factors Affecting Snow Depth Measurements

In calculating snow depth based on the grid DTMs, it appeared that at some grid points the ground surface elevation

exceeded the snow surface elevation, which resulted into negative values of snow depth. Such points were distributed on the gauging flume at the outlet, the steep slopes along the stream, or the relatively gentle slopes above the tree line (Fig. 7). All of these points are thought to be the place where the ground surface elevation was overestimated due to either interpolation errors resulting from lower pulse density, typically on the water surface in the deeply incised stream channels (Fig. 8), or measurement errors caused by lodging of the dense vegetation cover such as bamboo grasses which literally covered the true ground against the laser pulse (Fig. 9). While these negative values might not substantially affect

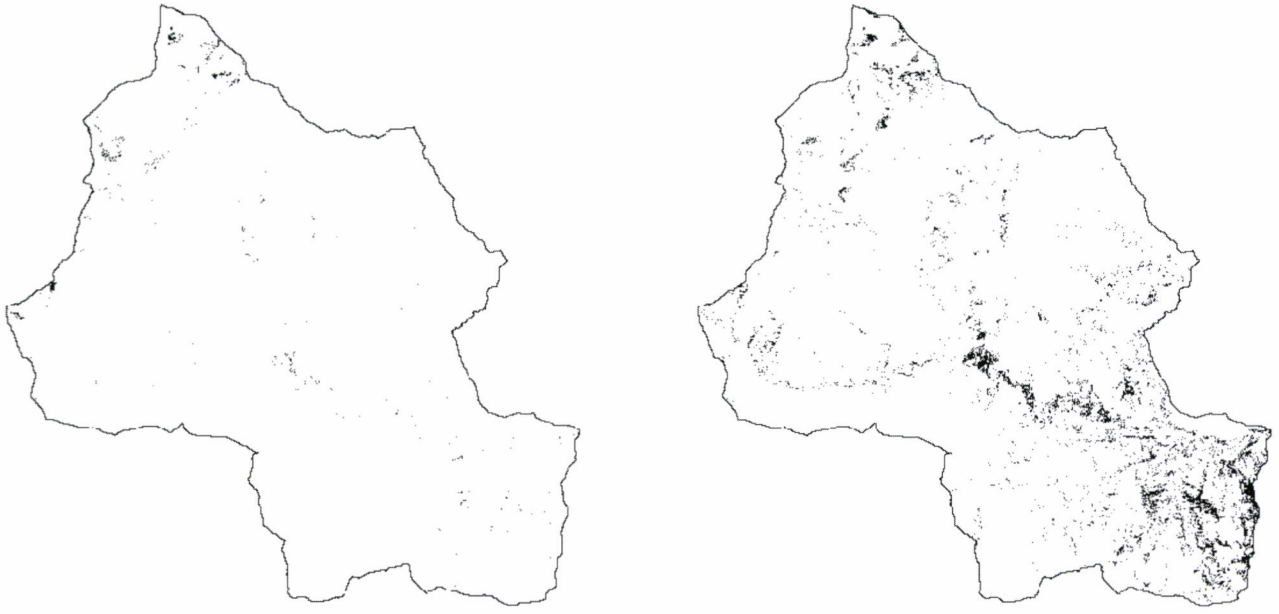

Fig. 7 Locations of grid points having negative snow depth for the mid (left) and the late (right) winter periods

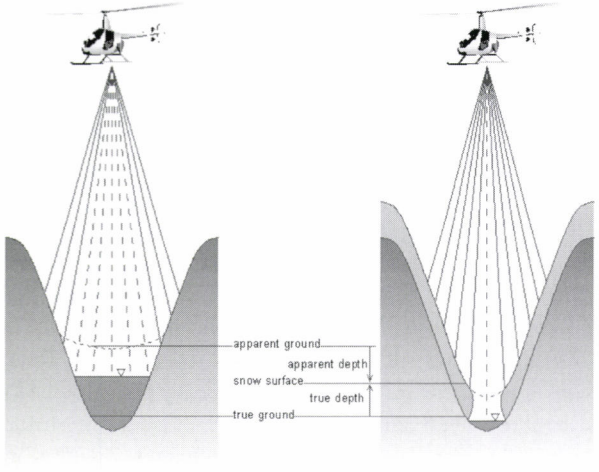

Fig. 8 Schematic illustration of the cause of negative snow depth as influenced by the water surface in a deeply incised stream channel
Solid and dash lines indicate the paths of laser pulses which were reflected and absorbed, respectively. Dot lines indicate the interpolated ground surface.

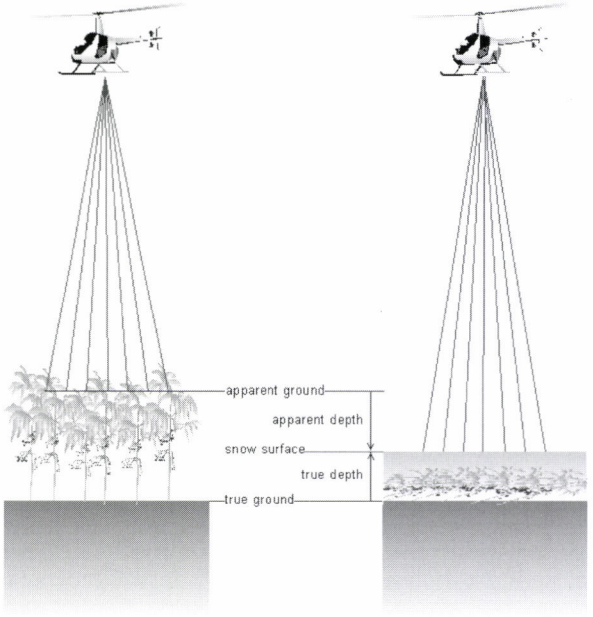

Fig. 9 Schematic illustration of the cause of negative snow depth as influenced by lodging of the dense vegetation cover due to the weight of snow

catchment-scale water balance due to its small fraction relative to the entire catchment area (0.4 and 4.6% for the mid and the late winter periods, respectively), it should be noted that some of the other grid points could be under similar conditions while the calculated snow depth at them happened to be positive.

CONCLUSION

The results of this study suggest that the airborne laser scanner could measure snow depth at the flat opening accurately and was useful to capture spatial and temporal patterns of snow depth over the watershed. An important finding of the study concerns the inverse relationship between snow depth and elevation for the highest part of the watershed, which might have been overlooked by conventional ground-based snow surveys. However, careful interpretation of the results is needed in places where calculated snow depth could be negative as a result of overestimation of the ground surface elevation, typically as influenced by the water surface in a deeply incised stream channel or by lodging of the dense vegetation due to the weight of snow. Further research on the measurement of snow depth on steep slopes and/or under tree canopies is recommended.

ACKNOWLEDGEMENTS

This study was conducted as a part of the "Development of eco-friendly management technology of water and agro-forested-aqua-ecosystem in watershed and estuary areas" project funded by the Ministry of Agriculture, Forestry and Fisheries. The laser data presented in this paper were obtained with the technical assistance of the Aero Asahi Corporation. Additionally, the authors thank anonymous reviewers who provided valuable comments on this manuscript.

LITERATURE CITED

AKIYAMA, M. and SATO, H.P., (2006): Snow depth distribution derived from airborne LiDAR data and estimation of snow water equivalent volume. J. Jpn. Soc. Photogrammetry and Remote Sensing **45**: 24-33 (in Japanese with English abstract)

ARMSTRONG, R.L. and BRODZIK, M.J., (2001): Validation of passive microwave snow algorithms. Remote Sensing and Hydrology 2000. IAHS Publ. **267**: 87-92

DERKSEN, C., WALKER, A. and GOODISON, B., (2005): Evaluation of passive microwave snow water equivalent retrievals across the boreal forest/tundra transition of western Canada. Rem. Sen. Environ. **96**: 315-327

HIRATA, Y., (2005) Influence of transmittance and sampling density of laser beams in forest measurements of a *Cryptomeria japonica* stand with an airborne laser scanner. Jpn. J. For. Plann. **39**: 81-95 (in Japanese with English abstract)

MURAKAMI, S. and YAMANOI, K., (2003): Long-term changes in altitudinal distribution of snow water equivalent in Takaragawa Forest Watershed Experiment Station. J. Jpn. Soc. Hydrol. and Water Resour. **16**: 131-141 (in Japanese with English abstract)

NÆSSET, E. and ØKLAND, T., (2002): Estimating tree height and tree crown properties using airborne scanning laser in a boreal nature reserve. Rem. Sen. of Environ. **79**: 105-115

OKAMOTO, T., KUROKAWA, U., MATSUURA, S., ASANO, S. and MATSUYAMA, K., (2004): Adaptability of an airborne laser scanner to determine a snow depth distribution on a mountain area. J. Jpn Soc. Hydrol. and Water Resour. **17**: 529-535 (in Japanese with English abstract)

PULLIAINEN, J., (2006): Mapping of snow water equivalent and snow depth in boreal and sub-arctic zones by assimilating space-borne microwave radiometer data and ground-based observations. Rem. Sen. Environ. **101**: 257-269

SAITO, K., HAYASHI, M., NUMATA, Y., MAYA, M. and TAKATSUKI, Y., (1999): Snow cover monitoring using remote sensing data. J. Remote Sensing Soc. of Jpn. **19**: 51-56 (in Japanese)

SEIDEL, K. and MARTINEC, J., (2004): Remote Sensing in Snow Hydrology. Springer, 150pp

TANI, M., (1996): An approach to annual water balance for small mountainous catchments with wide spatial distributions of rainfall and snow water equivalent. J. Hydrol. **183**: 205-225

TARBOTON, D., BLÖSCHL, G., COOLEY, K., KIRNBAUER, R. and LUCE, C., (2000): Spatial snow cover processes at Kühtai and Reynolds Creek, in Grayson, R. and Blöschl, G. (*eds.*) Spatial patterns in catchment hydrology. Cambridge University Press: 158-186

WOODHOUSE, I.H., (2006): Introduction to microwave remote sensing, CRC press, 370p

YAMADA, S., (1943): Report of a hydrological experiment in the Takaragawa Forest Watershed Experiment Station. Tokyo Regional Forest Office, Tokyo: 121-182 (in Japanese)

(Received 22 January 2007)
(Accepted 12 May 2007)

Article

Expectation of LiDAR on Forest Measurement in Kyoto Protocol

Masahiro Amano*

ABSTRACT

Since United Nations Conference on Environment and Development, the world community has formally recognized that forests have a crucial role to play mitigating global warming and it is necessary to evaluate their role through repeatable, verifiable, and transparent scientific data analyses. The Kyoto Protocol and a subsequent document, the Intergovernmental Panel on Climate Change (IPCC) Special Report and Good Practice Guidance for Land Use, Land Use Changes and Forestry, recommended establishing a scientifically neutral method to evaluate and monitor forest land changes and forest biomass dynamics with international standards. Satellite remote sensing has been identified as one tool that can be used to measure forest area, rates of change in land use, location of forest activities, etc. Also satellite data has many advantages that are not only transparent and verifiable but also cost effective, including periodic data acquisition that is internationally available. When negotiators decided the modality of the forest inventory scheme of Kyoto Protocol, they relate it to the imaged characteristics of satellite remote sensing data. But the utility of data from satellites has some difficulties in estimating growing stock changes, and in distinguishing some type of forest activities, such as thinning. In this context LiDAR has a potentiality to provide measures for estimating carbon stock changes, greenhouse gas emissions, and removals associated with forest lands under UNFCCC and Kyoto Protocol. The definition of forest under Kyoto Protocol requires the minimum threshold of forest area, tree crown density, and tree height to be determined within specific ranges. Satellite data have not work well to separate forests according to such a precise threshold. However, LiDAR will be able to provide enough information to judge whether stands will be able to satisfy the definition of a forest. This report discusses the advantages of LiDAR from the view point of the inventory scheme under Kyoto Protocol.

Keywords: LiDAR, Kyoto Protocol, Land Use, Land Use Changes and Forestry (LULUCF)

INTRODUCTION

Since Russia submitted an instrument of ratification for Kyoto Protocol to the United Nations Framework Convention (UNFCCC) on November 18, 2004, the Protocol was entered into force on the 90days later- on February 16, 2005. Japan has promised to reduce annual average of the greenhouse gas (GHG) emissions in the first commitment period of the Kyoto Protocol - from 2008 to 2012 - 6% less than the GHG emission in 1990. Therefore Japanese Government developed a Kyoto Protocol Target Achievement Plan in April 2005. This Plan called for the securing of carbon credit of 13million t from the forest sector, which is equivalent to 3.8% of the 6% overall reduction. However, Japanese greenhouse gas emissions in 2002 had increased 7.6% above the 1990 level and 8% more in 2003. Thus, a 14% reduction from the 2003 greenhouse gas emission levels is required in order to achieve the target. Therefore, it is important to achieve the targets from the forest sector if the overall targets have any chance of being realized.

Of the six greenhouse gases identified in the Kyoto Protocol, CO_2 is the gas that is absorbed by the forest. A country's reporting responsibility requires that the calculations be made using the standard established by UNFCCC. This paper considers how LiDAR measurements might contribute to the reporting on the amount of CO_2 absorbed by the forest under the UNFCCC requirements.

Corresponding author: Masahiro Amano
* School of Human Science, Waseda University
2-579-15 Mikajima, Tokorozawa, Saitama 359-1192
Japan
Tel:+81-4-2947-6740 Fax:+81-4-2947-6801
amano@waseda.jp

BACKGROUND: WHY FOREST IS VALUED IN THE KYOTO PROTOCOL

Between 1850 and 1998, human activities emitted approximately 270 billion t of carbon through the use of fossil fuel and cement production. Also, land use change, primarily deforestation, generated additional emissions of 136 billion t of carbon. According to the latest FAO statistics, the area of global forests continued to decline by approximately 12.5million ha every year in 1990s (FAO, 2001) and the volume of carbon emissions due to land use change is still high. Although the carbon in the atmosphere is sequestrated by ocean and terrestrial ecosystem, the net increased in the atmosphere carbon has been 176 billion t because the gas emissions exceeded the amount absorbed. In terms of CO_2 concentrations in the atmosphere, it increased from 285 ppm to 366 ppm between 1850 and 1998 (IPCC, 2000). It is estimated of the gas emissions due to land use change, 87% is from conversion of forest land to other purposes, deforestation and forest fire. The remaining 13% is due to cultivation of field grasses. On the other hand, 2.3 billion t of carbon are absorbed by the land every year. In the terrestrial ecosystem, 466 billion t of carbon is stored in the biomass and 2 trillion t of the carbon is stored in the soil. Reduction of the temperate forests and boreal forests started 5000 years ago in Mediterranean area and China, and a large amount of forests were reduced in North America in the 19th century. However, since later than middle of the 20th century, the forest area has been stable or expanding in North America. In recent years, the volume of the carbon absorbed annually has been 170million t in the US and of 110million t in the Western Europe. According to FAO statistics, forest in advanced countries absorbed 880million t of carbon annually (FAO, 2000). With these facts,

At the insistence of the US and Oceania countries, the carbon absorbed and stored by the forest, field grass, and soil became a part of carbon reductions measured in the Kyoto Protocol. For example, if the forest absorbs 300 thousand t of carbon in the country where its emission reduction target is 1million t, the actual amount of emission cuts required is only 700 thousand t of carbon. The role of the forest is addressed in four parts in the Kyoto Protocol: the 3rd and 4th terms of the Article 3, which defines reduction of the greenhouse gas through domestic forests; Article 6, which describes reduction of the greenhouse gas through the cooperation among industrial countries (Annex I countries); and Article 12, which determines reduction of the greenhouse gas through the cooperation between industrial countries and developing countries. Although the articles of the Kyoto Protocol were agreed by COP3 in 1997, the modalities based on these articles were not determined until the 4 years later at Marrakesh Accords (COP7).

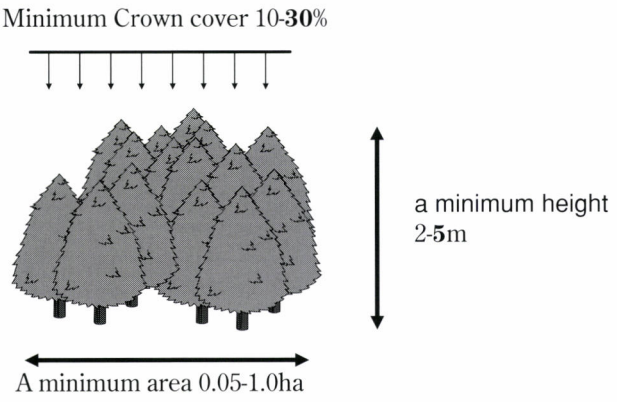

Fig. 1 Definition of Forest under UNFCCC

ITEMS REGARDING FORESTS DETERMINED IN THE KYOTO PROTOCOL

Definition of the "Forest".

Each country has already determined the definition of the forests by their law, the situations of land uses, and/or the condition of the land coverage. Thus it will be lack of the universal scale in calculation of the absorbed amount of carbon by forest in each country as long as the definition is universally undetermined. As shown in Fig. 1, the Kyoto Protocol requests that each country should formulate the definition of the forest by crown cover, mature tree height, and the minimum area of the forest. However, the threshold values are to be determined within the range shown in the Fig. 1 according to the natural and social conditions of each country.

Direct Human-induced Activity in the Article 3.4

The Article 3.4 describes "The net change in greenhouse gas emissions by sources and removals by sinks resulting from direct human-induced land-use change and forestry activities, limited to afforestation, reforestation and deforestation since 1990, measured as verifiable changes in carbon stocks in each commitment period, shall be used to meet the commitments under this Article of each Party included in Annex I". This article defines "forestation" as the reforestation and/or afforestation on lands that were used for purposes other than forest prior to 1990. In other words, when the area that had been used for other than the forests as of December 31, 1989 became forest, the average of the changes in carbon stock in 5 years associated with increase or decrease of accumulation in the land from 2008 to 2012 will be considered as amount absorbed or emitted. Regarding reduction in forests, when the forest as of December 31, 1989 is changed to an alternative land use forest before December 31, 2012, the average of the changes in carbon stock on the land in each year between 2008 and 2012 will be recorded. In the case

where the forest persists, the forest is treated as absorbing the carbon. However, if severe forest thinning and final cutting are implemented between 2008 and 2012 and the storage in 2012 is less than the storage in 2008, this situation will be considered as an emission. In the former case where forest land has been converted to agriculture, there are no large changes made in the carbon stock with the time passed, unlike the forest, and therefore the carbon balance will be reported as "zero".

Additional Human-induced Activity in the Article 3.4

The Article 3.4 targets the greenhouse gas reduction through acceleration of the carbon sequestration capacity by adding the human-induced activities to the existing forests while the Article 3.3 describes the evaluation of the absorbed amount of the forest newly established. With the precondition of application mainly from the second commitment period, the Article 3.4 of the Protocol describes "The Conference of the Parties serving as the meeting of the Parties to this Protocol shall, at its first session or as soon as practicable thereafter, decide upon modalities, rules and guidelines as to how, and which, additional human-induced activities related to changes in greenhouse gas emission by sources and removals by sinks in the agricultural soils and the land-use change and forestry categories shall be added to, or subtracted from, the assigned amounts for Parties ~". However, concrete modalities are not included in the Protocol. Also, there is a sentence in the end of the 4th Terms of the Article 3, "A Party may choose to apply such a decision on these additional human-induced activities for its first commitment period, provided that these activities have taken place since 1990." In the Marrakesh Accords developed by COP7, the additional human-induced activity includes a. *vegetation restoration*, b. *agricultural land management*, c. *grass field management*, d. *forest management*. If there is any additional activity desired to apply in the first commitment period, it shall be selected and reported. Japan considers the forest management as an essential item for achievement of the reduction target.

There were various discussions regarding how to determine the activity as the forest management, and for the tentative target limited to the first commitment period, it reached the consensus on the forest with any human-induced activities after 1990 as the source of absorption. However, the contents of the human-induced activities are not discussed at the negotiating scene of Kyoto Protocol. There are various perspectives that some countries consider that the forest stands covered by the forest planning and the forests in the area with fire prevention taken are subjected to the forest management activity to satisfy Kyoto Protocol. Some countries consider only forests with actual specific operations, such as thinning, weeding and fertilizer activities implemented after 1990, shall be subjected to forest management activities that satisfy Kyoto. Since this is a politically sensitive issue and forest operations differ depending on the natural and social environments in each country, the current view is that the decision on the standards and definitions be left to each country. Also, the current view is that the evaluations are to be conducted by the countries and will determine whether the evaluation decision would be appropriate at the time that the inventory report is received by the secretariat office of the United Nations Framework Convention on Climate Change (UNFCCC).

EXPECTATION OF LIDAR MEASUREMENT ON KYOTO PROTOCOL

For the evaluation of forest CO_2 absorption in the Kyoto Protocol, the negotiator's first concern was the utilization of satellite remote sensing technique. The Protocol requires the measurement with transparent and verifiable method and report, at the same time, if the remote sensing data are used, it is easy to ensure the transparency and to verify the result obtained. However, there are some problems that would not be solved by the satellite data alone and that occurred in the process of establishment of the concrete rules such as the regulations in the 3rd and 4th terms of the Article 3. These regulations require the measurement not only of above-ground biomass but also debris on the ground, below-ground biomass and soil carbon, some of which are impossible to be measured by satellite remote sensing tools. The author is expecting the resolution of many problems by complementary utilization of the LiDAR, which may work as regional/national sampling tool to provide detail forest resource profiling, and swath sampling data, which include proxies of each carbon pool requested by Kyoto Protocol. Major points are as follows.

Utilization of LiDAR for Definition of Forest

Japan is planning to determine for three thresholds of forest definitions as following; the minimum area of the forest is 0.3 ha, the crown cover is 30%, and tree height is about 5m. The negotiators of each country who have been involved in preparation of the Protocol thought that these forests would be easily categorized by the satellite remote sensing technique. However, using only spectral information, it is difficult to determine the forest area where the crown cover of 30% is strictly the threshold value and there are various tree species. Also, 3D data are required for determining the tree height data. However, it's relatively easy to lay out the tree crown and other gap parts, and to calculate the average forest stand height in terms of the study example to which the LiDAR is applicable. In addition, one of key factors needed to get good estimation of tree height and differentiate forests with specific crown cover is a size of footprint of LiDAR

Afforestation, Reforestation and Deforestation in the Article 3.3 and LiDAR Utilization

It has been assumed that to detect areas of afforestation, reforestation and deforestation would be easy using satellite remote sensing data. However, it's actually difficult to differentiate the young forests with tree height of 1-2m after the operations of afforestation and reforestation from the grass field and farm land. Also, it's found that there were many misinterpretations for differentiation between temporary bare land after harvest and that following replanting or conversion of land use to other purposes. This suggests that it is difficult to determine changes in the land coverage or the land use by the satellite remote sensing data alone, although general satellite remote sensing data easily detects many changes in the land coverage. These considerations suggest that continuous monitoring of the afforestation, reforestation and deforestation of the specific location after 1990 will be impossible with the sound accuracy of the current satellite remote sensing data in the business-level. Therefore the forests with the afforestation, reforestation and deforestation will need to be collected as administrative information, at least for a while.

If the LiDAR will be able to detect the terrain properly where the remaining materials of the forest land are built along the contour lines for afforestation, and young forests regularly planted, the detection of afforestation, reforestation and deforestation with the remote sensing will be easy.

Utilization of LiDAR for Additional Human-induced Activity under the Article 3.4

Article 3.4 addresses forests that are sequestering carbon, i.e., forest zones, and forests that are losing carbon through, for instance, thinning. In Japan, the forested area that is periodically thinned is large relative to that forested area that is completely harvested and reforested. It is necessary to determine the difference in the number of standing trees in order to differentiate whether the forests are thinned or not. As with crown cover, it is not easy to estimate the number of standing trees by the satellite remote sensing data. However, the estimation of the stand density using the LiDAR is not difficult. In this case it is possible to differentiate the thinned forests and the forests without thinning, from the relation between the tree height and the stand density,

FUTURE OF KYOTO PROTOCOL AND REMOTE SENSING

Even though the administrative data and conventional forest inventory system are utilized for the report in the first commitment period, there is no choice but to establish the new remote sensing data-oriented reporting system in consideration of transparency and verifiability for the second session. Besides the report to the Protocol, agriculture and forests are reported separately in the national inventory for the greenhouse gas emission of the UNFCCC. However, in the guidelines to be revised in 2006, the national land will be divided into six land uses and be reported collectively. Also, any changes made in the land use shall be reported separately. Therefore monitoring of the land use on a nationwide scale is necessary and the guideline emphasizes utilization of the remote sensing techniques. Regarding the forest sector, a report of the CO_2 absorption with a high accuracy will be available if the measurement of the change in forestry biomass by the LiDAR is periodically undertaken. Judging from the trend of current negotiation, e.g., a report is required every 5 years, the dependence on the ground survey is not rational in terms of data collection and processing. Therefore establishment of the forest biomass monitoring system, which is a combination of permanent monitoring plots with remote sensing by LiDAR, is desired.

ACKNOWLEDGEMENT

The author gratefully thanks for Dr. Roger Sedjo of the Resources for the Future, Washington DC, US. He provided helpful comments on this manuscript. This work was supported by the Global Environment Research Fund of the Ministry of Environment, Japan.

LITERATURE CITED

FAO, (2000): Forest Resources of Europe, CIS, North America, Australia, Japan and New Zealand, United Nations, 158pp

FAO, (2001): Global Forest Resources Assessment 2000, FAO, 9pp

IPCC, (2000): Land Use, Land-Use Changes, and Forestry, Cambridge University Press, 5pp

Hori, S., Hayashi, H., Amano, M., Matsumoto, M. and Awaya, Y., (2002): Development of ARD determination in the Article 3.4 using satellite data, Aerial Photogrammetry for Forest, **197**: 1-7 (in Japanese)

(Received 22 January 2007)
(Accepted 10 September 2007)

Article

Stability of Surface LiDAR Height Estimates on a Point and Polygon Basis

Michael A. Wulder[*1], Steen Magnussen[*1], David Harding[*2], Nicholas C. Coops[*3], Paul Boudewyn[*1] and David Seemann[*1]

ABSTRACT

Airborne scanning LiDAR (Light Detection and Ranging) data has significant potential to update, audit, calibrate, and validate operational stand-level forest inventories by providing information on canopy height, vertical structure, and ground elevation. However, using LiDAR data as an operational data source in a sampling context requires repeatable and consistent attribute estimation (i.e. height), from data collected over several acquisition flight lines. We examined the consistency of LiDAR height estimates obtained from the Scanning LiDAR Imager of Canopies by Echo Recovery (SLICER) instrument over Jack pine (*Pinus banksiana*, var. Lamb) and black spruce (*Picea mariana*, var. Mill.) forest stands in central Saskatchewan, Canada. Two analyses were undertaken: first, estimated tree heights derived from pairs of LiDAR returns, acquired from multiple flight lines and within 9m of a single LiDAR footprint, were compared to assess the consistency of height estimates (point stability); secondly, height estimates from multiple flight lines within individual forest inventory polygons were compared to assess the consistency of within-polygon estimates of tree height (polygon stability). The point stability analysis indicated that over all forest classes estimates of height were consistent, with 94% of LiDAR returns (n = 15,896) having a pair-wise height difference within ± 5m. On a polygon basis, both between- and within-flight line standard deviations were considered. Results indicated that the within-polygon variability in estimated tree heights was captured by LiDAR data collected over any portion of a polygon. This result suggests that the inventory polygons are homogenous with regards to height (and related variability) and may be characterized with LiDAR, independent of actual flight path.

Keywords: LiDAR, forest inventory, Landsat, SLICER, BOREAS

INTRODUCTION

Both private forest companies and public forest management agencies require information collected at a range of spatial scales to facilitate short and long term planning. Strategic information is needed to plan for timber production in anticipation of market trends and needs over long time horizons. Since this type of planning is often conducted over a discrete forest management unit, it is possible to rely on information from an objective field sample (HOLMGREN, 2004). However, the actual allocation of forest operations across a landbase requires estimates of forest variables for each and every forest stand. Given that a full-fledged, field based forest inventory is both operationally and cost prohibitive in most jurisdictions, the ability to estimate forest stand parameters by remote methods is necessary.

For industrial forest management activities the almost universal method used to derive spatial information on forest structure and condition is through the manual interpretation of tree heights from large-scale stereo aerial photography, supported by a sample of field site visits for calibration and quality assurance. Whilst tree height is not the only, or often the primary, driver of forest inventories (often stand volume or diameter at breast height is what is required (NELSON *et al.*, 2003)), there is generally (especially in young to mature forest stands) a strong relationship between height and diameter, volume, stand density and ultimately production. Aerial photography, like most optical remotely sensed imagery, provides only a 2-dimensional representation of forests, which

Corresponding author: Michael A. Wulder
[*1] Canadian Forest Service (Pacific Forestry Centre), Natural Resources Canada, Victoria, British Columbia, Canada
[*2] Code 921, Geodynamics Branch, NASA Goddard Space Flight Centre, Greenbelt, Maryland, United States of America
[*3] Department of Forest Resource Management, 2424 Main Mall. University of British Columbia, Vancouver, Canada

requires inference to be applied when estimating vertically distributed parameters (WULDER, 1998). Some examples of factors which affect the accuracy of height estimation in forest inventory include film emulsion, scale, focal length, time of day, shape of tree, character of shadow, character of the forest (e.g., stand density, complexity of stratification), topography, observer skill, and measurement technique (AVERY and BURKHART, 2002). Alternatively, airborne scanning LiDAR (Light Detection and Ranging) data provide a 3-dimensional representation of forest structure. Laser altimetry determines the distance from a sensor to a target using a beam of light and recording the time taken for the light to travel to the target object and return. This 3-dimensional view of forest structure allows for estimates of vertically distributed elements of the forest, making LiDAR data well suited to measurement of individual trees (NÆSSET and OKLAND, 2002), tree heights (MAGNUSSEN and BOUDEWYN, 1998), and canopy heights (NELSON, 1997).

LiDAR systems applied to forestry applications can be categorized as either 'discrete return' or 'full waveform' systems and differ from one another with respect to how they vertically and horizontally sample a canopy's three-dimensional structure (LIM *et al.*, 2003). Discrete return systems typically allow for two (first and last) or sometimes up to five, returns to be recorded for each pulse. Conversely, a full waveform LiDAR system senses and records the amount of energy returned to the sensor at a series of equal time intervals. In either case, the sensor produces a beam which results in a circular sampling area (i.e., footprint), which increases in size with distance from the sensor. The footprint for most discrete return systems is on the order of 0.2 to 0.9 m. For the full waveform systems, the footprint size may vary from 8m to 70m (MEANS, 1999; HARDING, 2000; LIM *et al.*, 2003). Recently, Hug *et al.* (2004) introduced the LiteMapper-500 capable of waveform digitization over a small footprint (0.4m at flying at 800m above ground level) based on the RIEGL LMS-Q560 laser scanner.

The SLICER (Scanning LiDAR Imager of Canopies by Echo recovery) instrument is an example of a full waveform LiDAR system which can be flown high and fast enabling the characterization of large areas in a short mobilization period (BLAIR *et al.*, 1994; HARDING, 2000). The instrument is also well suited for flying transects enabling sampling and attribute extension. SLICER also provides for an intermediate scale of information (footprint 5-10m) between small-footprint discrete systems and satellite based systems such as the GLAS (ZWALLY *et al.*, 2002). The SLICER instrument has demonstrated capability to accurately estimate forest canopy heights in both deciduous (LEFSKY *et al.*, 1999) and coniferous (MEANS *et al.*, 1999) dominated stands. LiDAR data has also been shown to accurately estimate biomass and other structural forest attributes, over a wide range of species and structural vegetation types, although most studies have focused on single dataset calibration (LEFSKY *et al.*, 2005). More recently, LiDAR technology has gained widespread acceptance for large-scale operational mapping. Recent examples include applications in Norway (NÆSSET, 2004) and the US state of Delaware (NELSON *et al.*, 2003). HUDAK *et al.* (2002) demonstrated an approach for extrapolation of small footprint LiDAR vertical information through the use of auxiliary image data. WULDER and SEEMANN (2003) used SLICER data and segmented Landsat to update a polygon based forest inventory.

The use of LiDAR data as a sampling tool raises a number of issues related to updating, calibrating, and validating standard forest inventory. To address these issues, we investigate the stability of height estimates on a per point basis comparing multiple LiDAR returns at the same location, and the agreement between multiple LiDAR flight lines through individual forest inventory polygons in a homogenous forest.

METHODS

Study Area

The data used for this analysis was established as part of the Boreal Ecosystem - Atmosphere Study (BOREAS) in central Saskatchewan, Canada (SELLERS *et al.*, 1995). For the purposes of this study, a 7,500km² study area was defined to represent a variety of boreal forest species types and forest conditions (Fig. 1). The study area is approximately 115km (E-W) and 65 km (N-S) and is located within the Saskatchewan Plains Region of the Great Plains Province of North America. The topography of the study area is gently undulating, with elevations ranging from 400 to 700m (SELLERS *et al.*, 1995).

The mixed forest in central Saskatchewan is close to the southern limit of the boreal forest and composed of aspen (*Populus tremuloides* Michx.) and white spruce (*Picea Glauca*) in well drained sites, and Jack pine (*Pinus banksiana*, var.

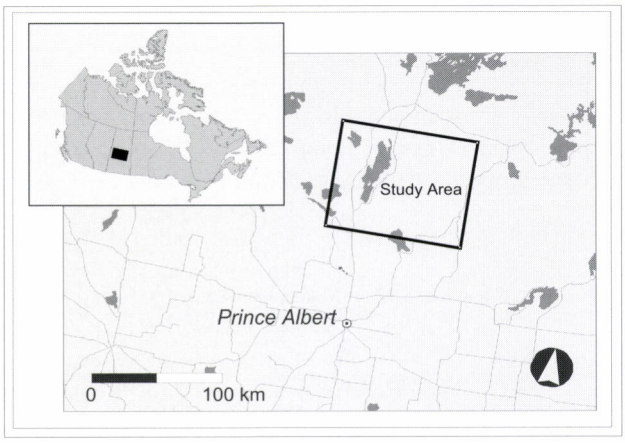

Fig. 1 Study area denoted in black is bounded by the geographic extents 54° 19' N and -106° 0' E (Northwest corner), to 53° 39' N and -104° 15' E (Southeast corner).

Lamb) and black spruce (*Picea mariana*, var. Mill.) on drier sites with coarse textured soils. In poorly drained areas, bogs support black spruce and small proportions of tamarack (*Larix laricina* var. Du Roi) (ROWE, 1977; LOWE *et al.*, 1996). Also present are fen areas, which are composed mostly of sedge vegetation with discontinuous cover of tree species such as tamarack. Forest disturbance is largely the result of localized logging operations and fire. Recent fires have generally been limited in extent and frequency through a comprehensive forest fire suppression program (SELLERS *et al.*, 1995).

Forest Inventory (GIS) and Landsat-5 TM Imagery

The provincial forest inventory system in Saskatchewan is based on interpretation and digitization of air photos on an approximate 15 year completion cycle (GILLIS and LECKIE, 1993). Inventory validation is undertaken through field visits and the establishment of temporary sample plots. The forest inventory data provided for this study is of variable vintage, with 82.7% of the inventory compiled in 1984; 3.8% compiled before 1984, and 13.5% compiled after 1984. To account for the differing vintage between the LiDAR data and the GIS data, a Landsat Thematic Mapper (TM) scene (Path 37, Row 22) acquired from July 1994, was classified to provide an indication of land cover classes commensurate with the field and LiDAR acquisition programs. The classified image data also provides for an indication of the within polygon land cover characteristics with greater spatial detail than the forest inventory data. The image was geocorrected using a first-order polynomial and a nearest neighbour resampling algorithm, resulting in a root mean square error of approximately 24 metres. The Landsat TM imagery was then classified using a hyperclustering and labeling approach based upon an established protocol (WULDER *et al.*, 2003). Using this approach, 241 initial spectral clusters were generated and subsequently merged down to represent the following general land cover classes: coniferous, deciduous, mixed-wood, shrub, herb, bryoids, wetland (treed), wetland (non-treed), exposed land, and water bodies. These classes were then further generalized using a polygon decomposition process whereby the proportion of land cover classes within each forest inventory polygon was determined (WULDER and FRANKLIN, 2001). The land cover class that represented the greatest amount of area in the inventory polygon was then assigned to the polygon. The forest inventory polygons provide a spatial context for the comparison of the differing LiDAR flight lines. The forest inventory polygons are also the units that are subject to updating in an operational context (e.g., WULDER and SEEMANN (2003)).

SLICER LiDAR Data

The SLICER instrument, developed at the NASA Goddard Space Flight Center, is a scanning modification of a profiling laser altimeter (BLAIR *et al.*, 1994). The SLICER is a LiDAR system that digitizes the backscattered return signal resulting in the capture of a full waveform. The instrument records the vertical distribution of illuminated surfaces within the laser footprint. The SLICER data used in this study was collected as part of the BOREAS project in July of 1996 (HARDING, 1998). Based upon the sensor configuration, the vertical resolution of the SLICER is approximately 1m, with a horizontal resolution of approximately 9m, and with five adjacent footprints resulting in an approximate 45m wide swath. In this study the footprint diameter was approximately 9m, varying by approximately ± 5% (or ± 45cm), due to laser divergence and changes in the distance from the aircraft to the ground.

The BOREAS LiDAR data was processed from the raw data into variables representing key components of the sensed waveform (HARDING, 2000). The height recorded for each LiDAR pulse was determined as difference between the "ground start" variable (i.e., ground inferred from the distribution of energy indicating a terminal location), and the detected laser returns indicative of the canopy top. The geolocation of the height value for each LiDAR footprint was also required in order to compare different height estimates. The location of the footprint is referenced to the first detected reflection (i.e. the canopy top). Accordingly, the absolute geo-location accuracy of footprint locations is limited by the degree of elevation change within the footprint, the differential GPS positioning of the aircraft, information on the laser pointing as established by an Inertial Navigation System (INS), and the encoding of the scanning mirror angle. Tag time errors in the independently recorded data streams, where the range and angle are in one data stream and GPS information in another, may introduce occasional geo-location errors. As a result, the footprint location accuracy can be expected to be at the scale of the laser footprint, in this case about 9m.

Stability Analysis

To undertake the point stability analysis, the following procedure was used (as illustrated in Fig. 2):

- For every LiDAR return, the height was computed from the SLICER data stream;
- A 9m radius buffer was then placed around each LiDAR return;
- LiDAR returns from adjacent SLICER flight lines were then overlaid on the buffered returns;
- Any pair of LiDAR hits which fell within the 9m buffer were tagged, the difference in height calculated, and the horizontal distance between the LiDAR returns recorded. The pair-wise selection of points was done on a flight line-by-flight line basis.

For the polygon stability analysis (as illustrated in Fig. 2):

- The forest inventory polygons were buffered by 9m to reduce any edge effect and geo-location issues.

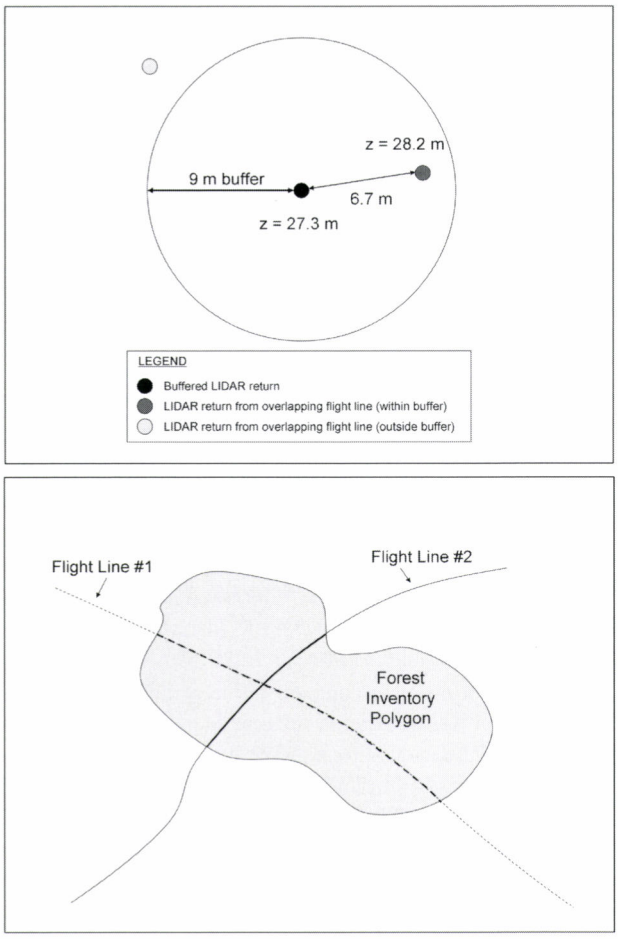

Fig. 2 For the point stability analysis (top panel) a 9m buffer was applied to each LiDAR return. The height of LiDAR returns from adjacent SLICER flight lines that fell within the 9m buffer were recorded, as was the horizontal distance between the two returns. For the polygon stability analysis (bottom panel), the within- and between- flight line standard deviations were compared to assess the pattern of variation in LiDAR heights.

- The SLICER flight lines were overlaid on the buffered forest inventory polygons.
- An analysis of variance (ANOVA) was then applied to the LiDAR height observations, stratified by polygon, to assess polygon height stability.
- Within polygon standard deviation of the hits between flight lines and within flight lines was compared to assess the pattern of variation in the LiDAR heights. The within line standard deviation is a measure of the variability of height values that may be expected for an individual flight line within a polygon. Low values indicate little variability in height values, likely cover type related, such as for water or wetlands, while a high value indicates that the height values may represent a mixture of tree tops, canopy openings and within crown hits, with the mixture and the values determined by the forest cover type.
- The between line standard deviation indicates the agreement of mean canopy height values of individual flight lines passing through a polygon. A low value indicates a high accuracy of the mean LiDAR canopy height of a flight line and that a single flight line across a polygon can provide a reliable estimate of the average canopy height in the polygon.

RESULTS

Point Stability Analysis

Analysis of the adjacent SLICER flight lines indicates that 18,507 individual LiDAR hits fell within the 9m footprint of a second hit. The height differences for measurements taken within the same footprint zone were then stratified by the nominal distance between paired measurements. By overlaying the lidar returns on the Landsat derived land cover classification, the relationship between the two height estimates used in the pairwise comparison of (purportedly) the same cover type, and the degree to which their footprints overlap, can be examined.

As a control, LiDAR returns occurring over water were investigated separately. For LiDAR returns over water, the height difference between pairs of LiDAR hits, spaced at 0 to 1m through to 8 to 9m, was always less than 1 meter, indicating that multiple measures of height, even when separated by a horizontal distance of up to 9m, were accurate. Observed differences are likely the results of errors in of GPS and INS adjustments, and possibly in some cases, shoreline encroachment.

An example from a Landsat TM-classified coniferous forest cover type is presented in Fig. 3; a large majority of pairs of hits were within ± 5m of each other. This figure also indicates a number of pairs of LiDAR hits increases as a function of distance, with approximately 200 pairs of LiDAR hits occurring within 1m of each cell, increasing to over 1600 for pairs within 9m of each other. By comparison, the observations for a deciduous forest cover type (Fig. 4) show less uniform and less consistent differences. Adjacent pairs have height differences ranging from 0 to over 10m for nominal distances between returns of 3m to 9m. Results for a mixed forest cover type (Fig. 5) were, as expected, intermediate relative to results for areas dominated by coniferous and deciduous species.

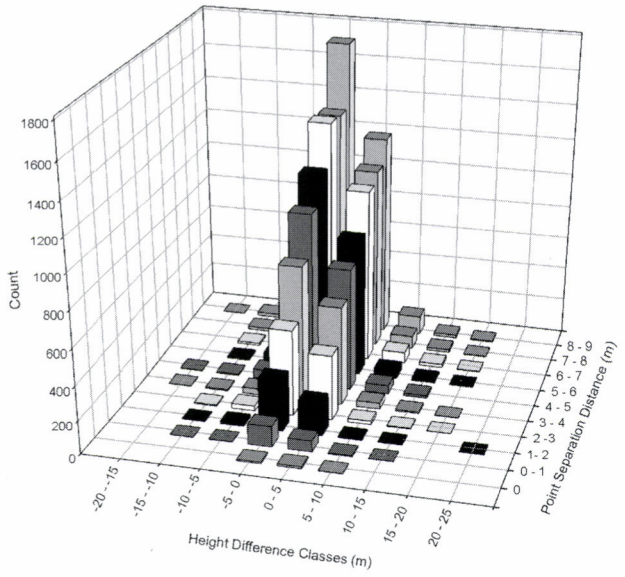

Fig. 3 Bar graph illustrating variability of SLICER height estimates as a function of multiple measures of the same location and area, stratified as coniferous land cover class.

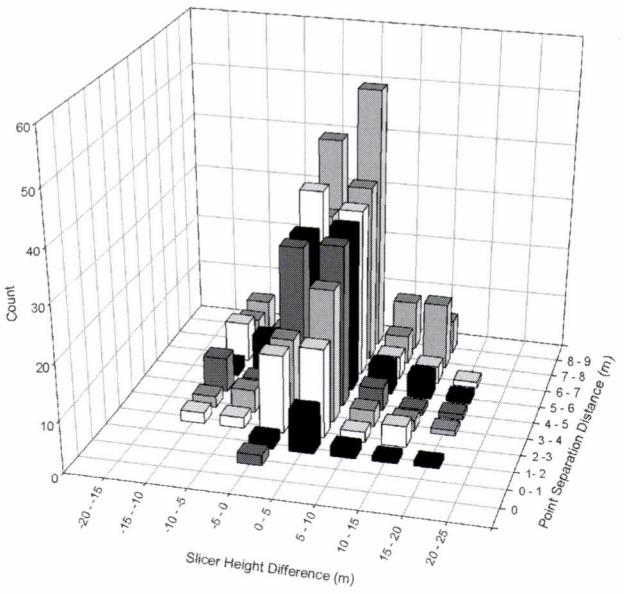

Fig. 5 Bar graph illustrating variability of SLICER height estimates as a function of multiple measures of the same location and area, stratified as mixed-wood land cover class.

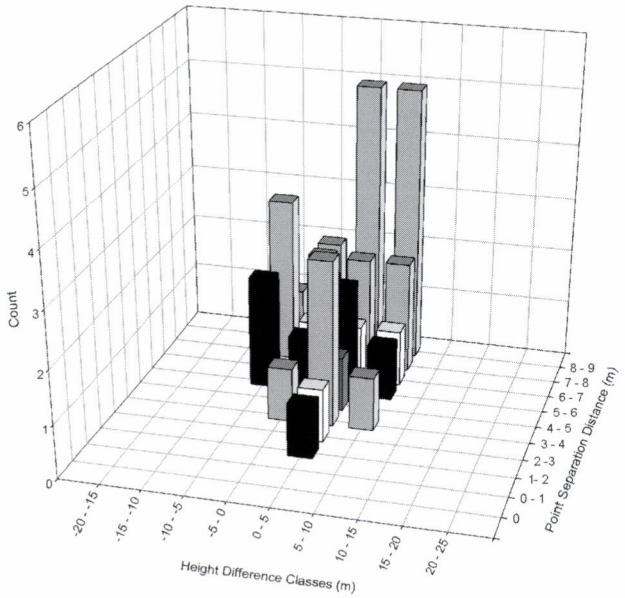

Fig. 4 Bar graph illustrating variability of SLICER height estimates as a function of multiple measures of the same location and area, stratified as deciduous land cover class.

Within Polygon Stability Analysis

In total, 360 polygons were intersected with 2 or more flight lines, representing 152,292 LiDAR returns. Most polygons had only two flight lines, with only 5% of polygons having more than 5 flight lines (Table 1). Only polygons with 2, 3, or 4 flight lines were included in the analysis. The within polygon stability analysis is undertaken through an analysis of variance (ANOVA) generating the within flight line and among flight line height variability of the forest inventory polygons. As a comparison, 5,919 LiDAR heights from multiple flight lines over three water polygons were used with a between line mean standard deviation of 0.15m and a within line mean standard deviation of 0.69m. The low values for both the between and within flight line variation, indicate, as expected both a high precision [variation within a flight line] and accuracy [variation between flight lines] of LiDAR data taken over flat surfaces. Corresponding results for vegetated surfaces reflects the variation sensed in the surface cover and its spatial distribution.

Of the 360 forested inventory polygons with multiple flight lines, the majority (275) were classed as coniferous from the Landsat imagery. The remaining forested polygons were either deciduous or mixed forest classes. Due to a lack of variation between cover types, the forest cover types were pooled and the tables illustrating within and between polygon standard deviation results are combined for all forest cover-types.

Over all classes, the between line results indicate, for example, that when 2 flight lines are flown over a polygon the estimates of mean polygon canopy height are within ± 1 meter of agreement in 73% of the examined polygons and within ± 2 meters in 89% of cases (Table 2). As the number of flight lines per inventory polygon increases, the agreement between the heights decreases, with only 53% of polygons having height estimates within ± 1m.

Within polygon, similar trends are noted in the within line variability which indicates that along the flight line, height varies considerably with variation up to ± 5m in nearly 90% of cases (Table 3). As more flight lines are added into the polygon this variation actually increases with approximately 80% of the polygons having ± 5m of height variation. The results indicate that each flight line is in close agreement in the variation detected; however, each flight line encounters different height structures within the polygon. This confirms that the polygons are in reality, not entirely homogenous and there is height variability within each stand; yet, each overpass is capturing the heterogeneity within the stand as a whole, in a similar manner. A caveat to this interpretation is a requirement that the inventory polygons used for context are not too old, with age as an indicator of the possibility of disturbance (e.g., fire, blow-down, or harvest) having occurred, potentially in a variable manner within the polygon, and subsequently captured with the lidar.

Table 1 Frequency of occurrence of flight lines collecting data on the same polygon.

# flight lines	# polygons
2	264
3	56
4	22
5	5
6	6
7	2
8	3
9	1
10	1
Total polygons	360

DISCUSSION

The provincial forest inventory program in Saskatchewan requires the measurement of tree heights to the nearest 5 m class (GILLIS and LECKIE, 1993, p. 53). The results from the SLICER LiDAR data indicates that the precision of single point-based measurements are well within the jurisdictional requirement in coniferous forests stands, with 93% of all paired LiDAR hits within 9m distance of each other being within ± 5m in height. This result increases to 95% of all paired hits being within ± 5m in height at distances less than 2m apart. In the case of deciduous forest stands, 82% of all paired LiDAR hits within 9m of each other are within ± 5m in height, which increases to 96% of all paired hits being within ± 5m at distances less than 5m apart.

As previously discussed, the SLICER LiDAR is a full waveform LiDAR instrument covering a moderate spatial footprint area (9m). The instrument detects "ground start" which is triggered by a return of the laser pulse above a preset threshold. Given a 9m footprint, in most cases the top of a tree canopy is likely to be within the footprint (assuming a tree crown size approximately commensurate with the footprint) making the "ground start" indicator a robust and significant predictor of tree height. The precision of these measures as demonstrated in this paper supports this view. Caution should be taken however when applying these results to small footprint LiDAR surfaces. In these cases, the footprint is much less (< 50cm) with a discrete sampling distance such as 1.5 - 5m. Thus the probability of a hit at the very apex of the crown is also less likely. As a result, small footprint LiDAR estimates

Table 2 Relative frequencies of between line standard deviations of canopy heights in GIS polygons.

		Between line standard deviation (m)							
		0 to 1	1 to 2	2 to 3	3 to 4	4 to 5	> 5	count	mean
Number of lines per polygon	2	73.7%	16.1%	5.7%	2.4%	1.8%	0.3%	334	0.705m
	3	65.2%	23.6%	6.8%	2.2%	1.1%	1.1%	89	0.892m
	4	53.1%	28.1%	9.4%	0.0%	6.3%	3.1%	32	1.372m

Table 3 Relative frequencies of within line standard deviations of canopy heights in GIS polygons.

		Within line standard deviation (m)							
		0 to 1	1 to 2	2 to 3	3 to 4	4 to 5	> 5	count	mean
Number of lines per polygon	2	4.5%	14.4%	33.5%	24.0%	12.0%	11.7%	334	3.16m
	3	3.4%	13.5%	25.8%	24.7%	21.3%	11.2%	89	3.36m
	4	3.1%	18.7%	25.0%	28.1%	6.8%	18.8%	32	3.25m

of tree height whilst highly precise (i.e. repeat measurements are similar, tightly scattered around a mean that may be biased) are often significantly negatively biased. The stability of small footprint LiDAR estimates of height would be expected to be similar to the findings made here, with the variation found at the scale of the smaller footprint.

The results of this study also have implications for broad scale LiDAR applications, and possibly to space-borne LiDAR design. Forest stands are highly variable. The process of defining forest stand boundaries for inventory and management attempts to delineate stands of common structure, condition and species composition, however considerable variation still exists within each stand. This variability is well captured by LiDAR hits through the stand; however, these results also indicate that multiple hits along a scan line can capture this variation adequately. These findings may aid in the design of future space borne LiDAR instruments - the concentration of measurements along a single line may be preferable to a dispersion of returns across a larger number of flight lines.

CONCLUSIONS

In previous studies, the estimation of canopy height from LiDAR observations has proven effective and is becoming an accepted methodology for forest inventories. The consistency of LiDAR height estimates is critical for forest managers considering the application of LiDAR data into existing and new forest inventory data collection exercises. The consistency of the SLICER height data, on both a point and polygon basis, illustrate the utility of LiDAR in forest inventory surveys, for sampling of forest structural conditions (including transects), and studies requiring scaling of LiDAR measures.

Recording and evaluating multiple LiDAR hits within the footprint threshold around the same location indicates that variability in LiDAR heights is limited when the separation between observations is small. In consideration of the boreal forest cover of this central Saskatchewan study area; estimates of canopy height from multiple flight lines through individual polygons indicate an acceptable level of variability related to the path taken over the polygon. The between line standard deviations indicate, in the case of 2 flight lines through a polygon, that height estimates are within 1m in over 70% of cases. The within line standard deviations indicate that there is considerable variability of height values collected within each line. Considering both between and within line standard deviation results, we conclude that within each polygon there is variability in LiDAR heights and that this variability is well captured by collecting data over any portion of a polygon. These results, on a point and polygon basis, indicate the utility of LiDAR data as a sampling tool in a forest inventory context.

ACKNOWLEDGEMENTS

Xilin Fang, of the Forestry Branch of the Saskatchewan Parks and Renewable Resources, is thanked for provision of the forest inventory data. Joanne White, of the Canadian Forest Service, is thanked for assistance in drafting of the figures and editorial insights.

LITERATURE CITED

AVERY, T. and BURKHART, H., (2002): Forest Measurements (5th ed.). Toronto, Canada: McGraw Hill

BLAIR, J., COYLE, D., BUFTON, J. and HARDING, D., (1994): Optimization of an airborne laser altimeter for remote sensing of vegetation and tree canopies. Proceedings of IGARSS '94, Vol. II, Piscatawy, New Jersey: Institute of Electrical and Electronics Engineers : 939-941

GILLIS, M. and LECKIE, D., (1993): Forest inventory mapping procedures across Canada (Information Report PI-X-114). Forestry Canada, Petawawa National Forest Institute: Petawawa, Ontario. 79 pp.

HARDING, D., (1998): Airborne LiDAR observations of canopy structure at the BOREAS tower flux sites. Proceedings of IGARSS '98, Piscatawy, New Jersey: Institute of Electrical and Electronics Engineers : 1,550-1,552

HARDING, D.J., (2000): BOREAS Scanning LiDAR Imager of Canopies by Echo Recovery (SLICER): Level-3 Data. CD-ROM. Available by special arrangement with Oak Ridge National Laboratory Distributed Active Archive Center, Oak Ridge, Tennessee, U.S.A. [http://www.daac.ornl.gov]

HOLMGREN, J., (2004): Prediction of tree height, basal area and stem volume in forest stands using airborne laser scanning. Scandinavian Journal of Forest Research **19**: 543-553

HUDAK, A. T., LEFSKY, M. A., COHEN, W. B. and BERTERRETCHE, M., (2002): Integration of LiDAR and Landsat ETM+ data for estimating and mapping forest canopy height. Remote Sensing of Environment **82**: 397-416

HUG, C., ULLRICH, A. and GRIMM, A., (2004): LiteMapper-5600 - A Waveform-Digitizing LiDAR Terrain and Vegetation Mapping System. (In THIES, M., KOCH, B., SPIECKER, H. and WEINACKER, H., (Eds.) Proceedings of the ISPRS working group VIII/2, 'Laser-Scanners for Forest and Landscape Assessment'.) Freiburg, Germany, October 3 to 6, International Archives of Photogrammetry, Remote Sensing and Spatial Information Sciences, Vol. XXXVI: 8/W2. URL (accessed on December 11, 2006): http://www.isprs.org/commission8/workshop_laser_forest/HUG.pdf

LEFSKY, M., HARDING, D., PARKER, G. and SHUGART, H., (1999): Surface LiDAR remote sensing of basal area and biomass in deciduous forests of Eastern Maryland, USA. Remote Sensing of Environment **67**: 83-98

LEFSKY, M., HUDAK, A., COHEN, W. and ACKER, S., (2005): Geographic variability in LiDAR predictions of forest stand structure in the Pacific Northwest. Remote Sensing of Environment **95**: 532-548

LIM, K., TREITZ, P., WULDER, M., St-ONGE, B. and FLOOD, M., (2003): LiDAR remote sensing of forest structure. Progress in Physical

Geography **27**: 88-106

Lowe, J., Power, K. and Marsan, M., (1996): Canada's Forest Inventory 1991: Summary by Terrestrial Ecozones and Ecoregions (Information Report BC-X-364E). Canadian Forest Service, Pacific Forestry Centre: Victoria, British Columbia. 56 p

Magnussen, S. and Boudewyn, P., (1998): Derivations of stand heights from airborne laser scanner data with canopy-based quantile estimators. Canadian Journal of Forest Research **28**: 1016-1031

Means, J., Acker, S., Harding, D., Blair, J., Lefsky, M., Cohen, W., Harmon, M. and McKee, W., (1999): Use of a large-footprint scanning airborne LiDAR to estimate forest stand characteristics in the western Cascades of Oregon, Remote Sensing of Environment **67**: 298-308

Næsset, E. and Okland, T., (2002): Estimating tree height and tree crown properties using airborne scanning laser in a boreal nature reserve. Remote Sensing of Environment **79**: 105-115

Nelson, R., (1997): Modeling forest canopy heights: The effects of canopy shape, Remote Sensing of Environment **60**: 327-334

Nelson, R., Valenti, M., Short, A. and Keller, C., (2003): A multiple resource inventory of Delaware using airborne laser data. BioScience **53**: 981-992

Rowe, J.S., (1977); Forest Regions of Canada. Canadian Forest Service: Ottawa, Canada. 172p.

Sellers, P., Hall, F., Margolis, H., Kelly, B., Baldocchi, D., den Hartog, G., Cihlar, J., Ryan, M., Goodison, B., Crill, P., Ranson, K., Lettenmaier, D. and Wickland, D., (1995): The Boreal Ecosystem-Atmosphere Study (BOREAS): An Overview and Early Results from the 1994 Field Year. Bulletin of the American Meteorological Society **76**: 1549-1577

Wulder, M. A., (1998): Optical remote sensing techniques for the assessment of forest inventory and biophysical parameters. Progress in Physical Geography **22**: 449-476

Wulder, M. A., Dechka, J. A., Gillis, M. A., Luther, J. E., Hall, R. J., Beaudoin, J. and Franklin, S. E., (2003): Operational mapping of the land cover of the forested area of Canada with Landsat data: EOSD land cover program. The Forestry Chronicle **79**: 1-9

Wulder, M. A. and Franklin, S. E., (2001): Polygon decomposition with remotely sensed data: rationale, methods, and applications. Geomatica **55**: 11-21

Wulder, M. A. and Seemann, D., (2003): Forest inventory height update through the fusion of LiDAR data with segmented Landsat imagery. Canadian Journal of Remote Sensing **29**: 536-543

Zwally, H. J., Schutz, B., Abdalati, W., Abshire, J., Bentley, C., Brenner, A., Bufton, J., Dezio, J., Hancock, D., Harding, D., Herring, T., Minster, B., Quinn, K., Palm, S., Spinhirne, J. and Thomas, R., (2002): ICESat laser measurements of polar ice, atmosphere, ocean, and land. Journal of Geodynamics **34**: 405-445

(Received 22 January 2007)
(Accepted 28 September 2007)

Article

Regional Forest Inventory using an Airborne Profiling LiDAR

Ross Nelson[*1], Eæsset[*2], Terje Gobakken[*3], Göran Ståhl[*4] and Timothy G. Gregoire[*5]

ABSTRACT

A 5,159km profiling airborne LiDAR data set consisting of 56 parallel flight lines (fls) systematically spaced one kilometer apart acquired over the State of Delaware (USA) in y2000 are used to test the accuracy and precision of LiDAR-based forest inventory estimates. Nonparametric techniques is employed to develop simple linear regressions (SLRs) relating ground-measured biomass to laser height and crown closure. The ground-laser models are used to estimate total aboveground dry biomass at the county (3 counties in Delaware - 1,124km², 1,542km² and 2,539km²) and State (5,205km²) levels. The laser estimates are compared to U.S. Forest Service-Forest Inventory and Analysis (FIA) estimates from a 1999 ground-based survey of 215 FIA plots. In addition, the 56-fl data set is treated as a population and subsampled to test three variance estimators. The three variance estimators include weighted versions of the simple random sampling (SRS) estimator, a successive differences (SD) estimator, and a Newton's Method (NM) estimator. Results, constrained to this particular 56 fl data set and post-stratification, indicate the following: (1) Using all 56 fls in conjunction with the nonparametrically derived SLRs, LiDAR-based estimates of biomass are within 4%-24% at the county level and 14%-18% at the state level. (2) Across the 3 counties and State, considering the full range of flight line sampling intensities (from 2 to 28km between fls), the SRS estimator most closely tracks systematic sampling variability. The SD estimator is most conservative, consistently overestimating biomass variability by ~15%. (3) When a limited, more realistic range of inter-flight line distances from 2-6km between parallel fls is considered, the behavior of the SRS estimator changes markedly. The SD and NM estimators overestimate systematic standard errors (SEs) by ~18%, whereas the SRS estimator becomes the most conservative, overestimating systematic SEs by ~30%. This SRS role reversal from least to most conservative as the distance between fls decreases suggests that the fls spaced 2-6km apart are, in Delaware, spatially autocorrelated. We suggest that analysts employ the SD or NM estimators when fls are closely spaced, e.g., 2-6km apart. (4) Inclusion of prediction error, i.e., the residual noise around regression lines used to predict, for instance, biomass as a function of profiling LiDAR height measurements, adds approximately 0.7-1.2 t/ha (an 8-15% increase) to the biomass standard error, averaged across strata and sampling intensities. (5) The positive relationship between the distance between flight lines and the systematic standard error appears to be generally linear (albeit noisy) for a given cover type and study area. Figures are provided illustrating the empirical relationship between flight line distance and systematic SE, by stratum within study area. These may be used to guide the design of airborne LiDAR-based forest surveys on areas from 1,000-5,000km².

Keywords: profiling LiDAR, laser, systematic sampling

INTRODUCTION

Airborne lasers, both scanning and profiling, have been and are being used for regional forest inventory. Scandinavian researchers employ small footprint scanning LiDARs to conduct wall-to-wall forest inventories on 50 - 900km² parcels in Norway (NÆSSET, 2004a; b; NÆSSET *et al.*, 2004). The level of acceptance concerning the accuracy and reliability of the science, in fact, has risen to the point where private companies have commercialized their LiDAR-based forest inventory products (E. NÆSSET, T. AASLAND, pers. comm.). In the state of Delaware, profiling data have been used to estimate forest volume and biomass, impervious surface area, open water area (NELSON *et al.*, 2003a), carbon (NELSON *et al.*, 2004), and wildlife habitat area (NELSON *et al.*, 2005). In this study, that same Delaware profiling data set is used to look at additional questions regarding large-area sampling using airborne LiDARs.

The objectives of this study are threefold: (1) to report the accuracy and precision of regional airborne LiDAR-based forest inventory, (2) to investigate three different variance

estimators to see which best characterizes systematic sampling variability, and (3) to provide some level of guidance with respect to flight-line (fl) spacing in those situations where airborne laser profilers are used as sampling tools for large-area (1,000-5,000km²) forest inventory.

A small, portable airborne LiDAR profiler (NELSON *et al.*, 2003b) was used to systematically sample the State of Delaware, on the mid-Atlantic coast of the eastern United States, during the summer of y2000. Delaware is a small, relatively flat state encompassing 5,205km². According to a 1997 airphoto-based GIS (University of Delaware Spatial Analysis Laboratory - http://www.udel.edu/FREC/spatlab/, LA=April 23, 2007), approximately 34% of the state is forested, 44% supports agriculture, 18% is residential-urban, and 4% is inland water. Delaware is divided into three counties, urbanized Newcastle County to the north (1,124km²), and the more agrarian Kent County (1,542km²) and Sussex County (2,539km²) as one moves south. Profiling measurements were collected along 56 N-S fls spaced one kilometer apart. The shortest fl was 17km, the longest 153km; 5159km of profiling data were collected and analyzed. Post spacing was nominally 25cm., and at a flying altitude of 150m AGL, the spot size was ~37cm.

METHODS AND MATERIALS

Statistical procedures outlined in Nelson et al. (2004, see erratum) were used to develop county and state-level estimates of forest biomass, specifically total aboveground dry biomass. Nonparametric regression procedures were used to fit simple linear models to relate ground-measured dry biomass to laser height and crown closure. One hundred forty two - 40m Line Intercept Samples (LIS, see DEVRIES, 1986) were collected on the ground throughout the state in seven of eight strata, four forest strata-hardwood/deciduous, mixed-wood, conifer, wetlands, and three nonforest strata-agriculture, residential, and urban/barren. An eighth stratum, open water, was not sampled on the ground. One generic equation was developed across the strata to produce a non-stratified predictive equation. In addition, five stratum-level simple linear regressions were calculated, one for each of the four forested strata, and one collectively for the three nonforest strata. The wetlands equation was used to predict biomass in the open water strata. Stratified and non-stratified results were compared to see if stratification improved accuracy and/or increased precision. The single generic and five stratum-level equations used in this study are reported in Table 1.

Regional estimates of biomass depend on the use of predictive equations that relate biomass to laser measurements. In this study, the equations reported in Table 1 are used to calculate biomass on fl segments ≤40m long. Laser-based predictions are summed within fls, and fl estimates are averaged across the region to calculate county and state estimates. Variance calculations at the regional level reflect fl, not segment-level, variation. But the segment-level, laser-based predictions, i.e., the $\hat{b}$ or $\hat{b}_j$ in Table 1, upon which the entire laser inventory is based, are themselves average responses. There is scatter around a given prediction for a segment ≤40m that we implicitly ignore in our variance calculations, and that scatter is characterized by the root mean square error of the SLR.

In this study, we look at the effects of including this residual noise in the form of prediction error in our variance calculations. We account for scatter about a given predictive

Corresponding author: Ross Nelson
*1 Biospheric Sciences Branch, Code 614.4
NASA-Goddard Space Flight Center
Greenbelt MD 20771 USA
1-301-614-6632 (v)
1-301-614-6695 (fax)
Ross.F.Nelson@nasa.gov
*2 Department of Ecology and Natural Resource Management
Norwegian University of Life Sciences
P.O. Box 5003, NO-1432
Ås, Norway
47 64 96 57 34
Erik.Naesset@umb.no
*3 Department of Ecology and Natural Resource Management
Norwegian University of Life Sciences
P.O. Box 5003, NO-1432
Ås, Norway
47 64 96 57 55
Terje.Gobakken@umb.no
*4 Department of Forest Resource Management and Geomatics
Swedish University of Agricultural Sciences
90183 Umea Sweden
46-90-7865800
Goran.Stahl@resgeom.slu.edu
*5 J. P. Weyerhaeuser, Jr. Professor of Forest Management
School of Forestry and Environmental Studies
Yale University
360 Prospect Street
New Haven, CT 06511-2189 USA
1-203 432 9398
Timothy.Gregoire@yale.edu

Table 1. Non-stratified and stratified simple linear models used to predict biomass, $\hat{b}$, in tons/hectare, based on laser-measured heights, in meters, and crown closure, in percent.

		R^2	RMSE (t/ha)	n
Non-stratified model:				
	$\hat{b}=[(8788.5)(\bar{h}_{qc})+0.00]/1000.0$	0.66	63.59	142
Stratified models:				
hardwood	$\hat{b}_j=[(106.80)(\bar{h}_a)(g)-31959.9]/1000.0$	0.30	115.51	24
mixedwood	$\hat{b}_j=[(7259.2)(\bar{h}_a)-36636.0]/1000.0$	0.28	49.17	22
conifer	$\hat{b}_j=[(9342.0)(\bar{h}_{qa})-7412.9]/1000.0$	0.44	68.05	23
wetlands	$\hat{b}_j=[(506.1)(\bar{h}^2_{qc})+0.00]/1000.0$	0.95	24.16	22
ag/res/urb	$\hat{b}_j=[(6903.6)(\bar{h}_{qc})+0.00]/1000.0$	0.76	41.60	51

where $\bar{h}_a$=average height, all pulses in a segment ≤40m long; $\bar{h}_{qa}$=quadratic mean height, all pulses; $\bar{h}_{qc}$= quadratic mean height, canopy hits, and g=crown closure, 0-100%.

equation by adding a random normal component to each segment-level, laser-based prediction, e.g., for hardwoods:

$$\hat{b} = [(106.80)(\bar{h}_a)(g) + 31959.9]/1000.0 + (m)(s)\sqrt{1 + \mathbf{x}'_0(\mathbf{X}'\mathbf{X})^{-1}\mathbf{x}_0},$$

where m is a normally distributed random variable, m~N(0,1), s is the RMSE of the predictive regression reported in Table 1 (for hardwoods, s=115.51), $\mathbf{x}_0$ and $\mathbf{x}'_0$ is the current laser measurement and it's transpose, and $(\mathbf{X}'\mathbf{X})^{-1}$ is the inverse of the sum of squares and cross-products matrix of the independent variables used to fit the linear equation. This prediction noise, assumed to be homoskedastic and normally distributed, is added at the segment level.

RESULTS

Accuracy and Precision of the County and State Biomass Estimates

Accuracy figures were generated for systematic samples of 14 fls, 28 fls, and all 56 fls, for stratified and non-stratified models, with and without regression error included. The y2000 laser estimates are compared with y1999 US Forest Service-Forest Inventory and Analysis (FIA) estimates based on 215 ground plots. Fig. 1 illustrates the accuracy of the 14 and 56 fl samples for the stratified models; the figures for the other test cases are available upon request.

A number of observations are immediate. First, at this scale, there appears to be no perceptible difference between laser estimates or standard errors with or without regression error included. This is to be expected since the random variation about the predictive regression has an expected zero mean. Second, the laser-based estimates are more precise than FIA estimates, even when only 14 parallel fls spaced 4km apart are considered, though this observation is tentative due to additional considerations discussed below. Third, if we use the FIA estimates as the standard and assume unbiasedness, then the airborne LiDAR profiler underestimates FIA total biomass in Newcastle/Kent Counties, Sussex County, and Delaware by 4.5%, 21.9%, and 14.1%, respectively. These differences may be due to (1) biased laser prediction equations and/or (2) the fact that the estimates are not directly comparable. With respect to (1), there is preliminary evidence that suggests that these laser equations under-report biomass (G. PARKER, pers. comm.). With respect to (2), the FIA estimates reflect standing stocks on "timberland", i.e., "forest land producing or capable of producing crops of industrial wood (more than 20 ft^3 per acre per year) and not withdrawn from timber utilization" (GRIFFITH and WIDMANN, 2001). Twenty cubic feet/acre/year is equivalent to 1.4m^3/ha/yr. The laser estimates are based on biomass found in the four forest classes defined by photointerpreters working with 1992 color-infrared and 1997 B&W airphotos, a 1m spatial resolution, and a 1.6ha (4acre) minimum mapping unit. Though the FIA and laser estimates are not directly comparable, discussions with FIA personnel suggested that this particular comparison was the best possible given the inherent differences in sampling methodology and forest class definitions.

It must be noted that the laser-based confidence limits illustrated in Fig. 1 are probably not correct. There are at least two reasons to question the veracity of these laser confidence limits. First, recent evidence from a laser study in Quebec indicates that covariance terms can markedly increase the variance of county and state biomass estimates. County-level estimates of biomass are calculated as an area-weighted sum of stratum estimates within the county. The county-level estimate is, then, a linear sum, i.e., $b_{county} = w_1(b_1) + w_2(b_2) + ... + w_8(b_8)$, where the b's are biomass in tons/ha of strata 1 to 8 and w_1 to w_8 are area weights that sum to 1.0 (NELSON *et al.*, 2004; see Erratum, 2005). The variance of a linear sum is the sum of the weighted variances + all possible covariance terms, i.e., $\text{var}(b_{county})=w_1^2(\text{var}(b_1))+w_2^2(\text{var}(b_2))+...+w_8^2(\text{var}(b_8))+$

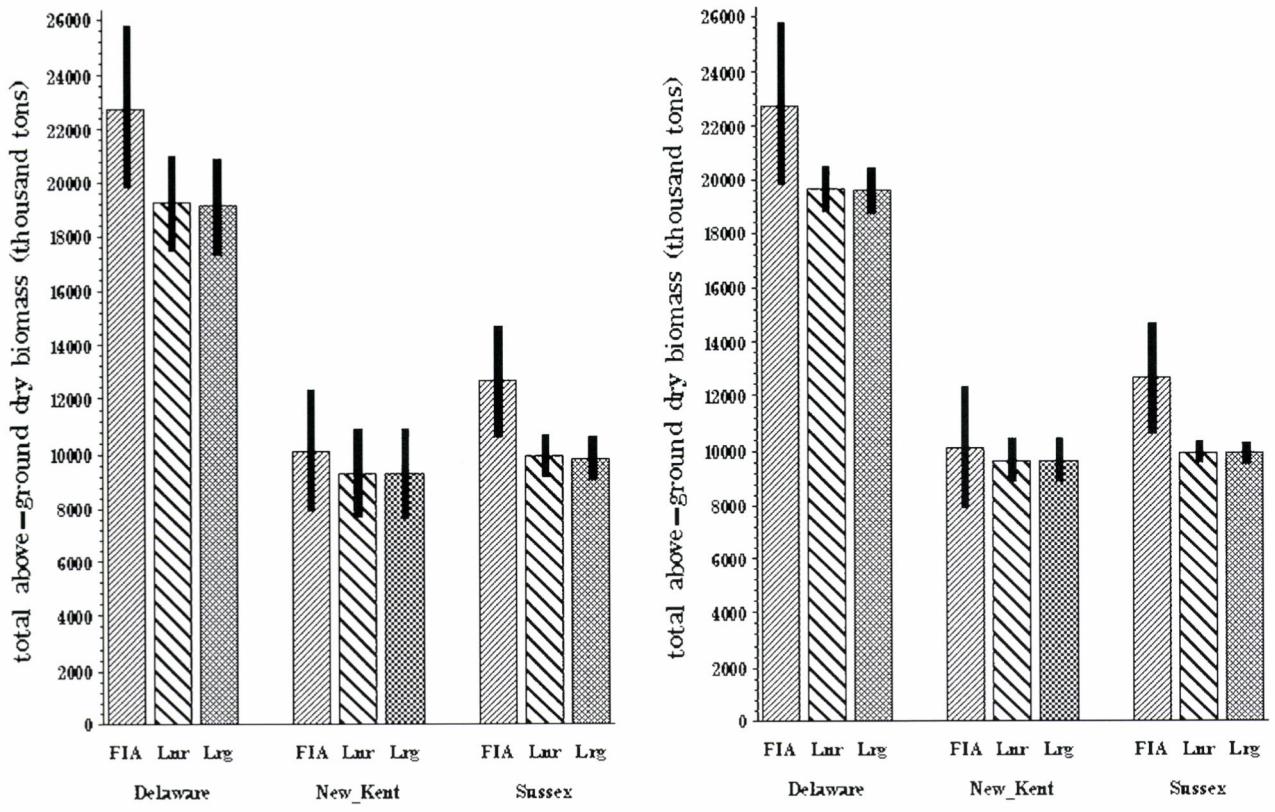

A. Total aboveground dry biomass
14 fls - nonparametric, stratified

B. Total aboveground dry biomass
56 fls - nonparametric, stratified

Fig. 1 Comparison of county and state USFS-FIA biomass estimates to stratified laser estimates based on (A) 14 fls-4km fl separation, and (B) 56 fls-1km fl separation. Laser estimates without and with regression error (Lnr and Lrg, resp.) included in calculations are shown. The black bars depict 95% confidence intervals calculated using a simple random sampling estimator.

$2w_1w_2(\mathrm{cov}(b_1, b_2))+2w_1w_3(\mathrm{cov}(b_1, b_3))+...+2w_7w_8(\mathrm{cov}(b_7,b_8))$

The cover type covariance terms were not taken into account in the calculation of the county-level confidence limits because we assumed that biomass estimates along flight lines are independent (hence the covariances = 0). In hindsight, this is probably a poor assumption. Likewise, the county-level covariance terms were not taken into account at the State level for the same reason. So those laser confidence limits in Fig. 1 may be biased downward. The second reason to question the veracity of the confidence intervals has to do with an offsetting inflationary effect that may occur when we treat a systematic sample of flight lines as a random sample. This problem is discussed directly below. The net effect of these two offsetting trends is unknown; research is underway to address the problems.

Variance Estimators for Laser Surveys

Fig. 1 depicts error bars calculated assuming that the systematically acquired fls were actually a random sample. Previous research has shown that the application of such an SRS estimator in a situation where data were actually systematically acquired may lead to an overestimation of the sampling variability (OSBORNE, 1942; NYYSSONEN *et al.*, 1967; 1971) if the study area is spatially ordered with respect to the dependent variable, e.g., biomass. Two alternative estimators might mitigate this SRS overestimation tendency (if it exists at all) - a successive differences (SD) estimator and the Newton's Method (NM) estimator (COCHRAN 1977). The SD estimator calculates fl variation based on weighted, squared differences between adjacent fls; the NM estimator works similarly but looks at three adjacent fls instead of two. The 3 candidate variance estimators, SRS, SD, and NM, were compared to empirical systematic sample variances by treating the 56 fl data set as a population. Formulas for the SRS, SD, and NM estimators, and the systematic standard error formula are provided below.

Simple random sample (SRS) variance of the stratum estimates:

For a given repetition or collection of sampled flight lines,

$$\hat{\text{var}}(\hat{b}_j) = \frac{\sum_{k=1}^{n_j} w_{jk}(\hat{b}_{jk} - \hat{b}_j)^2}{n_j - 1} \quad (1),$$

$$w_{jk} = \frac{l_{jk}}{\sum_{k=1}^{n_j} l_{jk}}, \text{and } \sum_{k=1}^{n_j} w_{jk} = 1.0,$$

where

$\hat{b}_j$ = an estimate of biomass/ha in the *jth* stratum across all n_j flight lines,

$\hat{b}_{jk}$ = an estimate of biomass/ha for the *jth* stratum, *kth* flight line,

l_{jk} = the length of interception of the *jth* stratum, *kth* flight line, and

n_j = the number of flight lines that intercept stratum *j*.

Note that n_j does not necessarily equal the total number of flight lines, n, flown over a study area because some flight lines may not intercept stratum *j*.

We condition on the particular post-stratified sample that we've selected, allowing us to treat n_j and l_{jk} as fixed quantities when, in fact, they're random variables. As a result of this condition, however, all inferences and conclusions drawn from study results are limited to the specific set of flight lines and to the particular post-stratification used in this study.

Successive differences (SD) variance of the stratum estimates:

For a given repetition where the sample size is n_j flight lines,

$$\hat{\text{var}}_{sd}(\hat{b}_j) = \frac{(n_j)\sum_{k=2}^{n_j}(w_{jk} + w_{j,k-1})^2(\hat{b}_{jk} - \hat{b}_{j,k-1})^2}{8(n_j - 1)}$$

(2, LINDEBERG 1926, eq. 4).

Newton's method (NM) variance of the stratum estimates:

For a given repetition where the sample size is n_j flight lines,

$$\hat{\text{var}}_{nm}(\hat{b}_j) = \frac{(n_j)\sum_{k=2}^{n_j-1}(w_{j,k-1} + 2(w_{jk}) + w_{j,k+1})^2(\hat{b}_{j,k-1} - 2(\hat{b}_{jk}) + \hat{b}_{j,k+1})^2}{96(n_j - 2)} \quad (3)$$

Equation 3 is derived from a nonweighted equivalent (COCHRAN 1977, pg. 225, eq. 8.45) and weights reported by LINDEBERG (1926, eq. 6).

In the simulation that we report below, equations 1, 2, and 3 were computed for each systematic sample. The average value of each was compared to the variance of $\hat{b}_j$ observed in the simulation. The latter is called the systematic variance.

Systematic variance:

Flight lines are systematically subsampled to calculate systematic variability at a particular sampling intensity. Sampling intensity is specified as a distance between adjacent, parallel airborne LiDAR flight lines.

$$\hat{\text{var}}_{sys}(\hat{b}_j) = \frac{\sum_{r=1}^{n_{sys}}(\hat{b}_{jr} - \hat{b}_j)^2}{n_{sys} - 1} \quad (4), \quad \text{where } \hat{b}_j = \frac{\sum_{r=1}^{n_{sys}} \hat{b}_{jr}}{n_{sys}} \quad (5)$$

and

$\hat{b}_{jr}$ = an estimate of of biomass per hectare for the *rth* systematic sample in the *jth* stratum for a given sampling intensity, and

n_{sys} = the number systematic sample observations for a given sampling intensity.

It turns out that the distance, in kilometers, between adjacent, systematically subsampled flight lines equals n_{sys}. This identity exists because we acquired flight lines 1km apart. This systematic variance is the standard against which the three variances estimators are compared.

The 56 parallel fls, acquired 1km apart, were divided into systematic samples 2km apart, 3km apart, 4km,... up to half the number of fls in the particular county or State. Newcastle County was transected by 31 fls, Kent by 36 fls, and Sussex County and Delaware by 56 fls. So systematic samples of fls spaced from 2 to15km apart were considered in Newcastle, 2 to18km apart in Kent, and 2 to 28km apart in Sussex and Delaware. For a given fl spacing and county/state, the "true" systematic variance was computed as a function of the squared difference between each systematic estimate of biomass and the average of the systematic estimates. The SRS, SD, and NM standard errors were compared with the systematic standard error to see which estimator most closely tracked systematic variability.

When we consider results based on the nonparametrically-derived, non-stratified and stratified SLR models across the full range of distances between flight lines and across all strata, the SRS estimator does the best job of tracking systematic sampling variability. The SRS estimator ranged from 93-105% of the systematic SEs. The comparable range for the SD estimator is 109-119%, and 97-118% for the NM estimator. A percentage less than 100% indicates that the estimator is underestimating the true systematic error; numbers greater than 100% indicate conservative estimates.

The relationships among the three estimators change when more realistic inter-flight line distances are considered. If we consider more closely spaced flight lines, i.e., from 2-6km between adjacent, parallel lines, then the SRS estimator becomes the most conservative, ranging from 111-151% of the systematic SEs. The SD and NM estimators are also conservative, but the estimator/systematic ratios collectively range from 109-133%.

These results, and the role reversal manifested by the

SRS estimator from least to most conservative, indicate that closely spaced flight lines, in Delaware, are spatially autocorrelated. This spatial autocorrelation inflates the SRS estimator. These results suggest that researchers should employ the SD or NM estimator if (1) they space their flight lines from 2-6km apart, (2) their study areas are on the order of 1000-5000km² in size, and (3) they believe that biomass is spatially ordered across the landscape. We would argue that many study areas show this spatial ordering. Delaware, for instance, supports more biomass on the western side of the State than on the wetter, sandier east side, and the N-S flight lines capture this biomass gradient.

Laser Sampling Error, by Stratum and Study Area

Fig. 2 depicts systematic standard errors for the non-stratified, nonparametrically fit SLR (the first equation in Table 1), with prediction error included, for the three counties and for the entire State. The areal extent of each stratum is reported as a percentage, in parentheses, next to the stratum name. In some cases, the stratum name (percentage) could not be noted directly on the plotted line. In these situations, an abbreviation is used (e.g., "res" for residential), and complete information listed to the left, in square brackets. Though the systematic errors reported in Fig. 2 are specific to the y2000 Delaware profiling lines and to our particular post-stratification, it is our hope that researchers might find this information useful when they design their own airborne laser-based forest inventory on areas encompassing 1,000-5,000km².

We should note that systematic errors depicted Fig. 2 do not suffer from the vagaries associated with missing covariance terms and estimator differences discussed at the end of Results Section A and the beginning of Section B (above). These systematic errors are our ground reference information; they are, in fact, true systematic sampling errors. We continue to search for estimators that more closely track

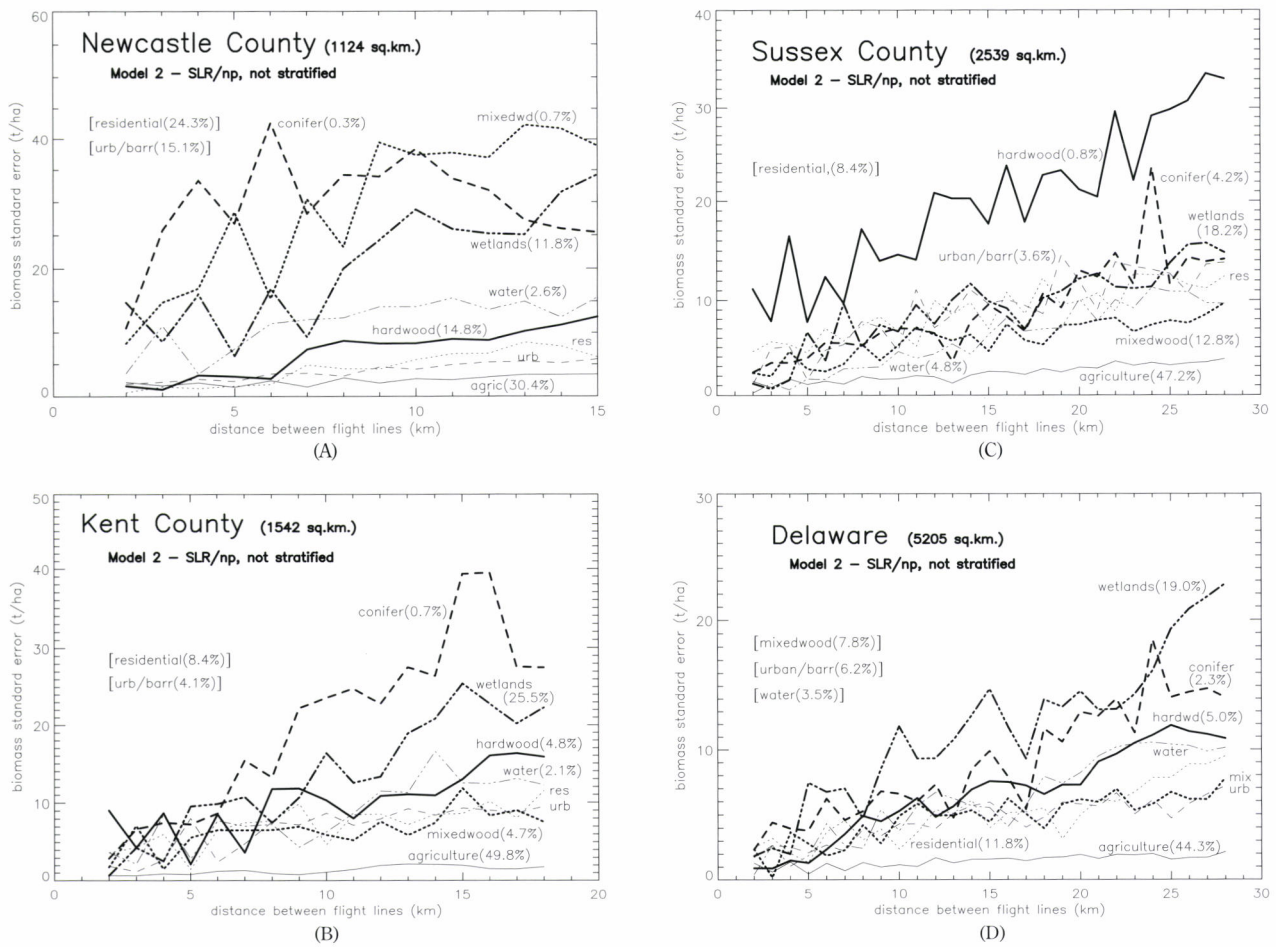

Fig. 2 Distance between flight lines versus systematic standard errors of estimate (t/ha) for eight strata in 4 study areas: (A) Newcastle County, (B) Kent County, (C) Sussex County, and (D) Delaware. Bold lines are forested strata; light lines are nonforest strata. Numbers in parentheses following the stratum name report the percentage, by area, of that particular stratum in the County or State.

these systematic errors.

Although the relationships are noisy due to the relatively limited population and small sample sizes, trends are apparent. Arguably, systematic SEs appear to increase linearly as the distance between flight lines increases. Larger study areas support smaller SEs due to the fact that a laser will measure strata more frequently given a fixed distance between flight lines. Note that the upper limits of the Y-axes increase as the size of the study areas decrease. With respect to laser sampling, the best-case scenario would be a requirement to sample a low biomass, ubiquitous stratum on a large study area, e.g., the agriculture stratum in Delaware. The worst-case scenario is the opposite, i.e., the requirement to measure a relatively rare cover type on a small study area that supports high and/or inherently variable biomass loads, e.g., the conifer or mixedwood strata in Newcastle County.

Stratification

In this study, stratification did not consistently improve the strength of the predictive models (Table 1) or consistently decrease standard errors. Looking at differences between non-stratified and stratified SEs for forested strata, we found that use of the stratified equations increased SEs, i.e., decreased precision, by 2.5 ± 4.3 t/ha, averaged across all sampling intensities and study areas. The precision of the nonforest strata, conversely, increased on average, with SEs decreasing by 1.0 ± 1.4 t/ha. The net effect across all 8 strata was an overall reduction in precision, or an average systematic SE increase of 0.8 ± 3.7 t/ha if stratified predictive models were employed to estimate biomass.

SUMMARY

The laser-based estimates of total aboveground dry biomass underestimated FIA totals by 4-24% at the county level and 14-18% at the state level. Though the two inventories are not directly comparable, the level of disagreement suggests that better methods need to be developed to relate airborne LiDAR profiling measurements to ground-measured biomass. In particular, we note the weak linear relationships between LiDAR height measurements and ground-based estimates of hardwood and mixedwood biomass. Popescu et al. (2003) made similar observations concerning mid-Atlantic hardwood versus pine cover types on a study area in central Virginia, approximately 500km SW of our Delaware study area. K. Zhao (2007, pers. comm.) demonstrated that hardwoods put more woody biomass into lateral growth, weakening the height-dbh and therefore the height-biomass relationship on which LiDAR researchers depend. He asserts, and we concur, that better, more effective hardwood models are needed.

Fig. 2 provides guidance to airborne LiDAR researchers designing flight plans for large-area forest inventory. The figure reports standard errors that might be expected in eight different strata on four different study areas ranging in size from 1,100 to 5,200km^2.

Of the three variance estimators considered, the SD and NM estimators, though conservative, mitigate the overestimation tendencies of all three estimators when flight lines are spaced 2-6km apart. Based on these results, we suggest that analysts employ the SD or NM variance estimators in situations where the flight lines are closely spaced and/or where a regional biomass gradient exists roughly perpendicular to the direction of the systematic, parallel flight lines. The use of the SD or NM estimators should be considered a stopgap while work continues to identify a variance estimator that more closely tracks systematic sampling variability.

LITERATURE CITED

Cochran, W. G., (1977): Sampling Techniques, 3rd ed., John Wiley & Sons, NY. 428 pp

DeVries, P. G., (1986): Sampling Theory for Forest Inventory. Springer-Verlag, NY. 399 pp

Griffith, D. M. and Widmann, R. H., (2001): Forest statistics for Delaware: 1986 and 1999. Resource Bull. NE-151, Newtown Square, PA: U. S. Dept. of Agriculture, Forest Service, Northeastern Research Station. 58 pp

Lindeberg, J. W., (1926): Zur Theorie Der Linientaxierung. Acta Forestalia Fennica **31**(6): 3-9

Næsset, E., (2004a): Practical Large-scale Forest Stand Inventory Using a Small-footprint Airborne Scanning LiDAR. Scandinavian Journal of Forest Research **19**: 164-179

Næsset, E., (2004b): Accuracy of Forest Inventory Using Airborne Laser scanning: Evaluating the First Nordic Full-scale Operational Project. Scandinavian Journal of Forest Research **19**: 554-557

Næsset, E., Gobakken, T., Holmgren, J., Hyyppä, H., Hyyppa, J., Maltamo, M., Nilsson, M., Olsson, H., Persson, Å. and Söderman U., (2004): Laser Scanning of Forest Resources: The Nordic Experience. Scandinavian Journal of Forest Research **19**: 482-499

Nelson, R., Short, E. A. and Valenti, M. A., (2003a): A Multiple Resource Inventory of Delaware Using Airborne Laser Data. BioScience **53**(10): 981-992

Nelson, R., Parker G. and M. Hom., (2003b): A Portable Airborne Laser System for Forest Inventory. Photogrammetric Engineering and Remote Sensing **69**(3): 267-273

Nelson, R., Valenti, M., Short, A. and Keller, C., (2004): Measuring Biomass and Carbon in Delaware Using an Airborne Profiling LiDAR. Scandinavian Journal of Forest Research **19**(6): 500-511 [Erratum. 2005, 20: 283-284.]

Nelson, R., Keller C. and Ratnaswamy, M., (2005): Locating and Estimating the Extent of Delmarva Fox Squirrel Habitat Using an Airborne LiDAR Profiler. Remote Sensing of Environment, **96** (3-4): 292-301

Nyyssönen, A., Kilkki, P. and Mikkola, E., (1967): On the Precision of Some Methods of Forest Inventory. Acta Forestalia Fennica **81**: 60 pp

Nyyssönen, A., Roiko-Jokela, P. and Kilkki, P., (1971): Studies on improvement of the efficiency of systematic sampling in forest inventory. Acta Forestalia Fennica **116**: 26 pp

OSBORNE, J. G., (1942): Sampling Errors of Systematic and Random Surveys of Cover-type Areas. Journal of the American Statistical Association **37**(218): 256-264

POPESCU, S. C., WYNNE, R. H. and NELSON. R. F., (2003): Measuring individual tree crown diameter with lidar and assessing its influence on estimating forest volume and biomass. Canadian Journal of Remote Sensing **29**(5): 564-577

(Received 19 January 2007)
(Accepted 7 June 2007)

Article

Conifer Plantation Volume Estimation by Remote Sensing without Parameter Fittings

Gen Takao[*1, *2], Satoshi Ishibashi[*1], Masayoshi Takahashi[*1], Tatsuo Sweda[*3], Hayato Tsuzuki[*3] and Tomoko Kusakabe[*4]

ABSTRACT

The objective of the present study is to develop a transparent and verifiable model of volume estimation for conifer plantations using remote sensing. The model is to be independent from observation, that is, ground truths are not necessary for parameter fitting and model construction. To achieve it, the estimation process is divided into two steps: direct measurements of physical parameters of stand, and a stand volume estimation by an external model. As an external model, we adopt the stand density chart, which is a robust and general model of stand volume growth and estimation based on a semi-empirical growth model of even-aged stands. It can estimate a stand volume from a dominant height and a density, which can be directly measured by remote sensing. In the present study, firstly, the iso-height curves, a sub-model of the stand density chart, are created from the external inventory data. Then, the dominant heights and densities are directly observed by means of the airborne remote sensing. Finally stand volumes are estimated by the observed dominant heights and densities using the iso-height curves. We found that the new iso-height curves predicted the stand volume very well. The dominant height estimation was reasonably accurate, too. However, there was a room for improvement for the stand density estimation. This method will contribute the implication of the remote sensing technology to forest management by sharing the concept and values with foresters.

Keywords: LiDAR, aerial photograph, stand density chart, iso-height curve, external model

INTRODUCTION

Application of LiDAR has been studied in forest resource and structure estimations from varied aspects (Lim *et al.*, 2003; Naesset *et al.*, 2004). Majority of the studies have depended on fully statistical approaches, in which both the model construction and its evaluation depend statistically on ground truths, like the classic optical remote sensing. For practical purpose of forest management, however, more preferable are universal models that require neither model selection nor parameter fitting for each observation campaign. Such models can reduce the cost of observation since they require neither the ground truths for model construction nor the complex processes of model selection.

It can be achieved by a two-step approach. At first, physical attributes of forest stands are directly measured by remotely sensed data, and secondly they are transferred to a model, which is external and independent from the remotely sensed data, for estimating an aimed attribute. LiDAR is an appropriate tool to directly measure the spatial dimensions of forest. Omasa *et al.*, (2003) estimated carbon storage of some Japanese cedar plantations by LiDAR height measurements coupled with an external model derived from the inventory data.

Foresters have been keen for developing models for inventory that can estimate the resources by a fewer measurable dimensions while be robust through a wider region. The stand density chart (Ando, 1982) is one of such

Corresponding author: Gen Takao
[*1] Hokkaido Research Center, Forestry and Forest Products Research Institute, Sapporo 062-8516, Japan
[*2] Current affiliation: Center for International Forestry Research, P.O. Box 0113 BOCBD, Bogor 16000, Indonesia
[*3] Forest Resources Planning, Ehime University, Matsuyama 790-8566, Japan
[*4] School of Human Science, Waseda University, 2-579-15 Mikajima, Tokorozawa, Japan

models, which describes the relationships among stand density, dominant height and volume, and their growths, for a species in a region. The model structure is semi-empirical, and the parameters are to be estimated by number of inventory data. It can be a good external model combined with the dominant height and density measurements by remote sensing.

In the present study, we propose a new two-step procedure to estimate the stand volume of conifer plantations in a region; direct measurements of dominant height and density as the first step, followed by a stand volume estimation by the iso-density curve as the second step. By the results, we discuss the source of biases and the possible implication of the procedure.

METHOD

Study Area and Data

A study area of 10km length by 600m width was set on conifer plantations in a national forest near City of Tomakomai, Hokkaido, Japan (Fig. 1), which located on gentle and flat slope at base of a volcano, Mt. Tarumae. The elevation of the area inclined from ca 50m in the east end up to ca 200m in the west end. Either of four major species, namely *Picea jezoensis*, *P. glehnii*, *Abies sachalinensis* and *Larix leptolepis*, was planted in about 65% of the plantations. The mechanized stand management made unique linear planting patterns perpendicular to the forest roads especially at young stands. Undergrowth was dominated by ferns and/or herbaceous plants, but they were relatively thin.

Airborne LiDAR along with natural color aerial photos were taken on the study area on September, 2002, whose specification can be found on Table 1. Digital Surface Model (DSM) with a pixel size of 1m square was derived by interpolating the first pulses. Digital Terrain Model (DTM) with the same pixel size was derived by interpolating the last pulses that had the local minimum altitude within a surrounded 5m by 5m square. Finally, Digital Height Model (DHM) was calculated by subtracting DTM from DSM. Using the DSM and natural color aerial photos, digital orthophotos with the spatial resolution of 50cm were derived.

Ground measurement of stands was taken place in 2002 at 21 plots of different planted species and ages. Diameter at breath height (= 1.3m, DBH), height and species of each tree within plot were recorded. Stem volume for each tree was estimated by the DBH and the height using the volume tables provided by Forestry Agency. The area of the plots varied depending on the tree densities so that each plot consisted of

Table 1 Specification of the acquired LiDAR data

Sensor type	Optech ALTM1020
Acquisition date	12 - 14 SEP 2002
Ground speed	230km/h
Absolute altitude	ca 1,700m
Scan angle	± 10deg
Scan frequency	27Hz
Pulse frequency	25MHz
Pulse density	> 1pt/m² (ground)
Divergence Angle	0.2mrad
Footprint	34cm
Vertical accu.	± 0.15m
Horizontal accu.	± 0.85m

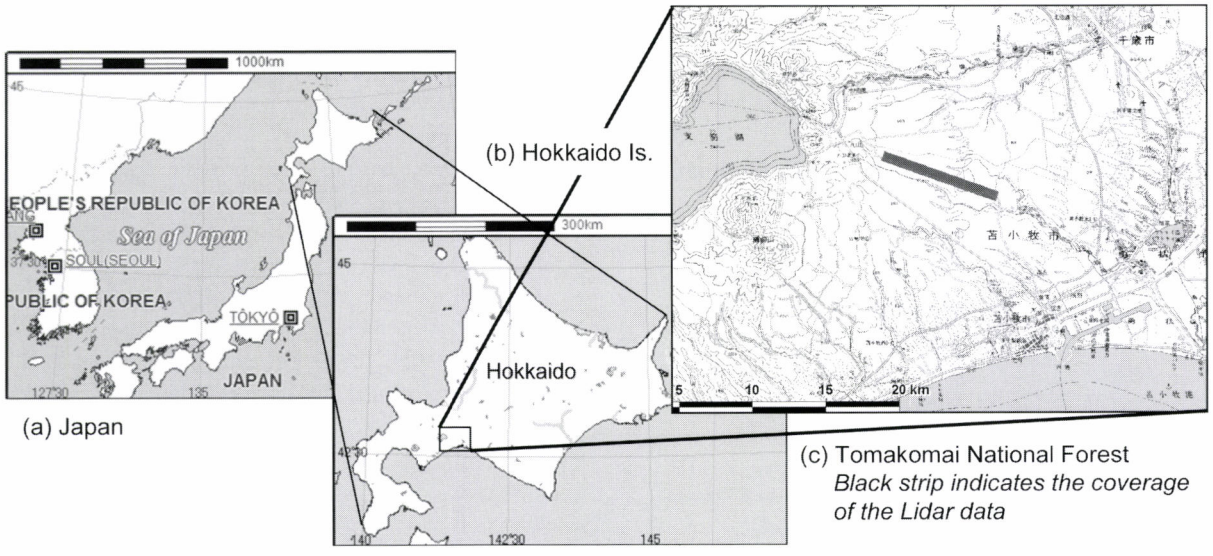

Fig. 1 Study site - Tomakomai, Hokkaido, Japan

at least 30 planted trees and at least three iterations of the planting pattern but not exceed 1,000m². As a consequence, the area of plot varied from 150m² up to 1,000m², the number of pulses within the plot from 148 to 1612, and the number of trees from 22 to 92. Note that the numbers of trees less than 30 were measured at plots of 1,000m². The locations of the plots were identified by either a simple survey or an interpretation of the orthophotos. Additional measurement was also done in 2004 at another 19 plots, which were used only for evaluation of the iso-height curves.

Iso-height Curves

The stand density chart is a semi-empirical growth model mainly applied to single age monoculture plantations, which describes the relationship among the stand density, the stand volume and the self thinning regardless of the stand age (ANDO, 1982). In Japan, stand density charts have been provided for major plantation species and regions by Forestry Agency, local governments, and/or other organizations so that forest managers can plan their operations and estimate the harvests of their plantations.

In the stand density chart, stand volume V [m³/ha] is calculated with stand density N and mean tree height H [m] by the iso-height equation (1) (ANDO, 1982).

$$V = 1/\left(a_1 H^{-b_1} + a_2 H^{-b_2}/N\right) \quad (1)$$

where a_1, b_1, a_2, and b_2 are parameters depending on the species and the region but independent from the age. Eq. (1) indicates that a stand volume can be estimated only by the attributes that can be observed from above by remote sensing.

However, it is not the mean tree height but the dominant height that can be estimated from LiDAR data, and the dominant height H_t was not equivalent to the mean height H. Thus, the eq. (1) should be redrawn as (2), and we should provide the iso-height curves for the species of our interests using the external plot measurements.

$$V = 1/\left(a_1 H_t^{-b_1} + a_2 H_t^{-b_2}/N\right) \quad (2)$$

External plantation measurements from overall Hokkaido Island (unpublished) were used to estimate the parameters in eq. (2) for each species of *P. glehnii*, *A. sachalinensis* and *L. leptolepis*. Numbers of the measurement were 165, 454 and 522 for the three species, respectively. Since not enough measurements were available for *P. jezoensis*, the parameters for *P. glehnii* were used for the species.

These parameters were estimated by fitting (2) to the above-mentioned external plantation measurements. The fittings were done numerically with two specific strategies. The first was that the variance of errors be equal independent of the stand volume, which was from a practical purpose to reduce the estimation error at higher stand volume. The second was that the criteria of fitness be the least ratio of contribution of the error instead of the least square of the error, by which underestimates at the higher stand volume, and vise versa, were to be avoided.

The derived iso-height curves were evaluated by the ground measurements.

Dominant Height Estimation

LiDAR pulses scarcely hit the tree tops, so it is difficult to estimate the dominant tree heights directly from those pulses. Instead, if a tree crown shape is simple and smooth, and the tree sizes and their crown shapes are similar to each other, the dominant tree height can be estimated as the limit of the crown height distribution.

Let F as the ratio of the projection area of the canopy higher than h [m] in a stand to the total stand area. The expected ratio of LiDAR pulses whose heights above terrain are higher than h in the stand is equal to F, given the pulses spread over the stand randomly or systematically. Plotting the height of all the pulses in the stand in the order of height and then normalizing the number of pulses into unity, an empirical relationship between h and F, i.e. $F = F[h]$ is derived (Fig. 2). The empirical h-F curves derived from the study plots seem linear in the middle part, although their overall shapes seem S-shaped with turns at the both ends.

If all the trees in a stand have a same size and a same shape of paraboloid of revolution, its h-F curve becomes completely linear as eq. (3);

$$F[h] = -sh + H_t, \text{for } H_t >= h >= 0, \quad (3)$$

where $s > 0$ is a parameter determining the width of crown. Even if all the tree shapes can be approximated as parabola,

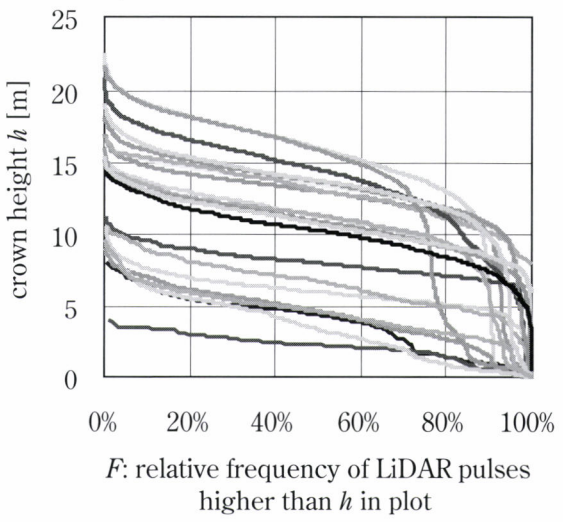

Fig. 2 Empirical h-F curves
Relative frequency, F, of LiDAR pulses higher than a given height from terrain, h. Each line represents the relative frequency in one of 19 study plots.

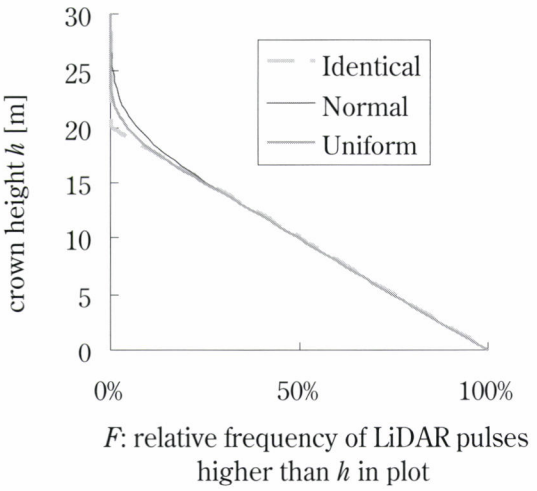

Fig. 3 Simulated relative frequencies of LiDAR pulses higher than h
A stand of 300 parabola-canopy trees with different size distributions; Identical: All trees have an identical shape with a height of 20m, Normal: All trees have similar shapes with the heights normally distributed with a mean of 20m and a standard deviation of 4m, Uniform: All trees have similar shapes with the heights uniformly distributed between 16m and 24m.

there should be a variation in the tree sizes in the real stands. In such a stand, h becomes higher than the linear relation for lower F (Fig. 3). On the other hand, in a real stand, h becomes lower than the linear relation for higher F due to the overlay of adjacent crowns, the existence of gaps, etc. All these effects can skew a linear h-F curve to an S-shaped one.

After the observation of the empirical h-F curves (Fig. 2) and the consideration of the h-F curve shapes as discussed above, we decided to estimate the dominant height, H_t, by eq. (3) fitted to a linear part of the h-F curve, assuming that the planted tree shapes are parabola. A portion of $50\% > F > 10\%$ in the h-F curve is arbitrary used to fit eq. (3) for each site.

They were evaluated by comparing with the 5 percentile height of trees of the plots.

Stand Density Estimation

Stand density was estimated by counting the tree tops on the orthophotos with a spatial resolution of 0.5m, which was as twice fine as the DHM, using Local Maximum Filter (LMF) (WULDER *et al.*, 2000). Only the green component of the orthophotos was used as B/W images for the analysis. For each plot, a small part of the orthophotos including the plot was extracted from a homogeneous part of the same compartment, the area of which varied from 0.1ha to .25ha depending on the stand condition. To decide the size of LMF, azimuthal semi-variograms for every 15 degree were derived for each plot. Since trees were planted linearly, the semi-variograms varied with the azimuth. Thus, the size of LMF window for a plot was decided as double the smallest range of the variograms, which was visually interpreted. The number of tree tops derived by LMF was then divided by the orthophoto area to derive the stand density N [trees/ha] for each plot.

The estimated density was compared with the measured density for each plot.

Stand Volume Estimation by Iso-height Curves

Stand volume of each plot was estimated from the dominant height derived from DHM and the stand density derived from the orthophoto by the iso-height curves (2) or (3). The estimations were evaluated by the ground measurements.

Table 2 Parameters for the iso-height curves

species	a_1	b_1	a_2	b_2
P.glehnii	0.0179	0.7463	13,261	3.3826
A.sachalinensis	0.9176	2.2106	1,349	2.4081
L.leptolepis	0.4546	1.7432	45,146	3.4458

RESULTS

Iso-height Curves

Prior to evaluate the estimations by LiDAR, the iso-height curves derived from the external measurements were evaluated by the ground measurements of our plots. Derived parameters for eqs. (2) and (3) are represented in Table 2 Fig. 4 shows the stand volume comparison between the ground measurements and their estimates from the iso-height curves. RMSE, bias, and the ratio of contribution of the estimates were 48.4m³/ha, −5.0m³/ha, and 94%, respectively.

Dominant Height Estimation

The dominant heights at the 21 plots in 2002 were estimated (Fig. 4). The coefficient of determination after the degree of freedom adjustment was 0.97. There were no significant differences found in the coefficient and intercept of regression from 1 and 0, respectively ($p > 0.4$). However, there was a bias of −0.5m. Regardless of species or height, the method earned very accurate estimations.

Stand Density Estimation

Among the plots used above, 19 plots were used for stand density estimation (Fig. 5); other 2 were dropped since there crowns were too small to be observed on the orthophotos. In the regression in log-log space, the coefficient of determina-

tion after the degree of freedom adjustment was 0.74. After dropping one plot, at where the sunlit floors through the thinned canopy were apparently mistaken as tree tops, still the coefficient was 0.76. The coefficient of regression was significantly different from 1 ($p < 0.0001$) in either cases. The bias was balanced as 0.0.

Stand Volume Estimation by Iso-height Curves

Finally, stand volumes were estimated from the LiDAR estimations of dominant heights and stand densities using the iso-height curves for the 19 plots (Fig. 7). RMSE, bias, and the ratio of contribution of the estimates were 53.0m³/ha, −20.9m³/ha, and 94%, respectively.

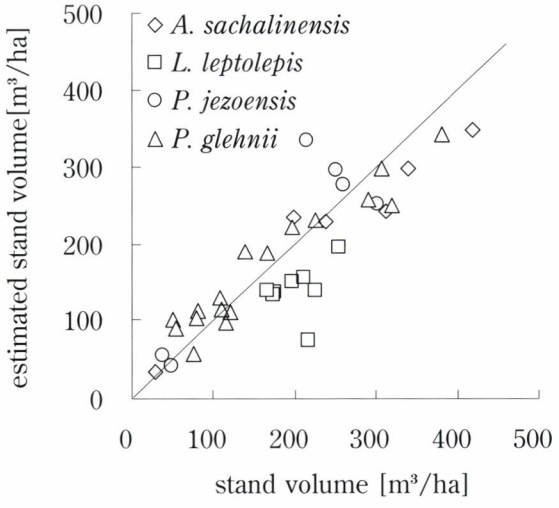

Fig. 4 Stand volume estimation from dominant height and density measured at the sample plots

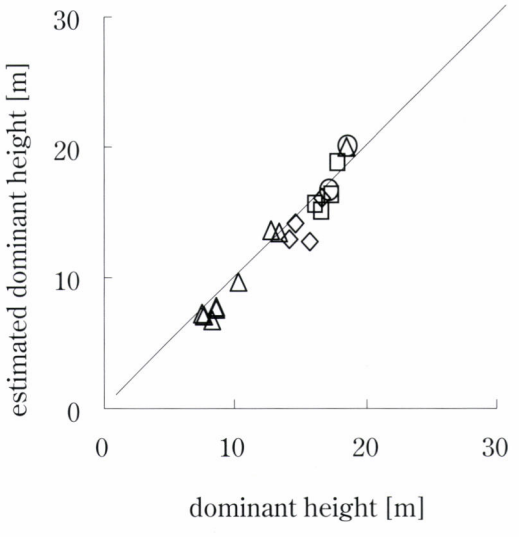

Fig. 5 Dominant height . measured vs. estimated
see Fig. 4 for legend

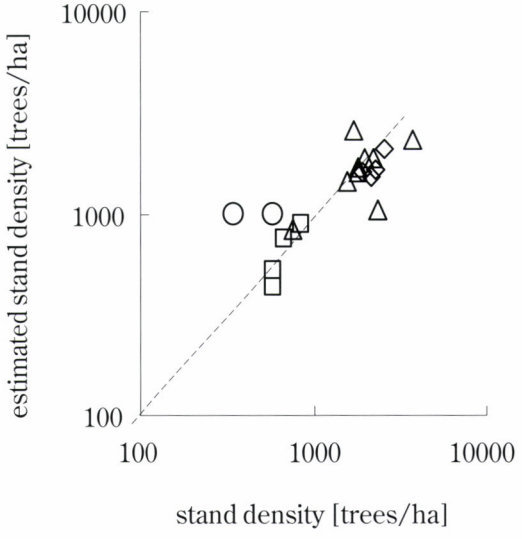

Fig. 6 Stand density - measured vs. estimated
see Fig. 4 for legend

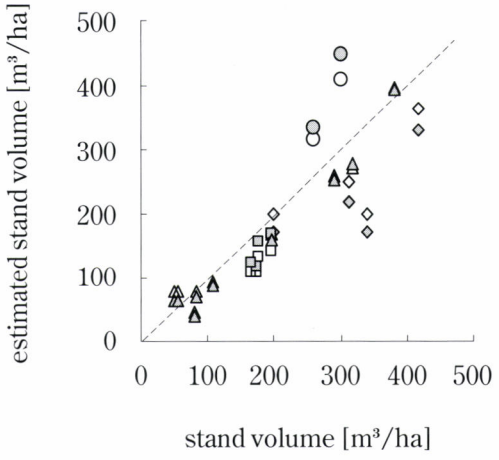

Fig. 7 Stand volume estimation from estimated dominant height and density by LiDAR
see Fig. 4 for legend

DISCUSSION AND CONCLUSION

Dominant height was estimated very accurately. The study site located on a flat and gentle slope, on which terrain affected very little to the LiDAR observation. What will be the effect on the dominant height estimation expected mathematically from steep slopes? In case the canopy shape is parabolic as eq. (3), a tree height estimation is expected to be overestimated as much as $\frac{\sqrt{s}}{4\pi}\tan^2\theta$ on flat slope with an inclination angle of θ. Suppose $\frac{\sqrt{s}}{4\pi}=1$, which is extremely large for a conifer, the tree height would be only 1m overestimated for a slope of θ = 45 deg. In case the canopy shape is cone like young trees, which had not been considered in the present study, there would be no estimation bias due to the slope. Thus, this dominant height estimation method is expected to be very stable.

The effect of the dominant height estimation bias on the stand volume estimation is represented as (4). The stand volume bias is very sensitive to the dominant height bias in general, and the bias is larger for taller trees for *A. sachalinensis* and *L. leptolepis*, although it is not always the case for *P. glehnii*.

$$\frac{\partial V}{\partial H_t}=\frac{a_1 b_1 H_t^{-b_1}+a_2 b_2 H_t^{-b_2}/N}{H_t}V^2 \qquad (4)$$

In the present study, we arbitrarily assumed the crown shape and size distribution of trees. Their structures and relationships with LiDAR data should be further studied in detail. Nevertheless, our results suggested that a wide range of canopy information, not necessarily at the tree tops, can earn a robust and straightforward estimation of the dominant height, given a crown shape model.

Stand density estimation was not sufficiently accurate. It needs a more accurate but still cost-effective method. Very high LiDAR DSM might be an alternative to aerial photos, however, it is not yet a practical option for operational forest management for the time being, since it is much more expensive than aerial photo to cover an area with a same spatial resolution. In addition, aerial photo would have an advantage in possibly screening the encroached broadleaf trees from the targeted conifers with its multispectral information.

The effect of the stand density estimation inaccuracy on the stand volume estimation is approximated when the inaccuracy is represented as the ratio as (5). In general, the bias is larger for taller and/or sparser stand.

$$\frac{\partial V}{\partial \ln N}=\frac{a_2 H_t^{-b_2}}{N}V^2 \qquad (5)$$

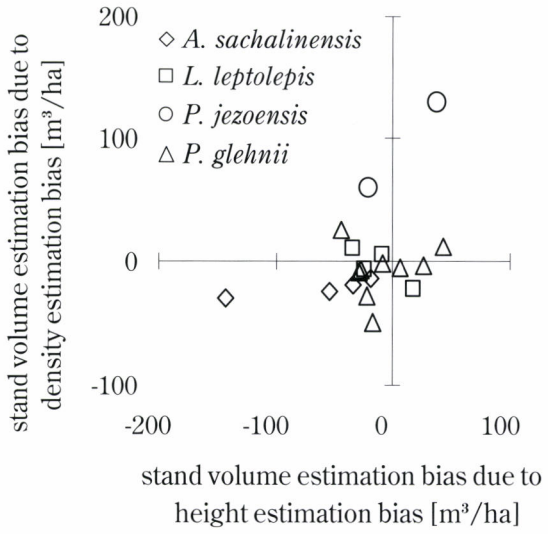

Fig. 8 Stand volume estimation bias due to height and density estimation bias

The bias contributions by the dominant height and density estimations were estimated for the 19 plots (Fig. 8). The stand density overestimates contributed to the volume overestimates in the old sparse *P. jezoensis* stands, while the dominant height underestimates contributed to the volume underestimates in the young dense *A. sachalinensis* stands. It is noted that the contributions of the two estimate biases were at similar order despite the height estimate's accuracy was far superior to the density estimate's.

The present study clearly defined the role of remote sensing to measure only what it can see, and demonstrated that the resultant methodology had not only a straightforward and robust structure combined with existing knowledge and data but also enough high estimation accuracy. However, there was room for improvement of the direct measurements by LiDAR, especially the stand density estimation. Site index, or the stand age, was not included in the present study, which should be addressed in future. Improving such sub-models would make the methodology to be more robust.

The proposed methodology not only offers the cost reduction by reducing the ground truth collections but also it can share with foresters the concept and values of forest resources derived from remote sensing using common language. It is a very important point of view for the implication of remote sensing to the real forest management, which has scarcely been achieved so far (HOLMGREN and THURESSON, 1998).

ACKNOWLEDGEMENT

The authors thank the Hokkaido Regional Forest Office, the National Forest, for the provision of the study site and the

cooperation for the study. This study was supported by "Global Environmental Research Fund" B-60, Ministry of Environment, Japan.

LITERATURE CITED

ANDO, T., (1982): Stand density management, Norin-shuppan, 126pp (in Japanese)

HOLMGREN, P. and THURESSON, T., (1998): Satellite remote sensing for forestry planning- a review. Scandinavian Journal of Forest Research **13**: 90-110

LIM, K., TREITZ, P., WULDER, M., ST-ONGE, B. and FLOOD, M., (2003): LiDAR remote sensing of forest structure. Progress in Physical Geography **27**(1): 88-106

NÆSSET, E., GOBAKKEN, T., HOLMGREN, J. *et al.*, (2004): Laser scanning of forest resources: the Nordic experience. Scandinavian Journal of Forest Research **19**(6): 482-499

OMASA, K., QIU, G.Y., *et al.*, (2003): Accurate Estimation of Forest Carbon Stocks by 3-D Remote Sensing of Individual Trees. Environmental Science and Technology **37**(6): 1198-1201

WULDER, M., NIEMANN, K. O. and GOODENOUGH, D. G., (2000) Local maximum filtering for the extraction of tree locations and basal area from high spatial resolution imagery. Remote Sensing of Environment **73**(1): 103-114

(Received 13 February 2007)
(Accepted 10 January 2008)

Article

Estimation of Stand Attributes in *Cryptomeria japonica* and *Chamaecyparis obtusa* Stands from Single Tree Detection using Small-Footprint Airborne LiDAR Data

Yasumasa Hirata[*1], Naoyuki Furuya[*2], Makoto Suzuki[*3] and Hirokazu Yamamoto[*4]

ABSTRACT

Stand attributes such as stand density, stand height, stand volume, are important factors for sustainable forest management. This study aimed to estimate stand attributes in *Cryptomeria japonica* and *Chamaecyparis obtusa* stands in Japan from single tree detection using small-footprint airborne LiDAR data. Twenty circular sample plots of 0.04ha were established for this study. Their stand densities were estimated from the number of treetops derived from airborne LiDAR data using the local maximum filtering method. Stand densities derived from the field survey in the sample plots were compared with those obtained from airborne LiDAR data. The coefficient of determination between them was 0.92. Stand densities which were estimated from the airborne LiDAR data, were underestimated in both young and mature stands. Stand heights, which were estimated from the airborne LiDAR data, were slightly overestimated, but they were almost the same as the mean heights of dominant standing trees. Allometric equations between diameter at breast height (DBH) and crown area obtained from airborne LiDAR data were determined for each of two species, i.e., *Cryptomeria japonica* and *Chamaecyparis obtusa*, and DBH of individual trees was estimated from the airborne LiDAR data. Stand volumes were estimated from the cumulative individual volumes, which were derived from volume formulas with two variables, i.e., DBH and height, both obtained from airborne LiDAR data. Stand volumes derived from the field survey were compared with those obtained from the airborne LiDAR data. The coefficient of determination was 0.86. Stand volumes which were estimated from the airborne LiDAR data, were underestimated because of the lack of suppressed tree volume; however, the degree of underestimation was relatively low.

Keywords: airborne LiDAR, stand attribute, single tree, *Cryptomeria japonica*, *Chamaecyparis obtusa*

INTRODUCTION

Sustainability has recently been a key issue in forest management, particularly after the UNCED (United Nations Conference on Environment and Development), which is commonly known as the Earth Summit, convened in Rio de Janeiro in June 1992 (FUJIMORI, 1996). Some initiatives for sustainable forest management, such as the Montreal Process (MCDONALD and LANE, 2004; SIRY *et al.*, 2005), the MCPFE (Ministerial Conferences on the Protection of Forests in Europe) Process replacing the Helsinki Process (MAYER, 2000; PARVIAINEN and FRANK, 2003), the ITTO Process (ITTO, 2005), as used as present criteria and indicators for the conservation and sustainable management of forests. Japan is a signatory of the Montreal Process and the extent of area by forest type and

Corresponding author: Yasumasa Hirata
[*1] Shikoku Research Center, Forestry and Forest Products Research Institute, 2-915 Asakura-nishi-machi, Kochi, 780-8077, Japan
e-mail: hirat09@affrc.go.jp
[*2] Department of Forest Management, Forestry and Forest Products Research Institute, 1 Matsuno-sato, Tsukuba, 305-8687, Japan
[*3] University Forest in Chiba, Graduate School of Agricultural and Life Sciences, The University of Tokyo, 770 Amatsu, Kamogawa, 229-5503, Japan
[*4] Graduate School of Agricultural and Life Sciences, The University of Tokyo, 1-1-1 Yayoi, Bunkyo-ku, Tokyo, 113-8657, Japan

by age class or successional stage must be monitored as indicators (MIURA and NAKASHIMA, 1996). These indicators are fundamental to understanding present forest conditions and monitoring their changes, and are essential for forest management planning.

Japan has two independent forest inventory systems (HIRATA *et al.*, 2007). One is the forest inventory stipulated by the forest planning system based on the forest law, in which forest registers and forest planning maps are prepared. The other is the forest resource monitoring survey, which is based on a systematic sampling on a national-wide 4km grid (PLANNING DIVISION IN FOREST AGENCY, 2004). The former is based on sub-compartments and the rapid compilation of GIS data on them gives us some understanding of the distribution and composition of Japanese forests. However, information about stand attributes in forest registers is not necessarily reliable because it is sometimes input without field confirmation. In addition, this inventory system sometimes involves multiple forest types. As a result, only dominant species and their ages in the sub-compartment are demonstrated on the polygon of forest planning maps.

The latter system was started in 1999 in both private and national forests to better understand Japanese forest conditions and their changes (IEHARA, 1999). The forest resource monitoring survey aims to prepare objective data, which are essential for planning regional forest management and for obtaining national statistics of forest resources. They are also required to understand biodiversity, productivity of forest ecosystems, and the carbon cycle. The results are reflected in the National Forest Plan. However, the sampling plot area of the latter system is 0.1ha per 16km^2, so we can estimate some indicators of the Montreal Process with it, but not the extent by forest type at the management level.

Remotely sensed data, especially from satellites and aerial photographs, is used to identify forest patches and their spatial attributes. At present, three-dimensional data and high-resolution data, both spatial and spectral, are available (LEFSKY and COHEN, 2003). Airborne LiDAR (Light Detection And Ranging) data is a type of three-dimensional data and previous studies have investigated its accuracy in estimating stand attributes such as tree height (NÆSSET, 1997; MAGNUSSEN *et al.*, 1999; NÆSSET and BJERKNES, 2001; ST-ONGE *et al.*, 2003), number of stems (NÆSSET and BJERKNES, 2001; MALTAMO *et al.*, 2004), stand volume (MALTAMO *et al.*, 2004), as well as individual tree attributes (HYYPPÄ and INKINEN, 1999; HYYPPÄ *et al.*, 2001; PERSSON *et al.*, 2002; HIRATA, 2005a; 2005b; TAKAKHASHI *et al.*, 2005a; 2005b). This study aims to estimate stand attributes in *Cryptomeria japonica* and *Chamaecyparis obtusa* stands in Japan using small-footprint airborne LiDAR data.

MATERIALS AND METHODS

Study Area and Sample Plots

The study area is located in the Tokyo University Forest (35°10' N, 140°07' E; 50-370m above sea level) about 100km southeast of Tokyo in Chiba Prefecture. Established in 1894, it is the oldest university forest in Japan. The University Forest covers an area of about 2,171ha, 40% of which is plantations and the rest is natural or semi-natural forests. The mean monthly temperature of this warm-temperate zone forest is 14.0°C, with the highest mean of 24.1°C in midsummer and the lowest of 4.6°C in winter. Annual precipitation is 2,182mm, concentrated from June to September and with little precipitation from November to March. More than 280 species of trees and 800 species of herbs, including 150 species of ferns, are recorded on the vegetation list. Most of the plantations consist of *Cryptomeria japonica* and/or *Chamaecyparis obtusa* (UNIVERSITY FOREST, THE UNIVERSITY OF TOKYO).

Twenty circular sample plots of 0.04ha were established in *Cryptomeria japonica* and *Chamaecyparis obtusa* stands, with ages ranging from 19 years to 102 years. The coordinates at the centers of all sample plots were positioned with DGPS to co-register airborne LiDAR data. DBH of all standing trees in the sample plots was measured and the species were recorded. Stand densities in the sample plots were calculated from the number of standing trees per 0.04ha. Mean DBH of sample plots ranged from 11.5cm to 58.0cm and stand densities from 300trees/ha to 3,925trees/ha.

Tree height measurement is always time- and labor-intensive. Hence, the height-diameter curve is used to estimate tree height instead of actual measurements (INOUE and YOSHIDA, 2004). The height of more than 40% of standing trees was measured in each sample plot and the height of other trees was estimated from the Näslund formula, a type of height-diameter curve, as follows:

$$h=bh+d^2/(a+bd)^2 \quad (1)$$

where, bh is breast height, h is tree height, d is DBH, and a and b are constants. The mean tree height in the sample plots varied from 6.3m to 32.4m.

Airborne LiDAR Data

The ALMAPS-G4 (Asahi Laser Mapping System), which consists of the ALTM 3100 laser scanning system (Optech, Canada), GPS airborne and ground receivers, and the inertial measurement unit (IMU) reporting the helicopter's roll, pitch and heading, were used to acquire airborne LiDAR data. The laser scanner system transmits laser pulses at 1,064nm (near-infrared) and receives the first and last echoes of each pulse. The elapsed time between transmittance and reception is

measured to calculate the distance between the system and the object.

Airborne LiDAR data were acquired on 14 August 2005. The flight altitude of the helicopter above the ground was about 500 meters and the average flight speed was approximately 19.4m/sec. The pulse repetition frequency of LiDAR was 70kHz and the scan frequency was 27Hz. Its maximum scan angle (off nadir) was 18°. The beam divergence was 1.2 mrad. Therefore, the footprint diameter was approximately 60cm. The interval between footprints was about 25cm. Both first pulse and last pulse were acquired to identify forest canopy and topography in rugged terrain.

Data from a region of interest (ROI), which was 200m in width and 1,700m in length, was selected for this study. A digital elevation model (DEM) and a digital surface model (DSM) for the study area were prepared from the airborne LiDAR data with 25cm cell size. Data for the digital canopy model, which delineates canopy height from the ground, were calculated by subtracting the DEM from the DSM.

Data Analysis

Treetops in the study area were identified from DCM using a local maximum filtering method (WULDER *et al.*, 2000). Forest gaps were masked to avoid overestimating the number of treetops. Areas that were considered gaps were confirmed using a threshold which was decided from a histogram of DCM. The number of treetops in each sample plot was counted and used to calculate the stand density in each sample plot. Stand densities derived from the field survey of the sample plots were compared with those obtained from the airborne LiDAR data.

Individual tree heights were determined as the values of DCM at the positions of treetops. Because suppressed trees cannot be observed from an aircraft, we assumed that individual tree heights derived from the reverse image of DCM corresponded to those obtained from the field survey according to the size of the largest ones. Mean tree heights that were derived from the airborne LiDAR data were calculated for all sample plots. Mean tree heights corresponding to trees identified from the airborne LiDAR data and those of all trees for all sample plots were also calculated. Both types of mean tree heights from the field survey were compared with those obtained from the airborne LiDAR data.

Individual crowns were identified from a reverse image of DCM by a watershed method with the gap mask. Here, we also assumed that crown areas derived from the reverse image of DCM corresponded to DBHs obtained from the field survey according to the size from the largest ones. We investigated the allometric relationship between DBH and crown area, which could be expressed with the following equation:

$$y=ax^b \tag{2}$$

where x is the independent variable, y is the dependent variable, and a and b are constants. Using the crown area from the airborne LiDAR data and the DBH from the field survey, a and b of Eq. (2) were determined for each species with the least-squares method. Individual volume was calculated from a volume formula with two variables, i.e., DBH and tree height derived from both the airborne LiDAR data and the field survey. The formula is written as follows:

$$\log v=p \log d+q \log h+r \tag{3}$$

where, v is volume, and p, q and r are constants which were determined by the DBH class for *Cryptomeria japonica* and *Chamaecyparis obtusa* respectively (PLANNING DIVISION IN FOREST AGENCY, 1970): (Table 1). Stand volume was calculated from the accumulation of individual volumes in each sample plot. Stand volumes derived from the field survey of the sample plots were compared with those obtained from the airborne LiDAR data.

Analysis was mainly conducted using GIS and the image processing software TNTmips version 6.7 (MicroImages Inc., USA).

Table 1 Constants in the volume formulas in Southern Kanto Region for *Cryptomeria japonica* and *Chamaecyparis obtusa* by diameter class

Cryptomeria japonica			
Diameter class	p	q	r
4-10cm	1.753904	1.040853	- 4.172632
12-30cm	1.849344	1.008086	- 4.219069
32-40cm	1.944187	0.894801	- 4.211821
42 and over cm	1.600066	1.075361	- 3.921218
Chamaecyparis obtusa			
Diameter class	p	q	r
4-10cm	1.906941	0.942734	- 4.230151
12-20cm	1.867405	1.108487	- 4.354186
22 and over cm	1.710344	1.175119	- 4.229853

RESULTS AND DISCUSSION

Stand densities obtained from the airborne LiDAR data were plotted against stand densities derived from the field survey in the sample plots (Fig. 1). The regression line fitting to the data by the least-squares method had an intercept of 127.7trees/ha and a slope of 1.07. The coefficient of determination (R^2) between them was 0.92 and RMS error (RMSE) was 369.9trees/ha. Stand densities, which were estimated from the airborne LiDAR data, were underestimated in both young and mature stands. In young stands, neighboring treetops are close together, making it difficult to distinguish them with the local maximum filtering method. In mature stands, some suppressed trees cannot be observed after growth competition because of canopy layer. Particularly, the stands densities were extremely underestimated in four plots of *Chamaecyparis obtusa* stands, where stands were considerably overcrowding because thinning operations were delayed or had not been performed. Relatively high RMSE was due to these underestimations. HIRATA (2005a) showed that thinning intensity affected extraction rate of treetops from DCM derived from airborne LiDAR data in a *Cryptomeria japonica* stand. This result suggested that thinning operation also affected estimation of stand density using airborne LiDAR in *Chamaecyparis obtusa* stands.

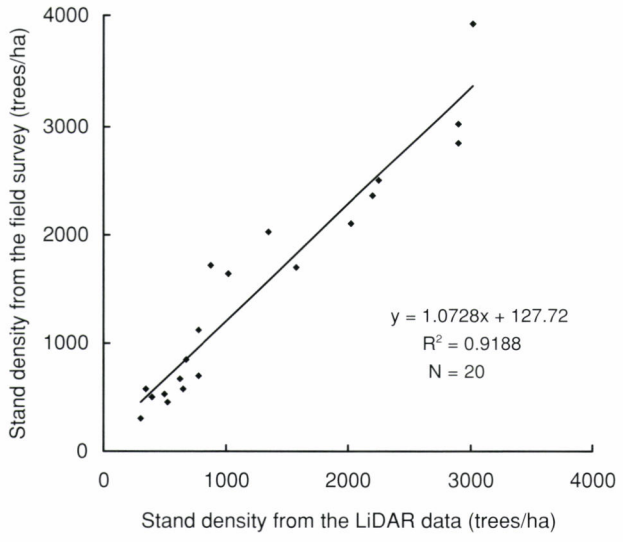

Fig. 1 Relationship between stand densities derived from the airborne LiDAR data and those obtained from the field survey for the sample plots

Mean tree heights obtained from the airborne LiDAR data were plotted against those corresponding to dominant trees and the mean of all standing trees derived from the field survey in the sample plots (Fig. 2 and Fig. 3), with regression analysis results presented in Table 2. R^2 were high in both analysis for dominant trees and all standing trees in the sample plots, and RMSE for dominant trees is smaller than one for all standing trees. Stand heights, which were estimated from the airborne LiDAR data, were slightly underestimated in young stands and overestimated in mature stands in both analysis for the dominant trees and the all standing trees. In mature stands, some suppressed trees normally cannot be measured

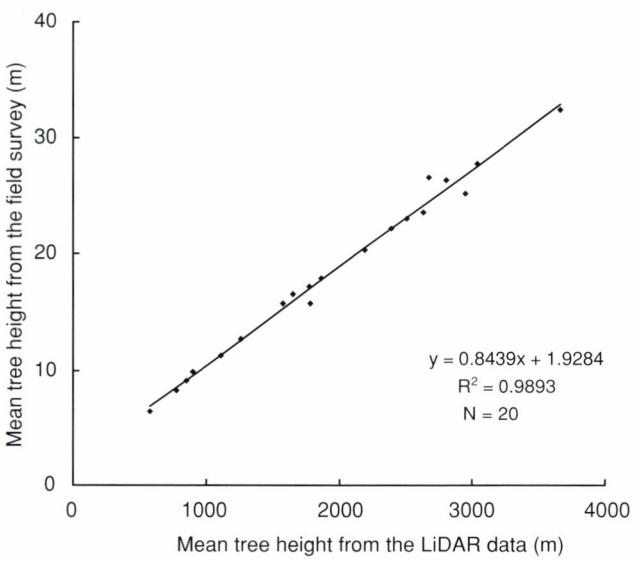

Fig. 2 Relationship between mean tree heights derived from the airborne LiDAR data and those of all standing trees obtained from the field survey for the sample plots

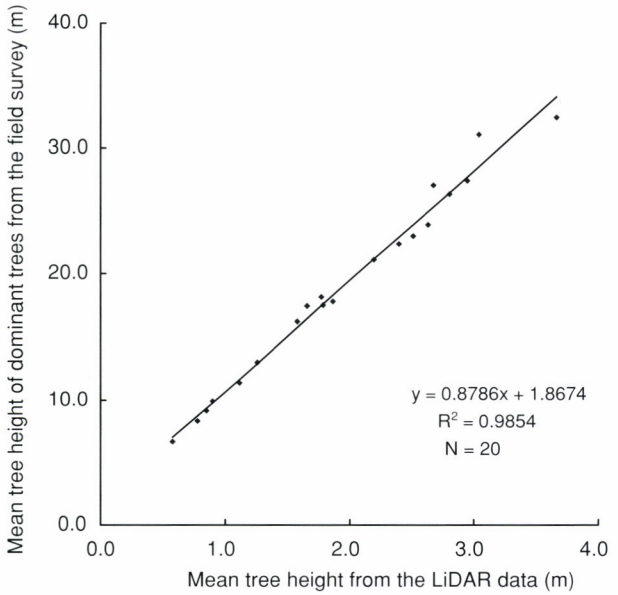

Fig. 3 Relationship between mean tree heights derived from the airborne LiDAR data and those of dominant trees obtained from the field survey for the sample plots

Table 2 The results of the regression analysis between mean tree height obtained from the airborne LiDAR data and those derived from the field survey for the sample plots

Tree height	Intercept	Slope	R^2	RMS error (m)
All trees	1.93	0.84	0.99	1.89
Dominant trees	1.87	0.88	0.99	1.46

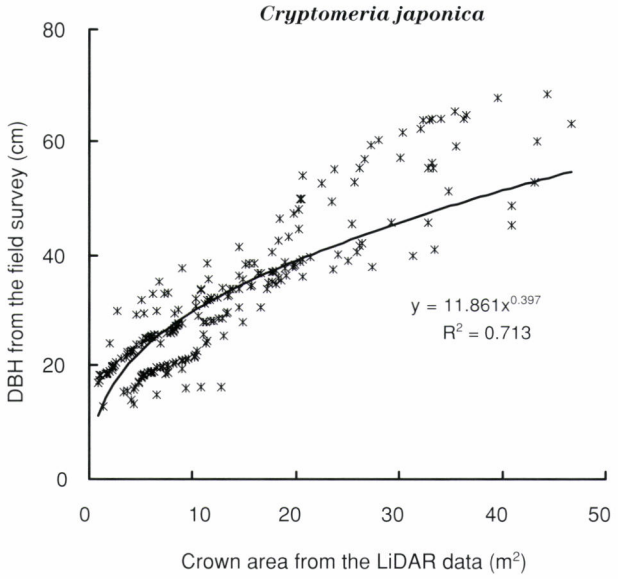

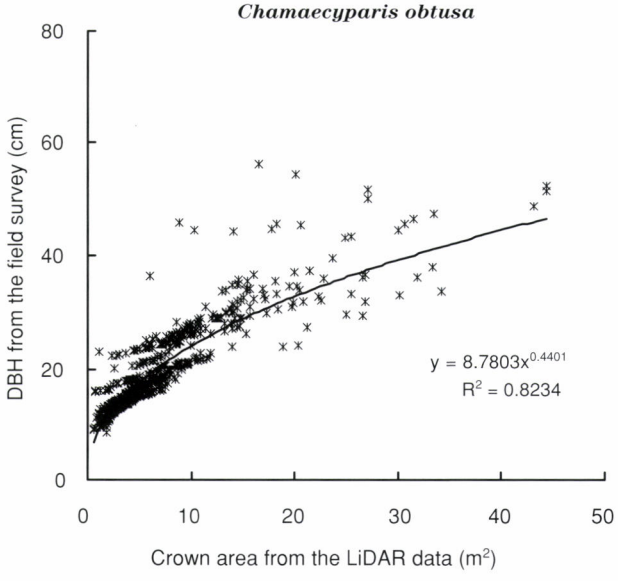

Fig. 4 Allometric relationships between crown area derived from the airborne LiDAR data and DBH obtained from the field survey for *Cryptomeria japonica* and *Chamaecyparis obtusa*

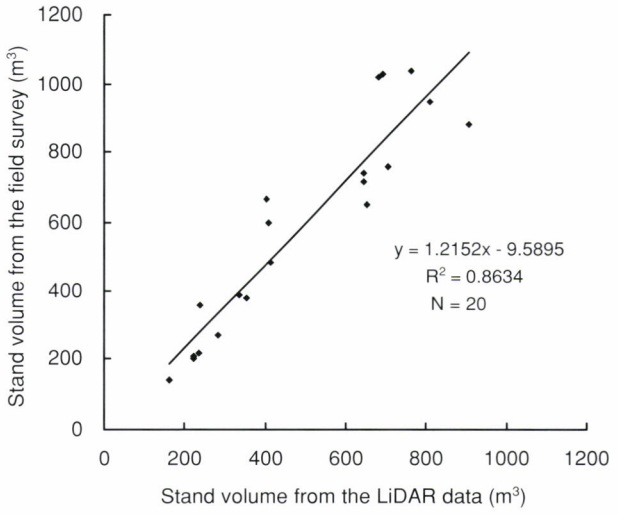

Fig. 5 Relationship between stand volumes derived from the airborne LiDAR data and those obtained from the field survey for the sample plots

by airborne LiDAR, therefore, mean height derived from airborne LiDAR data become large as compared with the stand height from the field survey.

The generalized allometric equation (Eq. 2) between DBH (d) and crown area (c) derived from airborne LiDAR data for *Cryptomeria japonica* and *Chamaecyparis obtusa* was determined with the least-squares method as follows (Fig. 4):

Cryptomeria japonica: $d=11.861c^{0.397}$
Chamaecyparis obtusa: $d=8.7803c^{0.4401}$

Stand volumes obtained from two variables, i.e., DBH and tree height, which were estimated from airborne LiDAR data, were plotted against stand volumes derived from the field survey in the sample plots (Fig. 5). The regression line fitting to the data by the least-squares method had an intercept of 9.6m³/ha and a slope of 1.22 (R^2 = 0.86; RMSE 153.5m³/ha). Stand volumes, which were estimated from the airborne LiDAR data, were underestimated because of lack of suppressed tree volume data, but the degree of underestimation was relatively low.

CONCLUSIONS

In this study, we estimated stand attributes in *Cryptomeria japonica* and *Chamaecyparis obtusa* stands in Japan from single tree detection using small-footprint airborne LiDAR data.

The findings are summarized below:

1. Stand densities, which were estimated from the airborne LiDAR data, were underestimated in young and mature stands. The regression line fitting to the data by the least-squares method had an intercept of 127.7 trees/ha and a slope of 1.07 (R^2 = 0.92; RMSE 369.9 trees/ha).
2. Stand heights, which were estimated from the airborne LiDAR data, were slightly overestimated, but they were the almost the same as the mean heights of dominant standing trees. The regression line fitting to the data of mean heights of all standing trees in the sample plots by the least-squares method had an intercept of 1.93m and a slope of 0.84 (R^2 = 0.99; RMSE 1.89) and the regression line fitting to the data of mean heights of dominant trees in the sample plots by the least-squares method had an intercept of 1.87m and a slope of 0.84 (R^2 = 0.99; RMSE 1.46).
3. Stand volumes, which were estimated from the airborne LiDAR data, were underestimated because of a lack of data on suppressed tree volume; however, the degree of underestimation was relatively low. The regression line fitting to the data by the least-squares method had an intercept of 9.6m^3/ha and a slope of 1.22 (R^2 = 0.86; RMSE 153.5m^3/ha).

Recently, airborne LiDAR data has come to be used in many domains of forestry. Some new experimental applications for airborne LiDAR data include quality assessment of forest structure as habitats of birds and animals (Hinsley *et al.*, 2002; Nelson *et al.*, 2005), snow depth estimation in a watershed for water control (Okamoto *et al.*, 2004), design of forest roads (Aruga *et al.*, 2005), change detection of forests (Yu *et al.*, 2006), and climatic damage assessment (Takao *et al.*, 2005; Taguchi *et al.*, 2006). In these studies, forest attributes are key factors derived from airborne LiDAR data, which are used to evaluate wildlife habitats, watershed and topographic properties, and change detection. Our results indicated that there are several ways that airborne LiDAR data can be used as alternative methods of undertaking inventory as well as ecological studies and others.

ACKNOWLEDGEMENTS

Funding for this research was provided by the Ministry of Agriculture, Forestry and Fisheries of Japan. We would like to thank the staff of the Tokyo University Forest in Chiba for their valuable assistance. We would also like to thank Yukihide Akiyama, Tohru Inoue, Koji Ohmori, Hidekazu Kobayashi, Junihi Takanuki, Toshiya Ueda, Hideo Suzuki, Daisuke Matsuda and Takeshi Yamamoto at Aero-Asahi Co. for the laser scanner data acquisition, and their pre-processing.

LITERATURE CITED

Aruga, K., Sessions, J. and Akay, A.E., (2005): Application of an airborne laser scanner to forest road design with accurate earthwork volume. J. For. Res. **10**: 113-123

Fujimori, T., (1996): Why do we need "sustainable forest management" now? Sinrin Kagaku **16**: 57-58 (in Japanese)

Hinsley, S.A., Hill, R.A., Graveau, D.L.A. and Bellamy, P.E., (2002): Quantifying woodland structure and habitat quality for birds using airborne laser scanning. J. Functional Ecol. **16**: 851-857

Hirata, Y., (2005a): Influence of transmittance and sampling density of laser beams in forest measurement of a *Cryptomeria japonica* stand with an airborne laser scanner. Jpn. J. For. Plann. **39**: 81-95 (in Japanese with English summary)

Hirata, Y., (2005b): Relationship between tree height and topography in a *Chamaecyparis obtusa* stand derived from airborne laser scnner data. J. Jpn. For. Soc. **87**: 497-503 (in Japanese with English summary)

Hirata, Y., Matsumoto, M. and Iehara, T., (2007): Japanese national forest inventory and its spatial extension by remote sensing. Proc. FIA Symposium **8**: (in press)

Hyyppä, J. and Inkinen, M., (1999): Detecting and estimating attributes for single trees using laser scanner. The Photogrammetric J. Finland **16**: 27-42

Hyyppä, J., Kelle, O., Lehikoinen, M. and Inkinen, M., (2001): A segmentation-based method to retrieve stem volume estimates from 3-d tree height models produced by laser scanners. IEEE Trans. on Geosci. and Remote Sens. **39**: 969-975

Iehara, T., (1999): New Japanese national forest resource monitoring survey. Sanrin **1384**: 54-61 (in Japanese)

Inoue, A. and Yoshida, S., (2004): Allometric model of the height-diameter curve for even-aged pure stands of Japanese cedar (*Cryptomeria japonica*). J. For. Res. **9**: 325-332

ITTO, (2005): Revised ITTO criteria and indicators for the sustainable management of tropical forests including reporting format. ITTO, Yokohama, 40 pp

Lefsky, M.A. and Cohen, W.B., (2003): Selection of remotely sensed data. *In* Wulder, M.A. and Franklin, S.E. (eds.), Remote sensing of forest environments - concepts and case studies -. 13-46. Kluwer Academic Publishers, Boston/Dordrecht/London

Magnussen, S., Eggermont, P. and LaRiccia V. N., (1999): Recovering tree heights from airborne laser scanner data. For. Sci. **45**: 407-422

Maltamo, M., Eerikäinen, K., Pitkänen, J., Hyyppä, J. and Vehmas, M., (2004): Estimation of timber volume and stem density based on scanning laser altimetry and expected tree size distribution functions. Remote Sens. of Environ. **90**: 319-330

Mayer, P., (2000): Hot spot: Forest policy in Europe: achievements of the MCPFE and challenges. Forest Policy and Econ. **1**: 177-185

McDonald, G.T. and Lane, M.B., (2004): Converging global indicators for sustainable forest management. For. Policy and Economics **6**: 63-70

Miura, S. and Nakashima, K., (1996): Criterion 1: Conservation of biodiversity. Sinrin Kagaku **16**: 59-60 (in Japanese)

Næsset, E., (1997): Determination of mean tree height of forest

stands using airborne laser scanner data. ISPRS J. Photogrammetry and Remote Sens. **52**: 49-56

NÆSSET, E. and BJERKNES, K.-O., (2001): Estimating tree heights and number of stems in young stands using airborne laser scanner data. Remote Sens. of Environ. **78**: 328-340

NELSON, R., KELLER, C. and RATNASWAMY, M., (2005): Locating and estimating the extent of Delmarva fox squirrel habitat using an airborne LiDAR profiler. Remote Sens. Environ. **96**: 292-301

OKAMOTO, T., KUROKAWA, U., MATSUURA, S., ASANO, S. and MATSUYAMA, K., (2004): Adaptability of an airborne laser scanner to determine a snow depth distribution on a mountain area. J. Jpn. Soc. Hydrol. and Water Resour. **17**: 529-535

PARVIAINEN, J. and FRANK, G., (2003): Protected forests in Europe approaches-harmonising the definitions for international comparison and forest policy making. J. Environ. Manage. **67**: 27-36

PLANNING DIVISION IN FOREST AGENCY, (1970): Volume table of standing tree in Eastern Japan. J-FIC, Tokyo, 333 pp (in Japanese)

PLANNING DIVISION IN FOREST AGENCY, (2004): A handbook for forest planning duties. J-FIC, Tokyo, 1400pp (in Japanese)

SIRY, J.P., CUBBAGE, F.W. and AHMED, M.R., (2005): Sustainable forest management: global trends and opportunities. For. Policy and Econ. **7**: 551-561

ST-ONGE, B., TREITZ, P. and WULDER, M.A., (2003) Tree and canopy height estimation with scanning lidar. *In* WULDER, M.A. and FRANKLIN, S.E. (eds.), Remote sensing of forest environments - concepts and case studies -. 489-510. Kluwer Academic Publishers, Boston/Dordrecht/London

TAGUCHI, H., USUDA, Y., FUKUI, H. and FURUKAWA, K., (2006): Development a method for forest snow damaged area detection using the combination of high resolution satellite optical sensor imagery and LiDAR data. J. Jpn. Soc. Photogrammetry and Remote Sens. **45**(1): 14-21 (in Japanese with English summary)

TAKAHASHI, T., YAMAMOTO, Y., SENDA, Y. and TSUZUKU, M., (2005a): Estimating individual tree height of sugi (*Cryptomeria japonica* D. Don) plantations in mountainous areas using small-footprint airborne LiDAR. J. For. Res. **10**: 135-142

TAKAHASHI, T., YAMAMOTO, Y., SENDA, Y. and TSUZUKU, M. (2005b): Predicting individual stem volumes of sugi (*Cryptomeria japonica* D. Don) plantations in mountainous areas using small-footprint airborne LiDAR. J. For. Res. **10**: 305-312

TAKAO, G., UTSUGI, H., SASAKI, S., IIDA, S., ABE, S. and TOBITA, H., (2005): Evaluation of windthrow damage in a deciduous broad-leaved forest using airborne LiDAR. J. Jpn. Soc. Photogrammetry and Remote Sens. **44**(6): 18-21 (in Japanese)

UNIVERSITY FOREST, GRADUATE SCHOOL OF AGRICULTURAL AND LIFE SCIENCE, THE UNIVERSITY OF TOKYO, http://www.uf.a.u-tokyo.ac.jp/english2/chiba/chiba.html

WULDER, K., OLAF NIEMANN, K., and GOODENOUGH, D.G., (2000): Local maximum filtering for the extraction of tree locations and basal area from high spatial resolution imagery. Remote Sens. Environ. **73**: 103-114

YU, X., HYYPPÄ, J., KUKKO, A., MALTAMO, M. and KAARTINEN, H., (2006): Change detection techniques for canopy height growth measurements using airborne laser scanner data. Photogrammetric Engineering & Remote Sens. **72**: 1339-1348

(Received 26 February 2007)
(Accepted 5 November 2007)

GUIDE FOR CONTRIBUTORS

Please refer to the following guidelines when submitting a new manuscript to the JOURNAL OF FOREST PLANNING ("the *Journal*"), of the Japan Society of Forest Planning ("the *Society*"), so that your manuscript may be handled expeditiously.

Type of Papers: Each paper is classified into one of three types: article, review, or short communication. A paper should be a report of original research that has not been submitted elsewhere (other than as an abstract).

Contributors: The first author of a paper of any type should be a member of the *Society* unless he/she is invited by Chief Editor. The authors can apply for memberships on submission.

Copyright: The *Society* reserves all rights to the papers for the *Journal*. Written permission by the Chief Editor is required for reproduction or republication.

Decision for Publication: The Editorial Board makes the decision to accept, reject, or suggest corrections of a manuscript in accordance with the results of reviews by knowledgeable referees selected by the Editorial Board.

Manuscript: Manuscripts should be written in English in line with the guidelines in "Manuscripts Preparetion" below. For the sake of prompt manuscript handling, authors are highly encouraged to provide an electronic manuscript as well as the printed ones.

English: All authors whose first language is *not* English should ask a native speaker to refine the written English before submission.

Final Manuscript and Authors' Corrections: When the manuscript is accepted, the authors will be asked to send the final manuscript in both printed and electronic forms. The required formats will be indicated in the final manuscript instruction. The author's proof will be sent only once for misprint corrections.

Expenses on Publication: Authors will be charged the following items on publication of the paper.

- Page charge: ¥6,000 per printed page
- Color pages/special printings: actual expense
- Reprints (exceeding 50 copies): ¥20,000/50 copies
- Annual membership (for authors without membership): ¥2,500

(All prices are subject to change.)

Submission and Inquiry: One original copy and one complete photocopy of the manuscript, and a submission form should be sent to Chief Editor, whose address can be found on the inside cover of the *Journal*. An electronic file of the abstract in text format on a floppy diskette should be attached if available. Inquiries about submission may also be sent to the Chief Editor.

Manuscripts Preparation

Style: A manuscript should be arranged as follows: (1) Title of paper, authors' full names and affiliations with addresses, (2) Abstract, (3) Keywords (no more than five), (4) Main Text, (5) Literature cited, (6) Figures and tables, (7) Messages to Editors.

Typing: Manuscripts should be typewritten, double-spaced on one side of A4 (or Letter size) white paper with margins of 3cm on top, bottom and both sides. The desired location of tables and figures should be indicated in the text with red ink in the right margins.

Text Style: Text to be printed in *italic*, **bold** and SMALL CAPITAL fonts should be indicated by single, wavy and double underlines, respectively.

Abstract: An abstract is required for any type of papers, and should be no more than 500 words.

Literature Cited: Literature cited should be listed alphabetically by first author's surname (family name). For the style, consult the examples given below. Literature in the text may be cited by author's surname and year of publication in parentheses after the statement concerned. If there are more than two authors, citations should quote the surname of the first author and the words "*et al.*". All author's names should be included in the list.

LEVITT, J., (1972): Responses of plants to environmental stresses. Academic Press, New York & London, 697pp

YAMAMOTO, N. and SASAKI, S., (1976): Electron microscope study on polysome formation duriog pine seed germination. J. Jpn. For. Soc.58:65-66

Tables: Tables must be numbered with Arabic numerals according to their sequence in the text (Table 1, Table 2 etc.). Each table should be prepared on a separate sheet. Each table should have a brief and self-explanatory title. Any explanation for tables should be given as a footnote at the bottom of the table.

Figures: Figures must be numberd with Arabic numerals according to their sequence in the text. Each figure should be prepared on a separate sheet. Each figure's legend should be prepared on another separate sheet. Figures should be of publication quality. Color figures can be included for an extra printing charge. A figure for color printing should be indicated by a note, "COLOR", on the margin of the sheet.

Submission Form: The submission form should be filled out and attached to the manuscript on submission. The form can be found at the last page of the *Journal*. Non-member authors can apply for memberships of the Society at the time of submitting their paper by enclosing the application form, which can be found on the inside of the back cover of the *Journal*.

Text File: The abstract should be saved as a text file on a floppy diskette. The file should be arranged as follows: (1) Title of paper, authors' full names and affiliations with addresses, (2) Abstract. The floppy diskette should be an MS-DOS formatted 3.5". The file name should be the prefix"a_ (underscore)" followed by the surname of the first author, and then the suffix".txt"(e.g. "a_koshika.txt"). The title and authors of the manuscript should be noted on the surface label of the diskette.

(May, 2001)
(revised September, 2002)

JOURNAL OF FOREST PLANNING
Submission Form

1 . Date of submission: _____

2 . Name of author(s): _____

_____

3 . Title of manuscript: _____

_____

4 . Correspoding author: _____

5 . Affiliated institution: _____

6 . Mailing address: _____

_____

Telephone: _____ Fax: _____

E-mail: _____

Maililng address in Japanese (if available): _____
（確実に郵送できるように送付先を研究室名等までお書きください）

_____

_____

7 . Classification of manuscript*: ☐ article ☐ review ☐ short communication
*Plaese tick one of the boxes.

8 . Number of pages including abstracts: _____

9 . Number of tables: _____ Number of figures: _____

10. Necessary number of reprints: _____

11. Please tick either which apply:
☐ The written English has been proofread by a native speaker.
☐ I am from an English-speaking country.

Filled by the Editorial Board

受付番号 _____

受付日 _____ 受理日 _____

Japan Society of Forest Planning
Membership Application Form
(for a person who lives except in Japan)

To join the "Japan Society of Forest Planning", please copy and fill out this membership application form and send it to secretary of the Japan Society of Forest Planning.

An individual membership fee for one year (from April to next March) is ¥2,500 and member of this society can receive Journal of Forest Planning (2 issues/year). Organization membership fee is ¥2,500 for each issue of Journal of Forest Planning.

(Please Print or Type Clearly)

Name: (Last) _____ (First) _____ (Middle) _____

Company/Organization: _____

Street/P.O.: _____

City: _____ State: _____ Zip: _____ Country: _____

Phone: _____ Fax: _____ E-Mail: _____

Type of Membership:

Except in Japan

☐ Individual	¥2,500/year
☐ Organization	¥2,500/issue

In Japan

☐ Individual	¥5,000/year
☐ Individual(student)	¥2,000/year
☐ Organization	¥2,500/issue

Payment:

☐ Bank Transfer Iwate bank, Ueda branch,
Account No. : 2002757
Account Name : Shinrinkeikaku-gakkai

This form should be sent to : The Japen Society of Forest Planning
Iwate University,
3-18-8 Ueda, Morioka, Iwate 020-8550, Japan
Fax : +81-19-621-6135

Japan Society of Forest Planning